TURBULENT EXCHANGE OF OZONE AND NITROGEN OXIDES BETWEEN AN AMAZONIAN RAIN FOREST AND THE ATMOSPHERE

A dissertation submitted to the
FACULTY OF BIOLOGY, CHEMISTRY AND GEOSCIENCES
AT THE UNIVERSITY OF BAYREUTH

for the degree of
DR. RER. NAT.

presented by
Udo Rummel
Dipl.-Meteorol.
Born in Göppingen

April 2005

TURBULENTER AUSTAUSCH VON OZON UND STICKOXIDEN ZWISCHEN EINEM AMAZONISCHEN REGENWALD UND DER ATMOSPHÄRE

Der vollständige Abdruck der von der Fakultät für Biologie, Chemie und Geowissenschaften der Universität Bayreuth genehmigten Dissertation zur Erlangung des akademischen Grades
Doktor der Naturwissenschaften (DR. RER. NAT.)

Erstgutachter: Prof. Dr. Thomas Foken
Zweitgutachter: Prof. Dr. Cornelius Zetzsch

Tag des Kolloquiums: 07. November 2005

Die vorliegende Arbeit entstand von Juni 1998 bis April 2005 am Max-Planck-Institut für Chemie, Abt. Biogeochemie, als Teil des LBA-EUSTACH Projektes, finanziert im Rahmen des "Environmental and Climate Programm" (ENV4-CT97-0566) der Europäischen Union und der Max-Planck-Gesellschaft.

Summary

Amazonia, the world's largest tropical rain forest area is facing rapid development, mainly caused by slash and burn activities. The change in land use, primarily to agricultural and pasture areas, has sustainable influence on the atmospheric input and the deposition of constituents like ozone (O_3) and nitrogen oxides (NO_x), which are of high relevance for tropospheric chemistry. To asses the effect of land use change on tropospheric chemistry, a good knowledge of the exchange of those trace gases between the primary rain forest ecosystem and the atmosphere is necessary. So far, experimental information from tower based canopy-scale and leaf-scale measurements focusing on exchange processes is very limited. Within the framework of the LBA-EUSTACH project 1999 two experiments were carried out in Rondônia, southwest Amazonia, to estimate the exchange of ozone and nitrogen oxides between a tropical rain forest ecosystem and the atmosphere during the wet and the dry season, respectively.

Ozone deposition was determined by eddy covariance measurements above the canopy. The data obtained during the end of the regional wet season confirm the results of the only previous study reporting on directly measured O_3 fluxes above the Amazonian rain forest. Mean daytime maxima of -11.0 nmol m^{-2} s^{-1} and 2.3 cm s^{-1} for ozone flux and deposition velocity, respectively, show the rain forest to be an effective sink for ozone during the wet season. At the end of the dry season, under conditions of high atmospheric humidity deficit, the ozone uptake by the forest canopy was significantly reduced. A consequence of this strongly reduced uptake was a substantial in-canopy O_3 storage during day, which was removed in the first half of the night, by considerable non-stomatal deposition and chemical destruction.

Ozone deposition was simultaneously determined at an old pasture site which was deforested 22 years before the LBA-EUSTACH experiment. The measurements at this site showed an ozone deposition velocity ~35% and ~25% lower than the rain forest values for the end of the wet and dry season, respectively. Since cattle pastures represent the largest part of converted forest land in Rondônia, this difference may represent the effect of deforestation on the regional O_3 surface sink. Based on land cover information provided by LANDSAT images, the current regional O_3 deposition average for central Rondônia was estimated to be ~85% of the original sink provided by the native rain forest cover.

NO soil emissions were determined by an eddy covariance system which was positioned within the trunk space. Nighttime measurements resulted in mean values from 3.5 ng N m^{-2} s^{-1} to 4.8 ng N m^{-2} s^{-1}, in good agreement with emission fluxes obtained by concomitant dynamic soil chamber measurements.

A further aim of the experiment was to characterize the turbulence structure throughout the canopy during two intensive measuring periods. Detailed analysis of high frequency time series of several scalar quantities above and within the canopy revealed, during daytime, the frequent appearance of ramp pattern, the “finger print” of coherent turbulent structures. This enabled (i) to estimate a mean residence time of air within the part of the canopy which is directly coupled to the atmosphere above by these short, extreme, exchange events, and (ii) to determine ozone fluxes by a surface renewal model based on coherent air motion.

To assess the relevance of in-canopy processes as turbulent transport, uptake by vegetation, soil deposition, and chemical reactions to the ecosystem exchange of ozone and nitrogen oxides, their characteristic time scales where analyzed.

For the first time NO_2 profiles were measured within a tropical rain forest. By combining these results with all available wet season data on leaf level exchange in a stationary budget approach, a reduction of soil-emitted NO_x by vegetation up to 25% was obtained. This value is considerably smaller than that obtained by previous model studies. Direct comparison to the NO_x budget of the old cattle pasture indicated the primary rain forest ecosystem to be a higher NO_x source, and suggests therefore, that deforestation is reducing the biogenic NO_x emission in southwest Amazonia on a long term basis, if no fertilizer is used.

Zusammenfassung

Der Amazonische Regenwald wird zunehmend durch Abholzung und Brandrodung reduziert. Die damit verbundene Landnutzungsänderung hin zu weide- und landwirtschaftlich genutzten Flächen, verändert auch nachhaltig den atmosphärischen Eintrag und die Deposition troposphärenchemisch relevanter Substanzen wie Ozon (O_3) und Stickoxiden (NO_x). Zur Bewertung der Auswirkungen von Landnutzungsänderung auf atmosphärenchemische Prozesse ist eine möglichst genaue Kenntnis des Austausches dieser Spurengase zwischen dem primären Regenwaldsystem und der Atmosphäre notwendig. Bisher gibt es kaum Messungen zum Austauschverhalten tropischer Regenwald-ökosysteme bezüglich O_3 und NO_x - weder auf Bestands- noch auf Blattniveau. Im Rahmen des LBA-EUSTACH Projektes wurden 1999, während der Regen- und der Trockenzeit im Südwesten Amazoniens, im Staat Rondônia, Feldexperimente zur Bestimmung des Austausches von Ozon und Stickoxiden zwischen einem tropischen Regenwaldökosystem und der Atmosphäre durchgeführt.

Die Ozondeposition wurde durch Eddy-Kovarianzmessungen über dem Bestand bestimmt. Die Ergebnisse der Messungen, die am Ende der regionalen Regenzeit stattfanden, bestätigen die einzigen, zuvor über dem Amazonischen Regenwald durchgeführten, direkten Ozonflussmessungen. Die mittleren Tagesmaxima des Ozonflusses und der Depositionsgeschwindigkeit von -11.0 nmol m^{-2} s^{-1} bzw. 2.3 cm s^{-1} zeigen, dass der Wald während dieser Periode eine sehr effektive Ozonsenke darstellt. In der Endphase der Trockenzeit, unter Bedingungen mit hohem atmosphärischen Luftfeuchtedefizit, war die Ozonaufnahme durch den Waldbestand während des Tages drastisch reduziert. Als Folge der verringerten Aufnahmefähigkeit trat während des Tages eine beachtliche Ozonspeicherung innerhalb des Bestandes auf, die während der ersten Nachthälfte durch nicht-stomatäre Deposition und chemische Prozesse wieder abgebaut wurde.

Parallel wurde die O_3 Deposition über einer 22 Jahre zuvor gerodeten Weidenfläche bestimmt. Die Messungen dort ergaben eine, im Vergleich zum Regenwald um ~35% bzw. ~25% geringere Depositionsgeschwindigkeit am Ende der Regen- bzw. Trockenzeit. Da Viehweiden im Staat Rondônia den größten Anteil der genutzten Rodungsflächen ausmachen, repräsentieren diese Verhältnisse wahrscheinlich in guter Näherung den Effekt der Abholzung auf die regionale Oberflächensenke von Ozon. Die Kombination der Ergebnisse mit Landnutzungsinformation aus LANDSAT-Satellitenbildern ergab, dass die gemittelte O_3 Deposition für Zentral-Rondônia aktuell ungefähr 85% der ursprünglichen Deposition bei vollständiger Oberflächenbedeckung durch Regenwald beträgt.

Bodenemissionen von NO wurden durch ein Eddy-Kovarianzmesssystem innerhalb des Stammraumes bestimmt. Für nächtliche Messungen ergaben sich, in guter Übereinstimung mit

Resultaten gleichzeitig durchgeführter Bodenkammermessungen, mittlere Werte zwischen 3.5 ng N m^{-2} s^{-1} und 4.8 ng N m^{-2} s^{-1}.

Ein Schwerpunkt der Experimente war es, während zwei Intensivmessphasen die Turbulenzstruktur innerhalb des Waldbestandes zu charakterisieren. Eine detaillierte Analyse der hochfrequenten Zeitreihen verschiedener Skalare über und im Bestand zeigte während des Tages ein häufiges Auftreten von Rampenmustern, einem Indiz für kohärente Turbulenzstrukturen. Dies ermöglichte tagsüber (a) die Bestimmung der mittleren Aufenthaltszeit der Luft in dem Teil des Bestandes, der durch diese kurzen, extremen Austauschereignisse direkt an die Atmosphäre darüber gekoppelt ist, und (b) die Anwendung eines auf kohärenter Luftbewegung basierenden Surface Renewal Modells zur Bestimmung des O_3 Flusses.

Um den Einfluss von Prozessen wie turbulentem Transport, Aufnahme durch die Vegetation, Bodendeposition und chemischen Reaktionen im Pflanzenbestand auf den Ökosystemaustausch von Ozon und Stickoxiden abzuschätzen, wurden deren charakteristische Zeitskalen analysiert.

Weiter wurden erstmalig NO_2 Profile in einem tropischen Regenwald gemessen. Durch die Kombination dieser Resultate mit den Daten aller, für die Regenzeit auf Blattniveau zur Verfügung stehenden Austauschmessungen, in einem stationären Budgetansatz, ergab sich eine Reduktion der Boden NO_x Emission durch die Vegetation von bis zu 25%. Dieser Wert ist wesentlich geringer als durch bisherige Modellrechnungen bestimmt. Im direkten Vergleich zur NO_x-Bilanz der relativ alten Viehweide, stellt der primäre Regenwald damit eine größere netto NO_x-Quelle dar, was darauf hindeutet, dass auf lange Sicht, ohne den Einsatz von Dünger, die biogene Emission von NO_x durch Abholzung des tropischen Regenwaldes in Südwest-Amazonien reduziert wird.

List of Manuscripts

The present cumulative thesis consists of five manuscripts. One manuscript has been publisched. Four manuscripts are in the submission process currently.

Printed Manuscript

Rummel, U., C. Ammann, A. Gut, F.X. Meixner, and M.O. Andreae, Eddy covariance measurements of nitric oxide flux within an Amazonian rainforest, *Journal of Geophysical Research*, *107(D20)*, 8050, doi:10.1029/2001JD000520, 2002 (Appendix C)

Manuscripts for Submission

Rummel, U., C. Ammann, G.A. Kirkman, M.A.L. Moura, S. Rottenberger, U. Kuhn, J. Kesselmeier, T. Foken, M.O. Andreae, and F.X. Meixner, Seasonal ozone deposition to a tropical rain forest in southwest Amazonia, for submission in *Agricultural and Forest Meteorology*, 2005 (Appendix B).

Rummel, U., C. Ammann, T. Foken, and F.X. Meixner, Characterization of turbulent air motion within and above a tropical rain forest in Amazonia,, for submission in *Boundary-Layer Meteorology*, 2005b (Appendix D)

Rummel, U., C. Ammann, T. Foken, M.O. Andreae, and F.X. Meixner, Application of a surface renewal model for the determination of heat, carbon dioxide, and ozone fluxes from a tropical rain forest in Amazonia, for submission in *Atmos. Chem. Phys*, 2005c (Appendix E)

Rummel, U., C. Ammann, M.O. Andreae, and F.X. Meixner, Wet season NO_x exchange between an Amazonian rain forest and the atmosphere-implication from time scale analysis, for submission in *Atmospheric Environment*, 2005d (Appendix F)

Acknowledgement

I would like to thank my “doctorfather” Prof. Thomas Foken for accepting to be the examiner of this thesis, for his interest in the scientific subject, and for his constructive contributions in several discussions.

I am especially indebted to Prof. Franz Meixner who initiated and supervised this work. He offered me the opportunity to work in an international and interdisciplinary environment with a high degree of independence. I much appreciate his enthusiasm, encouragement, support and friendship.

Special thanks go to my friend and former colleague Dr. Christof Ammann (Air Pollution Climate group (TP 11.3) FAL-Reckenholz, P.O.Box, CH-8046 Zürich, Switzerland). For the great teamwork in the rain forest and many fruitful discussions back in Europe. I profited a lot from his micro-meteorological expertise.

I would like to thank the other co-authors and colleges for their important contributions to the manuscripts: Drs. Grant Kirkman, Andreas Gut, Stefanie Rottenberger, Uwe Kuhn, Jürgen Kesselmeier, Meinrat. O. Andreae (Max Planck Institute for Chemistry in Mainz), Marcos A. L. Moura (Departamento de Meteorologia, Centro de Ciencia Exatas e Naturais, Universidade Federal de Alagoas, Maceió Alagoas, Brazil).

Thanks also to Prof. Günter Helas (Max Planck Institute for Chemistry in Mainz) for his support and to my other former and present colleges from the Max Planck Institute for Chemistry in Mainz. Especially the LBA-EUSTACH crew is gratefully acknowledged: Drs. Pascal Guyon, Greg Roberts, Jens Beck, Saskia van Dijk, Bim Graham as well as Günter Schebeske, Michael Welling, Annette Solf, Ulrich Renk, Monika Scheibe, and Jörn von Jouanne. I really enjoyed the cooperative and pleasant atmosphere at the IBAMA camp in Jaru.

I am greatful to the staff at INCRA (Instituto Nacional de Colonização e Reforma Agrária), especially Jaõ Luis Esteves, Eduardo Conceição, and Claudionor Rodrigues. Further, to Carlos Brãndao and the staff of IBAMA (Instituto Brasileiro do Meio Ambiente e dos Recursos Naturais Renováveis) in Ji-Parana, to Beatriz E. Gomes and Wesley Saores (Universidade Federal de Rondonia, Ji Parana) and to Sr. Afonso Pereira de Andrade the owner of the Fazenda Nossa Senhora Aparecida.

Contents

Synthesis

1 Introduction

1.1 Tropical Deforestation

Today 3869 million ha, which is about 30% of the earth's land surface is covered by forests [*FAO*, 2001]. Compared to an estimated 50% coverage 8000 years ago [e.g. *Ball*, 2001] a remarkable decrease of forested area took place. Although forest extent is on a long-term basis coupled to climatic variations, the reduction is especially in the last centuries mainly a consequence of anthropogenic land conversion. Just in the relative short time period from 1850 to 1990 the global forest cover was reduced by approximately 20% [*Houghton*, 1999].

Historically, the extent of deforestation was much larger in temperate regions than in the tropics. Growing population entailed by rapidly increasing food demand, was one of the main driving forces for development and cultivation of large forest areas, when the economy of today's industrialized countries was dominated by agriculture. In recent decades, deforestation has been extremely high in the tropics. While in non-tropical areas the global forest cover between 1990 and 2000 was increasing by 2.9 million ha/year due to reforestation programs and sustainable forestry practice, the tropical forest area was reduced by -12.3 million ha/year during this time period [*FAO*, 2001].

The worlds largest area of tropical forest with 851 million ha can be found in South America where the rain forest of the Amazon Basin contributes most of it. To illustrate the vast spatial dimension of the Amazon Basin it is shown in Figure 1 together with western and parts of central Europe. About 75% of the south American rain forest area belongs to Brazil, where rubber exploitation at the beginning of the twentieth century initiated serious deforestation activities. Cattle ranching on large scale and exploration of oil and other mineral resources were also driving forces for development of forested areas in the Amazon region. After construction of main access roads like 1965 the BR364 in the Brazilian state of Rondônia, the forest clearing process was further accelerated by governmental-induced colonization programs. The rapid progressing deforestation from 1978 to 1999 is documented in Figure 2 by a LANDSAT image chrono-sequence of a ~26500 km^2 large area in northwest Rondônia [*Roberts et al.*, 2002]. Over this time period a typical fishbone like pattern of pastures, agricultural fields, and forest patches is replacing the primary rain forest, spreading out from the BR364. The average deforestation rate in central Rondônia increased between 1990 and 1999 from ~1.2% per year to ~3.4% per year [*Roberts et al.*, 2002].

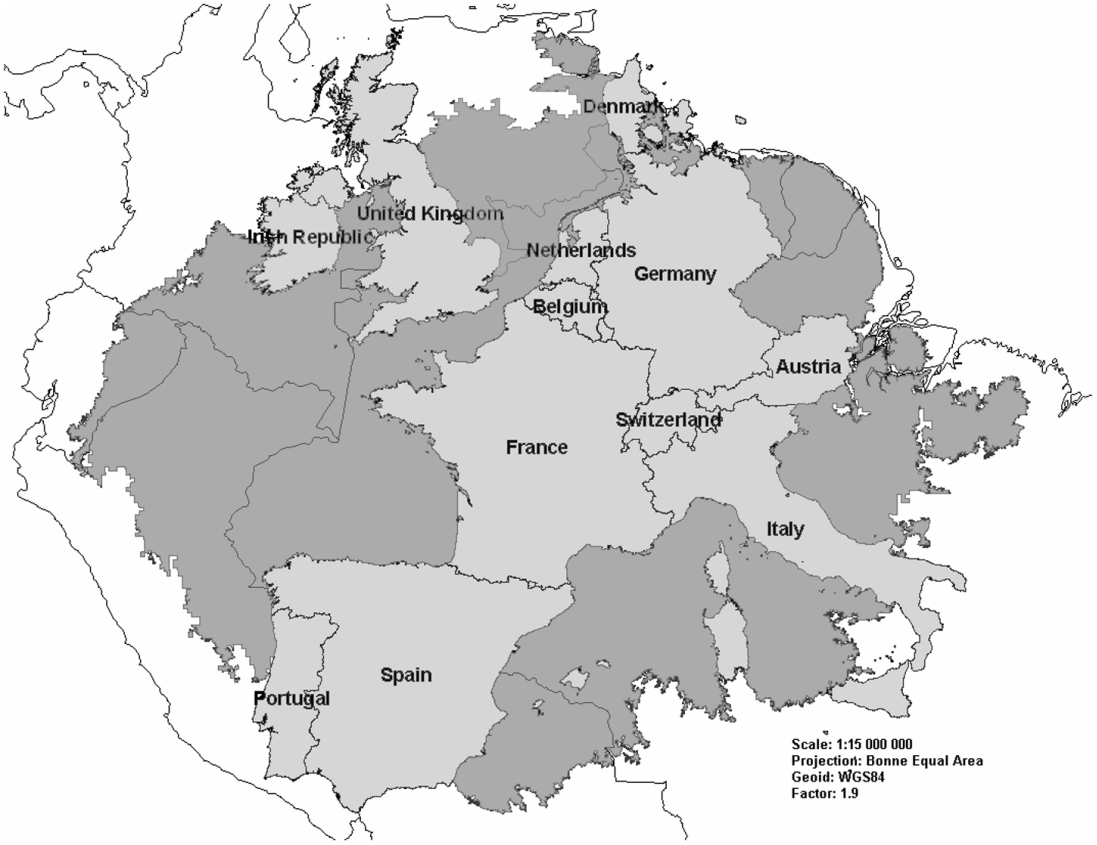

Figure 1: *The spatial dimension of the Amazon Basin (dark gray) compared to western and parts of central Europe (light gray).*

In view of the ambitious development program for Brazilian Amazonia described in the "Avanca Brasil" (Forward Brazil) no change in trend is likely in the near future. The program intends massive infrastructure measures like road paving, river channelling, port improvements, and expansion of energy production to the value of 45 billion US$ until 2009 [*Carvalho et al.*, 2001].

Since the large rain forests play an important role in the ecologic balance of the tropics deforestation is expected to have far reaching effects in many environmental respects. The high biodiversity with complex plant-animal interaction of the Amazonian forest makes this system susceptible for disturbance. Deforestation was found to influence the local climate by altering physical surface characteristics, e.g. increasing surface albedo, decreasing net surface radiation and roughness length, which seems to result in a reduction of evapotranspiration and precipitation in several numerical simulations [see *Werth and Avissar*, 2002].

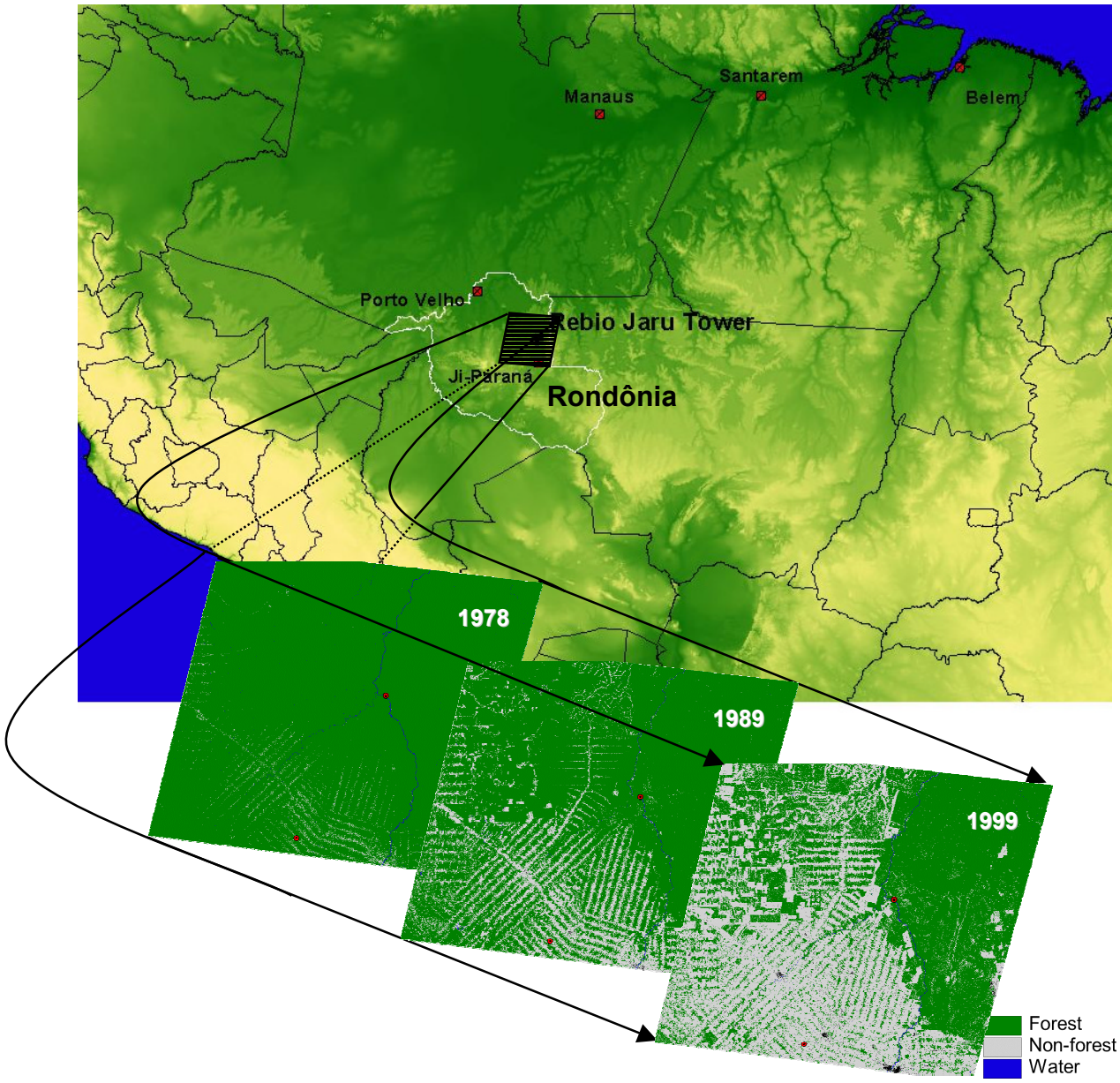

Figure 2: *LANDSAT (Multispectral Scanner: MSS and Thermic Mapper: TM) land cover chrono-sequence of northwest Rondônia [Roberts et al., 2002], which illustrates the deforestation progress in southwest Amazonia. The area of the shown section is ~26500 km^2.*

Due to the large biomass of the Amazon forest (Brazil alone holds 27% of the global above ground woody biomass [*FAO*, 2001]), it plays an important role in the global carbon cycle, in terms of both carbon turnover and storage [e.g. *Houghton et al.*, 1998]. Therefore tropical deforestation, especially slash and burn practice, is a considerable contribution to the anthropogenic emission of the principal greenhouse gas carbon dioxide CO_2.

Further, the surface exchange of reactive trace gases like ozone O_3 and its photochemical precursor constituents nitrogen oxides NO_x ($NO+NO_2$) and hydrocarbons may be significantly changed by deforestation and therefore strongly affect the O_3 budget in the tropical troposphere.

1.2 O_3 Chemistry

The highly reactive trace species O_3, which is quantitatively an atmospheric impurity, is of supreme importance for (i) the atmosphere's chemical composition and (ii) the biosphere, influencing life on Earth in several respects.

About 90% of O_3 is present in the stratosphere. In this layer it is produced by photodissociation of molecular O_2:

$$O_2 + h\upsilon\ (\lambda \le 240\,nm) \longrightarrow O + O \tag{1}$$

$$2\left(O + O_2 + M \longrightarrow O_3 + M\right) \tag{2}$$

$$Net: \quad 3O_2 + h\upsilon \longrightarrow 2O_3 \tag{3}$$

Here M is e.g. an air molecule that carries of excess energy and $h\upsilon$ is the product of the Planck constant and the frequency of radiation at wavelength λ. The stratospheric layer of maximum O_3 mixing ratios between about 20 km and 60 km height is mainly responsible for the absorption of UV radiation with wavelengths between ~200 nm and 320 nm (Hartley band of O_3, see (4)), and therefore protecting the biosphere from harmful radiation.

Compared with the stratosphere, O_3 mixing ratios in the troposphere are relatively small (10% only) but are of fundamental relevance for many environmental issues, particularly in that layer. Tropospheric O_3 is the third most important greenhouse gas after CO_2 and CH_4 [e.g. *Portmann et al.*, 1997; *IPCC*, 2001], providing the third largest increase in direct radiative forcing since the pre-industrial era. Because O_3 is highly phytotoxic (e.g. causing significant reduction of agricultural productivity [*Heck et al.*, 1984]) and detrimental to human health [*McKee*, 1993], an increase in tropospheric O_3 mixing ratios would be of serious environmental concern. On the other hand, tropospheric O_3 has a strong influence on the chemical composition of the atmosphere, since it is a key precursor of the hydroxyl radical OH. The hydroxyl radical is in turn particularly important since it is the primary oxidant of the atmosphere and is responsible for the removal of constituents like methane CH_4, carbon monoxide CO, and many other organic substances which otherwise would be inert in the troposphere [*Levy*, 1971].

OH is generated through the photolysis of tropospheric O_3 at wavelengths shorter than 320 nm as follows:

$$O_3 + h\upsilon\ (\lambda \le 320\,nm) \longrightarrow O(^1D) + O_2 \quad (4)$$

$$O(^1D) + H_2O \longrightarrow 2OH \quad (5)$$

Although UV radiation is strongly attenuated in higher atmospheric regions, considerable amounts of electronically excited $O(^1D)$ atoms are produced in the troposphere by (4). While the majority of $O(^1D)$ is deactivated by collision with N_2 or O_2, a small portion has enough energy to react with H_2O to form OH by (5). The OH formation by O_3 photolysis is strongly favored by high UV intensities and water vapor concentrations why the oxidation of trace gases occurs mainly in the tropical troposphere [*Crutzen*, 1986].

The global annual mean tropospheric O_3 budget is controlled by downward transport of stratospheric O_3 (550 ± 300 Tg yr^{-1}), net in situ photochemistry (150 ± 300 Tg yr^{-1}), and surface deposition (700 ± 300 Tg yr^{-1}). The quantification of these terms is given by *Lelieveld and Dentener* [2000], based on a compilation of several 3D global chemistry-transport model estimates. The net in situ photochemistry is the difference of much larger production and loss terms, in the order of 3000 Tg yr^{-1} to 3500 Tg yr^{-1}. Due to a relative short tropospheric lifetime of O_3 and its precursor constituents, large regional differences can occur.

Tropospheric Ozone is formed by the photochemical oxidation of CO and hydrocarbons RH in the presence of nitrogen oxides NO_x ($NO + NO_2$) [e.g. *Crutzen*, 1979]. One generalized RH oxidation sequence is given by [*Chameides et al.*, 1992]:

$$RH + OH \longrightarrow R + H_2O \quad (6)$$

$$R + O_2 + M \longrightarrow RO_2 + M \quad (7)$$

$$RO_2 + NO \longrightarrow RO + NO_2 \quad (8)$$

$$RO + O_2 \longrightarrow HO_2 + RCHO \quad (9)$$

$$HO_2 + NO \longrightarrow OH + NO_2 \quad (10)$$

$$2\left(NO_2 + h\upsilon\ (\lambda \le 400\,nm) \longrightarrow NO + O\right) \quad (11)$$

$$2\left(O + O_2 + M \longrightarrow O_3 + M\right) \quad (12)$$

$$Net: \quad RH + 4O_2 + 2h\upsilon \longrightarrow RCHO + 2H_2O + 2O_3 \quad (13)$$

The initial reaction with OH leads to alkyl radicals R which quickly form peroxy radicals RO_2 through combination with O_2. If enough NO_x is available the peroxy radical reacts with NO, yielding NO_2 and a alkoxy radical RO. RO is also reacting with O_2, forming an aldehyde RCHO and HO_2. A

second NO_2 is produced by the oxidation of NO by H_2O. This NO_2 subsequently photodissociates ((11) and (12)), leading to net O_3 production. Additional O_3 can be produced from further photodissociation of RCHO.

As mentioned before, as a catalyst NO_x plays a key role in this reaction chain. Under low NO_x conditions reactions (14) and (15) are dominating, forming peroxides (ROOH, H_2O_2) [*Atkinson*, 2000]:

$$RO_2 + HO_2 \longrightarrow ROOH + O_2 \tag{14}$$

$$HO_2 + HO_2 \longrightarrow H_2O_2 + O_2 \tag{15}$$

As a consequence ozone consuming reactions like reaction (16) lead to a net O_3 reduction in the troposphere.

$$HO_2 + O_3 \longrightarrow OH + 2O_2 \tag{16}$$

The dependence of O_3 evolution on NO_x and hydrocarbon mixing ratios is depicted in Figure 3, as a result from a simplified photochemical box model according to *Chameides et al.* [1992]. This study shows a clear difference in the O_3 evolution between a polluted urban area and remote pristine sites like the marine boundary layer and the tropical rain forest. Whereas the high O_3 generation in the urban areas with sufficient NO_x is primarily controlled by the hydrocarbon reactivity (production rate of peroxy radicals), O_3 production at the remote sites is largely limited by the availability of NO_x. Although in tropical forest regions mixing ratios of reactive biogenic hydrocarbons (mainly isoprene) are high [e.g. *Zimmermann et al.*, 1988; *Kesselmeier et al.*, 2002; *Kuhn et al.*, 2002] the estimated O_3 production rates in these regions are not higher than in the marine boundary layer, where the O_3 formation is rather a consequence of background CO and CH_4 oxidation [*Crutzen et al.*, 1999].

In both cases, the NO_x mixing ratios are in the transition range from O_3 destruction to production regime (here ~30 ppt, representing the threshold between both regimes almost over three orders of magnitude of hydrocarbon mixing ratios), which illustrates the sensitivity of the background photochemistry to changes in NO_x emissions. But due to the abundance of highly reactive RHs, especially the tropical troposphere above rain forests has the potential to evolve into a regime of significant O_3 production in the case of increasing NO_x mixing ratios.

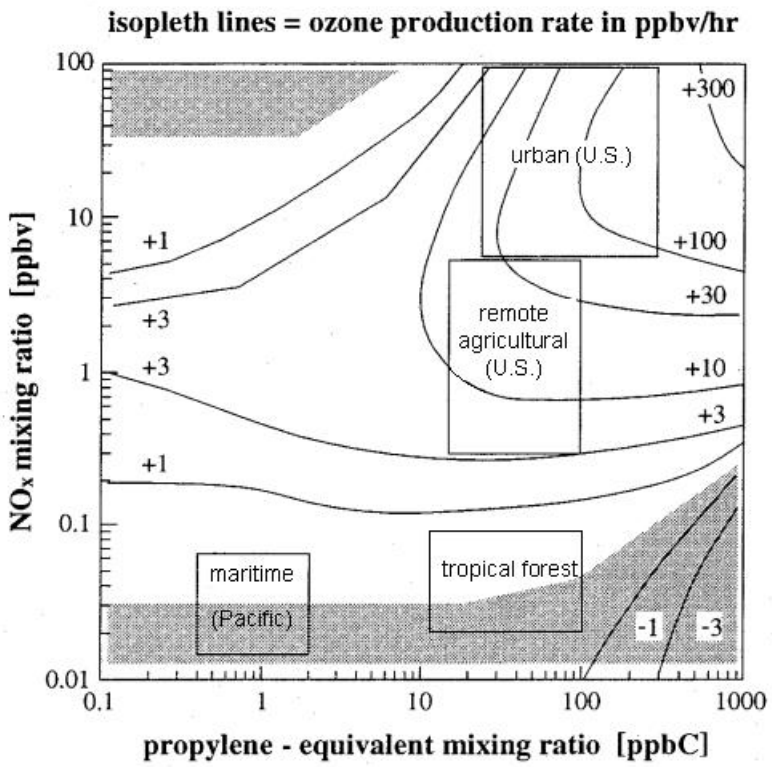

Figure 3: *Summary of non methane hydrocarbon / NO_x regimes and the corresponding ozone production / destruction rate after Chameides et al. [1992]. Non methane hydrocarbons are expressed in the reactivity-based scale propylene equivalent. Isopleth lines indicate the calculated (photochemical box model) net rates of ozone production / destruction at the corresponding mixing ratios. Shaded areas represent mixing ratio regions of net ozone destruction.*

1.3 Surface NO_x Exchange

A compilation of the mean global NO_x source estimates is listed in Table 1 [*IPCC*, 2001]. In total, anthropogenic emissions by fossil fuel combustion are the dominating NO_x sources, mainly concentrated in the industrial centers of the northern hemisphere. However, large parts of the globe may be still controlled by natural sources. Especially in remote continental areas, e.g. tropical rain forest regions, such as the Amazon Basin, the tropospheric NO_x budget, and therefore photochemical O_3 production, is also considerably influenced by biogenic emissions of NO from soils [*Jacob and Wofsy*, 1988; 1990].

Table 1: *Compilation of global tropospheric NO_x source estimates (Tg N yr^{-1}) [IPCC, 2001]* **.**

Reference:	[*Ehhalt*, 1999]	[*Holland et al.*, 1999]	[*Penner et al.*, 1999]	[*Lee et al.*, 1997]
Base year	~1985	~1985	1992	
Fossil fuel	21.0	20 - 24	21.0	22.0
Aircraft	0.45	0.23 - 0.6	0.5	0.85
Biomass burning	7.5	3 - 13	5 - 12	7.9
Soils	5.5	4 - 21	4 - 6	7.0
NH_3 oxidation	3.0	0.5 - 3	-	0.9
Lightning	7.0	3 - 13	3 - 5	5.0
Stratosphere	0.15	0.1 - 0.6	-	0.6
Total	**44.6**			**44.3**

The intense deforestation and burning activities in the Amazon basin affect the surface exchange of trace constituents in several ways. High amounts of NO_x are seasonally emitted by biomass burning during the dry season (typically June to October) affecting strongly the regional tropospheric chemistry [e.g. *Delany et al.*, 1985; *Andreae et al.*, 1988; *Crutzen and Andreae*, 1990].

Beside the NO_x emissions caused directly by the combustion processes, the deforestation and following land use change also affects the NO emissions of corresponding soils. The effect of forest-pasture conversion on soil NO emissions was found to be time-dependent [*Keller et al.*, 1993]. Whereas immediately after deforestation elevated NO emissions were registered [e.g. *Neff et al.*, 1995], they decrease below the original forest soil emissions at time scales of years [*Keller et al.*, 1993]. This stresses the necessity to consider age and land use history of pastures, to estimate the effect of deforestation on soil emission of a certain area [*Kirkman*, 2001]. Rain forest soil NO fluxes, measured in central and southwest Amazonia were found to be considerable with average values from 4 ng N $m^{-2}s^{-1}$ to 12 ng N $m^{-2}s^{-1}$ [*Kaplan et al.*, 1988; *Bakwin et al.*, 1990a; *Gut et al.*, 2002a].

To asses the net NO_x emission from a forest ecosystem, which is relevant to tropospheric chemistry, it is important to consider the impact of various processes within the vegetation layer on the NO emissions from soil. As illustrated in Figure 4, already in the canopy soil emitted NO can be oxidized to NO_2 by O_3 which is imported from aloft. The potential uptake of NO_2 by vegetation and soil surface is much faster than for NO. Together with largely attenuated short wave radiation within the forest, suppressing the photolysis of NO_2 back to NO, the original NO_x soil emission can be

considerably reduced on its way throughout the vegetation layer [*Jacob and Wofsy*, 1990; *Meixner*, 1994; *Ganzeveld et al.*, 2002a]. The efficiency of this reduction effect by the vegetation depends on the time scales of the interacting processes, namely turbulent transport, vegetation uptake, soil deposition, and chemistry. The vegetation influence is important for global soil NO_x emission estimates [e.g. *Yienger and Levy*, 1995; *Davidson and Kingerlee*, 1997; *Ganzeveld et al.*, 2002b], as well as for the assessment of the deforestation impact on regional NO_x input from ecosystems to the troposphere [*Kirkman*, 2001]. So far, most estimates and derived parameterizations, like the semi-empirical canopy reduction factor of *Yienger and Levy* [1995] are based on the model results of *Jakob and Wofsy* [1990] or directly on the experimental findings of the pioneering ABLE 2B (Atmospheric Boundary Layer Experiment) campaign performed during the 1987 wet season in central Amazonia [*Harriss et al.*, 1990]. *Jakob and Wofsy* [1990] calculated the original NO_x emission from forest soil to be reduced by ~75% and ~87% at the canopy top for day and night time situations, respectively. The substantial reduction they obtained was necessary to reconcile the experimental findings on NO soil emission [*Bakwin et al.*, 1990a] and NO_y mixing ratios (reactive oxides of Nitrogen: NO, NO_2, HNO_3, PAN, HNO_2, HNO_4, particulate nitrate, and alkyl nitrates) above the canopy [*Bakwin et al.*, 1990b]. However, a major drawback to their study is, that NO_2, which is an essential quantity to assess the vegetation reduction effect, was not available from their experimental data basis (ABLE 2B). Measured NO_2 mixing ratios are particularly helpful with regard to the potential bi-directionality of NO_2 leaf-air exchange associated with the existence of a compensation point (an ambient mixing ratio at which net NO_2 uptake by the plant changes to net emission).

Over the last twenty years, leaf level enclosure measurements on various plant species indicated the existence of a compensation point for NO_2 [e.g. *Johansson*, 1987; *Thoene et al.*, 1991; *Ludwig et al.*, 1992; *Rondon et al.*, 1993; *Rondon and Granat*, 1994; *Thoene et al.*, 1996; *Weber and Rennenberg*, 1996; *Sparks et al.*, 2001; *Hari et al.*, 2003]. Especially the results of *Sparks et al.* [2001], who found compensation points between 0.53 ppb and 1.6 ppb for 25 tropical tree species, underline a basic inconsistence between the findings of canopy and leaf scale investigations ("the NO_2 flux conundrum") as pointed out by *Lerdau et al.* [2000]. The ambient NO_2 mixing ratios of 0.04 ppb to 0.15 ppb postulated by *Jacob and Wofsy* [1990] in their model calculation for background conditions in central Amazonia were well below the compensation points found by enclosure measurements, suggesting rather an additional emission of NO_x by the tropical vegetation layer instead of the substantial uptake obtained with respect to the canopy scale measurements.

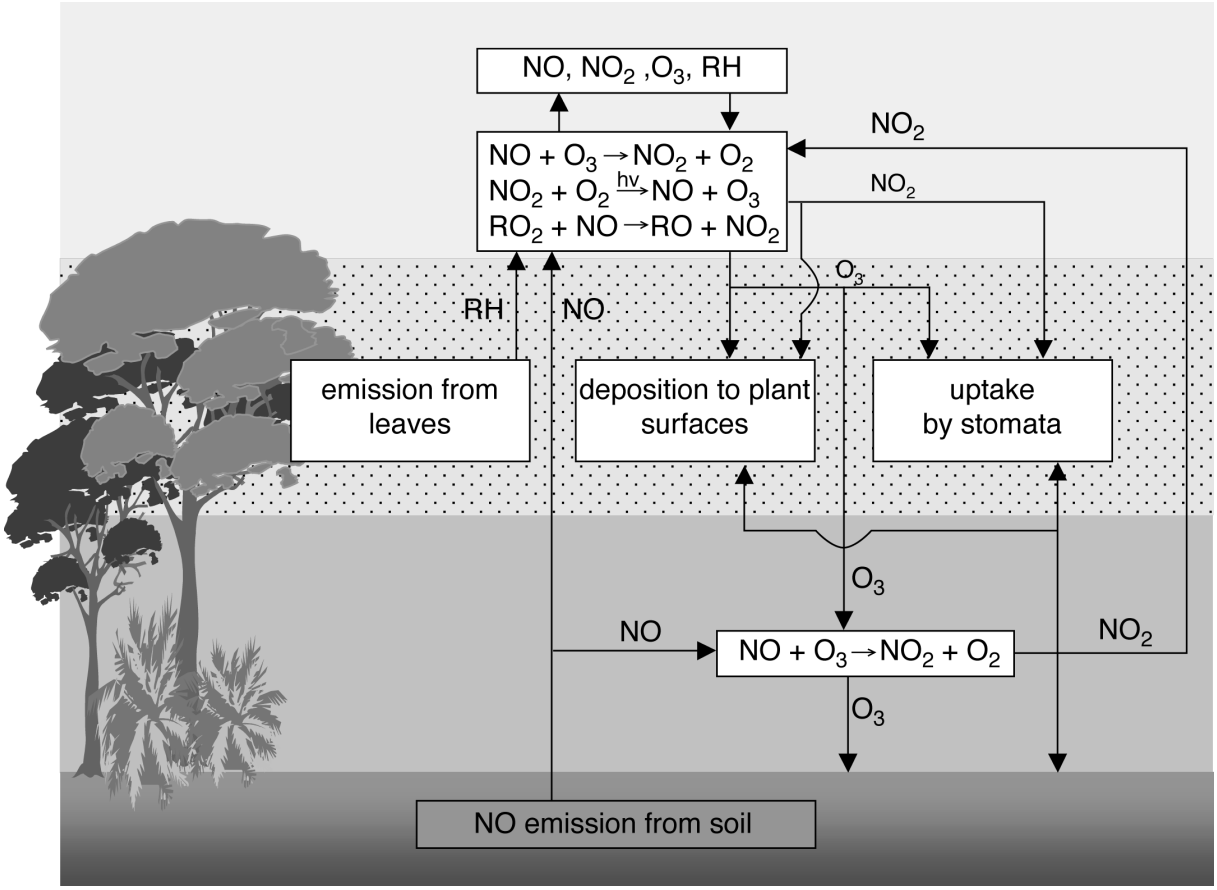

Figure 4: *Surface exchange and chemical processes influencing NO, NO_2, O_3 and RH (isoprene, terpenes) within and above a dense Forest. Modified after Coe et al. [1993].*

1.4 Turbulent Transport

Especially the atmospheric input of soil emitted reactive constituents like NO_x to the relative pristine environment of the remote forested tropical areas is largely dependent on the coupling of the vegetation layer to the atmosphere above. The way in which turbulent transport is established determines the temporal and spatial framework for all air-surface interactions and chemical reactions within and immediately above the canopy space.

Turbulent air motion within and above different plant canopies exhibits a number of similar peculiarities that distinguish it clearly from surface layer flows [see reviews of *Kaimal and Finnigan*, 1994; *Raupach et al.*, 1996; *Finnigan*, 2000]. Daytime turbulence throughout various vegetation layers was found to be dominated to a large extend by large-scale, spatially organized eddies (coherent turbulent structures) [cf. *Gao et al.*, 1989; *Raupach et al.*, 1989; *Paw U et al.*, 1992]. Their occurrence within a canopy is indicated by clearly skewed and kurtotic frequency distributions of wind

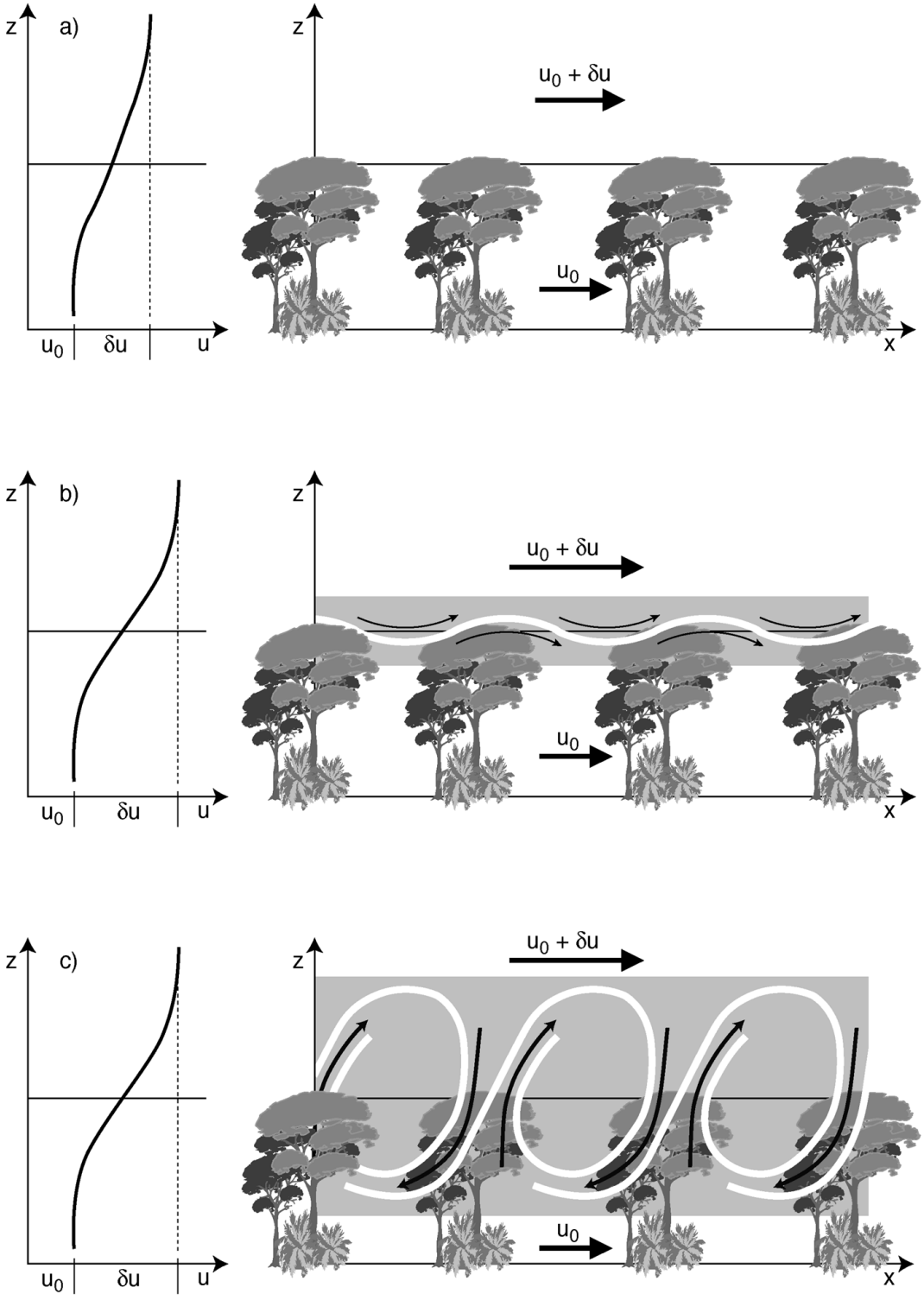

Figure 5: *Mixing layer of self-preserving coherent structures (emerging from Kelvin-Helmholtz instability at canopy height, initialized by a strongly inflected profile of horizontal flow velocity u. After Raupach et al. [1996] modified.*

speed components [e.g. *Baldocchi and Hutchison*, 1987; *Amiro and Davis*, 1988; 1990] as well as by distinct ramp pattern in high-frequency time series of scalar quantities [e.g. *Gao et al.*, 1989; *Paw U et al.*, 1992]. *Raupach et al.* [1996] proposed a mixing layer analogy that describes the universal canopy turbulence characteristics within and above vegetation rather than the traditional description as a perturbed boundary layer. They argued, that the air flow at the canopy-atmosphere interface resembles a plane mixing layer (a "boundary-free" shear flow, see e.g. *Ho and Huerre* [1984]) formed between two co-flowing fluid streams of different velocities (Figure 5 (a)). In both cases the corresponding mean longitudinal velocity profiles are inflected and inviscidly unstable to perturbations. It is believed that unstable modes, two-dimensional transverse Kelvin-Helmholtz waves (Figure 5 (b)), emerge at the canopy-atmosphere interface as the shear raises above a certain threshold level. Coherent structures (transverse vortices linked by braid regions of strained fluid) are formed through the "roll up" of the initial Kelvin-Helmholtz waves. Figure 5 (c) shows a schematic two-dimensional longitudinal section of these coherent structures (for a depiction of the three- dimensional flow which also exhibits the transverse structure evolution, see *Rogers and Moser* [1992] and *Finnigan* [2000]).

During daytime, the occurring coherent air motion is often dominating the transport of scalar quantities like heat and mass throughout the main part of the vegetation layer. Due to the relative large length scales of these transport relevant coherent structures, the flux of a constituent can be totally independent from its local gradient at the corresponding height (an extreme form of this effect are counter gradient fluxes [c.f. *Demnead and Bradley*, 1985]). Furthermore, the turbulent transport within the vegetation is highly intermittent, with short intense exchange events renewing the air within the canopy [e.g. *Coppin et al.*, 1986; *Gao et al.*, 1989; *Lee and Black*, 1993], separated by rather quiescent periods. During these interim periods turbulent mixing occurs on much smaller scales, restricting the heat and mass exchange between the vegetation layer and the atmosphere above.

Most experimentally obtained knowledge about forest canopy turbulence originates from wind tunnel investigations and field studies at temperate and boreal vegetation [for reviews see *Kaimal and Finnigan*, 1994; *Raupach et al.*, 1996; *Finnigan*, 2000]. Investigations which were focusing on turbulence characteristics of tropical rain forest canopies are scarce [*Fitzjarrald et al.*, 1988; *Pinker and Holland*, 1988; *Fitzjarrald and Moore*, 1990; *Fitzjarrald et al.*, 1990; *Kruijt et al.*, 2000]. It seems, that the specific architecture of rain forests with high leaf area index and huge canopy space together with the environmental conditions in the tropics, characterized by high humidity and radiative input during daytime, restrict a direct coupling of forest and atmosphere to the upper part of the vegetation layer. A point which raises the question, whether this is a principle characteristic of dense tropical forests, since the penetration depth of coherent turbulent structures is of great relevance to the net ecosystem export of biogenic NO_x (as well as e. g. for CO_2 and hydrocarbons). The penetration

depth is the height, down to which O_3 from the boundary layer is effectively transported and therefore where NO_2 is mainly formed by the reaction of O_3 with soil emitted NO. Consequently the penetration depth of O_3 defines the vegetation layer in which deposition of NO_2 is mainly occurring. In this layer, the timeframe of both processes, chemical transformation and surface deposition, is closely connected to the duration of quiescent periods between consecutive exchange events.

1.5 Dry Deposition of O_3 in the Tropics

In the tropics, the annual cycle of tropospheric ozone caused by the natural seasonality of atmospheric and surface conditions is affected by the coincidence of anthropogenic biomass burning activities with the dry season [e.g. *Crutzen et al.*, 1985; *Delany et al.*, 1985; *Logan and Kirchhoff*, 1986; *Kirchhoff et al.*, 1988 ; *Kirchhoff et al.*, 1990]. Here, O_3 mixing ratios of 50 to 100 ppb are frequently reached at altitudes between 1 km and 4 km, in haze layers which are partly of large horizontal extend [*Andreae et al.*, 1988; *Cros et al.*, 1988]. In the vicinity of burning areas of the Brazilian cerrado (savanna) even at the surface O_3 mixing ratios up to 80 ppb were found by *Kirchhoff et al.* [1996].

In remote areas of the tropics, without the influence of biomass burning, the seasonal variation of O_3 in the lower troposphere is mainly a consequence of varying exchange with higher atmospheric regions and terrestrial surfaces. During the wet season convective systems enhance the O_3 entrainment from the free troposphere and the stratosphere to the boundary layer [*Browell et al.*, 1990; *Jacob and Wofsy*, 1990]. Contrastingly, in the dry season O_3 input from aloft is rather small [*Jacob and Wofsy*, 1988] due to formation of the trade wind inversion by large scale subsiding air motion.

The surface exchange of O_3 and its precursors CO, hydrocarbons, and especially NO_x (Section 1.3) is crucial for the "natural" photochemical gain or loss of tropospheric O_3 (Section 1.2). Generally, dry deposition of O_3 was found to be the most important sink in the ozone budget of the lower troposphere. However, even for the rainforest, the main tropical biome, just a few experimentally derived estimates of the O_3 dry deposition exist up to now. For the dry season most of known estimates are rather crude, resulting from atmospheric boundary layer (ABL) or surface layer (SL) budget estimates, which base on a few vertical profiles of O_3 mixing ratio in the northern Congo [*Andreae et al.*, 1992; *Cros et al.*, 1992] and in the central Amazon [e.g. *Gregory et al.*, 1988; *Kirchhoff et al.*, 1988]. Recently, direct flux measurements applying an airborne eddy covariance system over northern Congo were made by *Cros et al*. [2000]. All these experiments have been performed in the corresponding dry season. However, they have indicated the importance of the tropical forest as an ozone sink and provided valuable flux information on a regional scale, by integrating large source areas. Due to their integral character, these measurements provide almost no information about the diel course of the O_3 flux. Tower based flux measurements with high temporal

resolution enable the investigation of those mechanisms which regulate the surface deposition of O_3. So far, there is only the wet season experiment (ABLE 2B) in the central Amazon, where tower based eddy covariance measurements of O_3 flux above a tropical rain forest have been performed for a 17 day period [*Fan et al.*, 1990].

Since ozone deposition is largely controlled by plant physiological mechanisms deforestation and changes in land use are expected to result in corresponding changes of ozone deposition. *Sigler et al.* [2002] made a first attempt to address this topic experimentally for wet season conditions by comparing their O_3 flux estimates from a cattle ranch (1999) in south west Amazonia with those O_3 flux data of *Fan et al.* [1990] which have been obtained 12 years before in the central part of the Amazon Basin. Their findings wait for verification, and for extension to dry season conditions in order to estimate the deforestation effect for the whole year.

2 Objectives of the Thesis

This study was embedded in the LBA-EUSTACH program (*European Studies on Trace gases and Atmospheric Chemistry as a contribution to the Large-scale Biosphere-Atmosphere experiment in Amazonia*). LBA-EUSTACH is an European contribution to the LBA project, an international research initiative designed to investigate the climatological, biogeochemical, ecological and hydrological functioning of Amazonia, and the impact of land use change on these functions.

The primary objective of the present work was to investigate the vegetation-atmosphere exchange of ozone and nitrogen oxides of a primary tropical rain forest. It was motivated by the scarcity of experimental information on that topic from one of the planet's largest forest ecosystems.

Two experiments were carried out to obtain information about the seasonal variation of O_3 deposition by eddy covariance measurements [*Rummel et al.*, 2005a]. Of particular interest was the behavior of the ecosystem under biomass-burning influenced dry season conditions. Comparison to simultaneously performed O_3 deposition measurements from a 22 years old cattle pasture [*Kirkman et al.*, 2002] were made to quantify the effect of deforestation on O_3 surface deposition.

Sub-canopy eddy covariance measurements of nitric oxide flux were performed at different heights [*Rummel et al.*, 2002] to determine the mean forest soil NO emissions, independently from a dynamic chamber measurement system [*Gut et al.*, 2002a] and to investigate its vertical evolution within the rain forest.

Besides the quantification of integral ecosystem fluxes, special emphasize was put on the characterization of turbulent transport mechanisms throughout the forest. One aim was to determine the vertical extent of the vegetation layer, which is typically coupled to the atmosphere above [*Rummel et al.*, 2005b].

Further to determine average residence times of air within the rain forest [*Rummel et al.*, 2005c] in order to evaluate the dominating canopy processes by comparison to characteristic time scales of chemistry and uptake processes [*Rummel et al.*, 2005d].

A final objective of this study was to discuss a potential reduction of NO_x emissions through the vegetation on the basis of a budget approach, which is closely coupled to the measured NO_2 mixing ratio profiles [*Rummel et al.*, 2005d].

3 Experiment

3.1 Investigation Periods and Sites

The LBA-EUSTACH trace gas measurements were performed in two experiments in 1999. The first experiment (LBA-EUSTACH 1) took place during the wet-to-dry season transition in April/May, the second one (LBA-EUSTACH 2) in September/October during the reverse transition from dry-to-wet season. The experimental site is located in the Reserva Biológica Jarú (RBJ), a forest reserve 90 km north of the city Ji-Paraná in the state of Rondônia (southwest Amazonia), Brazil (see Figure 2). The vegetation cover of RBJ, owned by the Brazilian Environmental Protection Agency IBAMA (Instituto Brasileiro de Meio Ambiente e Recursos Renováveis), is a primary (terra firme) open rain forest with a closed canopy of about 32 m height. Single jutting trees reach heights up to 45 m. The understory consists mainly of palms (for a more detailed site description see e.g. *Rummel at al.* [2005a]).

Temporarily the IBAMA camp site, which is located 7 km south-southwest of the RBJ rain forest tower was used to determine O_3 deposition at leaf scale of a deciduous canopy tree. This permanent control post of IBAMA in the reserve is within a 1 km^2 patch of secondary forest (for a description see *Kuhn et al.* [2002] and *Rottenberger et al.* [2004]).

To assess the effect of deforestation and land cultivation on the surface exchange of the investigated trace gases, an additional measuring site was simultaneously operated at a commercial cattle ranch [see *Kirkman et al.*, 2002], named Fazenda Nossa Senhora Aparecida (FNS). This pasture, is about 45 km west-northwest of Ji-Paraná.

3.2 Measurements

The main platform for the micrometeorological and trace gas measurements was a scaffolding tower of 52 m height erected in 1991 [*Gash et al.*, 1996].

O_3 fluxes above the forest analyzed in *Rummel at al.* [2005a] were measured by a eddy covariance system at 53 m height, combining a three-dimensional sonic anemometer and a fast closed path chemi-

luminescence O_3 analyzer [*Güsten et al.*, 1992]. To measure O_3 deposition at leaf scale an dynamic (flow-through) branch cuvette system [see *Kuhn et al.*, 2002; *Rottenberger et al.*, 2004] was used together with a UV absorption O_3 sensor.

Sub-canopy NO fluxes in *Rummel at al.* [2002] were also measured by the eddy covariance method 11 m and 1 m above the forest floor. Sonic anemometers at both heights were sequentially combined with a NO chemiluminescence analyser for ten-day periods each. NO soil emission was determined by a dynamic chamber system operated 50 m north of the main tower. For details about the chamber system see *Gut et al*. [2002a].

In order to characterize turbulent transport mechanisms within and above the canopy in *Rummel at al.* [2005b], during temporally limited periods a third sonic anemometer was operated simultaneously to those at 53 m and 11 m height. It was alternately mounted at 42 m, 31 m, 20 m, and 1 m above the forest floor to derive mean profiles of single-point turbulence statistics.

The surface renewal approach in *Rummel at al.* [2005c] was in addition to O_3 and temperature T, also applied on high-frequency time series of H_2O and CO_2. These were measured by a closed-path differential infrared absorption analyzer at 53 m height.

Vertical profiles of O_3, NO, and NO_2 mixing ratios the basis of the budget approach in *Rummel at al.* [2005d] were measured above and throughout the forest canopy. The air sampling system consisted of eight TEFLON® tubes connecting the inlets at 0.3 m, 1.0 m, 4.0 m, 11.3 m, 20.5 m, 31.3 m, 42.2 m, and 51.7 m to a UV absorption O_3 analyzer, a gas phase chemiluminescence NO analyzer, and a photolytic NO_2 converter in the shelter at the tower base.

All Inlets at heights up to 4 m above ground were attached to a separate tripod located 15 m northeast of the main tower, where the surrounding area was closed off to minimize soil disturbance.

For short time periods the NO_2 photolysis frequency j_{NO2} was measured by a selective radiation sensor sequentially above and within the forest canopy at 51.7 m, 22 m, and 1 m height.

A detailed description of the experimental setup, the named measurements, as well as of additional supporting meteorological measurements is given e.g. in *Rummel et al.* [2005a].

4 Results and Discussion

4.1 Dry Deposition of O_3

4.1.1 Primary Rain Forest

In *Rummel et al.* [2005a], surface deposition, the main sink for tropospheric ozone was determined at different time and spatial scales. Tower based eddy covariance flux and mixing ratio profile measurements at the rain forest site, complemented by leaf level information form branch cuvette measurements revealed new information about seasonal and diel behavior of O_3 deposition to that tropical ecosystem type.

The eddy covariance measurements at the end of the wet season (LBA-EUSTACH 1) showed the tropical rain forest in the south western part of the Amazon basin to be an effective O_3 sink (Figure 6 (a)). Magnitude and diel variation of O_3 flux and deposition velocity (mean daytime maxima: -11.0 nmol m^{-2} s^{-1} and 2.3 cm s^{-1}) are comparable to the wet season O_3 deposition found for a tropical rain forest in central Amazonia by *Fan et al.* [1990].

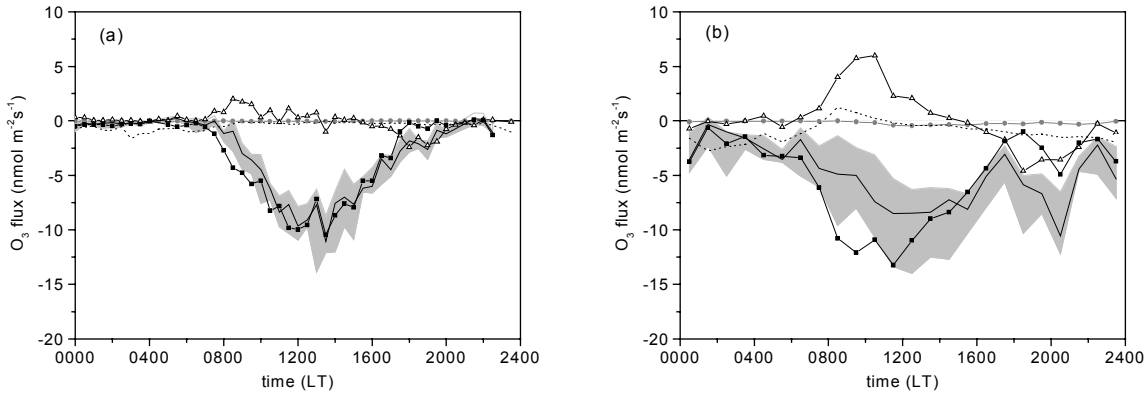

Figure 6: *Diel variation of mean (median) O_3 budget components for LBA-EUSTACH 1 (a) and LBA-EUSTACH 2 (b): O_3 flux measured at 53 m (black squares), O_3 storage within the column 0-53 m (open triangles), net "chemical" flux (chemical reactions of the NO-NO_2-O_3 triad: black dotted line), O_3 flux at the forest soil surface (gray circles), and O_3 flux corrected for storage (black line; gray area indicates its inter quartile range). Figure taken from Rummel et al. [2005a]*

The results of LBA-EUSTACH 2 provide the very first information about the diel course of O_3 deposition to a tropical rain forest under dry season conditions, partly influenced by substantial

biomass burning activities (Figure 6 (b)). In contrast to the regional scale information from former integral boundary layer budget estimates from central Amazonia, e.g. by *Gregory et al.* [1988], the tower based eddy covariance measurements enabled the investigation of mechanisms which regulate surface deposition of O_3. The results indicate, that the daytime O_3 deposition to the forest at the end of the local dry season was influenced by specific humidity deficit *SHD* and consequently controlled by stomatal aperture. Days characterized by moderate *SHD* values showed rather higher daytime O_3 fluxes than those days with extreme specific humidity deficits, although systematically higher O_3 mixing ratios occurred during the latter period. Therefore, the concurrence of high specific humidity deficits and O_3 mixing ratios partly up to 80 ppb above the canopy might be also caused by the limited daytime O_3 uptake of the forest (under extremely dry conditions), beside enhanced atmospheric O_3 production as a consequence of biomass burning.

The consequence of the strongly reduced uptake during the dry periods of LBA-EUSTACH 2 was a substantial in-canopy O_3 storage during day (Figure 6 (b)). The stored O_3 was finally removed in the first half of the night by considerable non-stomatal deposition, i.e. to vegetation surfaces like leaf cuticle and bark.

The occurrence of cuticular O_3 deposition was supported by branch cuvette measurements at a tropical deciduous tree species (*Hymenaea courbaril* L.) from the nearby IBAMA camp site. But the inferred mean cuticula resistance for O_3 of ~ 4000 s m^{-1} to 5000 s m^{-1}, derived through the application of a leaf resistance model according to *Baldocchi et al.* [1988], might be to high to explain the fast O_3 depletion after sunset solely by dry deposition on plant surfaces. This makes additional chemical sinks likely.

The second remarkable result is the almost identical relative diurnal course of the mean O_3 deposition to a branch of one tree species inferred from the cuvette measurements and the canopy scale O_3 flux obtained by the eddy covariance measurements. This clearly shows, that during daytime the O_3 deposition to the rain forest is dominated by the stomatal uptake of the crown species, which as a functional group are similar in their stomatal behavior [see *Roberts et al.*, 1990; 1993; *McWilliam et al.*, 1996].

4.1.2 The Impact of Deforestation

The O_3 fluxes obtained at the primary rain forest site (RBJ) [*Rummel et al.*, 2005a] were compared to O_3 deposition measurements simultaneously performed at the 22 years old cattle pasture (FNS) [*Kirkman et al.*, 2002]. The results showed a ~35% lower mean deposition velocity at FNS at the end of the wet season. At the end of the dry season the mean deposition velocity at the pasture site was

only ~25% lower compared to the forest. This smaller difference is mainly a consequence of enhanced canopy resistances at the forest as reaction on the high specific humidity deficits in the dry season.

Assuming both experiments to be representative for two equally long seasons (6 months each, which may be reasonable for Rondônia with respect to the monthly average *SHD* values [see *Culf et al.*, 1996]) after deforestation the regional O_3 surface sink would be about 70% of the original value for the extreme case of a total rain forest to pasture conversion. Since cattle pastures represent the largest part of converted forest land in Rondônia [*Fearnside*, 1980; *Roberts et al.*, 2002], this scenario might not be unrealistic.

For an estimate of the current state and the recent history in central Rondônia a simple up scaling approach was made in *Rummel et al.* [2005a] based on the LBA-EUSTACH results and the land cover information provided by the analysis of *Roberts et al.* [2002] for the two LANDSAT scenes P231, R67 (Ji-Paraná) and P231, R68 (Luiza).

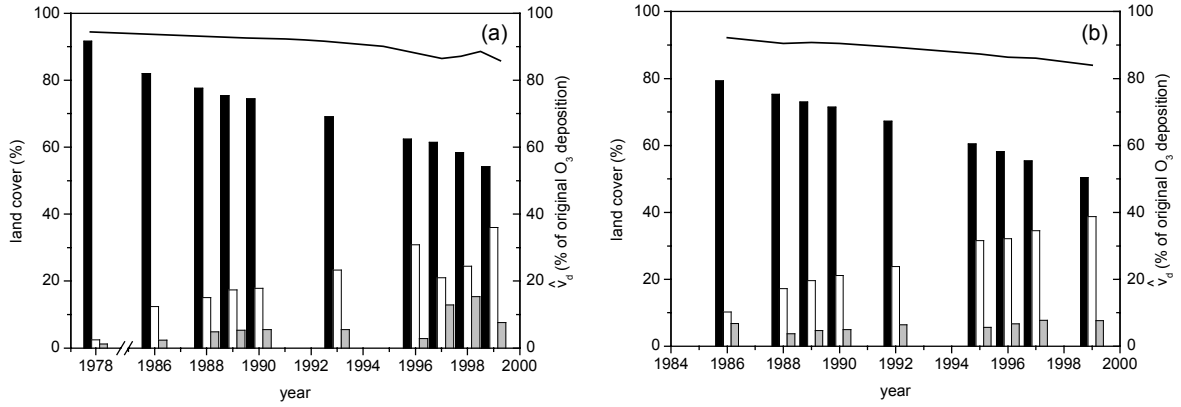

Figure 7: *Temporal evolution of the areal percentage of the three major land-cover classes (primary rain forest: black column, pasture: white column, and secondary growth: gray column) of two LANDSAT scenes: (a) Ji-Paraná (~26500 km^2) and (b) Luiza (~30000 km^2) in central Rondônia [Roberts et al., 2002]. The black line indicates the corresponding change of the areal O_3 deposition average in relation to the original forest cover. Figure taken from Rummel et al. [2005a]*

Figure 7 displays the land cover history of the two scenes from 1978 and 1986 to 1999 for Ji-Paraná and Luiza, respectively [*Roberts et al.*, 2002]. Both areas show a similarly reduction of the tropical rain forest cover from 82% and 79% in the year 1986 to 54% and 50% in 1999. The calculated reduction of the area averaged O_3 deposition for the same time period is from 93% to 86% and from 92% to 84% of the original tropical rain forest value.

4.2 The Fate of biogenic Soil NO Emission

The net effect of different chemical and physical processes in the vegetation layer on soil emitted NO (see Figure 4) is directly visible in the NO fluxes presented in *Rummel et al.* [2002].

Eddy covariance measurements of NO flux were carried out within the rain forest, 1 m and 11 m above the ground. Night time similarity between the cospectra of the sensible heat flux and the NO flux enabled to correct the considerable high-frequency attenuation of the NO eddy covariance measurements, which was mainly caused by the sensor separation under low wind conditions. The total effect of high-frequency attenuation was estimated to 20.9 ± 4.6% for the system at 1 m and 5.2 ± 1.5% for the one at 11 m above ground.

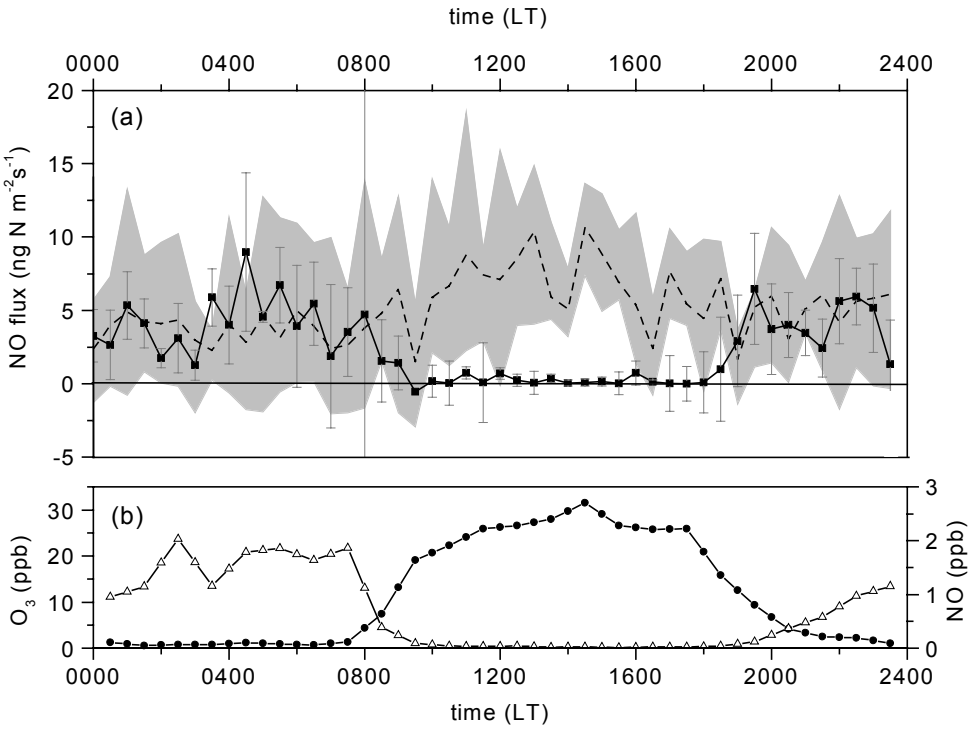

Figure 8: *Mean diurnal course from 23 September to 01 October of (a) the NO flux measured by the eddy covariance system at 11 m height (full squares), NO soil emissions measured by the dynamic chambers (mean: dashed line; range: grey shaded area) and (b) NO (open triangles) and O3 (solid circles) mixing ratio at 11.3 m height . The vertical bars indicate the variability of the eddy covariance results over the averaging period. Figure taken from Rummel et al. [2002]*

At night biogenic NO is transported into the crown region of the forest. This is demonstrated by the generally good agreement between the NO fluxes measured by eddy covariance of 3.5 ± 0.14 ng N m^{-2} s^{-1} and 4.8 ± 0.39 ng N m^{-2} s^{-1} (in 1 m und 11 m height, respectively) and the mean

NO soil emission rates of 3.9 ± 0.14 ng N m^{-2} s^{-1} and 5.2 ± 0.31 ng N m^{-2} s^{-1}, obtained independently by a dynamic chamber system [*Gut et al.*, 2002a] for the two ten day investigation periods, respectively. Figure 8 (a) shows the corresponding results of the flux measurements at 11 m height.

During daytime, NO flux as measured by the eddy covariance method was significantly reduced. At 11 m height the daytime NO flux was already close to zero (Figure 8 (a)), indicating that nearly all soil emitted NO was reacting with entrained O_3, forming NO_2 within the lowest meters of the forest. How much of the NO_x (NO + NO_2), originating from the soil emission, is able to leave the vegetation layer depends largely on the turbulent transport throughout the canopy.

4.3 Turbulence Characteristics within and above the dense Rain Forest Canopy

The analysis of the turbulence structure within and above the rain forest is presented in *Rummel et al.* [2005b]. A distinct coupling appeared between the main part of the canopy and the atmosphere above during daytime. Especially in windy conditions with wind speeds ≥ 2 m s^{-1}, as indicated by transport of mean turbulent kinetic energy TKE, high kurtosis and negative skewness of the vertical wind fluctuations in the stem space, large scale eddies have sufficient energy to penetrate deep into the stably stratified lower part of the forest. In agreement to the findings of *Kruijt et al.* [2000] the lower part of the canopy is most of the time not included in the direct exchange with the atmosphere above the vegetation layer. But this layer is mostly limited to the first meters above the forest floor and therefore much shallower than in the forest canopy in central Amazonia where just the upper third of the canopy was directly coupled to the roughness sublayer [*Kruijt et al.*, 2000].

Contrastingly, to the daytime situation, at night the whole sub-canopy space is mostly decoupled from the atmosphere above the forest. A strong inversion throughout the upper crown layer and above it isolates the stem space below most of the time. Unstable stratification in the isolated stem space initiates an internal convection. The resulting sub-canopy vertical turbulence structure is similar to that of the atmospheric mixing layer and can be closely described by the corresponding scaling approach (Figure 9). Here, the convective velocity scale w_* was calculated on the basis of the layer depth and the internal heat flux, resulting in the characteristic maximum of the σ_w^2/w_*^2 profile in the mid stem space.

As a consequence of this night time convection soil emitted NO is mixed up to the lower crown region [*Rummel et al.*, 2002]. Therefore occasionally occurring nocturnal turbulence enhancements, which break up the inversion layer may be able to effectively transfer accumulated NO to the atmosphere above the forest.

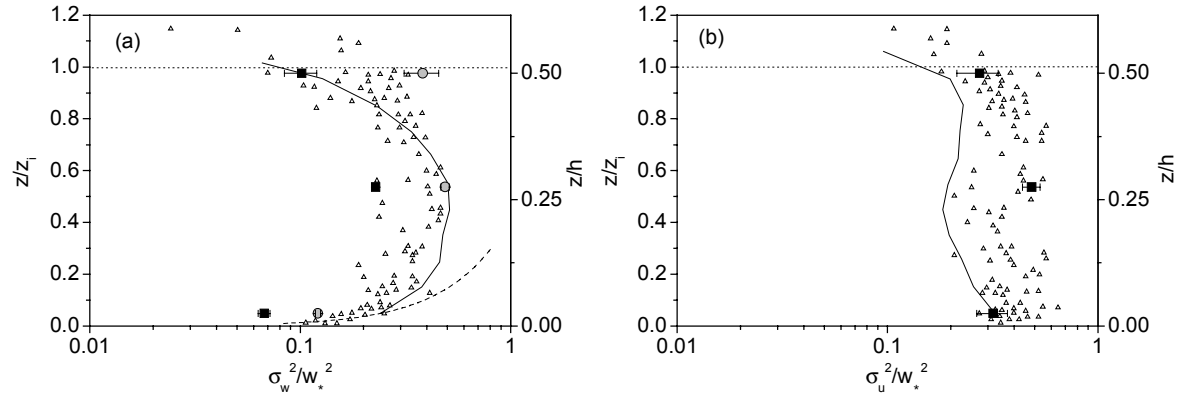

Figure 9: *Average night time profiles of vertical (a) and streamwise (b) velocity variance measured at three heights (1 m, 11 m, and 20 m), normalized by the squared convective velocity scale (calculated with buoyancy flux at 11 m: black squares; and in (a) at 1m:grey circles). Error bars represent standard errors. Height z is normalized by the assumed convective boundary layer height z_i (left axis) or the canopy height h (right axis). The lower dashed curve indicates the local free convection surface layer scaling after Kaimal et al. [1976]. The solid line shows the average convective layer results of laboratory model experiments carried out by Willis and Deardorff [1974]. Mixed layer data of two field experiments presented in Caughey and Palmer [1979] are displayed as open triangles. Figure taken from Rummel, et al. [2005b].*

4.4 Derivation of Transport Time Scales and Surface Renewal Analysis

For an intensive measuring period at the end of the wet season, a further characterization of the turbulent transport mechanisms with special emphasis on the heat and trace gas exchange is given by *Rummel et al.* [2005c]. Detailed analysis of high frequency scalar time series within and above the canopy revealed the frequent appearance of ramp pattern, the "finger print" of coherent turbulent structures, during daytime. These coherent structures establish a direct coupling between the upper 70-90% of the deep forest layer and the atmosphere above. The corresponding exchange of canopy air occurs mainly during short and strong events at the end of each ramp, a fact which enabled (i) to determine (by a wavelet detection scheme) the mean residence time of air in the main vegetation layer, as the mean time interval τ_s between consecutive ramps (Figure 10 (a)), and (ii) to determine scalar fluxes by a surface renewal model [*Paw U et al.*, 1995] which is based on this short coherent air motion.

On average, consecutive exchange events, which reached down into the stem space, were separated by a dimensionless time interval ($\tau_s\, u_*$) / h of about 1.6 (here u_* is the friction velocity above the forest and h is the canopy height), which is between 1.8 and 1.4, the results of earlier studies for temperate and boreal forests [*Collineau and Brunet*, 1993; *Chen et al.*, 1997]. For typical daytime situations, the

average residence times (turbulent time scales) were about 110 s for the crown layer and 160 s for the stem space of the forest (which is not reached by all events occurring at the vegetation-atmosphere interface), respectively.

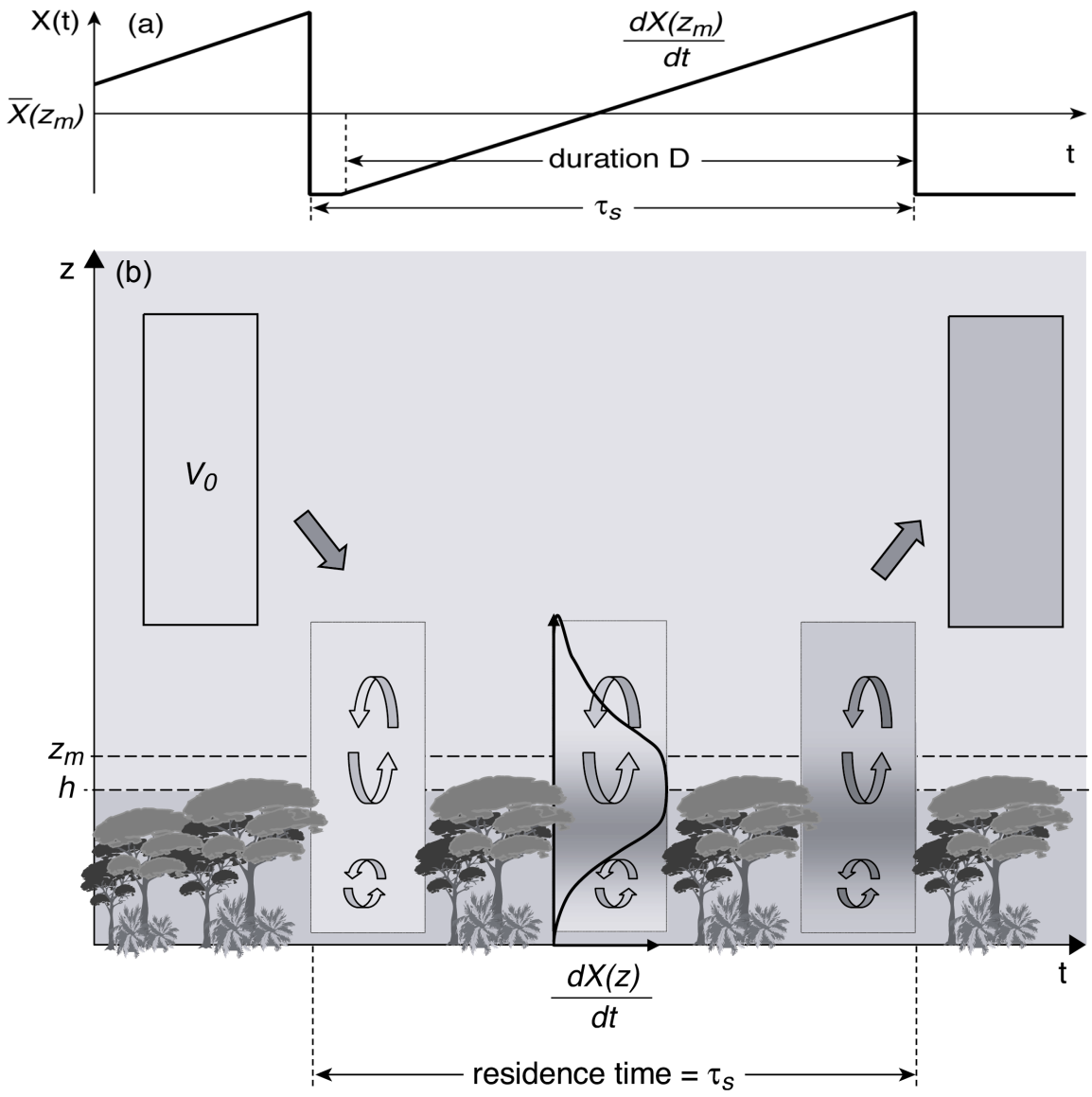

Figure 10: *Conceptual scheme of the air parcel motion on which the surface renewal approach is based. During the residence time τ_s, the volume V_0 is in contact with the canopy surface, and the scalar property X is exchanged. The mean duration D of the turbulent structures is directly related to the peak of the corresponding wavelet variance spectrum. The exchange results in a gradual increase (here for an emitted scalar quantity) in the time series X(t) measured at z_m until the parcel is replaced by another one. Small-scale turbulence and the source/sink distribution within V_0 control the vertical profile of the temporal change dX(z)/dt (the profile is indicated by the black curve in the middle volume). Figure modified from Rummel et al. [2005c].*

Typically, the characteristic ramp pattern was, in agreement with the mixing layer analogy suggested by *Raupach et al.* [1996], also pronounced in scalar time series measured well-above the forest canopy. This was the trigger to develop a conceptual picture for the surface renewal approach for tall dense canopies, in which a considerable part of the exchanged air parcels is located above the canopy (Figure 10 (b)). In that context, the model parameter α was supposed to reflect not just the vertical source/sink distribution of the scalar for forest canopies, as suggested in the originally work of *Paw U et al.* [1995], but it relates the average storage change within these air parcels of unknown vertical extent to the storage change within the considered air volume below the sensor height z_m. The latter is approximated by the mean temporal exchange of the scalar at z_m between the renewal events (for details see Section 2 of *Rummel et al.* [2005c]).

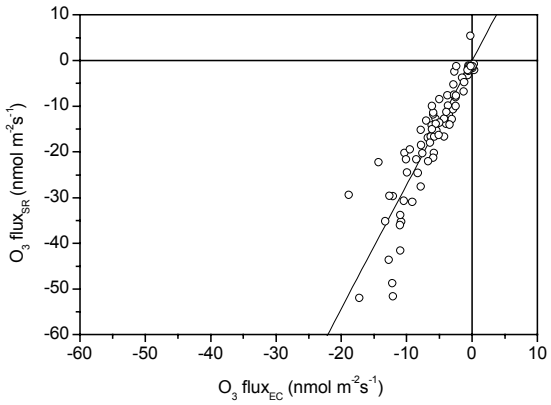

Figure 11: *Daytime O_3 flux above the canopy determined by the surface renewal (subscript SR) approach versus correspondent fluxes measured by eddy covariance (subscript EC). Figure taken from Rummel et al. [2005c]).*

During daytime hours the fluxes of the four measured scalars determined by the surface renewal approach agreed reasonably well with the fluxes obtained above the forest by the eddy covariance method (Figure 11 shows the result for ozone), which supports the assumed coherent air motion and the corresponding residence times to be characteristic for the main vegetation layer.

4.5 NO_x Canopy Reduction by a primary Rain Forest: Analysis of Processes and Quantification for Wet Season Conditions

The relative shallow layer close to the forest floor which was mostly decoupled from this direct exchange with the atmosphere above [see *Rummel et al.*, 2005b], turned out to play a crucial role for the net ecosystem emission of NO_x for daytime conditions. This is shown in *Rummel et al.* [2005d], where characteristic time scales of different canopy processes, namely turbulent transport, plant uptake, chemistry and soil deposition were compared. As in *Rummel at al.* [2005c], the data basis is

also the intensive investigation period at end of the wet season. In the lowest part of the canopy the transport time scale (or mean residence time) was considerably larger than the chemical time scale of NO oxidation by O_3 imported from aloft (Figure 12). This in concurrence with a negligible photolysis rate close to the ground ensured that during daytime nearly all soil emitted NO was transformed into NO_2 within the first 4 m above the forest floor. Consequently, almost the whole canopy depth contributes to the reduction of the created NO_2..

At night time the ratio of transport and chemical ($NO + O_3$) time scales is reversed in the lowest part of the canopy. This enables NO to reach higher regions of the forest. Therefore, in contrast to the daytime situation, when biogenic NO_x leaves the forest as NO_2, at night NO can (in the case of turbulent coupling) directly leave the canopy. Both results confirmed the measured in-canopy NO fluxes at 11 m in *Rummel et al.* [2002].

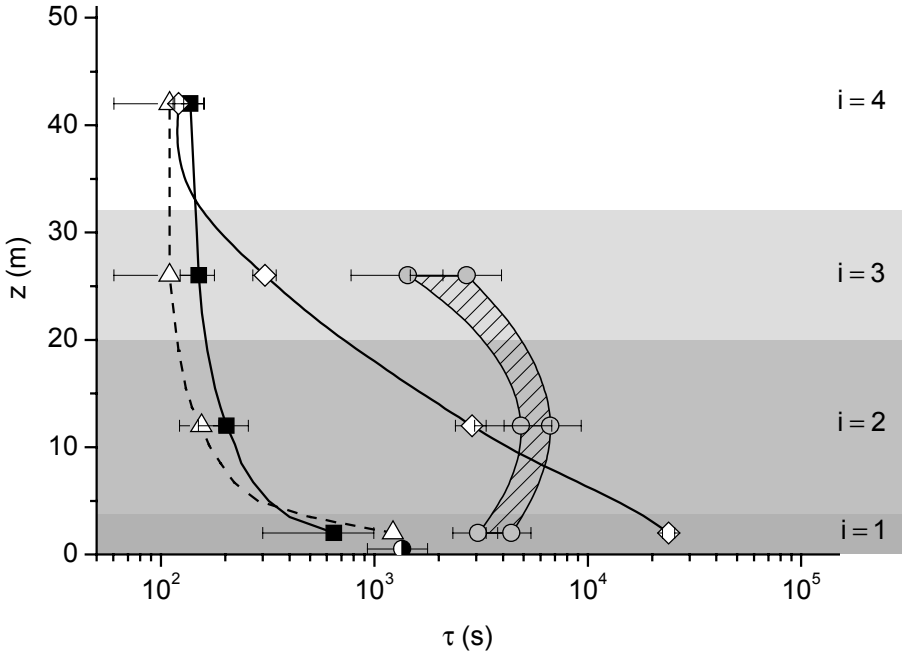

Figure 12: *Average vertical profiles (1000 LT-1400 LT) of NO_x exchange relevant time scales (chemical reaction with O_3: solid squares; photolysis: open diamonds; turbulent transport: open triangles; vegetation uptake NO_2: gray circles (the hatched area marks the range of NO_2 uptake time scales with and without mesophyll resistances); soil uptake: half open circle). Error bars represent standard deviations from the ensemble average. Figure taken from Rummel et al. [2005d].*

A clear advantage of the LBA-EUSTACH data set compared to former field studies is the availability of the first NO_2 mixing ratio profiles measured throughout a tropical rain forest. On the basis of mean NO_2 profiles and the assumption of steady state conditions, the NO_2 ecosystem uptake was assessed. Unfortunately the conundrum raised by *Lerdau et al.* [2000], about the existence of an

compensation mixing ratio for NO_2 exchange by leaves could also not be solved in this study. For this, beside canopy scale information, extensive leaf scale measurements of NO_2 exchange under environmental mixing ratio levels would be necessary. Three scenarios characterized by different NO_2 compensation points were calculated instead for daytime conditions. The resulting integral ecosystem NO_x reduction ranges from -3% (of average soil emission), in the case of NO_2 emitting vegetation, up to -25% for NO_2 uptake by all vegetation layers. The vegetation reduction of NO_x in the latter case is considerably smaller than in the prominent model estimations by *Jacob and Wofsy* [1990] and *Jacob and Bakwin* [1992], who got -75% and -60%, respectively, for a central Amazonian forest during daytime in the wet season. The difference is caused by the lower LAI and distinctively higher mesophyll and cuticula resistances used in the leaf model for the RBJ tropical forest in southwest Amazonia. Although canopy scale measurements showed some indication for NO_2 cuticula resistances as low as used by *Jacob and Wofsy* [1990] (1000 s m^{-1}), there is experimental evidence by leaf level cuvette field and greenhouse measurements for a NO_2 minimum cuticula resistance of ~ 4000 s m^{-1}. Based on this cuticula resistance the mean nocturnal NO_x reduction is also about -25%.

5 Conclusion

In order to asses the effect of deforestation on biosphere-atmosphere NO_x exchange of southwest Amazonian ecosystems, Table 2 (negative sign represents deposition) compiles the experimental information gained by the LBA-EUSTACH experiments. During LBA-EUSTACH 1, at the end of the local wet season, the RBJ rain forest was a clear source of biogenic NO_x [*Rummel et al.*, 2005d]. The FNS pasture site results for the same time period shows a balanced surface exchange of NO_x, if, as found for the forest soil, no significant difference occurs between NO emission of wet and dry season [*Gut et al.*, 2002a]. In that case the NO emission fluxes measured during LBA-EUSTACH 2 at FNS by *Kirkman et al.* [2002] can be transferred to the wet season. Although the NO_2 deposition to the pasture site might be somewhat overestimated by the usage of a molybdenum converter (to catalyze NO_2 to NO which was measured by the chemiluminescence analyzer), the NO_x input from the pasture to the troposphere was clearly lower than from the forest.

This difference between the RBJ forest and the FNS pasture reflects the general effect of converting tropical forest to agriculture on the corresponding NO soil emission. FNS is a relative old pasture with largely reduced soil N stocks since its first deforestation in 1977 [*Kirkman*, 2001]. Over timescales of several years and decades, soil nitrogen cycling at tropical pasture tends to slow down with age (from first deforestation) [e.g. *Neill et al.*, 1995; 1997] which is consequently resulting in a reduction of nitrogen trace emission to rates well below the original forest soil emissions [*Keller et al.*, 1993]. Therefore, without fertilizer usage, on a long term basis, deforestation and establishment of pastures (the main use of converted land in Rondônia) is most likely not resulting in a significant

increase of the net input of biogenic NO_x to the lower troposphere. Especially when the relative low NO_x reduction of -25% by the RBJ rain forest vegetation layer is considered. A value which is principally caused by comparatively high mesophyll and cuticula resistances for leaf uptake of NO_2 [*Gut et al.*, 2002b; *Rummel et al.*, 2005d] and supported during daytime by partly effective turbulent transport of O_3 into, and NO_2 out of the forest canopy [*Rummel et al.*, 2005c; 2005b]. The successful application of a surface renewal model in *Rummel et al.* [2005c] indicated coherent turbulent structures to be mainly responsible for the direct coupling of a deep forest layer and the atmosphere. During nighttime the fact that biogenic NO_x reaches higher canopy layers mainly as NO [*Rummel et al.*, 2002] which is hardly deposited at plant and soil surfaces provides the low NO_x reduction percentage.

Table 2: *Mean (24 h) NO_x exchange in ng N m^{-2} s^{-1} for the tropical rain forest at Reserva Biológica Jarú (RBJ) and the pasture at the commercial cattle ranch Fazenda Nossa Senhora Aparecida (FNS). Negative signs represent deposition.*

	LBA-EUSTACH 1		LBA-EUSTACH 2	
Quantity	RBJ	FNS	RBJ	FNS
NO soil emission	4.7[a]	0.7[b]	4.0[a]	0.7
NO_2 deposition	-1.2 ±0.2[c]	-0.7[d]	-5.0 ±0.9[e]	-3.9[d]
net NO_x exchange	3.5	±0	-1.0	-3.3

[a] RBJ NO soil emission by *Gut et al.* [2002a] [see also *Rummel et al.*, 2002].
[b] FNS NO soil emission during LBA-EUSTACH 1 assumed to be equivalent to findings during LBA-EUSTACH 2 by *Kirkman et al.* [2002].
[c] RBJ NO_2 deposition by *Rummel et al.* [2005d]
[d] FNS NO_2 deposition represents an upper limit since the measurements were performed with a molybdenum converter, possibly including contributions of other NO_y components.
[e] RBJ NO_2 ecosystem deposition here was calculated equivalently to the wet season results of *Rummel et al.* [2005d] but based on the LBA-EUSTCH 2 data and dry season stomatal resistances of *McWilliam et al.* [1996].

In contrast to the long term effect, significantly enhanced soil NO emission (compared to the forest soil emission) was found at recently established pastures, particularly within the first year after deforestation [*Keller et al.*, 1993; *Neff et al.*, 1995; *Weitz et al.*, 1998]. Increased availability of soil inorganic nitrogen (NO_3^- and NH_4^+), mainly as a consequence of lacking vegetation uptake immediately after slash and burn activities, are most likely the reason for this higher soil NO emission [*Neill et al.*, 1999]. The following decline of soil inorganic nitrogen and connected NO emission depends largely on land-use and cultivation activities. In his model study, *Kirkman* [2001] investigated

the effect of FNS's land-use history on the corresponding soil NO emission. He obtained a significant NO emission enhancement within the first year after the primary deforestation. During the following time period of about 11 years, the soil NO emission was relatively constant at 65%-75% of the original forest soil emission level. Afterwards a further decline of the NO emission occurred towards the low measured emission level in 1999, 22 years after the deforestation. It becomes clear, that on the short and midrange time scale the effect of transforming tropical forest to pasture on the input of biogenic originating NO_x into the atmosphere is largely dependent on the magnitude of NO_x reduction by the original forest ecosystem. Based on the canopy reduction obtained for the RBJ forest by *Rummel et al.* [2005d] and the results of *Kirkman* [2001] for FNS, the effect of deforestation and pasture establishment on the net biogenic NO_x emission in Rondônia is relatively small over almost one decade. Considering the fact, that the found relative NO_x reduction of -25% ranges at the lower end of the estimates obtained by canopy models for tropical forests [*Jacob and Wofsy*, 1990; 1992; *Ganzeveld et al.*, 2002a], an increase of biogenic NO_x emission by forest-pasture transformation over this first decade seems to be likely if no NO_2 leaf compensation mixing ratio exists. To clarify the possible existence of NO_2 emission by tropical trees due to leaf compensation mixing ratios and its influence on the forest NO_x budget under wet season conditions experimentally, it is necessary to complement comprehensive canopy scale experiments like LBA-EUSTACH in future by extensive branch cuvette measurements with highly sensitive NO_2 sensors (or converters).

However, the impact of long term development and pastoral land use on the input of NO_x into the tropical troposphere is not restricted to the gradually decreasing biogenic soil emission. Beside this effect, development and colonization of originally forested land comes along with growing infrastructure and consequently increasing anthropogenic NO_x emissions caused by fossil fuel combustion. Anthropogenic impact on NO_x mixing ratios above the RBJ forest was clearly visible during LBA-EUSTACH 2 at the end of the dry season in Rondônia. Despite similar NO soil emission (Table 2), intensive biomass burning activities resulted in NO_x mixing ratios 6-10 times higher than during LBA-EUSTACH 1 (see Figure 13). The dry season NO_2 ecosystem deposition for the RBJ rain forest in Table 2 was calculated equivalently to the budget approach of *Rummel et al.* [2005d] but based on the LBA-EUSTCH 2 data and dry season stomatal resistances of *McWilliam et al.* [1996]. Both ecosystems were net NO_x sinks during the LBA-EUSTCH 2 campaign. Due to the much lower NO soil emission of the old pasture, the net NO_x uptake of FNS was about 3 times higher than the net uptake found for the forest ecosystem. This difference in net NO_x uptake between the two ecosystems during the burning season was most likely smaller for a considerable time period after deforestation, taking into account the temporal evolution of soil NO emission mentioned above.

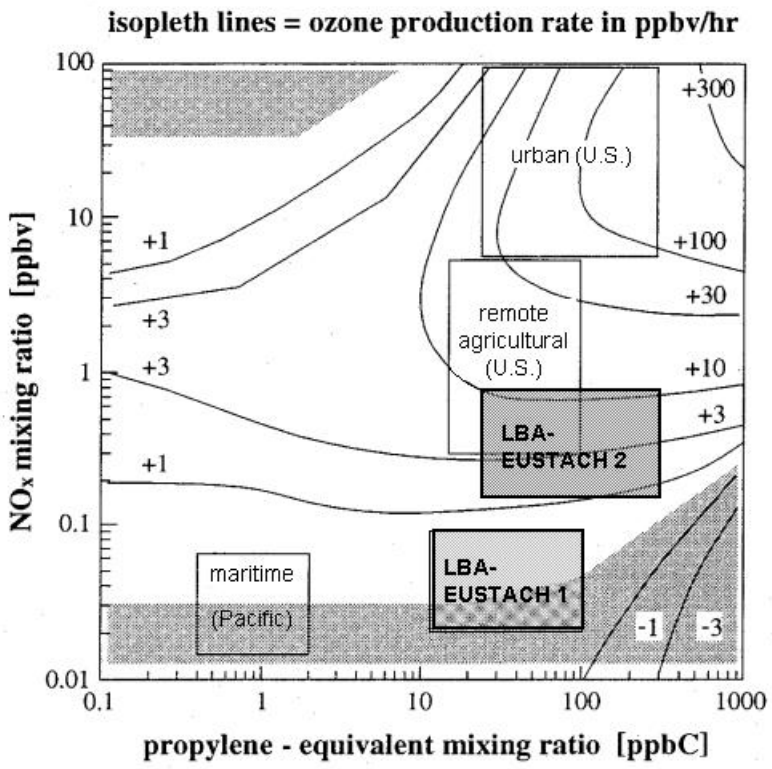

Figure 13: *Ozone production/destruction rate after Chameides et al. [1992] like Figure 3. Additionally shown is the range of the NO_x and total non methane RH's (in propylene reactivity equivalent) mixing ratios during LBA-EUSTACH 1 and 2.*

Figure 13 shows again the O_3 production/destruction rate resulting from photochemical box model calculations of *Chameides et al.* [1992] (see also Figure 3) with the corresponding mixing ratios of NO_x and total non methane RH's. The original Figure is complemented by the midday (when due to well mixed conditions, surface values can be assumed to represent approximately the boundary layer mixing ratios) mixing ratio ranges measured during both LBA-EUSTACH experiments above the RBJ forest. At the end of the local wet season, during LBA-EUSTACH 1, the mixing ratio ranges of the O_3 precursors were comparable to the background levels found in central Amazonia 14 to 19 years before [*Kaplan et al.*, 1988; *Zimmermann et al.*, 1988]. The conditions during that experiment were at the transition range between local photochemical O_3 destruction and production. Totally different is the situation at the end of the dry season (LBA-EUSTACH 2) under biomass burning influence. The mixing ratios of ozone precursors, already comparable to values in agricultural regions of northern America, are clearly shifted into the O_3 production range, providing the high daytime O_3 levels which were measured during this time of the year [*Rummel et al.*, 2005a].

But the sensitivity of the O_3 production rate on the mixing ratios of nitrogen oxides shown in Figure 13 is also illustrating the high potential in the developing regions of the Amazon to get

enhanced O_3 levels in the lower troposphere over the whole year. The increasing amount of seasonally independent NO_x emissions by fossil fuel combustion and fertilizer deployment together with the considerable reduction of the surface O_3 sink strength by, (i) deforestation, found in *Rummel et al.* [2005a], and (ii) lower O_3 uptake capability of the remaining rain forest in developing regions due to the likely feedback of high O_3 mixing ratios and plant damage will propagate such a development.

References

Amiro, B. D., and P. A. Davis, Statistics of atmospheric turbulence within a natural black Spruce forest canopy, *Boundary-Layer Meteorology*, *44* (3), 267-283, 1988.

Amiro, B. D., Comparison of turbulence statistics within 3 boreal forest canopies, *Boundary-Layer Meteorology*, *51* (1-2), 99-121, 1990.

Andreae, M. O., E. V. Browell, M. Garstang, G. L. Gregory, R. C. Harriss, G. F. Hill, D. J. Jacob, M. C. Pereira, G. W. Sachse, A. W. Setzer, P. L. Silva Dias, R. W. Talbot, A. L. Torres, and S. C. Wofsy, Biomass-burning emissions and associated haze layers over Amazonia, *Journal of Geophysical Research*, *93* (D2), 1509-1527, 1988.

Andreae, M. O., A. Chapuis, B. Cros, J. Fontan, G. Helas, C. Justice, Y. J. Kaufman, A. Minga, and D. Nganga, Ozone and Aitken nuclei over Equatorial Africa: Airborne observations during DECAFE 88, *Journal of Geophysical Research*, *97* (D6), 6137-6148, 1992.

Atkinson, R., Atmospheric chemistry of VOCs and NO_x, *Atmospheric Environment*, *34*, 2063-2101, 2000.

Bakwin, P. S., S. C. Wofsy, S.-M. Fan, M. Keller, S. Trumbore, and J. M. da Costa, Emission of nitric oxide (NO) from tropical forest soils and exchange of NO between the forest canopy and atmospheric bounday layers, *Journal of Geophysical Research*, *95* (D10), 16'755-16'764, 1990a.

Bakwin, P. S., S. C. Wofsy, and S. M. Fan, Measurements of Reactive Nitrogen-Oxides (NO_y) within and above a Tropical Forest Canopy in the Wet Season, *Journal of Geophysical Research-Atmospheres*, *95* (D10), 16765-16772, 1990b.

Baldocchi, D., A multi-layer model for estimating sulfur dioxide deposition to a deciduous oak forest canopy, *Atmospheric Environment*, *22* (5), 869-884, 1988.

Baldocchi, D. D., and B. A. Hutchison, Turbulence in an Almond Orchard - vertical variations in turbulent statistics, *Boundary-Layer Meteorology*, *40* (1-2), 127-146, 1987.

Ball, J. B., *Global forest resources; history and dynamics*, Blackwell Science, Oxford, 2001.

Browell, E. V., G. L. Gregory, R. C. Harriss, and V. W. J. H. Kirchhoff, Ozone and aerosol distributions over the amazon basin during the wet season, *Journal of Geophysical Research*, *95* (D10), 16887-16901, 1990.

Carvalho, G., A. C. Barros, P. Moutinho, and D. Nepstad, Sensitive development could protect Amazonia instead of destroing it, *Nature*, *409*, 131, 2001.

Caughey, S. J., and S. G. Palmer, Some aspects of turbulence structure through the depth of the convective boundary layer, *Quarterly Journal of the Royal Meteorological Society*, *105*, 811-827, 1979.

Chameides, A. L., F. C. Fehsenfeld, M. O. Rodgers, C. Cardelino, J. Martinez, D. D. Parrish, W. Lonneman, D. R. Lawson, R. A. Rasmussen, P. Zimmermann, J. Greenberg, P. Middleton, and T. Wang, Ozone precursor relationships in ambient atmosphere, *Journal of Geophysical Research*, *97* (D5), 6037-6055, 1992.

Chen, W., M. D. Novak, T. A. Black, and X. Lee, Coherent eddies and temperature structure functions for three contrasting surfaces. Part 2: Renewal model for sensible heat flux, *Boundary-Layer Meteorology*, *84*, 125-147, 1997.

Coe, H., M. W. Gallagher, and T. W. Choularton, NO_x and O_3 exchange above a forest canopy in southern Scottland, in *General assessment of biogenic emissions and deposition of nitrogen compounds, sulphur compounds and oxidants in Europe;*, edited by J. Slanina, G. Angeletti, and S. Beilke, pp. 189-200, Comission of European Communities, Directorate-General for Science, Research and Development, Brussels (B), 1993.

Collineau, S., and Y. Brunet, Detection of Turbulent Coherent Motions in a Forest canopy Part 2: Time-scales and conditional averages, *Boundary-Layer Meteorology* (66), 49-73, 1993.

Coppin, P. A., M. R. Raupach, and B. J. Legg, Experiments on scalar dispersion within a model-plant canopy. 2. An elevated plane source, *Boundary-Layer Meteorology*, *35* (1-2), 167-191, 1986.

Cros, B., R. Delmas, D. Nganga, B. Clairac, and J. Fontan, Seasonal trends of ozone in Equatorial Africa: experimental evidence of photochemical formation, *Journal of Geophysical Research*, *93* (D7), 8355-8366, 1988.

Cros, B., J. Fontan, A. Minga, G. Helas, D. Nganga, R. Delmas, A. Chapuis, B. Benech, A. Druilhet, and M. O. Andreae, Vertical profiles of ozone between 0 and 400 meters in and above the African Equatorial forest, *Journal of Geophysical Research*, *97* (D12), 12877-12887, 1992.

Cros, B., C. Delon, C. Affre, T. Marion, A. Druilhet, P. E. Perros, and A. Lopez, Sources and sinks of ozone in savanna and forest areas during EXPRESSO: Airborne turbulent flux measurements, *Journal of Geophysical Research*, *105* (D24), 29347-29358, 2000.

Crutzen, P. J., The role of NO and NO_2 in the chemistry of the troposphere and the stratosphere, *Annual Review of Earth and Planetary Sciences*, *7*, 443-472, 1979.

Crutzen, P. J., A. C. Delany, J. Greenberg, P. Haagenson, L. Heidt, R. Lueb, W. Pollock, W. Seiler, A. Wartburg, and P. Zimmermann, Tropospheric chemical composition measurements in Brazil during the dry season, *Journal of Atmospheric Chemistry*, *2*, 233-256, 1985.

Crutzen, P. J., The role of the tropics in atmospheric chemistry, in *The Geophysiology of Amazomia*, edited by R.E. Dickinson, pp. 107-130, John Wiley, New York, 1986.

Crutzen, P. J., and M. O. Andreae, Biomass burning in the tropics: impact on atmospheric chemistry and biogeochemical cycles, *Science*, *250*, 1669-1678, 1990.

Crutzen, P. J., M. G. Lawrence, and U. Pöschel, On the background photochemistry of tropospheric ozone, *Tellus*, *51 A-B*, 123-146, 1999.

Culf, A., J. L. Esteves, A. d. O. Marques Filho, and H. R. da Rocha, Radiation, temperature and humidity over forest and pasture in Amazonia, in *Amazonian Deforestation and Climate*, edited by J.H.C. Gash, C.A. Nobre, J.M. Roberts, and R.L. Victoria, pp. 175-191, John Wiley and Sons, Chichester, 1996.

Davidson, E. A., and W. Kingerlee, A global inventory of nitric oxide emissions from soils, *Nutrient Cycling in Agroeecosystems*, *48*, 37-50, 1997.

Delany, A. C., P. Haagenson, S. Walters, A. Wartburg, and P. J. Crutzen, Photochemically produced ozone in the emission from large-scale tropical vegetation fires, *Journal of Geophysical Research*, *90* (D1), 2425-2429, 1985.

Demnead, O. T., and E. F. Bradley, Flux-gradient relationships in a forest canopy, in *The Forest-Atmosphere Interaction*, edited by B.A. Hutchison, and B.B. Hicks, pp. 421-442, D. Reidel Publishing Company, Oak Ridge, Tennesee, 1985.

Ehhalt, D. H., Gas phase chemistry of the troposphere, in *Global aspects of atmospheric chemistry*, edited by Deutsche Bunsen-Gesellschaft für Physikalische Chemie, R. Zellner guest editor, Springer Verlag, New York, 1999.

Fan, S. M., S. C. Wofsy, P. S. Bakwin, D. J. Jacob, and D. R. Fitzjarrald, Atmosphere-biosphere exchange of CO_2 and O_3 in the central Amazon forest, *Journal of Geophysical Research*, *95* (D10), 16851-16864, 1990.

FAO, Global forest ressources assessment 2000, FAO Forestry Pap. No. 140, UN Food Agric. Org., Rome, 2001.

Fearnside, P. M., The effects of cattle pastures on soil fertility in the Brazilian Amazon:consequences for beef production sustainability, *Tropical Ecology*, *21*, 125-137, 1980.

Finnigan, J., Turbulence in plant canopies, *Annual Review of Fluid Mechanics*, *32*, 519-571, 2000.

Fitzjarrald, D. R., B. L. Stormwind, G. Fisch, and O. M. R. Cabral, Turbulent transport observed just above the Amazon forest, *Journal of Geophysical Research*, *93* (D2), 1551-1563, 1988.

Fitzjarrald, D. R., K. E. Moore, O. M. R. Cabral, J. Scolar, A. O. Manzi, and L. D. D. Sa, Daytime turbulent exchange between the Amazon forest and the atmosphere, *Journal of Geophysical Research-Atmospheres*, *95* (D10), 16825-16838, 1990.

Fitzjarrald, D. R., and K. E. Moore, Mechanisms of nocturnal exchange between the rain forest and the atmosphere, *Journal of Geophysical Research*, *95* (D10), 16839-16850, 1990.

Ganzeveld, L. N., J. Lilieveld, F. J. Dentener, M. C. Krol, and G.-J. Roelofs, Atmosphere-biosphere trace gas exchanges simulated with a single-column model, *Journal of Geophysical Research*, *107*, 10.1029/2001JD000684, 2002a.

Ganzeveld, L. N., J. Lilieveld, F. J. Dentener, M. C. Krol, A. J. Bouwman, and G.-J. Roelofs, Global soil-biogenic NO_x emissions and the role of canopy processes, *Journal of Geophysical Research*, *107*, 10.1029/2001JD001289, 2002b.

Gao, W., R. H. Shaw, and K. T. Paw U, Observation of organized structure in turbulent flow within and above a forest canopy, *Boundary-Layer Meteorology*, *47*, 349-377, 1989.

Gash, J. H. C., J. M. Nobre, J. M. Roberts, and R. L. Victoria, An overview of ABRACOS, in *Amazonian Deforestation and Climate*, edited by J.H.C. Gash, J.M. Nobre, J.M. Roberts, and R.L. Victoria, John Wiley, New York, 1996.

Gregory, G. L., E. V. Browell, and L. S. Warren, Boundary-layer ozone - an airborne survey above the Amazon Basin, *Journal of Geophysical Research-Atmospheres*, *93* (D2), 1452-1468, 1988.

Güsten, H., G. Heinrich, R. W. H. Schmidt, and U. Schurath, A novel ozone sensor for direct eddy flux measurements, *Journal of Atmospheric Chemistry*, *14*, 73-84, 1992.

Gut, A., S. M. van Dijk, M. Scheibe, U. Rummel, M. Welling, C. Ammann, F. X. Meixner, M. O. Andreae, and B. E. Lehmann, NO emission from an Amazonian rain forest soil: Continuous measurements of NO flux and soil compensation concentration, *Journal of Geophysical Research*, *107* (D20), 8057, doi: 10.1029/2001JD000521, 2002a.

Gut, A., M. Scheibe, S. Rottenberger, U. Rummel, M. Welling, C. Ammann, G. A. Kirkman, U. Kuhn, F. X. Meixner, J. Kesselmeier, B. E. Lehmann, J. Schmidt, E. Müller, and M. T. F. Piedade, Exchange fluxes of NO_2 and O_3 at soil and leaf surfaces in an Amazonian rain-forest, *Journal of Geophysical Research*, *107* (D20), 8060, doi:10.1029/2001JD000654, 2002b.

Hari, P., M. Raivonen, T. Vesala, J. W. Munger, K. Pilegaard, and K. M., Ultraviolet light and leaf emission of NO_x, *Nature*, *422*, 134, 2003.

Harriss, R. C., M. Garstang, S. C. Wofsy, S. M. Beck, R. J. Bendura, J. R. B. Coelho, J. W. Drewry, J. M. Heoell Jr., P. A. Matson, R. J. McNeal, L. C. B. Molion, J. W. Navarro, V. Rabine, and R. L. Snell, The Amazon boundary layer experiment: Wet season 1987, *Journal of Geophysical Research*, *95* (D10), 16721-16736, 1990.

Heck, W. W., W. W. Cure, L. J. Rawlings, A. S. Zaragoza, H. E. Heagle, R. J. Heggestad, L. W. Kohut, L. W. Kress, and P. J. Temple, Assessing impacts of ozone on agricultural crops, II,

Crop yield functions and alternative exposure statistics, *J. Air Pollut. Control Assoc.*, *34*, 810-817, 1984.

Ho, C. M., and P. Huerre, Perturbed free shear layers, *Annual Review of Fluid Mechanics*, *16*, 365-424, 1984.

Holland, E. A., F. J. Dentener, B. H. Braswell, and J. M. Sulzman, Contemporary and pre-industrial reactive nitrogen budgets, *Biogeochemistry*, *46*, 7-43, 1999.

Houghton, R. A., E. A. Davidson, and G. M. Woodwell, Missing sinks, feedbacks, and understanding the role of terrestrial ecosystems in the global carbon balance, *Global Biogeochemical Cycles*, *12*, 25-34, 1998.

Houghton, R. A., The annual net flux of carbon to the atmosphere from changes in land use 1850-1990, *Tellus*, *51B*, 298-313, 1999.

IPCC, *Climate Change 2001: The Scientifc Basis - Contribution of Working Group I to the Third Assessment Report of the International Panel on Climate Change (IPCC)*, Cambridge University Press, Cambridge, 2001.

Jacob, D. J., and S. C. Wofsy, Photochemistry of biogenic emissions over the Amazon forest, *Journal of Geophysical Research-Atmospheres*, *93* (D2), 1477-1486, 1988.

Jacob, D. J., and S. C. Wofsy, Budgets of reactive nitrogen, hydrocarbons, and ozone over the Amazon-Forest during the wet season, *Journal of Geophysical Research*, *95* (D10), 16737-16754, 1990.

Jacob, D. J., and P. S. Bakwin, Cycling of NO_x in tropical forest canopies, in *Microbial Production and Consumption of Greenhouse Gases*, edited by W.B. Whitman, pp. 237-253, American Society of Microbiology, Washington, D.C., 1992.

Johansson, C., Pine forest: A negligible sink for atmospheric NO_x in rural Sweden, *Tellus (B)*, *39*, 426-438, 1987.

Kaimal, J. C., J. C. Wyngaard, D. A. Haugen, O. R. Cote, Y. Izumi, S. J. Caughey, and C. J. Readings, Turbulence structure in the convective boundary layer, *Journal of Atmospheric Science*, *33*, 2152-2169, 1976.

Kaimal, J. C., and J. J. Finnigan, *Atmospheric boundary layer flows*, 280 pp., Oxford University Press, New York, Oxford, 1994.

Kaplan, W. A., S. C. Wofsy, M. Keller, and J. M. da Costa, Emission of NO and deposition of O_3 in a tropical forest system, *Journal of Geophysical Research*, *93* (D2), 1389-1395, 1988.

Keller, M., E. Veldkamp, A. M. Weitz, and W. A. Reiners, Effect of pasture age on soil trace-gas emissions from a deforested area of Costa Rica, *Nature*, *365*, 244-246, 1993.

Kesselmeier, J., U. Kuhn, S. Rottenberger, T. Biesenthal, A. Wolf, G. Schebeske, M. O. Andreae, P. Ciccioli, E. Brancaleoni, M. Frattoni, S. T. Oliva, M. L. Botelho, C. M. A. Silva, and T. M. Tavares, Concentrations and species composition of atmospheric volatile organic compounds (VOC) as observed during the wet and dry season in Rondonia (Amazonia), *Journal of Geophysical Research*, *107* (D20), 8053, doi:10.1029/2000JD000267, 2002.

Kirchhoff, V. W. J. H., E. V. Browell, and G. L. Gregory, Ozone measurements in the troposphere of an Amazonian rain forest environment, *Journal of Geophysical Research*, *93* (D12), 15850-15860, 1988.

Kirchhoff, V. W. J. H., I. M. O. Dasilva, and E. V. Browell, Ozone measurements in Amazonia - dry season versus wet season, *Journal of Geophysical Research*, *95* (D10), 16913-16926, 1990.

Kirchhoff, V. W. J. H., J. R. Alves, F. R. da Silva, and J. Fishman, Observations of ozone concentratios in the Brazilian cerrado during the TRACE A field expedition, *Journal of Geophysical Research*, *101* (D19), 24029-24042, 1996.

Kirkman, G. A., The surface exchange of trace gases in the tropics and savannas, Dissertation thesis, University of Mainz, 2001.

Kirkman, G. A., A. Gut, C. Ammann, L. V. Gatti, A. M. Cordova, M. A. L. Moura, M. O. Andreae, and F. X. Meixner, Surface exchange of nitric oxide, nitrogen dioxide, and ozone at a pasture in Rondonia, Brazil, *Journal of Geophysical Research*, *107* (D20), 8083, doi: 10.1029/2001JD000523, 2002.

Kruijt, B., Y. Malhi, J. Lloyd, A. D. Nobre, A. C. Miranda, M. G. P. Pereira, A. Culf, and J. Grace, Turbulence statistics above and within two amazon rain forest canopies, *Boundary-Layer Meteorology*, *94*, 287-331, 2000.

Kuhn, U., S. Rottenberger, T. Biesenthal, A. Wolf, G. Schebeske, P. Ciccioli, E. Brancaleoni, M. Frattoni, T. M. Tavares, and J. Kesselmeier, Isoprene and monoterpene emission of Amazonian tree species during the wet season: Direct and indirect investigations of controlling functions, *Journal of Geophysical Research*, *107* (D20), 8071, doi:10.1029/2001JD000978, 2002.

Lee, D. S., I. Köhler, E. Grobler, F. Rohrer, R. Sausen, L. Gallardo-Klenner, J. G. J. Olivier, F. J. Dentener, and A. F. Bouwman, Estimations of global NO_x emissions and their uncertainties, *Atmospheric Environment*, *31* (12), 1735-1749, 1997.

Lee, X., and A. Black, Atmospheric turbulence within and above a Douglas-Fir stand. Part 2: eddy fluxes of sensible heat and water vapour, *Boundary Layer Meteorology*, *64*, 369-389, 1993.

Lelieveld, J., and F. J. Dentener, What controls tropospheric ozone?, *Journal of Geophysical Research*, *105* (D3), 3531-3551, 2000.

Lerdau, M., J. W. Munger, and D. J. Jacob, The NO_2 flux conundrum, *Science*, *289*, 2291-2293, 2000.

Levy, H., Normal atmosphere: Large radical and formaldehyde concentrations predicted, *Science*, *173*, 141-143, 1971.

Logan, J. A., and V. W. J. H. Kirchhoff, Seasonal variations of tropospheric ozone at Natal, Brazil, *Journal of Geophysical Research*, *91* (D7), 7875-7881, 1986.

Ludwig, J., P. Weber, F. X. Meixner, and H. Rennenberg, Surface fluxes of NO and NO_2 by a dynamic chamber technique - Laboratory studies on wheat, in *Field measurtements and interpretation of species related to photooxidants and acid deposition*, edited by G. Angeletti, S. Beilke, and L. Slanina, pp. 257-265, Comission of the European Comunities, Directorate-Generale for Science, Brussels (B), 1992.

McKee, D. J., Tropospheric ozone, human health and agricultural impacts, Lewis, Boca Raton, Fla., 1993.

McWilliam, A.-L. C., O. M. R. Cabral, B. M. Gomes, J. L. Esteves, and J. M. Roberts, Forest and pasture leaf gas exchange in south-west Amazonia, in *Amazonian deforestation and climate*, edited by J.H.C. Gash, C.A. Nobre, J.M. Roberts, and R.L. Victoria, pp. 266-285, John Wiley & Sons, Chichester, 1996.

Meixner, F. X., Surface exchange of odd nitrogen oxides, *Nova Acta Leopoldina*, *70* (288), 299-348, 1994.

Neff, J. C., M. Keller, E. A. Holland, A. M. Weitz, and E. Veldkamp, Fluxes of nitric oxide from soils following the clearing and burning of secondary tropical rain forest, *Journal of Geophysical Research*, *100* (D12), 25913-25922, 1995.

Neill, C., M. C. Piccolo, P. A. Steudler, J. M. Melillo, B. J. Feigl, and C. C. Cerri, Nitrogen dynamics in soils of forests and active pastures in the western Brazilian Amazon basin, *Soil Biology and Biochemistry*, *27*, 1167-1175, 1995.

Neill, C., M. C. Piccolo, C. C. Cerri, P. A. Steudler, J. M. Melillo, and M. Brito, Net nitrogen mineralization and net nitrification rates in soils following deforestation for pasture across the southwestern Brazilian Amazon basin landscape, *Oecologia*, *110*, 243-252, 1997.

Neill, C., M. C. Piccolo, J. M. Melillo, P. A. Steudler, and C. C. Cerri, Nitrogen dynamics in Amazon forest and pasture soils measured by ^{15}N pool delition, *Soil Biology and Biochemistry*, *31*, 567-572, 1999.

Paw U, K. T., Y. Brunet, S. Collineau, R. H. Shaw, T. Maitani, J. Qiu, and L. Hipps, On coherent structures in turbulence above and within agricultural plant canopies, *Agricultural and Forest Meteorology*, *61*, 55-68, 1992.

Paw U, K. T., J. Qiu, H. B. Su, T. Watnabe, and Y. Brunet, Surface renewal analysis: a new method to obtain scalar fluxes, *Agricultural and Forest Meteorology*, *74*, 119-137, 1995.

Penner, J. E., D. H. Lister, D. J. Griggs, D. J. Dokken, and M. McForland (eds.), Aviation and the global atmosphere, in *A Special Report of IPCC Working Groups I and III*, pp. 373, Cambridge University Press, Cambridge, 1999.

Pinker, R. T., and J. Z. Holland, Turbulence structure of tropical forest, *Boundary-Layer Meteorology*, *43*, 43-63, 1988.

Portmann, R. W., S. Solomon, J. Fishman, J. R. Olson, J. T. Kiehl, and B. Briegleb, Reactive forcing of earth's climate due to tropical tropospheric ozone production, *Journal of Geophysical Research*, *102*, 9409-9417, 1997.

Raupach, M. R., J. J. Finnigan, and Y. Brunet, Coherent eddies in vegetation canopies, in *Australian Conference on Heat and Mass Transfer*, pp. 75-90, University of Canterbury, 1989.

Raupach, M. R., J. J. Finnigan, and Y. Brunet, Coherent eddies and turbulence In vegetation canopies - the mixing-layer analogy, *Boundary Layer Meteorology*, *78*, 351-382, 1996.

Roberts, D. A., I. Numata, K. Holmes, G. Batista, T. Krug, A. Monteiro, B. Powell, and O. A. Chadwick, Large scale mapping of land-cover change in Rondonia using multitemporal spectral mixture analysis and decision tree classifiers, *Journal of Geophysical Research*, *107* (D20), 8073, doi:10.1029/2001JD000374, 2002.

Roberts, J., O. M. R. Cabral, and L. F. Deaguiar, Stomatal and Boundary-Layer Conductances in an Amazonian Terra- Firme Rain-Forest, *Journal of Applied Ecology*, *27* (1), 336-353, 1990.

Roberts, J., O. M. R. Cabral, G. Fisch, L. C. B. Molion, C. J. Moore, and W. J. Shuttleworth, Transpiration from an Amazonian rainforest calculated calculated from stomatal conductance measurements, *Agricultural and Forest Meteorology*, *65*, 175-196, 1993.

Rogers, M. M., and R. D. Moser, The three-dimensional evolution of a plane mixing layer: the Kelvin-Helmholtz rollup, *Journal of Fluid Mechanics*, *243*, 183-226, 1992.

Rondon, A., C. Johansson, and L. Granat, dry deposition of nitrogen dioxide and ozone to coniferous forests, *Journal of Geophysical Research*, *98* (D3), 5159-5172, 1993.

Rondon, A., and L. Granat, Studies on dry deposition of NO_2 to coniferous species at low NO_2 concentrations, *Tellus*, *46B*, 339-352, 1994.

Rottenberger, S., U. Kuhn, A. Wolf, G. Schebeske, S. T. Oliva, T. M. Tavares, and J. Kesselmeier, Exchange of short-chain aldehydes between Amazonian vegetation and the atmosphere, *Ecological Applications*, *14* (4), 247-262, 2004.

Rottenberger, S., U. Kuhn, A. Wolf, G. Schebeske, S. T. Oliva, T. M. Tavares, and J. Kesselmeier, Formaldehyde and acetaldehyde exchange during leaf development of the Amazonian deciduous tree species *Hymeaea courbaril*, *Atmospheric Environment*, *in press*, 2005.

Rummel, U., C. Ammann, A. Gut, F. X. Meixner, and M. O. Andreae, Eddy covariance measurements of nitric oxide flux within an Amazonian rainforest, *Journal of Geophysical Research*, *107(D20)*, 8050, doi:10.1029/2001JD000520, 2002.

Rummel, U., C. Ammann, G. A. Kirkman, M. A. L. Moura, S. Rottenberger, U. Kuhn, J. Kesselmeier, T. Foken, M. O. Andreae, and F. X. Meixner, Seasonal ozone deposition to a tropical rain forest in southwest Amazonia, *Agricultural and Forest Meteorology*, *for submission*, 2005a.

Rummel, U., C. Ammann, T. Foken, and F. X. Meixner, Characterization of turbulent air motion within and above a tropical rain forest in Amazonia, *Boundary-Layer Meteorology*, *for submission*, 2005b.

Rummel, U., C. Ammann, T. Foken, M. O. Andreae, and F. X. Meixner, Application of a surface renewal model for the determination of heat, carbon dioxide, and ozone fluxes from a tropical rain forest in Amazonia, *Atmos. Chem. Phys.*, *for submission*, 2005c.

Rummel, U., C. Ammann, M. O. Andreae, and F. X. Meixner, Wet season NO_x exchange between an Amazonian rain forest and the atmosphere-implication from time scale analysis, *Atmospheric Environment*, *for submission*, 2005d.

Sigler, J. M., J. D. Fuentes, R. C. Heitz, M. Garstang, and G. Fisch, Ozone dynamics and deposition processes at a deforested site in the Amazon basin, *Ambio*, *31* (1), 21-27, 2002.

Sparks, J. D., R. K. Monson, K. L. Sparks, and M. Lerdau, Leaf uptake of nitrogen dioxide (NO_2) in a tropical wet forest: implications for tropospheric chemistry, *Oecologia*, *127*, 214-221, 2001.

Thoene, B., P. Schröder, H. Papen, A. Egger, and H. Rennenberg, Absorption of atmospheric NO_2 by spruce (Picea abies L. Karst.) trees. 1. NO_2 influxe and its correlation with nitrate reduction, *New Phytol.*, *117*, 575-585, 1991.

Thoene, B., H. Rennenberg, and P. Weber, Absorption of atmospheric NO_2 by spruce (Picea abies) trees. 2. Parameterization of NO_2 fluxes by controlled dynamic chamber measurements, *New Phytol.*, *134*, 257-266, 1996.

van Dijk, S. M., and J. Duyzer, Nitric oxide emissions from forest soils in the Netherlands, *Journal of Geophysical Research*, *104* (D13), 15955-15961, 1999.

Weber, P., and H. Rennenberg, Dependency of nitrogen dioxide (NO_2) fluxes to wheat(Triticum Aestivum L.) leaves from NO_2 concentration, light intensity, temperature and relative humidity determined from controlled dynamic chamber experiments, *Atmospheric Environment*, *30* (17), 3001-3009, 1996.

Weitz, A. M., E. Veldkamp, M. Keller, J. C. Neff, and P. M. Crill, Nitrous oxide, nitric oxide and methane fluxes from soils following clearing and burning of tropical secondary forest, *Journal of Geophysical Research*, *103* (D21), 28047-28058, 1998.

Werth, D., and R. Avissar, The local and global effects of Amazon deforestation, *Journal of Geophysical Research*, *107* (D20), 8087, doi: 10.1029/2001JD000717, 2002.

Willis, G. E., and J. W. Deardorff, A laboratory model of the unstable planetary boundary layer, *Journal of Atmospheric Science*, *31*, 1297-1307, 1974.

Yienger, J. J., and H. Levy, Empirical model of global soil-biogenic NO_x emission, *Journal of Geophysical Research*, *100* (D6), 11447-11464, 1995.

Zimmermann, P. J., J. P. Greenberg, and C. E. Westberg, Measurements of atmospheric hydrocarbons and biogenic emission fluxes in the Amazon boundary layer, *Journal of Geophysical Research*, *93*, 1407-1416, 1988.

Appendix A

Individual Contributions to the Publications

The results of the studies cumulated in this thesis were obtained in the frame of LBA-EUSTACH project in collaboration with other scientists. Therefore, several authors contributed to the manuscripts. The following sections specify my own and the contributions of the corresponding coauthors.

Appendix B

Rummel, U.[*], C. Ammann, G.A. Kirkman, M.A.L. Moura, S. Rottenberger, U. Kuhn, J. Kesselmeier, T. Foken, M.O. Andreae, and F.X. Meixner, Seasonal ozone deposition to a tropical rain forest in southwest Amazonia, for submission in *Agricultural and Forest Meteorology*, 2005a.

I performed the eddy covariance flux measurements and developed the online- and post processing data analysis software. Further, I made the comprehensive O_3 deposition analysis, and wrote the text of this manuscript.

C. Ammann realized and processed the trace gas profile measurements, which were used for calibration of the flux system and to determine the O_3 storage within the forest. The work profited from many constructive scientific discussions with him.

G.A. Kirkman provided the O_3 deposition data measured at the pasture site, which were separately published [*Kirkman et al.*, 2002].

M.A.L. Moura is a Brazilian counterpart who supported G.A. Kirkman at the Pasture site.

S. Rottenberger & U. Kuhn provided the pre-processed leaf level O_3 exchange data measured by their branch cuvette system mainly used for VOC exchange measurements.

J. Kesselmeier is the working group leader of S. Rottenberger and U. Kuhn.

T. Foken is the supervisor of the thesis. Discussions with him on flux data quality aspects were valuable for the analysis.

M.O. Andreae is a coordinator of the LBA-EUSTACH project and head of the Biogeo-chemistry Dept. at the Max-Planck-Institute.

[*] corresponding author of the specific publication

F.X. Meixner is the working group leader and my supervisor at the Max-Planck-Institute. This work profited from frequent scientific discussions with him.

Appendix C

Rummel, U.*, C. Ammann, A. Gut, F.X. Meixner, and M.O. Andreae, Eddy covariance measurements of nitric oxide flux within an Amazonian rainforest, *Journal of Geophysical Research*, *107(D20)*, 8050, doi:10.1029/2001JD000520, 2002.

I worked out and tested a possibility to measure eddy covariance fluxes with the commercial nitric oxide analyzer. I also realized the in canopy measurements and wrote the text for the manuscript.

C. Ammann contributed the trace gas and temperature profile measurements, which were used for calibration of the flux system and to characterize the atmospheric stability, respectively. The work profited from frequent scientific discussions with him.

A. Gut provided the NO soil emissions measured by dynamic chambers, which were separately published [*Gut et al.*, 2002].

F.X. Meixner is the working group leader and my supervisor at the Max-Planck-Institute.

M.O. Andreae is a coordinator of the LBA-EUSTACH project and head of the Biogeo-chemistry dept. at the Max-Planck-Institute.

Appendix D

Rummel, U.*, C. Ammann, T. Foken, and F.X. Meixner, Characterization of turbulent air motion within and above a tropical rain forest in Amazonia, for submission in *Boundary-Layer Meteorology*, 2005b.

I made the turbulence data measurements, analysis and derived all the results presented. I also wrote the text for the manuscript.

C. Ammann made valuable contributions in several scientific discussions.

T. Foken is the supervisor of the thesis and a person to turn to with respect to turbulence data quality evaluation.

F.X. Meixner is the working group leader and my supervisor at the Max-Planck-Institute. This work profited from frequent scientific discussions with him.

* corresponding author of the specific publication

Appendix E

Rummel, U.*, C. Ammann, T. Foken, M.O. Andreae, and F.X. Meixner, Application of a surface renewal model for the determination of heat, carbon dioxide, and ozone fluxes from a tropical rain forest in Amazonia, for submission in *Atmos. Chem. Phys*, 2005c.

I developed the modified conceptual picture of the surface renewal approach for tall dense canopies, made the turbulence data measurements, analysis, and derived all the results presented. I also wrote the text for the manuscript.

C. Ammann contributed the trace gas and temperature profile measurements, which were used in the analysis. Scientific discussions with him stimulated the progress of this work considerably.

T. Foken is the supervisor of the thesis and contributed to the work in discussions about wavelet analysis of turbulence data series.

F.X. Meixner is the working group leader and my supervisor at the Max-Planck-Institute. This work profited from frequent scientific discussions with him.

M.O. Andreae is a coordinator of the LBA-EUSTACH project and head of the Biogeochemistry dept. at the Max-Planck-Institute.

Appendix F

Rummel, U.*, C. Ammann, M.O. Andreae, and F.X. Meixner, Wet season NO_x exchange between an Amazonian rain forest and the atmosphere-implication from time scale analysis, for submission in *Atmospheric Environment*, 2005d

I made the time scale analysis and budget approach compiling the comprehensive data set of the LBA-EUSTACH experiments, and derived the results presented. I also wrote the text for the manuscript.

C. Ammann contributed and realized the trace gas and temperature profiles, which were used to determine the chemical and uptake time scales and to calculate the NO_x budget.

F.X. Meixner is the working group leader and my supervisor at the Max-Planck-Institute. This work profited from frequent scientific discussions with him.

M.O. Andreae is a coordinator of the LBA-EUSTACH project and head of the Biogeochemistry dept. at the Max-Planck-Institute.

* corresponding author of the specific publication

Appendix B

Seasonal Variation of Ozone Deposition to a Tropical Rain Forest in Southwest Amazonia

U. Rummel[a*], C. Ammann[b], G.A. Kirkman[a], M.A.L. Moura[c], S. Rottenberger[a], U. Kuhn[a], J. Kesselmeier[a], T. Foken[d], M.O. Andreae[a], and F.X. Meixner[a]

[a]*Max Planck Institute for Chemistry, Biogeochemistry Dept., D-55020 Mainz, Germany*

[b]*Air Pollution Climate group (TP 11.3), FAL-Reckenholz,P.O.Box, CH-8046 Zürich, Switzerland*

[c]*Departamento de Meteorologia, Centro de Ciencia Exatas e Naturais, Universidade Federal de Alagoas, Maceió Alagoas, Brazil*

[d]*University of Bayreuth,. Mikrometeorology Dept., D-95440 Bayreuth, Germany*

for submission in **Agricultural and Forest Meteorology**

Abstract

Within the LBA-EUSTACH project, tower based eddy covariance measurements of O_3 flux were performed above a Amazonian primary rain forest at the end of the local wet and dry seasons. Ozone deposition reveals distinct seasonal differences, which are primarily caused by extreme environmental conditions during the dry season, e.g. high humidity deficits and O_3 mixing ratios. At the end of the wet season the rain forest was an effective O_3 sink, documented by mean daytime maxima of -11.0 nmol m^{-2} s^{-1} and 2.3 cm s^{-1} for O_3 flux and deposition velocity, respectively. Contrastingly, a strongly reduced daytime O_3 uptake during dry periods was observed, which in turn (a) results in a large canopy storage effect, and (b) indicates the occurrence of considerable non-stomatal O_3 deposition after sunset. Leaf scale measurements support the occurrence of significant cuticular deposition, but the corresponding resistance of ~ 4000 s m^{-1} to 5000 s m^{-1} suggests chemical sinks to contribute substantially to the found nocturnal O_3 depletion. Measurements, simultaneously made at a 22 years old cattle pasture, enable the spatially and temporally direct comparison of O_3 dry deposition to a primary rain forest and a typical vegetation cover of deforested land in southwest Amazonia. The mean ozone deposition to the pasture was systematically lower. While at the end of the wet season, mean deposition velocity at the pasture site was about 35% lower than at the forest site, this difference was only about 25% under dry season conditions.

Keywords: Tropical forest; Eddy covariance; Ozone deposition, Deforestation

* corresponding author

1 Introduction

Tropospheric ozone O_3 is a constituent of the atmosphere with relevance for various environmental issues. As a secondary pollutant, formed by the photochemical oxidation of carbon monoxide CO and hydrocarbons in the presence of nitrogen oxides NO_x (Crutzen, 1979), high daytime mixing ratios arise mainly in industrialized areas of the northern hemisphere where anthropogenic emissions of precursors are extremely high (Chameides et al., 1992). But a gradual increase of O_3 together with CO and methane CH_4 is a global phenomenon (Crutzen and Andreae, 1990) and because of the detrimental impact of high O_3 levels on vegetation and human health an increasingly important problem. Furthermore, O_3 is an important greenhouse gas in the upper troposphere. On the other hand, O_3 is also a key precursor of the hydroxyl radical OH, the primary oxidant in the troposphere which is responsible for the removal of many reactive pollutants. Most oxidation of trace gases occurs in the tropical troposphere, where high UV intensities and water vapor concentrations favor the formation of OH by O_3 photolysis (Crutzen, 1986).

In the tropics, the annual cycle of tropospheric ozone due to natural seasonality of chemical and meteorological conditions is affected by the coincidence of anthropogenic biomass burning activities with the dry season (e.g. Crutzen et al., 1985; Delany et al., 1985; Kirchhoff et al., 1988; Kirchhoff et al., 1990; Logan and Kirchhoff, 1986). Here, O_3 mixing ratios of 50 to 100 ppb are frequently reached in haze layers at altitudes between 1 and 4 km and partly with large horizontal extend (Andreae et al., 1988; Cros et al., 1988). In the vicinity of burning areas of the Brazilian cerrado (savanna) even O_3 surface mixing ratios up to 80 ppb were found by Kirchhoff et al. (1996).

In remote areas of the tropics, without the influence of biomass burning, the seasonal variation of O_3 in the lower troposphere is mainly a consequence of varying exchange with higher atmospheric regions and terrestrial surfaces. During the wet season convective systems enhance the O_3 entrainment from the free troposphere and the stratosphere (Browell et al., 1990; Jacob and Wofsy, 1990), whereas in the dry season O_3 input from aloft is rather small (Jacob and Wofsy, 1988) due to formation of the trade wind inversion by large scale subsiding air motion. The surface exchange of O_3 and its precursors (CO, hydrocarbons, and NO_x) is crucial for the "natural" photochemical gain or loss of tropospheric O_3. Generally, dry deposition of O_3 was found to be the most important sink in the ozone budget of the lower troposphere. However, even for the rainforest, the main tropical biome, estimates of the O_3 dry deposition are up to now very scarce. For the dry season most of known estimates are rather crude, resulting from atmospheric boundary layer (ABL) or surface layer (SL) budget estimates, which base on a few vertical profiles

of O_3 mixing ratio in the northern Congo (Andreae et al., 1992; Cros et al., 1992) and in the central Amazon (e.g. Gregory et al., 1988; Kirchhoff et al., 1988). Recently, direct flux measurements applying an airborne eddy covariance system over northern Congo were made by Cros et al. (2000). All these experiments have been performed in the corresponding dry season. However, they have indicated the importance of the tropical forest as an ozone sink and they provided valuable flux information on a regional scale, by integrating large source areas. Only sporadic temporal information is available from these measurements. Tower based, high temporal resolution flux measurements enable the investigation of those mechanisms which regulate the surface deposition of O_3. So far, there is only one wet season experiment (ABLE 2B) in the Amazon, where tower based eddy covariance measurements of O_3 flux above a tropical rain forest have been performed for a 17 day period (Fan et al., 1990).

The present study as part of the LBA-EUSTACH campaigns (EUropean Studies on Trace gases and Atmospheric CHemistry as a contribution to Large-scale Biosphere–atmosphere experiment in Amazonia) (Andreae et al., 2002), particularly addresses the seasonality of ozone deposition to a tropical rain forest. For that purpose eddy covariance measurements of ozone flux were carried out at the end of the 1999 wet season (May), as well as the end of the 1999 dry season (September-October) at the RBJ tower site. In that context the O_3 uptake of the rain forest at canopy scale during periods with extremely high O_3 ambient levels as a consequence of intense biomass burning is of special interest.

To get a closer insight on the mechanisms of O_3 deposition at the leaf scale, ozone exchange was also measured by branch cuvettes on a deciduous tree species for a few days at a nearby site.

The Brazilian state of Rondônia is characterized by heavy deforestation and land use change (forest to pasture). The average deforestation rate in central Rondônia increased between 1990 and 1999 from ~1.2% per year to ~3.4% per year (Roberts et al., 2002). Since ozone deposition is largely controlled by plant physiological mechanisms these changes in land use are expected to result in corresponding changes of ozone deposition. Indeed, Sigler et al. (2002) have addressed this topic for wet season conditions by comparing their O_3 flux estimates at a Rondônian cattle ranch (1999) with those O_3 flux data of Fan et al. (1990) in central Amazonia, which have been obtained 12 years before. Taking advantage of the results of Kirkman et al. (2002), O_3 flux measurements which have been simultaneously performed at the rain forest and a pasture site (~ 60 km distance) during both seasons will be compared.

2 Experiment

2.1 Sites and Experimental Periods

The LBA-EUSTACH trace gas measurements were performed in two experiments in 1999. The first experiment (LBA-EUSTACH 1) took place during the wet-to-dry season transition in April/May, the second one (LBA-EUSTACH 2) in September/October during the reverse transition from dry-to-wet season. Herein, O_3 flux measurements were carried out from 4 to 22 May and from 21 September to 20 October, respectively. The experimental site (10°04´55´´ S, 61°55´48´´ W, 147 m a.s.l.), a former ABRACOS site (Gash et al., 1996) is located in the Reserva Biológica Jarú (RBJ), a forest reserve 90 km north of the city Ji-Paraná in the state of Rondônia (southwest Amazonia), Brazil (see Fig. 1). The vegetation cover of RBJ, owned by the Brazilian Environmental Protection Agency IBAMA (Instituto Brasileiro de Meio Ambiente e Recursos Renováveis), is a primary (terra firme) open rain forest with a closed canopy of about 32 m height (h_c). Single jutting trees reach heights up to 45 m. Due to their relevance for turbulence, an effective canopy layer height of 40 m (h) was defined for the analysis following Kruijt et al. (1996). The understory consists mainly of palms. Plant species at the measuring site have been characterized by McWilliam et al. (1996). The total LAI was measured (LI-COR LAI 2000, USA) to be about 5.6 (see Rummel et al. (2002) for the vertical LAI distribution).

The horizontal extent of the forest is partly limited. Within the west-northwest to southeast sector primary rain forest exists for several tens of km. In the remaining sector a river (Rio Machado) interrupts the vegetation. The minimum distance to the river (in southwest direction) is about 400 m. Beyond the river the area is covered by a mixture of plantations, secondary growth, and remaining patches of primary rain forest. On the LANDSAT image of Fig. 1 the fishbone pattern, typical for ongoing deforestation and colonization (activities which were promoted over the last 25 years in Rondônia by Brazilian authorities) can be seen to the west of the river, as well as in the southern part around Ji-Paraná.

Datasets from two additional sites, which are also visible at the satellite image (Fig. 1), are included in the analysis. Firstly, the IBAMA camp site, which is located 7 km south-southwest of the RBJ rain forest tower. This site is a permanent control post of IBAMA in the reserve. The camp is within a 1 km^2 patch of secondary forest (height: 10-15 m). At the end of the LBA-EUSTACH 2 experiment, from 25 to 31 October, ozone deposition was directly determined by branch cuvette measurements at a deciduous tree (*Hymenaea courbaril* L.), common in tropical rain forests (Kuhn et al., 2002a; Rottenberger et al., 2004). The second additional site is a commercial cattle ranch, named Fazenda Nossa Senhora Aparecida (FNS). This pasture,

also a former ABRACOS site, is about 45 km west-northwest of Ji-Paraná (Fig. 1). During both LBA-EUSTACH experiments Kirkman et al. (2002) determined exchange of ozone and nitrogen oxides betwen the atmosphere and *Brachiaria brizantha* grass (the predominant vegetation cover at FNS) by the inferential method, combining soil chamber and micrometeorological profile techniques.

Further information about all LBA-EUSTACH sites and campaigns are given by Andreae et al. (2002).

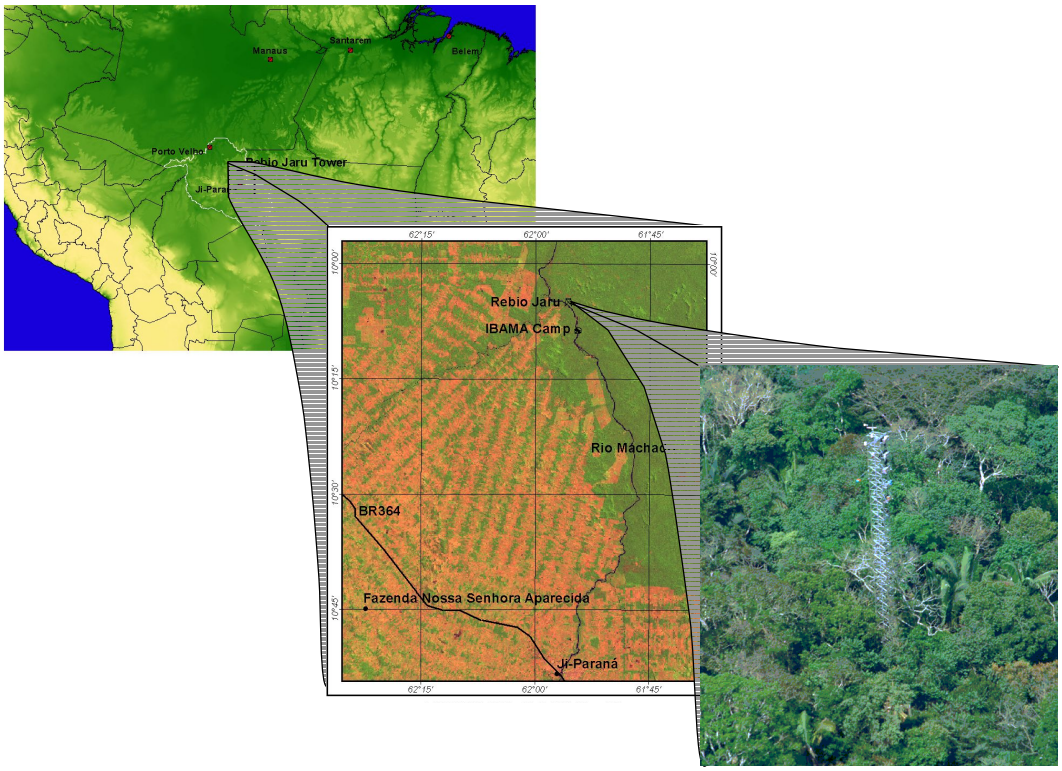

Fig. 1. Map and satellite image indicating the location of the LBA-EUSTACH sites Reserva Biológica Jarú (RBJ), Fazenda Nossa Senhora Aparecida (FNS), and the IBAMA camp in Rondônia. The tower site at RBJ is shown in the right image.

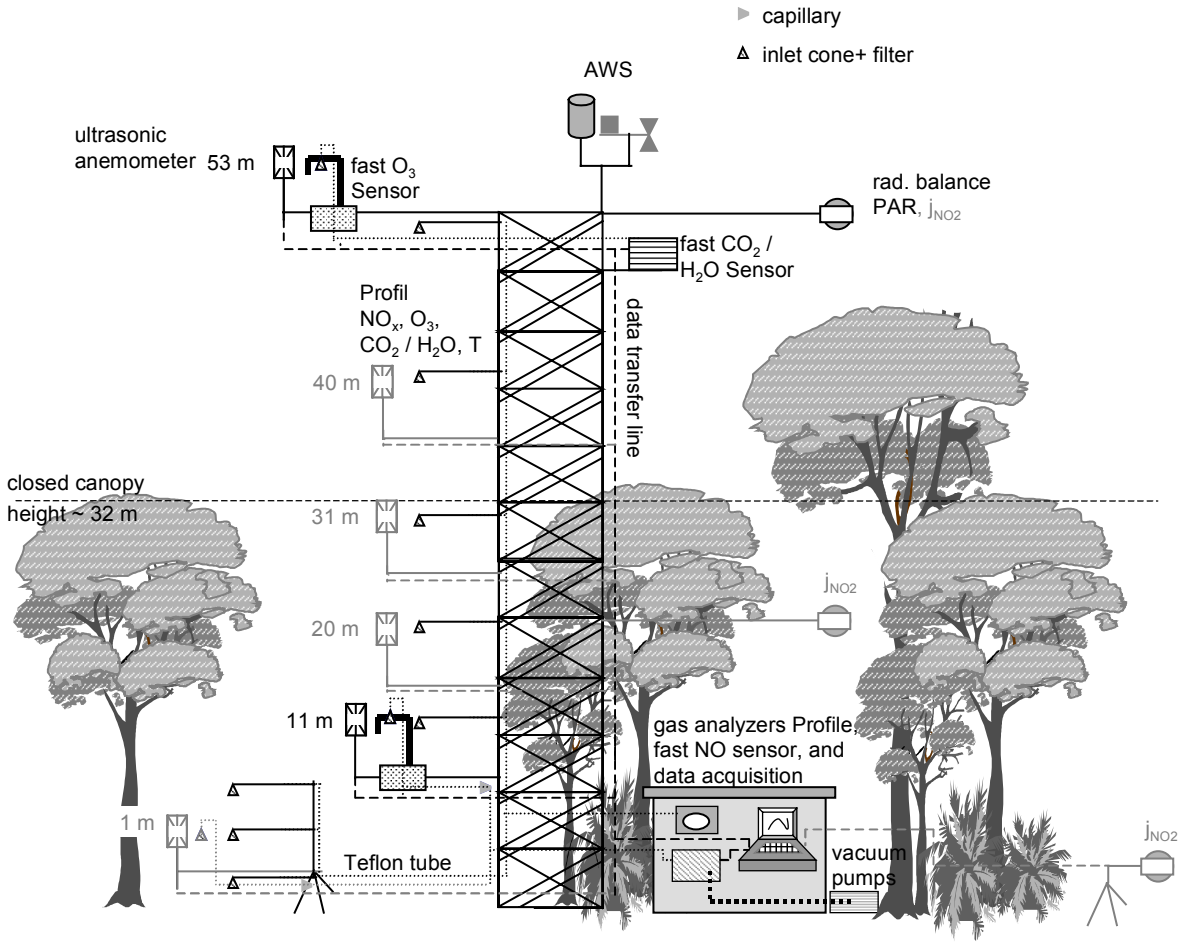

Fig. 2. Scheme of the cumulative experimental setup of the tower site at the Reserva Biológica Jarú (RBJ) during LBA-EUSTACH 1 and 2 campaigns. Periodically performed measurements are displayed in light gray (e.g. a 3rd sonic anemometer which was alternately operated at different heights)

2.2 *Instrumentation*

An aluminum scaffolding tower of 52 m height (see Fig. 1) erected in 1991 (Gash et al., 1996) was the main platform for the measurements conducted at the site RBJ. Fig. 2 and Fig. 3 show a comprehensive scheme of the experimental setup and the operation periods during the LBA-EUSTACH campaigns, respectively.

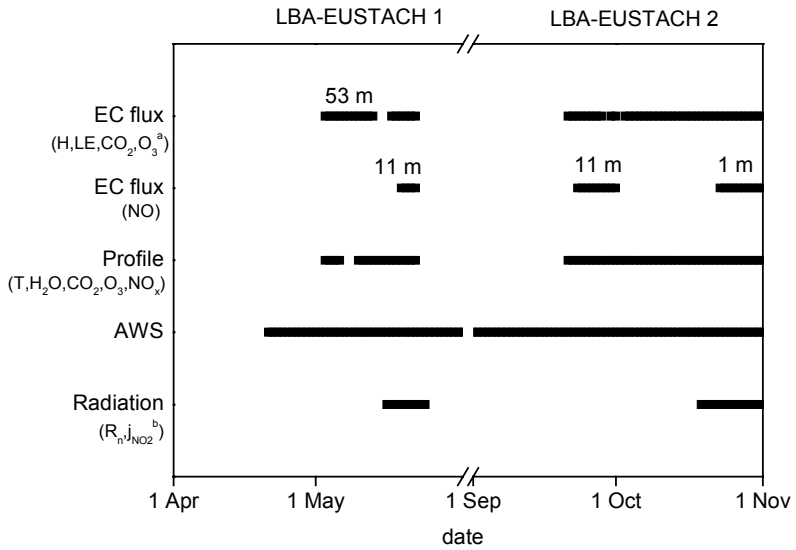

Fig. 3. Operation periods for different measuring systems at the RBJ tower during LBA-EUSTACH 1 and 2 campaigns. [a] Eddy covariance measurements of O_3 flux were just performed until 20 October1999. [b]Photolysis frequency j_{NO2} was measured at different heights (see Section 2.2.3).

2.2.1 Turbulence and fast Trace Gas Measurements

Fluctuations of the three wind velocity components (u, v, w) and virtual temperature (T_v) were continuously measured at 53 m (= 1.33 h) by a sonic anemometer (Gill Instruments, Solent Research 1012 K55, UK) mounted on a boom extending 4 m horizontally. High-frequency measurements of H_2O, CO_2, and O_3 mixing ratios were simultaneously performed at 1.33 h. For the H_2O and CO_2 measurements a closed-path differential infrared absorption analyzer (LI-COR LI-6262, USA) with a nominal response time of 0.1 s was used (e.g. Ammann, 1999; Aubinet et al., 2000; Moncrieff et al., 1997). The inlet of the air sampling system, consisting of a small funnel to keep out liquid water, was attached to the horizontal boom 20 cm from the head of the sonic anemometer. A 6.4 mm TEFLON® tube (inner diameter: 4.35 mm) of 8 m length connected the inlet through a 1 µm pore size filter (Gelman Acro 50) to the LI-6262 located in a ventilated housing 2 m below. A constant flow rate of about 7 L min^{-1} (turbulent flow) was provided by a combination of a mass flow meter (MKS 358C, Germany) and a rotation pump (Brey G12/07-N, Germany) downstream of the analyzer. The resulting lower pressure in the measuring cell of the analyzer was recorded by a piezoresistive pressure transducer (Data Instruments XT, USA) and considered for the calculation of CO_2 and H_2O mixing ratios together with the internal LI-6262 cell temperature. The analyzer was operated in the absolute mode with the reference cell connected to a closed air circuit containing a scrubber column (soda lime + $Mg(ClO_4)_2$).

The analytical basis of the fast O_3 analyzer (GFAS, Germany) is a surface chemi-luminescence reaction of O_3 with a marin dye layer on an aluminum plate in the sample air stream. The analyzing principle is described by Güsten et al. (1992), Güsten and Heinrich (1996) and Ammann (1999). The sensor was directly attached under the boom of the sonic anemometer. The sampling air was led to the O_3 analyzer by a tube of 0.5 m length and an inner diameter of 0.02 m. To prevent flow distortion by the tube, the inlet has been separated by 0.30 m from the head of the sonic anemometer. Turbulent flow in the tubing was ensured by a micro fan of the O_3 analyzer, maintaining a flow rate of ~ 100 L min^{-1}. The response time of the O_3 analyzer is well below 0.1 s (Ammann, 1999). The instrumental sensitivity of the O_3 analyzer was relative low from time to time, most likely caused by the extremely humid tropical environment.

All high-frequency data were sampled at 20.8 Hz. The trace gas signals were fed into the built-in analogue-to-digital converter of the sonic anemometer. The data were transferred via serial interfaces to a laptop computer in an air-conditioned shelter at the tower base.

For calibration purposes, the fast H_2O, CO_2, and O_3 measurements were referenced to their corresponding mixing ratios measured by the profile system at the same height.

2.2.2 Profile Measurements

Vertical profiles of H_2O, CO_2, O_3, NO, and NO_2 mixing ratios were measured above and throughout the canopy. The air sampling system consisted of eight 6.4 mm TEFLON® tubes connecting the inlets at 0.3 m, 1.0 m, 4.0 m, 11.3 m, 20.5 m, 31.3 m, 42.2 m, and 51.7 m to the analyzers in the shelter at the tower base. The individual tubes were bundled up in two opaque insulated main pipes, which were heated just above environmental air temperature to prevent condensation in the tubing system. All inlets at heights up to 4 m above ground were attached to a separate tripod located 15 m northeast of the tower, where the surrounding area was closed off to minimize soil disturbance. All tubes were continuously flushed through a purging pump and air from all heights was sequentially sampled by a TEFLON®valve manifold. Past the manifold the inlets to each trace gas analyzer were branched off from the main sampling stream. H_2O and CO_2 were sampled by a second LI-6262 analyzer, which was regularly calibrated by a dew point generator (LI-COR LI-610, USA) and gas standard cylinders in the case of CO_2. O_3 mixing ratios were measured with a UV absorption analyzer (Thermo Instruments TE49C, USA). For NO, and NO_2 a gas phase chemiluminescence analyzer (ECO Physics CLD 780 TR, Switzerland) combined with a photolytic converter (ECO Physics PLC 760, Switzerland) was employed (see Rummel et al., 2002). A gas-phase titration unit, which contains a UV lamp as O_3 source (ANSYCO SYCOS K/GPT, Germany) was used together with zero air and NO cylinder standards for combined O_3, NO, and NO_2 calibrations.

Two complete cycles of sequentially sampled profile data have been averaged to obtain corresponding half-hour data sets of vertically resolved H_2O, CO_2, O_3, NO, and NO_2 mixing ratios. Within one cycle, the dwell time at each height was 1.5 min with 30 s rejected because of adaptation processes. Due to different tubing length the delay times within the sample lines varied from ~1 s up to ~8 s from the lowest to the highest level. Mixing ratios of O_3, NO, and NO_2 were corrected for the gas-phase reaction $NO + O_3 \rightarrow NO_2 + O_2$ occurring within the tubes depending on the corresponding delay time (Beier and Schneewind, 1991). For data recording and controlling of the trace gas profile system, a laptop computer, equipped with a data acquisition device (National Instruments DAQPad-1200, USA) was used.

Air temperature profiles were determined by fine wire thermocouples (Omega, USA) recorded by a data logger / multiplexer system (Campbell 21X and AM25T, USA).

2.2.3 Measurement of Mean Meteorological Quantities and NO_2 Photolysis Frequency

During both LBA-EUSTACH campaigns an automatic weather station (AWS) above the forest canopy was continuously measuring air temperature *T* and relative humidity *rh* (Rotronic MP300, Switzerland), wind speed *ws* and direction *wd* (Young 05103-5, USA), precipitation (Campbell ARG100, USA), hydrostatic pressure *p* (Vaisala PTA427, Finland), and incoming short wave radiation S_R (LI-COR LI-200SZ, USA) at 53 m height.

At the end of both campaigns, net radiation R_n and the NO_2 photolysis frequency j_{NO2} were measured for a few days at 51.7 m height. R_n measurements were made by net radiometers during LBA-EUSTACH 1 (REBS Q6, USA) and LBA-EUSTACH 2 (DR Lange, Germany). For the remaining time periods the R_n dataset was complemented by R_n measurements from a neighboring tower site, 700 m northeast from the site here (Andreae et al., 2002). The NO_2 photolysis frequency was measured by a selective radiation sensor (Meteorologie Consult, Germany). The short periods were used to derive relationships between j_{NO2} above the forest and the simultaneously measured short wave radiation S_R, which was available for the whole experimental periods of LBA-EUSTACH 1 and 2. In addition to the measurements above the forest, j_{NO2} was also measured within the canopy at 22 m and 1 m height during LBA-EUSTACH 2. The attenuation of j_{NO2} with decreasing height below the canopy top was calculated with an exponential decay function fitted to the measurements made at these two heights.

2.2.4 Branch Cuvette Measurements

To measure ozone deposition at leaf scale a dynamic (flow-through) cuvette system was used, consisting of two identical enclosures with an inner TEFLON® surface (Volume ~ 75 l). The sample cuvette was containing the end of the branch under investigation, the

corresponding reference cuvette was empty to exclude artifacts caused by material properties. Both cuvettes were continuously flushed with an ambient air flow rate of about 40 L min^{-1}. A TEFLON® propeller provided well mixed conditions within the cuvettes (see Gut et al., 2002b). The system was mainly used to determine the exchange of volatile organic compounds VOCs and to investigate plant physiological parameters like transpiration and assimilation rates. A detailed description of these measurements and the system is given by Kuhn et al. (2002b) and Rottenberger et al. (2004). During the late LBA-EUSTACH 2 experiment an ozone sensor (Model 1003, Dasibi Environmental Corp., USA) was attached to the system probing alternately air from the branch and reference cuvette for 10 min each (sampling flow rate of ~1 L min^{-1}). From each 10 minute interval the first two minutes were discarded to avoid adaptation artifacts after the switching process. The average O_3 mixing ratio of the reference cuvette directly before and after probing the branch cuvette was used for the mixing ratio difference to calculate the ozone deposition flux at leaf level (see Eq. (11)).

3 Methods

3.1 Eddy Covariance Data Processing and Rejection Criteria

After an intensive spike and error control at the raw data, half hour averages of heat and trace gas fluxes were calculated. Time lags between the signals from sonic anemometers and trace gas analyzers were estimated by determining the maxima of correspondent covariance functions within preset time lag intervals. A linear detrending was applied to the time series followed by a two axis rotation of the wind field coordinates such that the average values of lateral and vertical wind speed equal zero (e.g. Aubinet et al., 2000). Currently the planar fit coordinate system by Wilczak et al. (2001) which is oriented at the terrain following streamlines (long term average of vertical wind speed is zero instead of the individual half hour values) is recommended by the FLUXNET community. A recalculation of the fluxes in this coordinate system to estimate the effect on the LBA-EUSTACH data is planed in future. Trace gas fluxes were corrected according to Webb et al. (1980) to account for flux contributions caused by air density fluctuations from sensible and latent heat exchange. Within sufficiently long inlet tubing of closed path analyzers temperature fluctuations are damped out (Leuning and Judd, 1996; Wienhold et al., 1994) making only the humidity correction necessary. But the short inlet system of the O_3 analysers is just damping a certain fraction of the temperature fluctuations (Ammann, 1999) which has to be considered adequately. High frequency flux loss caused by physical properties of sensors, setup, and data acquisition was corrected according to Moore (1986), Zeller et al. (1989), Lenschow and Raupach (1991), and Horst (2000), using the semi-empirical spectral formulations of Kaimal et al. (1972). The linear detrending was used in

order to keep the connected flux loss at low frequencies limited. It was estimated with a transfer function after Kristensen (1998) (see Aubinet et al., 2000) to about 6% during daytime. Due to the poor determination of the used model spectra in the low-frequency part for unstable daytime conditions, this correction was not applied. (for further discussion of low frequency flux loss, see Section 3.2).

To avoid influence of rapidly changing environmental conditions on the analysis, a stationarity test slightly modified from Foken and Wichura (1996) was applied to all derived variances and covariances. Data were rejected if the (co)variance averaged over 30 minutes deviated more than 100% from the average of the fluxes obtained from 10-minute subintervals (instead of 5-minute subintervals proposed by Foken and Wichura (1996)). Here, the unstable stratification within the tropical boundary layer and the occurrence of coherent turbulent structures are taken into account by the longer subintervals. The intension is to include the sometimes almost periodically occurring coherent turbulent structures (see Rummel et al. (2005)) in the analysis, whereas non-stationary conditions by single large scale events are excluded. Despite the longer subintervals the deviation limit of 100%, which is suggested by Foken et al. (2004) as an upper limit for flux data which are intended to be used for the determination of average values, is applied here. Two additional data rejection criteria were also considered. The first one considers instrumental failures, which Solent Research sonic anemometers show during calm conditions. At a lower limit of the friction velocity ($u_{*crit} \approx 0.01$ m s^{-1}) the corresponding momentum flux became systematically positive. Therefore all values below u_{*crit} were excluded. The second criterion concerns periods with disturbed upwind fetch. A detailed discussion of that point will be presented in the context of corresponding footprint analysis (Section 4.1.2)

After application of all rejection criteria and exclusion of instrumental failures the overall daytime (night time) data availability was reduced to 51% (35%) and 69% (50%) during the LBA-EUSTACH 1 and LBA-EUSTACH 2 experimental periods, respectively.

For the data set of the FNS pasture site similar rejection criteria were applied to make the measurements comparable to the results of the RBJ forest site. Beside the exclusion of instrumental failures, those time periods were rejected when the friction velocity was below $u_{*crit} \approx 0.01$ ms^{-1} or the upwind fetch was disturbed (see Kirkman et al., 2002). After the re-evaluation the daytime (night time) data, the data availability was 80% (47%) and 35% (25%) during the LBA-EUSTACH 1 and LBA-EUSTACH 2 experimental periods, respectively.

3.2 Energy Balance

Turbulent fluxes were determined in a way usually as usually done by the FLUXNET community (Aubinet et al., 2000; Baldocchi et al., 2001). The energy balance closure,

$$LE + H = R_n - G - S \quad (1)$$

as a method to assess the turbulent fluxes obtained by eddy covariance was recently investigated by Wilson et al. (2002) for 22 FLUXNET sites. The sum of the turbulent fluxes of latent and sensible heat ($LE+H$) from the vegetation surface is expected to be equivalent to all other energy sources and sinks within the air volume below. Here, R_n is the net radiation, G is the soil heat flux, and S is the volume integrated heat storage of air and biomass (assuming horizontal homogeneity). All remaining energy sources and sinks are supposed to be comparatively small. Relating half hourly averages of $LE+H$ to R_n-G-S by linear regression Wilson et al. (2002) obtained a slope range between 0.55 and 0.99, with a mean of 0.79 for temperate and boreal vegetation types (mainly forest). In order to reduce random error influence, these values are calculated by the "reduced major axis" method (RMA), the geometric mean of the regression slopes obtained by using both quantities alternately as dependent as well as independent variable. A similar imbalance missing between 10% and 30%, was found for three tropical forest sites in central Amazonia (Araujo et al., 2002; Fitzjarrald et al., 1988; Malhi et al., 1998). An exception represents a short experiment by Shuttleworth at al. (1984) who got a reasonable closure within 5% for the cumulative energy budget. Applying the RMA Method, corresponding regression values of 0.64 and 0.75 for the LBA-EUSTACH 1 and LBA-EUSTACH 2 experiments were obtained, which are well within the range observed for tall forest canopies.

Several possible reasons for that systematic gap in the surface energy balance are conceivable. For a survey and discussion see e.g. Foken (1998) and Wilson et al. (2002). Within the frame of the present study the focus is on those topics which may also be relevant for the determination of ozone fluxes. Beside possible instrumental problems, these are mainly related to (i) the way of data analysis for turbulent flux calculation and (ii) considering additional terms of the correspondent budget equation which may not be always negligible (see e.g. Baldocchi et al., 2000; Finnigan, 1999; Lee, 1998; Paw U et al., 2000). A re-evaluation of the long-standing discussion in micrometeorology about the adequate averaging period, which separates the turbulent and mean part of the flow and defines also the streamline following coordinate system, was recently presented by Finnigan at al. (2003) (see also Sakai et al. (2001)). Basically, an adequate averaging period should include the time scales of all flux contributing processes. The results of Finnigan at al. (2003), obtained at three different forest sites, are indicative for substantial flux contributions from atmospheric motion which occur at time periods longer than the standard averaging times of 15 min to 60 min. A successive increase of the averaging and rotation interval from 15 min to 4 h for the data of a forest site at central Amazonia resulted in a substantial improvement of the energy balance closure from originally 70% to about 100% (see also

Malhi et al., 2002). The quantitative increase of the fluxes was found to be site specific, depending on terrain complexity and environmental conditions. A scale analysis of turbulent fluxes by von Randow et al. (2002) from a tower site just 700 m northeast of the RBJ site has also indicated low frequency flux contributions during different experimental periods. Hence the potential improvement of the energy balance closure by using longer averaging periods and omitting trend removal, was investigated specifically for the LBA-EUSTACH 1 experiment, since the energy imbalance was larger during this first experiment. For heat fluxes, averaging times of 1 h, 2 h, and 4 h were used. The obtained RMA values are 0.69, 0.71, and 0.67, i.e. increasing the averaging time from 30 min up to 2 h results in an improvement of the energy balance closure of hardly 10%. A further increase up to 4 h entailed even in a decreased RMA value. Here one has to keep in mind the higher statistical uncertainty of the regression which comes along with a reduced sample size. Nevertheless, the rather poor closure of the energy balance at RBJ seems to have mainly other causes.

An additional point of uncertainty especially in tropical forest canopies with large amounts of biomass and incoming solar radiation is the storage term. Because no direct biomass temperature measurements were carried out, the storage term in Eq. (1) was estimated by a parameterisation according to Moore and Fisch (1986) derived for a central Amazonian forest canopy, which is based on air temperature and humidity measured above the vegetation.

A further point concerns the application of closed path measuring systems for the determination of water vapor fluxes. Baldocchi et al. (2001) reported from side by side comparison of closed- and open-path systems which showed 20% underestimation of the flux by the former, caused by adsorption and desportion of water vapor within the intake tubing.

This point as well as the storage uncertainty would not affect ozone flux estimates, whereas an underestimation of low frequency flux contributions would. Since longer averaging times did not result in a substantial improvement of the energy balance and a high temporal resolution is desirable for the investigation of the diurnal course of the ozone budget (especially during transition times), 30 min averages were maintained for the analysis in this study.

3.3 Instrumental Noise

Flux measurements are always affected by instrumental noise. Measurements of trace gas fluxes by eddy covariance are usually more influenced by the noise level of the gas sensor than by the noise of the corresponding sonic anemometer. Due to the fact that instrumental noise is usually characterized as “ ideal white noise” which does not correlate with the vertical velocity fluctuations, it has no systematic effect on the trace gas flux. But the associated statistical error directly affects the

magnitude of the minimal resolvable flux. A procedure offered by Lenschow and Kristensen (1985) was used to calculate the effective detection limit for the ozone flux which results in ~ 0.45 nmol m^{-2} s^{-1}. This has to be seen as an upper limit, since the worst case sensitivity of the O_3 analyzer (mentioned above) have been taken into account. The corresponding limits for latent heat and CO_2 fluxes were 0.2 W m^{-2} and 0.18 µmol m^{-2} s^{-1}, respectively.

3.4 Ozone Budget

Measuring turbulent fluxes of reactive trace gases like ozone above tall vegetation canopies makes it necessary to determine additional terms of the corresponding mass balance equation, in order to relate the measurements to the actual exchange at the plant-atmosphere interface. Assuming horizontal homogeneity (assuming advection to be negligible and single point measurements to be representative for the necessary spatial average in plant canopies (see Coppin et al., 1986; Raupach and Shaw, 1982)), the O_3 mass balance equation is given by (2):

$$F_{O_3}(z_m) + \frac{\partial}{\partial t}\int_0^{z_m}[O_3](z)\,dz = \int_0^{z_m} Ch_{net}(z)\,dz + \int_0^{z_m} D_S(z)\,dz + F_{O_3}(0) \qquad (2)$$

where $F_{O_3}(z_m)$ is the turbulent ozone flux at the measuring height z_m = 53 m. $F_{O_3}(0)$ is the soil deposition flux at the forest floor on the basis of measurements by Gut et al. (2002b). The second term at the left side represents the storage which is the vertically integrated temporal mixing ratio change within the considered air column between the soil surface and the measuring height. $D_S(z)$ is the actual deposition to plant surfaces, the main interest here. $Ch_{net}(z)$ represents the height dependent net effect of chemical processes, the difference between chemical production and loss rates. Based on the available mixing ratio measurements, $Ch_{net}(z)$ is limited to the photochemical triad of NO-NO_2-O_3:

$$NO_2 + h\upsilon \xrightarrow{j_{NO2}} NO + O \qquad (3)$$

$$O + O_2 \xrightarrow{k_1} O_3 \qquad (4)$$

$$NO + O_3 \xrightarrow{k_2} NO_2 + O_2 \qquad (5)$$

The second reaction (4) is very fast and can be considered as immediate. Therefore in this simplified system O_3 is formed as a direct result of NO_2 photolysis by solar radiation ($\lambda \leq 420$ nm). The oxidation of NO by O_3 (5) is reforming NO_2. The photolysis frequency j_{NO2} was determined as described in Section 2.2.3. The reaction rate of (5) was calculated as $k_2 = 17/T \times \exp(-1450/T)$ in units of ppb^{-1} s^{-1}. The equation system which is used for the calculation of $Ch_{net}(z)$ at each layer is described in Meixner et al. (1997). Despite their probable importance for ozone formation above the tropical forest (e.g. Jacob and Wofsy, 1988; Jacob and Wofsy, 1990), the influence of peroxy radicals RO_2 was not considered, due to the complete lack of experimental data about their mixing ratios.

3.5 Canopy Scale Resistances

For trace gases, like ozone, which are (i) exclusively depositing, (ii) reveal a zero substrate mixing ratio (cf. Laisk et al., 1989), and (iii) for which a negligible net effect of sources and sinks between the surface and the reference height z_m can be assumed, the dry deposition velocity (v_d) concept can be applied:

$$v_d = -\frac{F_{O_3}(z_m)}{[O_3](z_m)} \tag{6}$$

Normalizing the flux F_{O_3} by the mixing ratio [O_3] at the reference height enables the investigation of parameters affecting deposition rates independent of ambient mixing ratios. It also makes deposition rates measured above different surfaces comparable. According to the "big leaf" multiple resistance approach (e.g. Hicks et al., 1987), the surface part of dry deposition can be separated from its aerodynamic contributions. The big leaf concept assumes that all contributing sinks (although only referring to O_3 in the following, the approach can be adequately applied to other scalars) of a vegetation canopy can be represented by a single sink at the conceptual surface of the "big leaf" at the height $d + z_{0,O_3}$. Here d represents the displacement height of the canopy and z_{0,O_3} the roughness length for O_3 (see below). The assumption is that the reciprocal of v_d, the total resistance R_t to ozone transfer between z_m and the vegetation, consists of a serial alignment of the aerodynamic resistances R_a and R_b, and the bulk canopy resistance R_c:

$$\frac{1}{v_d} = R_t = R_a + R_b + R_c \tag{7}$$

R_a is the atmospheric resistance, characterizing the turbulent ozone transfer between z_m and the height $d + z_0$:

$$R_a = \frac{1}{k u_*}\left(\ln\left(\frac{z-d}{z_0}\right) - \Psi_{O_3}\left(\frac{z-d}{L}, \frac{z_0}{L}\right)\right) \tag{8}$$

Here z_0 the average roughness length for momentum was determined together with d by a formulation of Raupach (1994), which relies on canopy height and leaf area index (*LAI*). Roughness length was determined to 1.3 m and displacement height to 34 m. Furthermore, the dimensionless von Kármán constant k equals to 0.4, is the, u_* is the friction velocity, L is the Obukhov length, and Ψ_{O_3} is the integrated form of the universal function (stability correction) for O_3 assumed to be equivalent to that for sensible heat determined after Paulson (1970). R_b is an "excess" resistance (Baldocchi et al., 1987) introduced because in the quasi laminar boundary layer close to surfaces mass and energy transfer are dominated by molecular properties of the air, whereas momentum transfer is influenced by the pressure drag:

$$\begin{aligned} R_b &= \frac{1}{B u_*}\left(\frac{Sc}{\mathrm{Pr}}\right)^n \\ &= \ln\left(\frac{z_0}{z_{0,h}}\right)\frac{1}{k u_*}\left(\frac{Sc}{\mathrm{Pr}}\right)^n \end{aligned} \tag{9}$$

here the sublayer-Stanton number (B) is a measure of the difference in the transport of momentum and sensible heat (e.g. Owen and Thomson, 1963). The Schmidt number (*Sc*) is

about 1.07 for O_3 and the Prandtl number (Pr) is 0.72. Their ratio accounts for transfer differences between sensible heat and ozone in the quasi laminar boundary layer between the height of the virtual momentum sink ($d + z_0$) and the virtual height $d + z_{0,h}$ where the temperature reaches its surface value. As pointed out by Kramm et al.(1995; 2002) the usage of the relation $k / B = \ln (z_0 / z_{0,h})$ (cf. Chamberlain, 1966), which introduces a roughness length for heat, is limited to aerodynamically rough surfaces with $z_0 >> z_{0,h}$. This requirement is most likely fulfilled above the tropical forest canopy at the RBJ site. Formulation (9) was used with parameters suggested by Hicks et al. (1987) ($\ln (z_0 / z_{0,h}) = \ln (z_0 / z_{0,O_3}) \approx 2$ and $n = 2/3$), which is, because also used by Kirkman et al. (2002) at the FNS pasture site, advantageous for comparison purposes.

The bulk canopy resistance R_c determined as the difference of R_t and the sum of aerodynamic resistances ($R_a + R_b$) contains the contributions of all single deposition pathways occurring within the canopy. These may consist of (i) the transfer through the stomatal apertures of leafs and subsequent transfer into the mesophyll tissue, (ii) transfer to the leaf cuticle, (iii) deposition to other plant surfaces (e.g. bark), and (iv) to the soil surface.

To get an independent estimate of the canopy bulk stomatal resistance (R_s) a modified Jarvis-type model Jarvis (1976) was employed. Wright et al. (1996) optimised the model for the Jaru site with canopy resistance values determined by the Penman-Monteith formulation (Monteith and Unsworth, 1990). In contrast to the original model of Jarvis (1976) the modified version bases on climatic variables from a reference height above the canopy, assuming that the conditions at canopy height could be adequately described by the measurements above (see also Dolman et al., 1991). Wright et al. (1996) used a non-linear least square optimisation to calibrate the product of maximal stomatal conductance $G_{s,max}$, LAI, and functional relationships for specific humidity deficit SHD, temperature T, and short wave radiation S_R:

$$R_{s,O_3} = \frac{D_{H_2O}}{D_{O_3}} \left[G_{s,\max} LAI \, f(SHD) f(T) f(S_R) \right]^{-1} \tag{10}$$

To obtain the bulk stomatal resistance for ozone the original formulation of Wright et al. (1996) was calculated with data measured by the automatic weather station at the tower top and scaled by the ratio of the corresponding molecular diffusivities D_{H_2O} / D_{O_3}. For a description of the functional relationships and parameters of (10) see Appendix.

3.6 Leaf Scale Resistances

Measurements with the dynamic cuvette system (see Section 2.2.4) result in a so-called leaf scale resistance of ozone deposition. This resistance was estimated from the leaf level deposition flux $F_{O_3}^L$. $F_{O_3}^L$ was calculated according to:

$$F_{O_3}^L = \frac{([O_3]_S - [O_3]_R)Q}{A_L} \quad (11)$$

from the measured mixing ratio difference between the sample and the reference cuvette ($[O_3]_S$ - $[O_3]_R$), the corresponding flush rate Q, and the enclosed leaf area A_L. For the *Hymenaea courbaril* L. $A_L = 0.0986$ m^2 was determined by a calibrated scanner system. To distinguish leaf scale resistances from canopy scale resistances, the former are denoted by small letters in the following. The leaf resistance for ozone r_{L,O_3}, the reciprocal of the corresponding deposition velocity v_d^L, is determined as the quotient of the mixing ratio within the sample cuvette and $F_{O_3}^L$:

$$r_{L,O_3} = \frac{1}{v_d^L} = -\frac{[O_3]_S}{F_{O_3}^L} \quad (12)$$

To separate the different contributions to r_{L,O_3} the leaf resistance model according to Baldocchi et al. (1988) was considered:

$$r_{L,O_3}^m = \left(\frac{1}{r_{b,O_3} + \frac{D_{H_2O}}{D_{O_3}} r_s + r_{m,O_3}} + \frac{2}{r_{b,O_3} + r_{ct,O_3}} \right)^{-1} \quad (13)$$

The modeled leaf resistance r_{L,O_3}^m distinguishes two deposition pathways, through the stomata and – in parallel to that – through the leaf cuticula. The first part is characterized by three resistances in series: the leaf boundary layer resistance r_{b,O_3}, the stomatal resistance r_s scaled by the ratio of molecular diffusivities of H_2O and O_3, and the mesophyll resistance r_{m,O_3}. The second part of r_{L,O_3}^m consists of the sum of r_{b,O_3} and the cuticular resistance r_{ct,O_3}. The numerators of both quotients at the right hand side of Eq. (13) base on the assumption, that tropical trees, like many deciduous temperate species are mainly hypo-stomatous (stomata are only at one side of the leaf). For the cuvettes used here, Gut et al. (2002b) determined the leaf boundary resistance r_{b,O_3} to 30 s m^{-1}. The stomatal resistance r_s was calculated according to von Caemmerer and Farquar (1981).

4 Results and Discussion

Most results are given in terms of mean diel variations. For that medians were used because they are less affected by extreme outliers than arithmetic averages.

4.1 Environmental Conditions

4.1.1 Climate and General Meteorology

Fig. 4 shows the 10 year average distribution of monthly rainfall from the standard weather station closest to the RBJ site (Gash et al., 1996). A similar 30 year average distribution is presented by Andreae et al. (2002). Rondônia at the south-westerly border of Amazonia is characterized by a distinct dry season (June to August). Most of the rain falls from December to March. Also shown in Fig. 4 is the monthly rainfall during the two LBA-

EUSTACH campaigns measured above the RBJ forest. The values closely correspond to the 10 year data with somewhat less rain in May and a wetter September. Fig. 4 also indicates that the two campaigns were carried out during the wet-to-dry and the dry-to-wet season transition period, respectively.

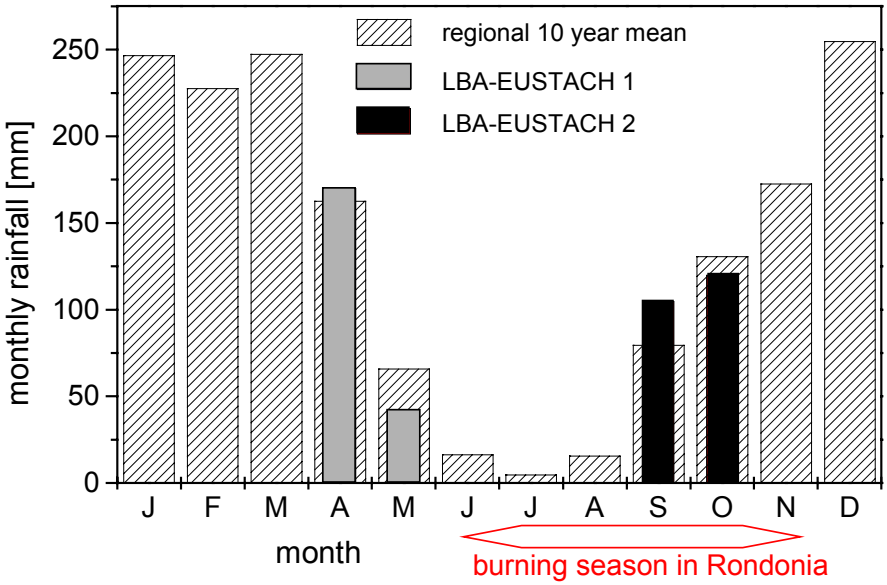

Fig. 4. Ten-year average monthly rain fall distribution from a standard weather station close to RBJ (Gash et al., 1996) and monthly rain fall measured during both experimental periods LBA-EUSTACH 1 and 2 (April-May and September-October 1999, respectively) at RBJ.

The latter was well within the time period of local biomass burning activities. With respect to climatic variables like incoming short wave radiation S_R, air temperature T, and specific humidity deficit *SHD,* the conditions during both transition experiments were rather characteristic for the preceding seasons.

The monthly average values of S_R, T, and *SHD* (measured at 53 m) for May 1999 (LBA-EUSTACH 1) are 16.7 MJ $m^{-2}day^{-1}$, 24.3 °C, and 2.5 g kg^{-1}, respectively, and are rather comparable to average values from January to March from the 2 year ABRACOS data set (end of 1991 to end of 1993) (Culf et al., 1996). These values are 16.4 MJ m^{-2} day^{-1}, 24.5 °C, and 2.4 g kg^{-1}, respectively, and are distinctively lower than the corresponding data for June (17.9 MJ m^{-2} day^{-1}, 25.4 °C, and 3.5 g kg^{-1}). The average S_R and T data of the period 21 September to 20 October 1999 (LBA-EUSTACH 2) are 19.9 MJ m^{-2} day^{-1} and 25.7 °C; they are almost identical to the October averages of the ABRACOS data, 19.8 MJ m^{-2} day^{-1} and 25.7 °C (Culf et al., 1996). The average specific humidity deficit during LBA-EUSTACH 2 is 5.2 g kg^{-1} and rather comparable to the 5 g kg^{-1} of the peak

dry season (July and August) of the ABRACOS data. That indicates, that the climatic conditions during LBA-EUSTACH 1 and 2 have been quite characteristic for the wet and dry season respectively.

The diel variation of mean S_R, T, SHD, and horizontal wind speed for both LBA-EUSTACH experiments is shown in Fig. 5. Incoming short wave radiation, air temperature, and specific humidity deficit show a considerable larger diel amplitude during LBA-EUSTACH 2, while horizontal wind speed exhibits only a weak diel variation during both experimental periods.

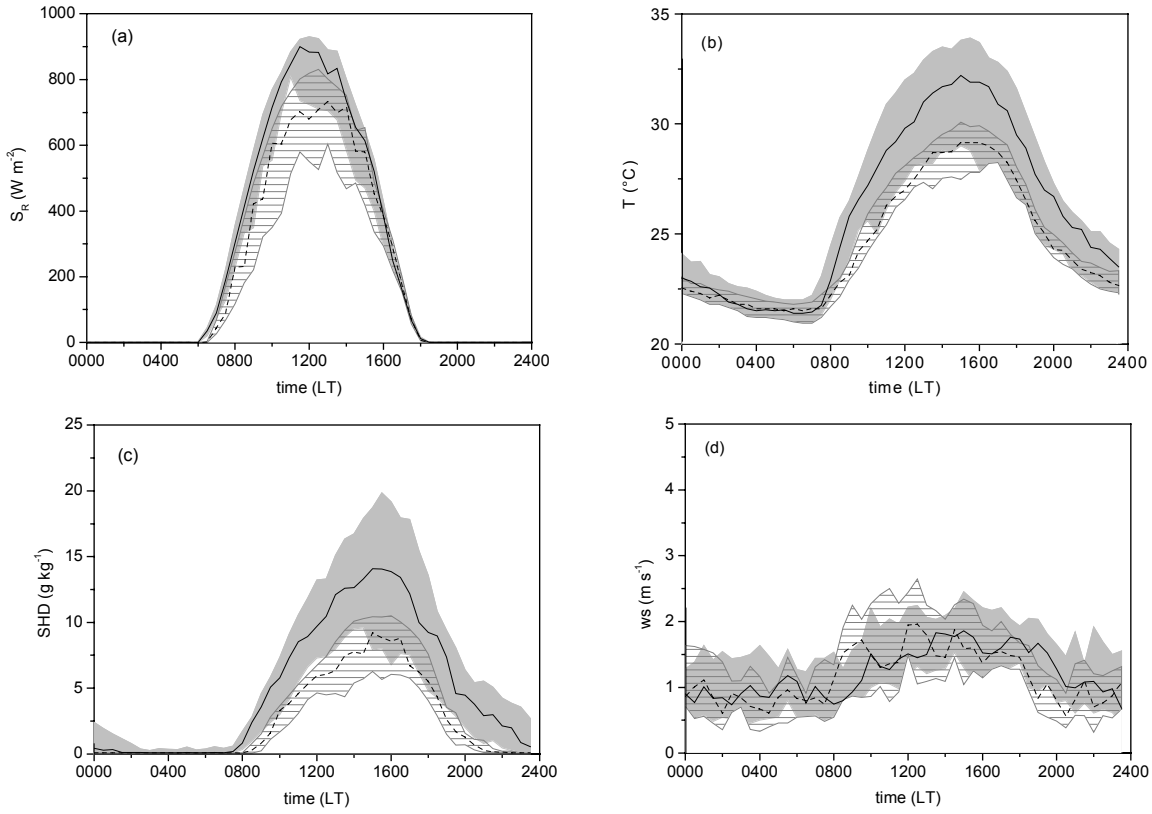

Fig. 5. Diel variation of mean (median) (a) incoming short wave radiation, (b) air temperature, (c) specific humisity deficit, and (d) wind speed measured on RBJ tower at 53 m. Medians (dashed black line) and inter quartile range IQR (gray hatched area) for LBA-EUSTACH 1; medians (black line) and IQR (light gray area) for LBA-EUSTACH 2.

4.1.2 Source Area Estimates

The vicinity of the Rio Machado (see Fig. 1) and the forest-pasture patches on the western side of the river makes a source area analysis for the flux measurements at the RBJ tower advisable. For that purpose the scalar Flux-Source Area Model (FSAM) after Schmid (1994; 1997) was used. The model determines numerically the upwind source area of a percentage P defined as the smallest possible area responsible for the contribution P to the flux measured by the sensors (i.e., the projected area of the fraction P of the total integrated source weight function). Like many Eulerian approaches the model also bases on atmospheric surface layer similarity assumptions (K-theory) and is therefore not intended for application in the roughness sublayer of forest canopies. Rannik et al. (2000) determined footprint (source weight) functions above a forest canopy with a Lagrangian stochastic model driven by parameterizations for turbulent flow within and above the canopy. According to their results for neutral stratification, including canopy turbulence and a leaf area weighted vertical source/sink distribution smears out the footprint function compared to surface layer flow above a source/sink level at displacement height. The effect decreases with increasing measuring height. Unfortunately no equivalent comparison was made for unstable stratification, the prevailing daytime conditions above the tropical forest. In a recent study (Rannik et al., 2003) the effect of stability on footprint functions was only discussed for a substance released from the forest ground. In contrast to these results, a comparison by Kaharabata et al. (1997) showed approximately agreement between the obtained source area dimensions after Schmid (1994) and the corresponding results from an modified surface layer approach according to Horst and Weil (1992). The approach of Horst and Weil (1992) was adjusted to tracer experiments conducted in the roughness sublayer of three boreal forests. Compared to this approach, the formulation according to Schmid (1994) seems to be a rather conservative one, which especially under unstable conditions tends to overestimate the source area dimensions. Considering the uncertainty of such tracer experiments and the results of the comparison by Rannik et al. (2000) the FSAM estimates might rather represent lower limits of the actual source area dimensions.

In this study, the 80% flux source areas were calculated separately for daytime (0600 LT to 1800 LT) and night time (1900 LT and 0500 LT) conditions. The results for LBA-EUSTACH 1 and LBA-EUSTACH 2 are shown in the form of two-dimensional frequency distributions in Fig. 6. The two-dimensional frequency distributions show how often each point in the terrain surrounding the tower has contributed to the corresponding 80%-source areas of any flux measured on RBJ tower at 53 m within these time intervals.

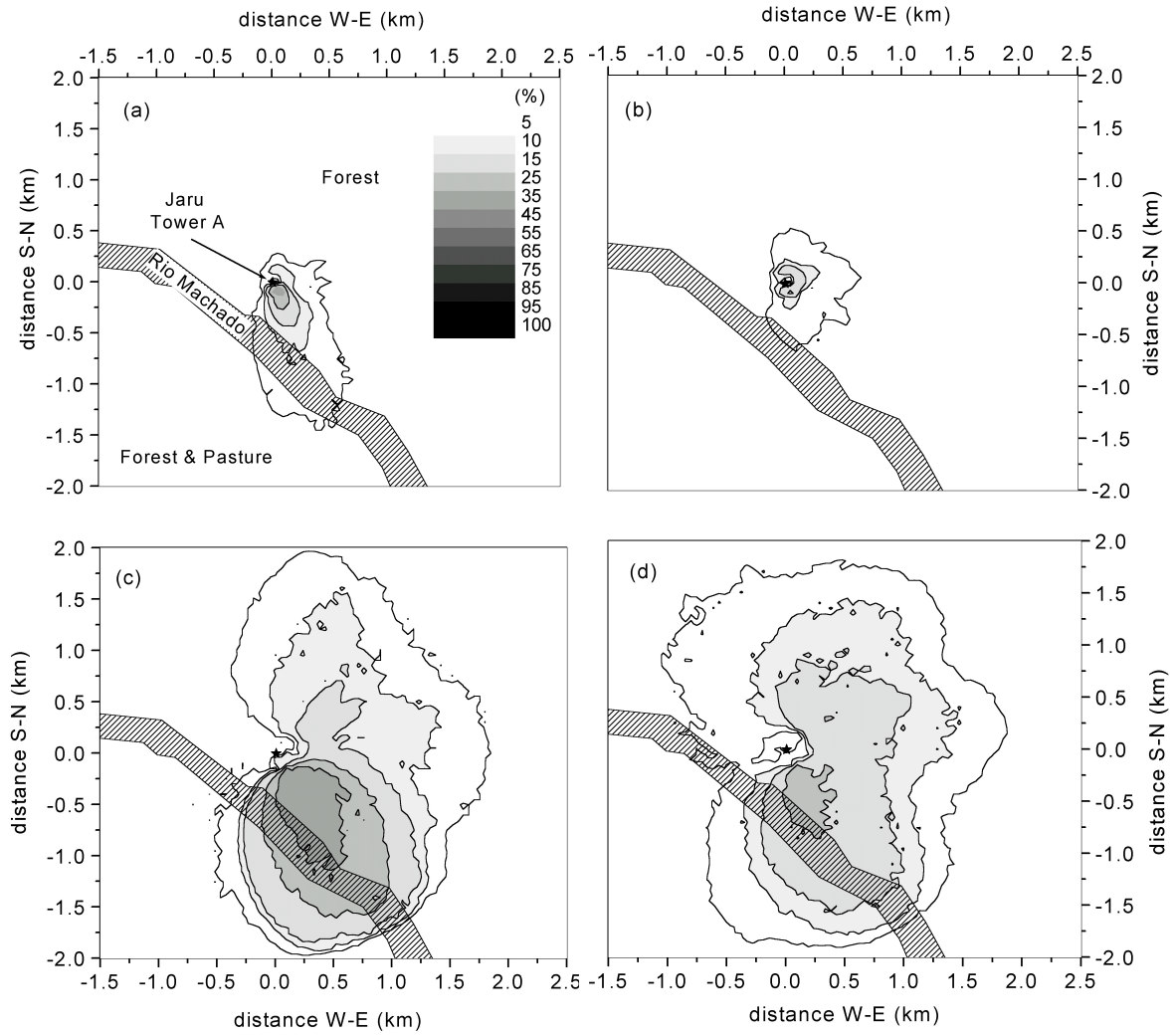

Fig. 6. Two dimensional frequency distributions (percent) showing how often each point in the terrain surrounding the tower was contributing to the 80% source area of any flux measured at the 53 m level of the RBJ tower. For LBA-EUSTACH 1 day (a) and night time (c) and LBA-EUSTACH 2 day (b) and night time (d). The river Rio Machado coordinates are from a Landsat TM image of August 1999 [G. A. Kirkman, personal communication]. The star denotes the position of the RBJ tower at (0 km; 0 km). In 1999, there was primary rain forest west of the river, while east of it a mixture a mixture of forest and pastures prevailed.

A common feature of both LBA-EUSTACH experimental periods is the clear dominance of easterly versus westerly wind components. During daytime, the unstable stratification ensured rather small source areas. For 90% of all daytime cases, the flux source area is not or barely influenced by the river. Those cases where source areas include parts of the river, occurred mainly in the early morning (just before sunset), when slightly stable stratification is still (already) prevailing. At night the situation is clearly

different. Due to the prevailing very stable stratification a significantly higher percentage of flux measurements is influenced by the Rio Machado and the forest/pasture vegetation mix west of it. During LBA-EUSTACH 1 (Fig. 6 (c)), the nighttime relative percentage of southerly winds with "river-affected" source area contribution is 35 - 40%, considerably higher than for LBA-EUSTACH 2. The LBA-EUSTACH 2 period is more characterized by a evenly distributed wind direction (Fig. 6 (d)).

Because nocturnal flux measurements during periods where wind directions from 150° - 300° were clearly influenced by surfaces different from primary rain forest, all corresponding data were excluded from the further analysis. On the other hand the contributions of these other surfaces to the flux source areas are rather low during daytime. Therefore only those data are excluded from the analysis where wind direction was from 225° - 280°. In this sector, flow distortion by the geometric structures of the scaffolding tower itself is expected to affect the turbulence substantially.

4.2 Seasonal Characteristics of Ozone Deposition

4.2.1 Mixing Ratio and Eddy Covariance Flux

Fig. 7 shows the diel variations of the mean ozone mixing ratio and the mean flux measured by eddy covariance at the top of the RBJ tower (51.7 m and 53 m respectively), 12 to 13 m above the effective canopy height *h*. As recently presented by Andreae at al. (2002), distinct differences especially in mixing ratio between both seasons are evident at RBJ.

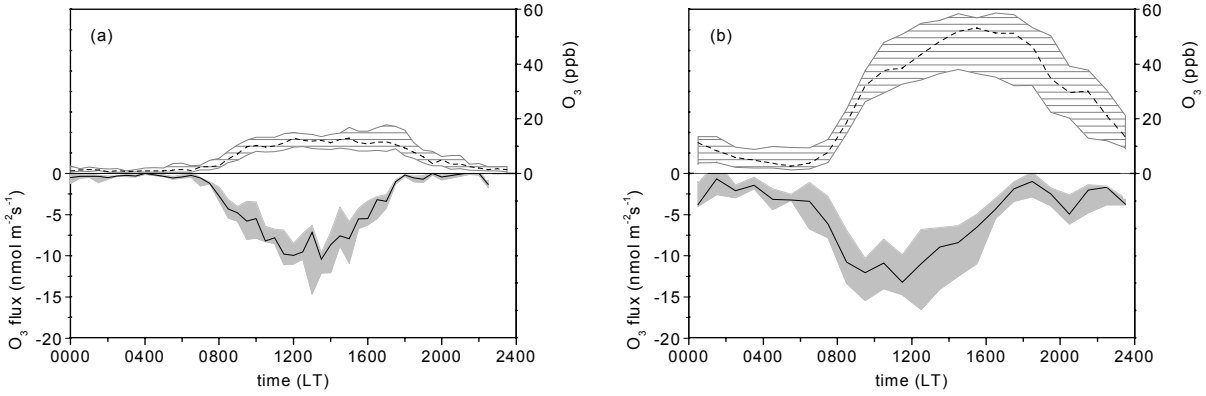

Fig. 7. Diel variation of mean (median) O_3 mixing ratio (median: dashed black line; inter quartile range (IQR): gray hatched area) and mean (median) O_3 flux (median: black line; IQR: light gray area) during LBA-EUSTACH 1 (a) and LBA-EUSTACH 2 (b). Mixing ratio and flux have been measured at RBJ tower at 51.7 m and 53 m, respectively.

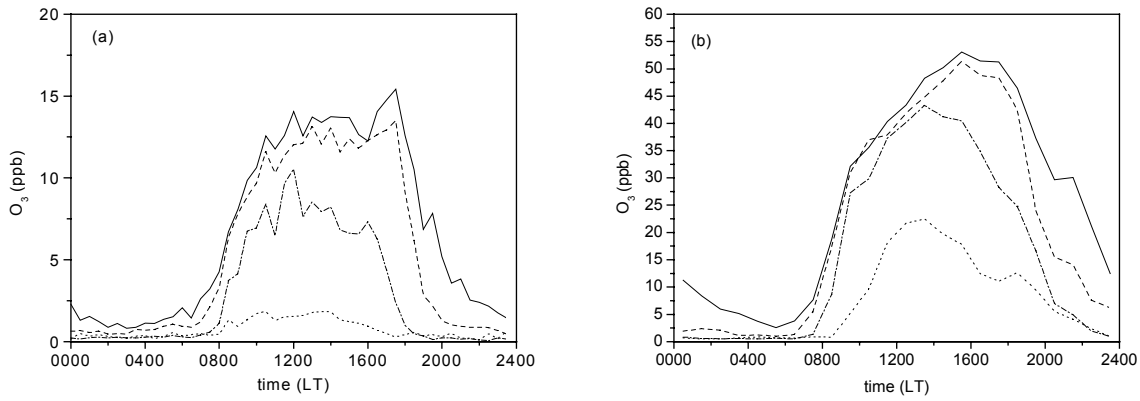

Fig. 8. Diel variation of mean (median) O_3 mixing ratio measured at 51.7 m (solid line), 31.3 m (dashed line), 11.3 m (dashed-dotted line), and 1 m (dotted line) during LBA-EUSTACH 1 (a) and LBA-EUSTACH 2 (b). Effective canopy height is ~ 40 m.

During the wet season, boundary layer ozone is mainly controlled by the convective input from the free troposphere, balanced by surface deposition and a weak net photochemical loss (Fan et al., 1990; Gregory et al., 1990; Jacob and Wofsy, 1990). Contrasting in the dry season, photo-chemical production, caused by massive biomass burning activities in the state of Rondônia and in the cerrado area (west and southwest of the Amazon basin), represents the main ozone source in the troposphere of tropical south America ((Andreae et al., 1988; Crutzen et al., 1985; Delany et al., 1985; Kirchhoff et al., 1996). This provides O_3 mixing ratios, which are approximately by a factor 4 higher than in the wet season. Remarkable is the mean diel variation of O_3 mixing ratios in both periods, with a strong decrease from about 1800 LT (sunset) towards sunrise (0600 LT). This is indicative for effective ozone reduction mechanisms and is typical for tropical forest sites with relative high biogenic soil emission of nitric oxide (NO) (Kirchhoff, 1988). General enhancement in the burning season is also visible in the eddy covariance O_3 flux, which shows mean daytime (0600 LT to 1800 LT) values of -9.0 nmol m^{-2} s^{-1} and mean night time (1900 LT to 0500 LT) values of -2.8 nmol m^{-2} s^{-1}. Corresponding values of the wet season are -5.3 nmol m^{-2} s^{-1} and -0.4 nmol m^{-2} s^{-1}, respectively. The relative increase of O_3 flux during daytime is only half the magnitude of the corresponding increase of O_3 mixing ratio. Besides the magnitude of the O_3 flux, the diel course of the O_3 flux exhibits a noticeable difference between the seasons. Whereas the O_3 flux during LBA-EUSTACH 1 shows a more or less symmetric behavior around 1300 LT, the diel variation in LBA-EUSTACH 2 has a clearly asymmetric form. Compared to the diel variation of the O_3

mixing ratio, the maximum of the downward O_3 flux is shifted towards the morning hours. A similar asymmetry and shift is evident, when one compares the diel variation of mean O_3 mixing ratios measured at different heights in the rain forest (31.3 m, 11.3 m, and 1.0 m) with that obtained above the canopy (51.7 m), as shown in Fig. 8. At daytime hours, the O_3 mixing ratios at heights above and within the crown layer (51.7 m and 31.3 m) where photochemical production occurs, show only small differences during both experimental periods. Deep in the forest (11.3 m and 1.0 m), where due to the attenuation of incoming short wave radiation O_3 import from above is the only O_3 source, relative high mixing ratios were reached during the first half of the day. Especially in the morning hours of LBA-EUSTACH 2 the massive increase of O_3 occurred nearly simultaneously throughout the upper two thirds of the canopy. Large O_3 fluxes are necessary to cause such a steep morning increase in O_3 mixing ratio. This massive O_3 input is due to the breakdown of the large O_3 gradients (see Gregory et al., 1988), between the nocturnal surface boundary layer (low O_3) and the so-called residual layer (a few tens to hundreds meters above ground; high O_3), caused by thermally driven turbulent mixing which starts shortly after sunrise. However, the corresponding downward transport of O_3 during these hours seems to exceed the uptake capacity of the forest. As a consequence, there will be an exceptionally large storage of ozone in the canopy. Therefore the storage term in the O_3 mass balance Eq. (2) has to be considered for the determination of the actual O_3 deposition to the rain forest deposition.

4.2.2 O3 Budget

Fig. 9 shows the diel variation of mean single and combined terms of the O_3 mass balance Eq. (2). As already mentioned above, marked seasonal differences in magnitude (and therefore importance) of individual processes are clearly visible. During daytime of LBA-EUSTACH 1 (Fig. 9 (a)), budget contributions of all considered processes were rather small compared to the measured O_3 flux. The net “chemistry” flux (due to chemical reactions of the NO -NO_2 -O_3 triad, ((3)-(5)) is negligible during daytime hours. This is in accordance with the wet season measurements over the rain forest in central Amazonia by Fan et al. (1990), where the diel variation of the mean O_3 flux was also hardly affected by any storage correction, although the mixing ratios at RBJ were higher than those in the central Amazon by a factor of two. Furthermore, the small influence of the O_3 storage term (also found usually for temperate forests (e.g. Lamaud et al., 2002; Munger et al., 1996)) indicates, that the diel variation of the actual O_3 surface deposition is in good approximation with the O_3 flux measured by eddy covariance 13 m above the effective canopy height. During night, the calculated chemical loss seems to exceed the storage corrected flux (especially during the second half of the night); this may be attributed to the considerably large

uncertainty of the flux and profile measurements, when O_3 sensors are close to their detection limits

During LBA-EUSTACH 2 (burning season), the mean mass balance terms were generally enhanced. But especially the storage term was tremendous due to the large diel variation of the O_3 mixing ratio in the air volume below the height of eddy covariance O_3 flux measurements (53 m). Around 1030 LT, the O_3 storage term was about 54% of the mean measured flux, while simultaneously the net "chemical" flux was almost zero. This means, that in contrast to the findings of LBA-EUSTACH 1, that there was a remarkable discrepancy between the amount of O_3 which was (i) transported downward through the plane of the measuring height and (ii) actually simultaneously deposited to the forest canopy. Compared to the daytime mean flux, the maximum of the storage corrected flux is shifted by approximately 2 hours towards the afternoon, where also higher O_3 mixing ratios occurred (see Fig. 7 (b) and Fig. 8 (b)). Besides that, it gets very clear from Fig. 9 (b), that a large part of the O_3 deposition occurs obviously after sunset (during the first half of the night). Between 1900 LT and 2000 LT values of the storage corrected O_3 flux are comparable to its daytime maximum. During LBA-EUSTACH 2 (burning season) the mean night time (1900 LT to 0500 LT) storage corrected O_3 flux of -4.0 nmol m^{-2} s^{-1} accounts for about 63% of the corresponding daytime (0600 LT to 1800 LT) flux (-6.4 nmol m^{-2} s^{-1}). For LBA-EUSTACH 1 this percentage is only 7% (-0.3 nmol m^{-2} s^{-1} and -4.4 nmol m^{-2} s^{-1}). Since stomata of the leafs are expected to be closed after sunset, the O_3 deposition to the leaves' cuticles and to other surfaces must be considerable in the burning season (for a more detailed discussion see also Sections 4.4 and 4.5). .

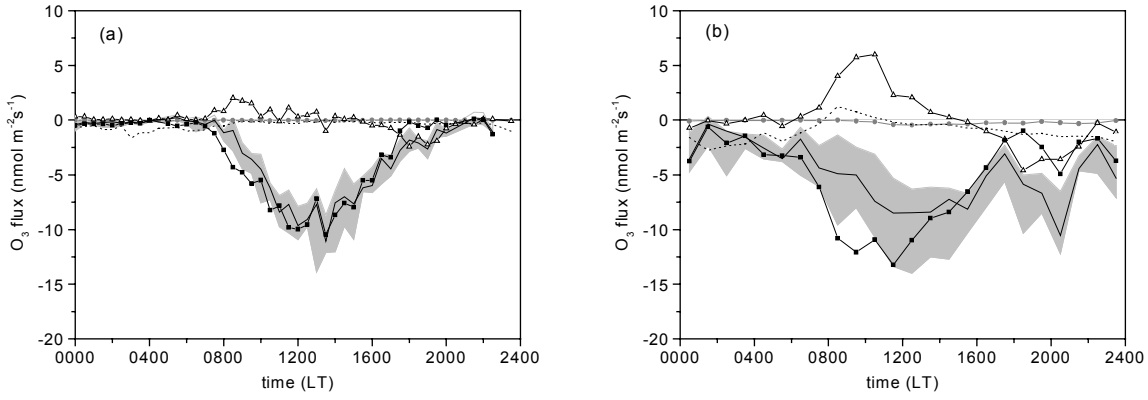

Fig. 9. Diel variation of mean (median) O_3 budget components (see Eq. (2)) for LBA-EUSTACH 1 (a) and LBA-EUSTACH 2 (b): O_3 flux measured at 53 m (black squares), O_3 storage within the column 0-53 m (open triangles), net "chemical" flux (chemical reactions of the NO-NO_2-O_3 triad, see Eqs. (3)-(5): black dotted line), O_3 flux at the forest soil surface (gray circles), and O_3 flux corrected for storage (black line; gray area indicates its inter quartile range).

In this context, the transition between day and night time O_3 deposition is also of interest. Around sunset (1800 LT) there is a local minimum of the storage corrected deposition flux (Fig. 9 (b)). At that time – about two hours after the sensible heat flux got negative – the surface layer over the forest canopy starts to stabilize with the growth of the nocturnal boundary layer (NBL) (Nobre et al., 1996). That means, that the lower part of the atmosphere (the NBL) starts to get decoupled from the rest of the daytime mixing layer and the downward turbulent O_3 flux in the NBL starts to break down. In this time period, it probably takes some time until the O_3 depletion in the developing NBL (by chemical loss and deposition) gets "recognized" throughout the whole canopy, which consequently enlarges the magnitude of the (negative) storage term. The nocturnal decrease of O_3 mixing ratio at all heights might be additionally intensified when the thermal stratification of the lower canopy space (ground to the crown region) gets unstable as a consequence of the development of a local temperature minimum in the crown region, where maximum radiative cooling occurs. The resulting convection in the lower canopy space provides an effective transport of ozone to surfaces within the lower canopy. This is strongly confirmed by the results of Gut et al. (2002b), who found at RBJ highest soil O_3 deposition fluxes at sunset and the following 3-4 hours. As a consequence of this internal instability, nitric oxide (NO), biogenically emitted from the soil, is also effectively mixed up into the canopy space, where it reacts with O_3 (Rummel et al., 2002).

4.2.3 Deposition Velocity

The diel variation of the mean O_3 deposition velocity v_d is displayed in Fig. 10 for both experiments. Deposition velocity was determined as the quotient of the storage corrected O_3 flux and the O_3 mixing ratio measured at 53 m and 51.7 m, respectively (see Eq. (6)). Therefore, it is not surprising that diel variations of mean v_d will reveal distinct seasonal differences as the relative increase of the O_3 flux from LBA-EUSTACH 1 to LBA-EUSTACH 2 was considerably less than the corresponding relative increase of the O_3 mixing ratio. Like the O_3 flux measured during LBA-EUSTACH 1, diel variation of mean deposition velocity shows also an almost symmetrical form, reaching noontime maximum of up to 2 cm s^{-1}. The mean night time deposition velocity of 0.45 cm s^{-1} is about 41% of the mean daytime value of 1.1 cm s^{-1}. The large variability of the nocturnal v_d data during LBA-EUSTACH 1 is most likely due to the uncertainty when calculating a quotient from two small values (O_3 flux and O_3 mixing ratio).

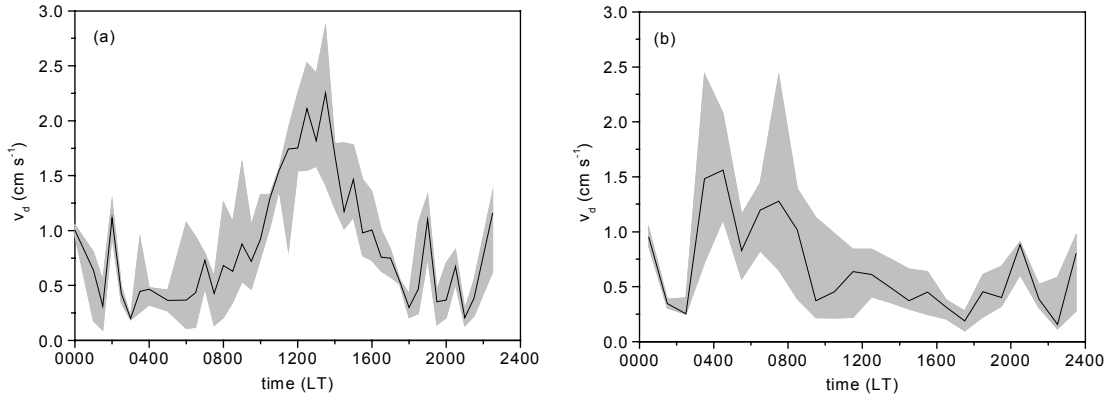

Fig. 10. Diel variation of mean (median) O_3 deposition velocity for LBA-EUSTACH 1 (a) and LBA-EUSTACH 2 (b); gray shaded areas indicate corresponding inter quartile ranges.

While the diel variation of v_d during LBA-EUSTACH 1 is mainly determined by the O_3 flux, its diel variation during the burning season is dominated by the large diel variation of the O_3 mixing ratio (Fig. 10 (b)). The deposition velocity shows two distinct maxima, one in the late night (around 0400 LT) and another right after sunrise (0730 LT). The first can certainly be attributed to the corresponding prevalence of very low O_3 mixing ratios during this period of the day. As indicated by the wide inter-quartile range, the uncertainty especially in the second half of the night is rather high, which arises from error prone low O_3 fluxes and mixing ratios, and a reduced data coverage as a consequence of frequently disturbed upwind fetch (see Section 4.1.2). The second maximum originates from the onset of turbulence, which happens just before the resulting steep increase of the O_3 mixing ratio. In the following daytime hours the deposition velocity is decreasing with a weak minimum around 1000 LT as a consequence of the storage correction. The peak around 2000 LT is also caused by the storage change. The mean daytime value of $v_d = 0.5$ cm s^{-1} is rather low, but comparable to findings above temperate forests (e.g. Lamaud et al., 2002; Munger et al., 1996). For night time hours the mean v_d is 0.6 cm s^{-1} and of comparable magnitude, bearing in mind the higher uncertainty.

4.2.4 Canopy Scale Resistances

In order to separate the bulk canopy processes of O_3 deposition from aerodynamic processes, the total resistance R_t (reciprocal of deposition velocity v_d) can be decomposed into the individual resistances R_a, R_b, and R_c (see Eqs. (7)-(9)). Fig. 11 (a)-(f) display the calculated resistances for both experimental periods. Turbulent aerodynamic (R_a) and quasi laminar boundary layer (R_b) resistances show

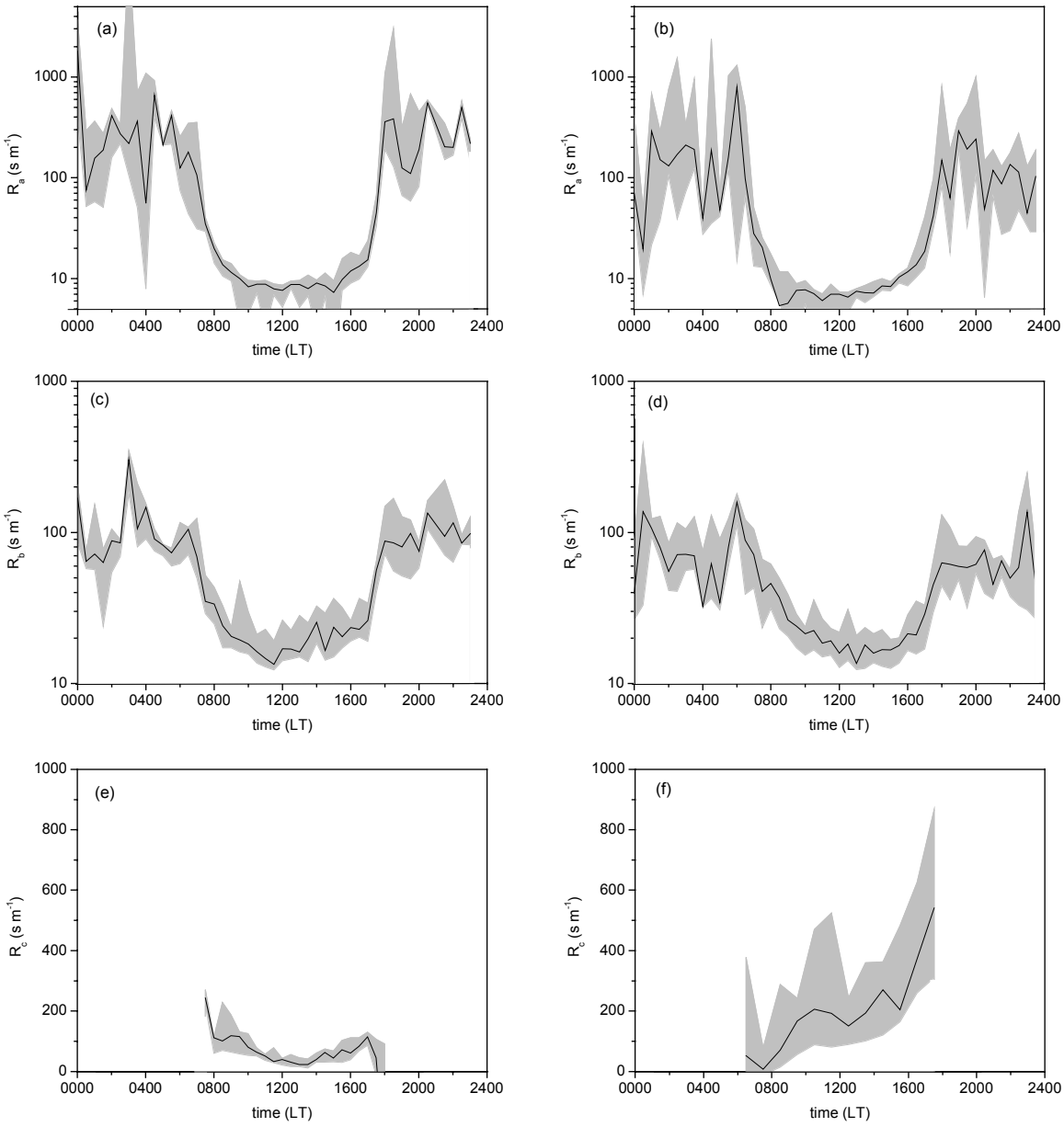

Fig. 11. Diel variation of mean (median) atmospheric (R_a), quasi laminar boundary layer (R_b), and bulk canopy resistance (R_c) at RBJ tower during LBA-EUSTACH 1 ((a), (c), and (e)) and LBA-EUSTACH 2 ((b), (d), and (f)). Corresponding inter quartile ranges are indicated by the gray shaded areas.

no significant differences between the seasons (see Fig. 11 (a)-(d)). In both cases mean daytime $R_a + R_b$ was about 30 s m^{-1}. At night, the mean $R_a + R_b$ of about 300 s m^{-1} during LBA-EUSTACH 1was higher than 180 s m^{-1} for LBA-EUSTACH 2. Although the resistances reveal high variability during both experiments, this supports the higher nocturnal

O_3 fluxes found during LBA-EUSTACH 2. The bulk canopy resistance $R_c = R_t - (R_a + R_b)$ is only shown for daytime hours, since the uncertainty of R_a and $R_t = 1/v_d$ prevents a meaningful determination at night time. It should be kept in mind, that R_c data right after sunrise and just before sunset reveal significant uncertainties for similar reasons. The different seasonal character of O_3 deposition is clearly mirrored by the tremendous difference of R_c during LBA-EUSTACH 1 and 2 (see Fig. 11 (e) and (f)). For LBA-EUSTACH 1, the daytime variation of mean R_c shows an analogous symmetrical form as the diel variation of the O_3 flux. A daytime mean value of $R_c = 50$ s m^{-1} is not much larger than the corresponding sum of $R_a + R_b$. Therefore the bulk canopy resistance seems to be only a weak limitation for O_3 uptake at the end of the wet season.

In big contrast R_c shows a strong diurnal trend during the late dry season (LBA-EUSTACH 2). It increases from low values (similar to wet season values) in the early morning up to about 500 s m^{-1} before sunset. The daytime mean is about 170 s m^{-1}. Unlike the findings of the first experiment, magnitude and diel variation of R_c during the burning season experiment provide an indication for a clear limitation of daytime O_3 deposition by bulk surface characteristics (which are most likely controlled by plant physiological processes). This result, somewhat unexpected, has to be considered as unique, since up to date, to my knowledge, there are no data available about diel variation of O_3 deposition to tropical forests during dry (burning) season.

4.3 Comparison with Results of former Experiments over Tropical Rain Forest

Table 1 gives a survey of experimental studies performed up to date and from which estimates of O_3 deposition to tropical rain forests have been deduced (regardless of season). All experiments took place in Amazonia and Equatorial Africa. For comparison purposes, (median) data of O_3 deposition velocities and fluxes were calculated for the two LBA-EUSTACH experiments, addressing the same time of day as corresponding studies listed in Table 1.

The only eddy covariance O_3 flux measurements at a tower site above a tropical forest canopy was carried out by Fan et al. (1990) during the wet season for 17 days within the framework of the ABLE 2B campaign (see Harriss et al., 1990). Fan et al. (1990) reported the tropical forest in central Amazonia (Reserva Ducke; 2° 57' S, 59° 57' W) to be an effective O_3 sink in April / May. The mean O_3 flux at daytime of -3.8 nmol m^{-2} s^{-1} is somewhat lower than the mean of -5.4 nmol m^{-2} s^{-1} obtained during LBA-EUSTACH 1, but with approximately two times lower mixing ratios at Reserva Ducke. Consequently, the mean daytime O_3 deposition velocity of 1.8 cm s^{-1} determined by Fan et al. (1990) was considerably higher than 1.1 cm s^{-1}, the mean v_d which was obtained for the same daytime period (0700 LT to 1700 LT)

at RBJ. The mean night time fluxes of -0.37 nmol $m^{-2} s^{-1}$ at Reserva Ducke and -0.36 nmol $m^{2} s^{-1}$ at RBJ are almost identical. The corresponding deposition velocities, 0.26 cm s^{-1} (Ducke) and 0.45 cm s^{-1} (RBJ) show a larger difference, but may be not significant in view of the already mentioned uncertainty of nocturnal v_d at low mixing ratios.

Fan et al. (1990) used a photochemical model (Jacob and Wofsy, 1990) to investigate the factors regulating the O_3 flux to the forest in the tropical boundary layer. They concluded that during the wet season (when the boundary layer is a weak net photochemical sink for O_3 (Jacob and Wofsy, 1990)) the O_3 deposition is mainly limited by the O_3 supply from the free troposphere. Their calculated O_3 flux showed only low sensitivity to the canopy surface resistance. The low magnitude and the symmetrical form of the diel variation of bulk canopy resistance obtained during LBA-EUSTACH 1 indicate also a rather weak limitation of the O_3 deposition by surface characteristics.

Table 1

A compilation of ozone deposition measurements within and above tropical rain forests. Values in brackets are measured fluxes (without storage term correction) and the corresponding deposition velocities. The Table continues on next page.

Location	Season / time	Flux[a]	v_d[b]	Method[c]	Reference
Central Amazonia, Manaus	wet / day	-3.8	1.8	EC	Fan et al. (1990)
	wet / night	-0.37	0.26		
South west Amazonia, Rondônia	end of wet / day[f]	-5.0	1.1	EC	LBA-EUSTACH 1[g]
	end of wet / night[f]	-0.36	0.45		
South west Amazonia, Rondônia	end of wet/ morning[e]	-5.8 (-6.6)	1.4 (1.5)	EC	LBA-EUSTACH 1

Table 1

Continued from previous page.

Location	Season / time	Flux[a]	v_d[b]	Method[c]	Reference
South west Amazonia, Rondônia	end of dry/ morning[e]	-7.7 (-11.1)	0.6 (0.8)	EC	LBA-EUSTACH 2
Central Amazonia (lat. cross section)	dry / day (morning)	-27	5	ABL	Gregory et al. (1988)
Northern Congo	end of dry / morning	-15	5	ABL	Cros et al. (1992)
Northern Congo / Central African Republic	begin of dry / morning	-13.1	1.5	EC	Cros et al. (2000)
	begin of dry / morning	-14.3	-	ABL	
Central Amazonia, Manaus (subcanopy)	dry / night (evening)	-9.3	1.8	G	Kaplan et al. (1988)
South west Amazonia, Rondônia (subcanopy)	dry / night (evening)	max. -1.2	max. 0.2	G/Ch	Gut et al. (2002b)
Central Amazonia, Manaus	dry / night (evening)	-18	-	G	Kirchhoff et al. (1988)
	dry / afternoon	-40	-	ABL	
Northern Congo	end of dry / night (evening)	-2.5	1.2	ABL	Andreae et al. (1992)
South west Amazonia, Rondônia	end of dry/ night[d]	-4.0 (-2.4)	0.6 (0.4)	EC	LBA-EUSTACH 2

[a] O_3 flux in nmol m^{-2} s^{-1}
[b] v_d in cm s^{-1}
[c] G: gradient (/Ch: soil chambers); ABL: atmospheric boundary layer budget estimate; EC: eddy covariance;
[d] Average flux between 1700 LT and 0700 LT comparable to the time period used for the O_3 depletion estimates of Kirchhoff et al. (1988) and Andreae et al. (1992).
[e] Average flux between 0800 LT and 1300 LT comparable to the time period used for the O_3 flux estimates of Gregory et al. (1988) and Cros et al. (2000)
[f] Daytime and night time averaging periods (0700 LT-1700 LT; 1700 LT-0700 LT) corresponding to Fan et al. (1990).
[g] All mean values for the LBA-EUSTACH experiments are expressed in medians.

In contrast to the wet season, the O_3 supply from the free troposphere to the boundary layer is during the dry season generally limited by the trade wind inversion as a consequence of large scale subsidence. On the other hand, as already mentioned, massive biomass burning activities represent a large additional O_3 source during that time of the year. But also under background conditions in the dry season boundary layer (not affected by biomass burning), Jacob and Wofsy (1988) got a net photochemical O_3 production from their model calculations. In contrast to the wet season, this "natural" photochemical O_3 production is a consequence of higher biogenic NO soil emissions (Kaplan et al., 1988), which provide the necessary NO_x mixing ratios. No significant differences have been found for the two LBA-EUSTACH experiments concerning biogenic soil NO emission from RBJ forest floor (Gut et al., 2002a). Despite this, mean afternoon mixing ratio of NO_x measured at 51.7 m during LBA-EUSTACH 2 (burning season) was about 390 ppt, considerably higher than 60 ppt observed during LBA-EUSTACH 1. Of course, intensity of deforestation and biomass burning activities is much higher in Rondônia (as a center of development in Brazil) than in central Amazonia. That means the higher NO_x mixing ratio and consequently the higher O_3 mixing ratio originates from biomass burning.

Despite the fact, that the total number of field experiments to determine O_3 deposition to rain forests is much larger for tropical dry seasons than for tropical wet seasons (see Table 1), no direct tower based flux measurements (eddy covariance) have been reported so far for tropical dry season. Moreover, the majority of experimental results is based on airborne measurements which focus on a much larger scale. The advantage of airborne methods, namely to integrate fluxes over larger areas and time intervals, is at the expense of (i) loosing information about diel variation and consequently (ii) missing the possibility to separate the contribution of individual processes.

Very high mean O_3 deposition rates of about -27 nmol m^{-2} s^{-1} and -40 nmol m^{-2} s^{-1} have been determined for central Amazonia with boundary layer budget approaches (Gregory et al., 1988; Kirchhoff et al., 1988). Gregory et al. (1988), whose O_3 profiles were obtained by aircraft measurements, assess their estimate as a rather lower limit for the deposition flux because possible boundary layer O_3 sources were not considered in their budget. However, as stated by them, their mean deposition velocity of ~ 5 cm s^{-1} seems to be unrealistically high. The huge deposition rate reported by Kirchhoff et al. (1988) would probably lead to a similar tremendous deposition velocity. Applying the modified Bowen ratio method to a few measured canopy profiles of NO and O_3 and using corresponding soil NO emissions Kirchhoff et al. (1988) obtained O_3 fluxes of -18 nmol m^{-2} s^{-1}. Kaplan et al. (1988) used the same method and the identical data set to estimate the O_3 flux for the lowest part of the forest (Reserva Ducke). They obtained a mean flux of -9.3 nmol m^{-2} s^{-1}

and a corresponding deposition velocity of 1.8 cm s^{-1}, which is considered to be very large for sub canopy conditions. Gut et al. (2002b) determined the O_3 soil deposition at the floor of the RBJ forest during LBA-EUSTACH 2 with the help of dynamic chamber measurements. Their results provide a maximum flux of -1.2 nmol m^{-2} s^{-1} and a corresponding v_d of 0.2 cm s^{-1}.

Ozone deposition rates measured above tropical forests in central Africa, mainly in Congo, are somewhat lower. An average O_3 flux of -15 nmol m^{-2} s^{-1} was obtained for early morning situations by Cros et al. (1992), using a budget approach on the basis of vertical profiles of O_3 mixing ratio from tethered balloon measurements. But the reported large variability of the estimates together with the rather unrealistic deposition velocities of ~ 5 cm s^{-1} make the results somewhat questionable. Recently, Cros et al. (2000) obtained O_3 fluxes of similar magnitude, around -13 to -15 nmol m^{-2} s^{-1}, during the morning hours by direct airborne eddy covariance measurements and by an atmospheric boundary layer budget approach. Using the results of the airborne eddy covariance measurements, they obtained mean O_3 deposition velocities of about 1.5 cm s^{-1}. The mean O_3 flux and v_d, with -7.7 nmol m^{-2} s^{-1} and 0.6 cm s^{-1} determined during LBA-EUSTACH 2 at RBJ tower for a comparable time interval (0800 LT to 1300 LT) are considerable smaller. But the airborne methods take not into account the storage change within and just above the forest, which was found to be large at RBJ especially if one is just focusing on the morning hours. The means of the non-storage corrected O_3 flux of -11.1 nmol m^{-2} s^{-1} and the corresponding deposition velocity of 0.8 cm s^{-1} are consequently closer to the results of Cros et al. (2000). In this context it might be interesting, that the measurements in Congo have been performed during the begin of the local dry season. Most likely, soil water conditions and the development state of deciduous tree species were different. Especially for O_3 deposition during daytime hours, when O_3 deposition might be largely controlled by stomata, different development plant stages could have a large impact. Therefore, a comparison with the results of LBA-EUSTACH 1 (transition from wet to dry season) might be more reasonable. The excellent agreement of the LBA-EUSTACH 1 mean deposition velocity of 1.4 cm s^{-1} (1.5 cm s^{-1}) for the storage corrected (uncorrected) O_3 deposition between 0800 LT and 1300 LT with the results of Cros et al. (2000) supports this hypothesis.

For a comparison of nocturnal O_3 deposition the development state of trees should play a minor role due to a negligible stomatal influence (comparable LAI assumed). For the Congo forest at the end of dry season nocturnal O_3 deposition was determined by Andreae et al. (1992) also by a budget approach using aircraft O_3 profile measurements. They estimated mean O_3 deposition fluxes and velocities of -2.5 nmol m^{-2} s^{-1} and 1.2 cm s^{-1}. Corresponding mean nocturnal values at RBJ during the LBA-EUSTACH 2

experiment (1700 LT to 0700 LT) are -2.4 nmol m^{-2} s^{-1} and 0.4 cm s^{-1}. Here again, for the comparison with aircraft measurements, the storage term was not considered in the RBJ O_3 deposition estimates. While the O_3 fluxes agree quite well, deposition velocities differ by a factor of three (obviously due to different mixing ratios). At night, the chemical loss of O_3 is considerable and depends mainly on the soil emission of NO which was not measured during the Congo experiment. Andreae et al. (1992) estimated the chemical contribution to O_3 deposition to about 35% by assuming the relative high NO dry season soil emissions measured by Kaplan et al. (1988) in central Amazonia. For comparison, at RBJ the integral chemical sink between the ground and the tower top accounted for 57% of the directly measured O_3 flux and for 35% of the storage corrected O_3 flux. Regardless of the finite difference in deposition velocity, both tropical rain forest ecosystems seem to have in common that a considerable fraction of non-stomatal deposition occurs during night.

The following Sections (4.4 and 4.5) will focus on dry season O_3 deposition, specifically on the influence of environmental and plant physiological parameters. This is due to the fact, that (i) so far the LBA-EUSTACH results show a much higher sensitivity of deposition on these aspects under the conditions of the dry season and (ii) there is a lack in canopy and leaf scale investigations of O_3 deposition to tropical rain forests for that season.

4.4 Short Term Variability during the Burning Season Experiment

Besides substantial differences between the seasons, O_3 mixing ratio exhibits also marked intra-seasonal variations during the burning season experiment LBA-EUSTACH 2. Corresponding time series of O_3 (1 h means) of O_3 mixing ratio, specific humidity deficit, incoming short wave radiation (all measured at RBJ tower top level), and average soil moisture (-0.01 m to -0.05 m) are shown in Fig. 12. The following discussion is emphasizing rather some suggested relations between O_3 mixing ratio, O_3 deposition flux, and selected environmental parameters, than the absolute temporal variations of these quantities.

Time series in Fig. 12 show a period of very high O_3 mixing ratio (up to 80 ppb) around half time of LBA-EUSTACH 2 (11 October). Similar high surface mixing ratios were found during the burning season in the Brazilian cerrado, e.g. at Porto Nacional, by Kirchhoff et al. (1996). At RBJ the highest mixing ratios occurred at the end of the dry and hot 10 day period (2 to 12 October), lacking any precipitation. This is clearly visible by decreasing moisture of the upper soil layer (Fig. 12 (d)) and the concurrent steady increase of specific humidity deficit *SHD* (Fig. 12 (b)). After that hot and dry period, O_3 mixing ratio was continuously decreasing towards the end of October, where levels of mixing ratios reached those at the end of the wet season (May 1999, see Fig. 8 (a)).

Confining to daytime values, time series of the O_3 mixing ratio and *SHD* show a very similar behavior throughout the whole experiment.

The scatter plot in Fig. 13 demonstrates this clearly. Data of both quantities, averaged from 1000 LT to 1800 LT, the time of day when the maximum values occur, are displayed for LBA-EUSTACH 1 and 2. Data of LBA-EUSTACH 2 are separated in two parts, those from 21 September to 20 October and from 25 to 31 October (period of branch cuvette measurements, see Section 2.2.4). Different relationships are observed for data ensembles from LBA-EUSTACH 1 and the first part of LBA-EUSTACH 2, which doubtlessly characterize wet and dry season conditions, respectively. Even for low *SHD* values higher O_3 mixing ratios are found during LBA-EUSTACH 2, demonstrating the general influence of biomass burning as an ozone source.

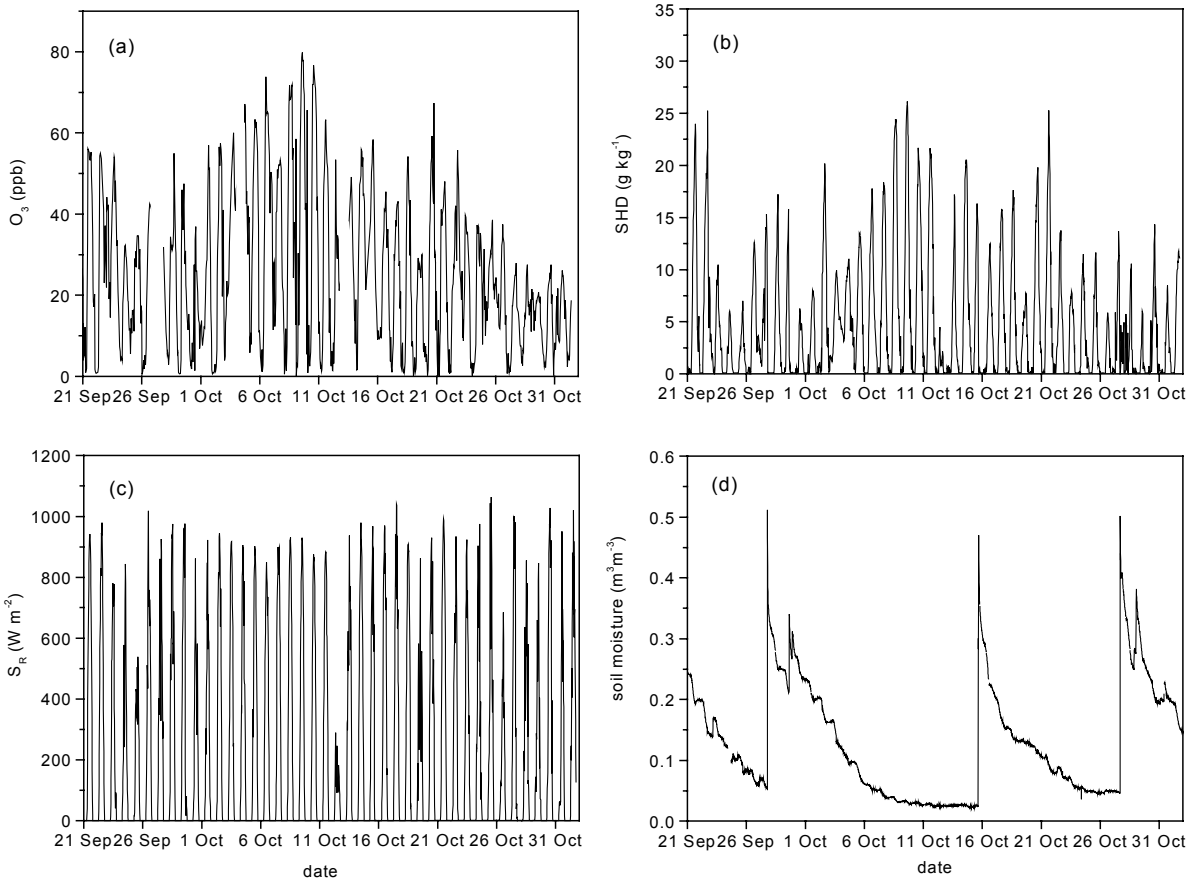

Fig. 12. Time series of O_3 mixing ratio (a), specific humidity deficit (b), incoming short wave radiation (c), and average soil moisture (-0.01 m to -0.05 m) (d) at RBJ tower during LBA-EUSTACH 2 (21 September to 01 November).

Another obvious difference to the LBA-EUSTACH 1 data is the larger slope of the O_3-*SHD* relation during LBA-EUSTACH 2. It sounds trivial, but this is a consequence of intensified biomass burning (enhanced levels of O_3 precursors) under dry conditions. On the other hand, the strong O_3 increase during daytime could also be due to low O_3 deposition as a consequence of reduced stomatal uptake at high specific humidity deficits. Next, O_3 mixing ratios versus *SHD* are considered for the period 25 to 31 October, where the branch cuvette measurements have been performed (Fig. 13). The corresponding data rank in between those of LBA-EUSTACH 1 and the first part of LBA-EUSTACH 2, indicating that data of the second part of LBA-EUSTACH 2 may be attributed to the (dry to wet) transition phase at the end of the latter experiment.

To test the hypothesis that the physiological limitation of O_3 deposition is related to high *SHD* values, the canopy scale measurements of the burning season were classified. For that, corresponding O_3 flux data have been separated on the basis of two specific humidity deficit categories, $SHD \leq 10$ g kg^{-1} and $SHD > 10$ g kg^{-1}. The critical value of 10 g kg^{-1} has been set equal to the maximum average *SHD* found in LBA-EUSTACH 1 (see Fig. 13). For both *SHD* regimes, corresponding diel variation of median measured O_3 flux, storage corrected O_3 flux, and the storage term, as well as bulk resistances R_c and R_{s,O_3} are shown in Fig. 14.

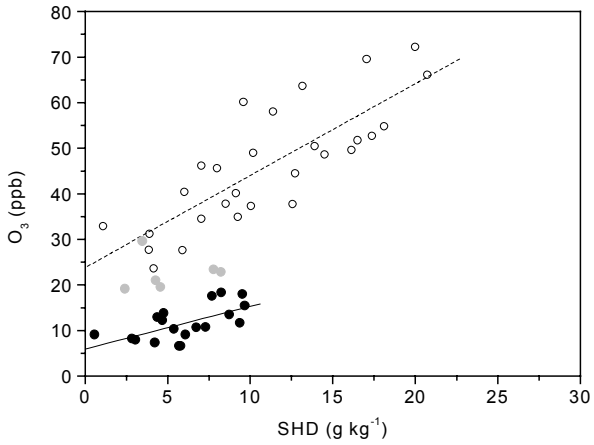

Fig. 13. Average O_3 mixing ratio versus average specific humidity deficit at RBJ tower during LBA-EUSTACH 1 (black full circles) and LBA-EUSTACH 2 (21 September to 20 October: open circles; 25 to 31 October: gray solid circles). Data points represent temporal averages between 1000 LT and 1800 LT.

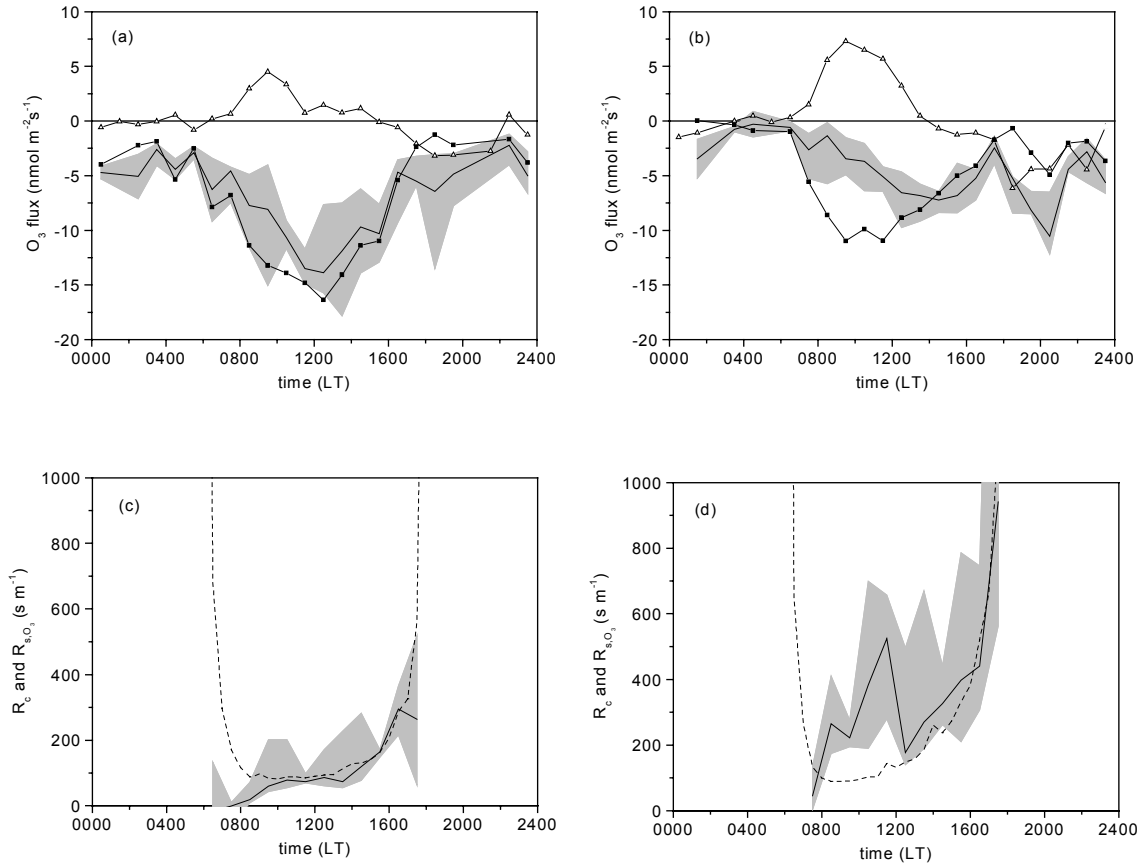

Fig. 14. Diel course of mean (median) O_3 flux measured at 53 m on RBJ tower (black squares), mean (median) O_3 storage within the column 0-53 m (open triangles), mean (median) storage corrected O_3 flux (solid line; gray shaded area indicates its inter quartile range IQR), mean (median) bulk canopy resistance R_c (solid line; gray shaded area indicates its IQR), and modeled stomatal resistance $R_{s,O3}$ (dashed line). Panels (a) and (c) represent conditions for average (1000 LT to 1800 LT) *SHD* category ≤ 10 g kg^{-1}, panels (b) and (d) for average *SHD* > 10 g kg^{-1}.

The general course of the directly measured O_3 flux shows a marked difference between both *SHD* regimes during daytime. Considering Fig. 14 (b), it becomes evident, that the form of the diel variation of the burning season fluxes (Section 4.2.1) is clearly dominated by those days when high specific humidity deficits prevailed: then the highest measured fluxes occur in the morning hours. Considering Fig. 14 (a) (*SHD* ≤ 10 g kg^{-1}), the behavior of measured O_3 flux is similar to that observed during LBA-EUSTACH 1 at the end of the wet season (see Fig. 7 (a)). The daily maximum occurs at the early afternoon and the form of the diel variation is more symmetric. The effect of storage correction on the O_3 flux is also very different for both *SHD* regimes due to the coincidence of high O_3 mixing ratios and *SHD* values > 10 g kg^{-1}. While in the low *SHD* regime the general daytime course of the

measured O_3 flux is not changed by corresponding storage correction (again a similar behavior as found for the entire LBA-EUSTACH 1 data, see Fig. 7 (a)), the maximum of the O_3 flux during days of high *SHD* regime is shifted towards the afternoon, when O_3 mixing ratios were the highest. The large effect of the storage correction is indicative for a clearly reduced daytime O_3 uptake capacity of the canopy under these dry conditions.

This limitation of O_3 deposition becomes already visible, when the magnitude of the not storage corrected fluxes for both *SHD* regimes are compared. For *SHD* $\leq$ 10 g kg^{-1} the mean daytime O_3 flux (0600 LT to 1800 LT) is -10.7 nmol m^{-2} s^{-1}, and significantly larger than -6.4 nmol m^{-2} s^{-1}, as observed for *SHD* > 10 g kg^{-1}. Considering the much higher O_3 mixing ratios in the latter case the difference is even more pronounced, when deposition velocities are compared. The corresponding mean values of v_d are 1.0 cm s^{-1} and 0.45 cm s^{-1}, respectively, calculated from the directly measured O_3 fluxes. For the storage corrected O_3 fluxes 0.84 cm s^{-1} and 0.29 cm s^{-1} were obtained, respectively. The fact, that significantly higher O_3 mixing ratios under high *SHD* regimes do not result in larger daytime O_3 fluxes supports the hypothesis that these O_3 mixing ratios are not only a consequence of intensified biomass burning activities. Obviously, also a physiologically reduced surface sink promotes the occurrence of very high daytime O_3 mixing ratios under dry conditions.

The bulk surface resistance R_c and the modeled stomatal resistance R_{s,O_3} agree well during most daytime hours in case of the low *SHD* regime (Fig. 14 (c)). This indicates, that daytime O_3 deposition is then mainly controlled by stomatal uptake. The deviation at the early morning and late afternoon hours is simply caused by the rather poor determination of the resistances during these periods, as already mentioned in Section 4.2.4. However, in the high *SHD* regime, larger deviations between R_c and R_{s,O_3} become evident (see Fig. 14 (d)). In the afternoon a significant increase of the stomatal resistance is observed and R_c and R_{s,O_3} show only minor differences; larger deviations can be seen in the morning hours. Here, mean R_c is clearly higher than the modeled bulk stomatal resistance R_{s,O_3}. This may be partly caused by an overestimation of the storage correction due to non-considered advective contributions to the O_3 budget (Eq. (2)). Especially during periods of high biomass burning activities such an influence can not be absolutely ruled out, although no systematic wind direction dependence was found. Another possibility to explain the differences between R_c and R_{s,O_3} may be the inadequate consideration of the developmental state of the canopy in the model Wright et al. (1996) (see Section 3.5). Especially during the end of the dry season, which is in the focus here, most deciduous tree species shed senescent foliage and develop fresh leaves. Rottenberger et al. (2005) investigated the

physiology of *Hymenaea courbaril* L. as a function of the developmental state and found, that at the begin of October at senescent, but especially at fresh leaves significantly higher stomatal resistances occurred compared to mature foliage towards the end of the month. While the O_3 flux measurements are largely influenced by that period at begin of October, the consideration of that period in the model calibration by Wright et al. (1996) is rather low. Especially the very dry period of 6 to 11 October, with highest O_3 mixing ratios (see Fig. 12 (a)) observed during the LBA-EUSTACH 2 experiment, is within that period. Depending on the fraction of deciduous trees at similar developmental state in the forest, the bulk stomatal resistance of the canopy (dominating R_c) might especially under high *SHD* regimes substantially deviate from the modeled R_{s,O_3} which is biased towards physiological behavior of mature foliage.

However as a consequence of coincidental occurrence of (i) dry conditions (high *SHD* values), (ii) the most likely high fraction of senescent and fresh canopy foliage, and (iii) intensive biomass burning activities, very high daytime O_3 mixing ratios can build up above tropical rain forests. These high afternoon O_3 mixing ratios were rapidly depleted by chemical loss and considerable surface deposition during the first half of the night. Since the leaf stomata are expected to be closed during the night, the O_3 surface deposition part of the nocturnal O_3 depletion must prefer other mechanisms, like deposition to the leaves' cuticles and other parts of the rain forest vegetation (e.g. bark, litter). To investigate specifically cuticular O_3 deposition, cuvette measurements at leave level are an adequate tool. Corresponding results from LBA-EUSTACH 2 are addressed next.

4.5 Leaf Scale Deposition of Ozone

Measurements of O_3 exchange on a tree-branch of *Hymenaea courbaril* L. have been performed applying a dynamic cuvette system (see Section 2.2.4) from 25 to 31 October 1999 (LBA-EUSTACH 2). Leaf scale O_3 resistances r_{L,O_3} have been determined from incoming and outgoing O_3 mixing ratios (see Section 3.6 Eqs. (12) and (13)). Fig. 15 (a) exhibits the diel course of median r_{L,O_3} together with that of $r_{s,O_3} = r_s\left(D_{H_2O} / D_{O_3}\right)$, the leaf scale stomatal resistance (see Eq. (13)), which was also determined by the branch cuvette measurements. There is no significant difference between r_{L,O_3} and r_{s,O_3} from 1100 LT to 1800 LT, indicating that daytime O_3 deposition is entirely controlled by stomatal aperture. The identity of the two resistances during that time period is also supporting the usual assumption, that the O_3 mesophyll resistance r_{m,O_3} (Eq. (13)) is negligible (see also Gut et al., 2002b). The mean values, averaged for daylight hours (0600 LT to 1800 LT) are 640 s m^{-1} for r_{L,O_3} and 770 s m^{-1} for r_{s,O_3}, where any significant differences would arise from the measurements during the

early morning hours. Contrastingly huge differences between r_{L,O_3} and r_{s,O_3} are obvious during night. Especially after sunset (1800 LT), in the first half of the night, when fast O_3 depletion resulted in huge storage corrections of O_3 fluxes at canopy level, a strong divergence of r_{L,O_3} and r_{s,O_3} is visible. However there is no significant reduction of the leaf resistance during that time, it ranges between 1000 and 3000 s m^{-1} during the whole night (mean: 1440 s m^{-1}, 1900 LT to 0500 LT). Although the difference to r_{s,O_3} is smaller in the second half of the night, there is still distinct additional O_3 deposition in parallel to any stomatal uptake. Within the branch cuvette, this can be attributed to O_3 deposition to the leaves' cuticles and to bark surfaces. This non-stomatal resistance does not show a systematic diel variation, such as found for coniferous forests by Rondon et al. (1993). They obtained a reduction of the non-stomatal resistances during daylight hours concluding a corresponding dependence on air temperature or solar radiation.

To elucidate the behavior of the non-stomatal O_3 deposition, the measured leaf scale O_3 resistances (r_{L,O_3}) are compared with those calculated by the leaf resistance model of Baldocchi et al. (1988), r^m_{L,O_3} (see Section 3.6, Eq. (13)). Still keeping the proved assumption $r_{m,O_3} \approx 0$ s m^{-1}, r^m_{L,O_3} was calculated with three different hypothetical values of O_3 cuticula resistances (r_{ct,O_3} = 1000, 2000, 4000 s m^{-1}). The comparison (r_{L,O_3} versus r^m_{L,O_3}) is shown in

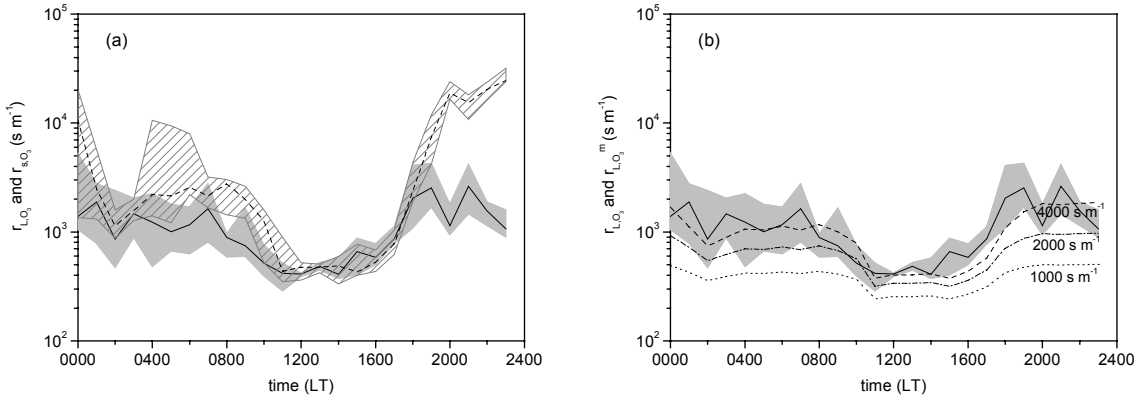

Fig. 15. (a): Diel variation of measured leaf scale O_3 stomatal resistance (median: dashed line; inter quartile range IQR: gray hatched area) and O_3 leaf resistance (median: solid line; IQR: light gray shaded area), both obtained by branch cuvette measurements at Hymenaea courbaril (IBAMA site). (b): Diel variation of measured and modeled O_3 leaf resistance for three different cuticula resistances (dashed line: 4000 s m^{-1}; dashed-dotted line: 2000 s m^{-1}; dotted line: 1000 s m^{-1}).

Fig. 15 (b). For r_{ct,O_3} = 4000 s m^{-1}, the diel variation of the modeled leaf resistance (r^m_{L,O_3}) agrees quite well with the measured one (r_{L,O_3}). The resulting mean values of r^m_{L,O_3} are 570 s m^{-1} (0600 LT to 1800 LT) and 1550 s m^{-1} (1900 LT to 0500 LT). These values compare well to the mean r_{L,O_3} data (640 s m^{-1} and 1440 s m^{-1}, respectively; see above). In a greenhouse experiment, Gut et al. (2002b) used the same type of dynamic cuvettes to investigate O_3 deposition to another young tropical deciduous tree (*Pouteria glomerata*), which is typical for the Amazon region. In contrast to the findings here, they obtained no significant O_3 deposition for night time, which is indicative for a very large cuticula resistance. This was supported by a statistically insignificant difference between r_{L,O_3} and r_{s,O_3} for daytime hours. According to the survey of non-stomatal O_3 deposition velocities from leaf level experiments by Kerstiens and Lendzian (1989) rather similar values for a variety of other plant species are known. The present results from *Hymenaea courbaril* L (mean: v_d^L of 7.0 × 10^{-2} cm s^{-1}) rank in the upper third of the reported range. These results show the potential for considerable nocturnal O_3 deposition if O_3 mixing ratios are high. Nevertheless, to explain the fast O_3 depletion during the first half of the night, additional sinks, most likely chemical reactions (besides (5)) are necessary.

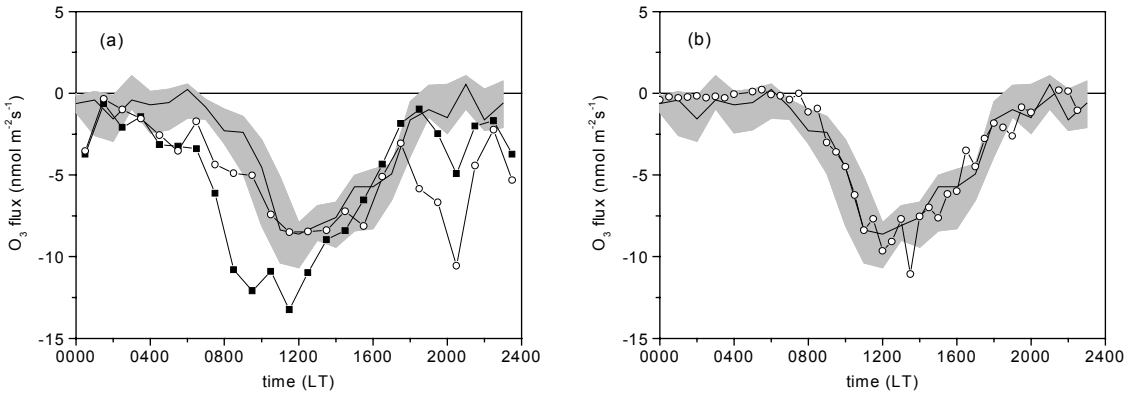

Fig. 16. Diel variation of the mean (median) up-scaled leaf level O_3 flux (median: solid line; inter quartile range: gray shaded area) and mean (median) canopy scale O_3 fluxes at RBJ tower site during (a) LBA-EUSTACH 2 (full squares: O_3 flux; open circles: storage corrected O_3 flux) and (b) LBA-EUSTACH 1 (open circles: storage corrected O_3 flux). Details see text.

Finally the leaf scale results of O_3 deposition are dicussed versus those obtained at the canopy scale. A direct comparison is not feasible, since both data sets have not gathered simultaneously. Moreover, there are general difficulties transferring results from measurements on single plants to the entity of forest canopies by so-called bottom-up scaling (e.g. Baldocchi et al., 1991). Especially here, where results of branch cuvette measurements, which have been performed on one single tree species, are compared with those obtained for the entire canopy of the RBJ rain forest with its large biodiversity – this seems to be, at a first glance, a hopeless undertaking. Therefore any comparison between leaf and canopy scale results is more qualitatively, i.e. it is not focusing on absolute values, the emphasize is rather on the relative behavior of mean diel variation. For this purpose, the O_3 fluxes, obtained from the cuvette measurements, were scaled up just by multiplication with the total *LAI* of 5.6 observed at RBJ. This rather crude scaling probably overestimates the real canopy O_3 deposition, because it is inherently assumed by this approach, that the O_3 deposition determined at crown level is vertically constant within the entire canopy. The diel variation of the up-scaled O_3 fluxes (25 to 31 October) are shown in Fig. 16 (a) together with the diel variation of measured (eddy covariance) O_3 fluxes, as well as the storage corrected canopy scale O_3 fluxes measured between 21 September and 20 October (see also Fig. 9 (b)). There is a marked difference between the up-scaled leaf level results and the eddy covariance O_3 fluxes, especially during the first half of day-light hours. Compared to that, the up-scaled leaf level O_3 flux shows a delayed increase and a more moderate slope during this time period. This different behavior nearly vanishes, if the storage corrected O_3 flux is compared with the up-scaled O_3 flux. Keeping in mind, that for cuvette based flux measurements no storage contribution has to be considered, the agreement between fluxes around noon is excellent. Nevertheless, one have to bear in mind that canopy and leaf scale measurements represent slightly different time periods (21 September to 20 October vs. 25 to 31 October, respectively). Therefore, the development growth state of the deciduous part of the RBJ canopy in early October might have been different from that of *Hymenaea courbaril* L. end of October. Secondly, during the time period of eddy covariance measurements, there were much higher O_3 mixing ratios than end of October. This may have two consequences: (i) cancellation of any major difference between canopy and leaf scale O_3 fluxes during day-light hours due to the expected overestimation of the latter (see above), and (ii) the considerable higher nocturnal canopy scale O_3 fluxes, especially during the first half of the night. Mean nocturnal leaf resistances (r_{L,O_3}), determined from the cuvette measurements, would allow relative high O_3 deposition fluxes, if higher O_3 mixing ratios would have been experienced end of October.

In this context, it is interesting to oppose up-scaled leaf level O_3 fluxes from end of October, to storage corrected canopy scale O_3 fluxes from LBA-EUSTACH 1 (May). As shown in Fig. 16 (b), there is an exceptionally good agreement between the diel variations of both quantities. At a first glance this is surprising, at least for the fact, the ambient O_3 mixing ratios in May have been somewhat lower than end of October (see Fig. 13). Obviously, the higher uptake capacity of the leaves (higher O_3 deposition velocity) in May have balanced the lower mixing ratios as well as possible differences which arise from up-scaling. But besides the coincidentally quantitative agreement of canopy scale and up-scaled leaf level fluxes, the more or less identical diel variation is most striking. This may be most likely due to (i) *SHD* regimes in May 1999 and end of October 1999 have been rather comparable (Fig. 13), and (ii) the developmental state of the *Hymenaea courbaril* L end of October, characterized by the presence of mostly mature leaves (Rottenberger et al., 2005) might correspond more to the developmental state of the RBJ canopy during the wet season than to that during the period 21 September to 20 October.

Finally, it should be stated generally, that during daytime the diel variation of O_3 deposition to the entire RBJ rainforest canopy seems to be very well characterized by the results of the leaf level measurements at a single deciduous tree. In addition the results suggest under dry season conditions the storage corrected eddy covariance flux (in contrast to the measured flux itself) to be a good measure for the actual O_3 uptake of the RBJ canopy during daytime.

4.6 Deforestation Impact on Ozone Uptake: Differences between Forest and Pasture

As mentioned above, O_3 deposition to (vegetated) surfaces counterweights the main sources in the O_3 budget of the lower tropical troposphere. Recalling, these are, depending on season, input from higher atmospheric regions and tropospheric photochemical production. The latter can be strongly enhanced by anthropogenic influences, like biomass burning. Any (large scale) change of land use will subsequently have consequences for the O_3 deposition to vegetated surfaces (and, in turn, the regional O_3 budget). This is particularly the case for Rondônia, where large areas of primary rain forest are continuously deforested and subsequent development to cattle pastures takes place. A first estimate of contrasting O_3 uptake by pasture and rain forest was recently made by Sigler et al. (2002). They reported O_3 fluxes from the Rondônian cattle pasture Fazenda Nossa Senhora Aparecida (FNS), measured in January – February 1999, to be about 60-70% of the O_3 fluxes measured at the primary rain forest Reserva Ducke (central Amazonia) by Fan et al. (1990) 12 years before.

Now, the measurements during LBA-EUSTACH 1 and 2 offer the unique possibility to establish another comparison, more direct and comprehensive, because also spatial and

temporal aspects of that question are addressed. The O_3 deposition data of Kirkman et al. (2002) obtained at FNS cattle pasture simultaneously with the O_3 flux measurements from the RBJ primary rain forest tower during LBA-EUSTACH 1 and 2 will be used. Fig. 17 displays the diel variations of median O_3 mixing ratios, fluxes and deposition velocities at both sites and for both seasons. Corresponding overall averages, based on the 24 individual hourly means, and the resulting percentage of O_3 deposition at FNS compared to O_3 deposition at RBJ, are listed in Table 2 for both measuring periods. Also listed are related values, taken from Sigler et al. (2002). To make their results comparable to ours, their Figure 6 was reevaluated and corresponding pasture-forest O_3 flux and deposition velocity ratios were determined.

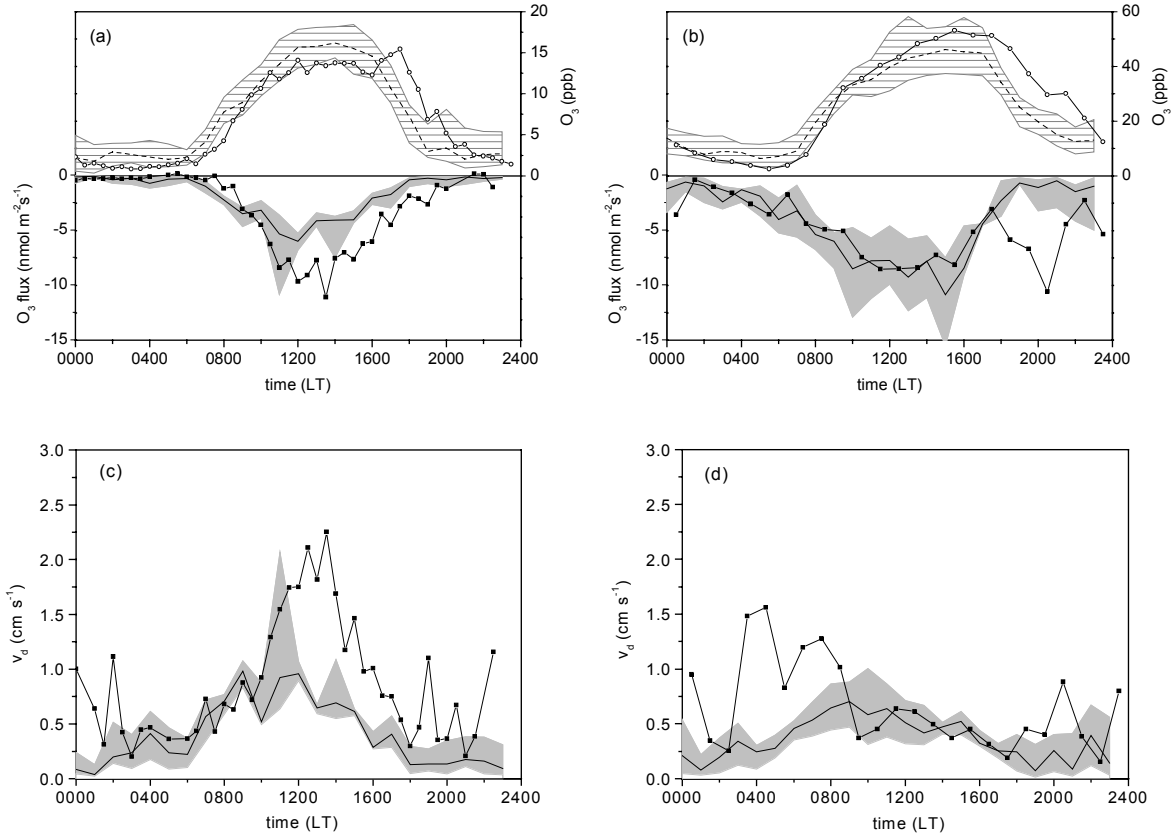

Fig. 17. Diel variation of mean (median) O_3 mixing ratio, flux and deposition velocity at FNS pasture site (median: solid line; inter quartile range: gray shaded area) and at RBJ forest site mean (median) storage corrected O_3 flux (full squares) during LBA-EUSTACH 1 (panels (a) and (c)) and LBA-EUSTACH 2 (panels (b) and (d)).

Based on the averages, the total O_3 flux to the grass pasture site was found to be ~ 70% of the flux obtained for the RBJ rain forest during LBA-EUSTACH 1 (May). As shown in Fig. 17 (a) the main part of this O_3 flux difference originates from daytime hours. With respect to the deposition velocity the resulting percentage is ~ 53%. Again the bulk of the v_d difference is a consequence of considerably higher O_3 deposition to the forest during daytime (Fig. 17 (c)). But as visible in Fig. 17 (a), daytime O_3 mixing ratios were not dramatically lower at RBJ compared to FNS. A considerable part of the larger v_d difference arises from nighttime hours at RBJ, where both low O_3 mixing ratios and fluxes occur. The deposition ratio as quotient from two small values is therefore rather uncertain at that time.

Table 2

Comparison of ozone flux (nmol $m^{-2}s^{-1}$) and deposition velocity (cm s^{-1}) measured at Rebio Jaru (RBJ) and Fazenda Nossa Senhora Aparecida (FNS) during both LBA-EUSTACH experiments: Average, standard deviation, and median. "Ratio" is the percentage of the corresponding pasture to forest value. Also listed are the average values and corresponding ratios based on the results of Sigler et al. (2002). "RD" is the Reserva Ducke rain forest site in central Amazonia (2° 57′ S, 59° 57′ W).

		LBA-EUSTACH[a]						Sigler et al. (2002)[b]		
Season	Quantity	Site	Av[c]	Ratio	StdDev[c]	Med[d]	Ratio	Site	Av[c]	Ratio
wet	O_3 Flux	RBJ	-2.93	70%	1.55	-2.97	65%	RD	-1.82	85%
		FNS	-2.04		1.31	-1.93		FNS	-1.55	
	$v_d(O_3)$	RBJ	0.88	53%	0.50	0.83	63%	RD	0.87	32%
		FNS	0.47		0.22	0.52		FNS	0.28	
Dry	O_3 Flux	RBJ	-5.69	82%	4.40	-5.82	75%			
		FNS	-4.68		2.95	-4.38				
	$v_d(O_3)$	RBJ	0.79	52%	0.62	0.52	77%			
		FNS	0.41		0.28	0.40				

[a] LBA-EUSTACH-1 data periods (end of wet season): 4 to 22 May 1999 (RBJ), 1 to 17 May 1999 (FNS). LBA-EUSTACH-2 data periods (end of dry season): 21 September to 20 October 1999 (RBJ), 24 September to 20 October 1999 (FNS).

[b] LBA-TRMM data period (wet season): January/February 1999 (FNS). ABLE 2B data period (wet season): 22 April to 8 May 1987 (RD) (Fan et al., 1990).

[c] 24 h average, based on 48 (24) individual half hour averages of LBA-EUSTACH 1 (2).

[d] Medians are calculated from the original data set of individual O_3 flux measurements and deposition velocities

Because data coverage during these nighttime periods is also often reduced (see Section 3.1), the overall averages are susceptible to extreme values. With respect to that point, overall medians may be a more robust measure for the pasture-forest O_3 deposition ratio. Based on medians the O_3 flux and deposition velocity at the pasture accounts for ~ 65% and ~ 63%, respectively, of the corresponding forest value. The v_d percentage, which expresses the flux ratio under equal environmental O_3 mixing ratios, is very much reflected in the daytime bulk canopy resistances. Mean R_c of the forest canopy is about 50 s m^{-1} during daytime, and therefore only half of the mean R_c of the pasture's canopy (100 s m^{-1}, Kirkman et al. (2002)).

During LBA-EUSTACH 2, there is a different picture. The O_3 flux ratio between the FNS pasture and RBJ forest is ~ 82% on average basis, and therefore clearly larger than during LBA-EUSTACH 1. Again, as shown in Fig. 17 (b), the ambient O_3 mixing ratios at both sites are not very different during daylight hours. However, the relative uncertain deposition velocities during the second half of the night (where lowest mixing ratios occur) are extremely influencing the overall deposition velocity average of RBJ. The average FNS-RBJ deposition velocity ratio of ~ 52% is therefore clearly biased by these values. To reduce the effect of some individual nighttime extremes, also the overall medians were used. Corresponding ratios result to 75% for the O_3 flux and to 77% for v_d. These percentages seem to be more reasonable, considering the similar ambient O_3 levels at both sites during LBA-EUSTACH 2. Fig. 17 (b) and (d) show, that – especially for the O_3 flux during daytime – there are virtually no significant differences between the two ecosystems. This is due to the different seasonal behavior of R_c at both sites. Whereas mean R_c for the RBJ primary rain forest during September-October was three times higher than in May (see Section 4.2.4), no significant difference of R_c was found between both seasons for the FNS pasture (Kirkman et al., 2002). The latter is most likely a consequence of a weaker response of R_c at FNS to specific humidity deficits (*SHD*). In contrast to the reduction of the (storage corrected) O_3 flux, which was observed at RBJ during the period of extremely high *SHD's* (6 to 12 October, see Fig. 12), O_3 fluxes at FNS were rather enhanced as a consequence of the simultaneously occurring high mixing ratios. This is in accordance with porometer based measurements of McWilliam et al. (1996). They found no significant dependence of the stomatal resistance at FNS on *SHD*, in contrast to a clear dependence of canopy species' stomatal resistance on *SHD* at the RBJ site. During both LBA-EUSTACH experiments soil moisture (-0.05 m) had also no systematic influence on the O_3 flux at the pasture. Since the grass canopy at FNS exhibited also considerable gaps, exposing bare soil patches, probably a large fraction of O_3 deposition was directly to the soil surfaces. In turn, this may be also a reason for the relative small daytime differences of R_c at FNS between the two

seasons. The main contribution to the difference of the (24 h-integrated) O_3 deposition between RBJ and FNS during LBA-EUSTACH 2 originates from the nighttime observations, as a consequence of (i) higher NO soil emission (Gut et al., 2002a; Kirkman et al., 2002), (ii) a larger LAI (non stomatal uptake), and (iii) higher aerodynamic surface roughness at the RBJ rain forest site. Considerably larger O_3 fluxes at RBJ (Fig. 17 (b)) occur during the first half of the night in accordance with the higher O_3 mixing ratios compared to FNS during that time of day.

Finally the results here are discussed with respect to those of Sigler et al. (2002). Recalling they performed their measurements in January-February 1999 (also at FNS pasture site) and compared the O_3 flux estimates to the wet season results for a primary central Amazonian rain forest (Reserva Ducke; RD) obtained 12 years before (Fan et al., 1990). The obtained O_3 flux ratio between the FNS and RD (calculated as described above) is ~85% (Table 2), which is somewhat larger than the corresponding ratio (70%) between FNS and RBJ during LBA-EUSTACH 1. Unlike similar daytime O_3 mixing ratios at FNS and RBJ during LBA-EUSTACH 1, mean O_3 mixing ratios at FNS were 2-3 times higher than at RD during the time periods considered by Sigler et al. (2002). Therefore, the corresponding FNS-RD O_3 deposition velocity ratio is much smaller, ~ 32%. Overall v_d averages at both rain forest sites, 0.87 cm s^{-1} at RBJ (LBA-EUSTACH 1) and 0.88 cm s^{-1} at RD (ABLE 2B, Fan et al. (1990)), agree very well. On the other hand, the average ozone deposition velocity obtained by Sigler et al. (2002) for FNS is 0.28 cm s^{-1}, clearly lower than 0.47 cm s^{-1} for FNS during LBA-EUSTACH 1. This difference may be due to different methods used by Sigler et al. (2002) and Kirkman et al. (2002) to obtain R_c for O_3 deposition in the "big leaf" multiple resistance approach. Whereas Kirkman et al. (2002) used vertical profiles of O_3 mixing ratio, wind speed and temperature to determine R_c for ozone during LBA-EUSTACH 1, Sigler et al. (2002) inferred $R_c(O_3)$ indirectly: they estimated it by surface exchange analogy between the O_3 flux and the latent heat flux.

On the basis of the findings during both LBA-EUSTACH experiments, a crude estimate of the forest-pasture transformation effect on O_3 deposition can be made for a whole year. Assuming both experiments to be representative for two equally long seasons (6 months each, which may be reasonable for Rondônia with respect to the monthly average *SHD* values (see Culf et al., 1996)) after deforestation the regional O_3 surface sink would be about 70% of the original value for the extreme case of a total rain forest to pasture conversion. Since cattle pastures represent the largest part of converted forest land in Rondônia (Fearnside, 1980; Roberts et al., 2002), this scenario might not be unrealistic. Whether this percentage is representative for whole Amazonia depends largely on the physiological response of the different rain forest canopies, e.g. in central Amazonia, and

on seasonal variations of environmental conditions like *SHD* and soil water availability.

For an estimate of the current state and the recent history in central Rondônia a simple up scaling approach was made. For that we made use of the LBA-EUSTACH results and the land cover information provided by the analysis of *Roberts et al.* (2002) for the two LANDSAT scenes P231, R67 (Ji-Paraná) and P231, R68 (Luiza). This is realized by Eq. (14):

$$\hat{v}_d(t) = \frac{\sum_{i=1}^{3}\left(\overline{v}_{d,i} A_i(t)\right)}{\overline{v}_{d,1}\sum_{i=1}^{3} A_i(t)} \cdot 100 \qquad (14)$$

Here, $\overline{v}_{d,i}$ is the mean deposition velocity for a whole year (again based on the assumption of both experiments to be representative for two equally long seasons) of land cover class *i*, with *i* = 1, 2, 3 corresponding to primary rain forest, pasture, and secondary growth, respectively. Secondary growth includes the whole spectrum of vegetation age (excluding primary rain forest and pasture), depending on the time when the land was abandoned. As a first guess for the mean deposition velocity of this class, $\overline{v}_{d,3}$ was assumed to be the average of the determined values for primary rain forest and pasture. $A_i(t)$ represents the area of the land cover class *i* within the investigated LANSAT scene at the time *t*. $\hat{v}_d(t)$ is therefore an area averaged deposition velocity normalized by the deposition velocity for primary rain forest (the original land cover) and expressed in percent.

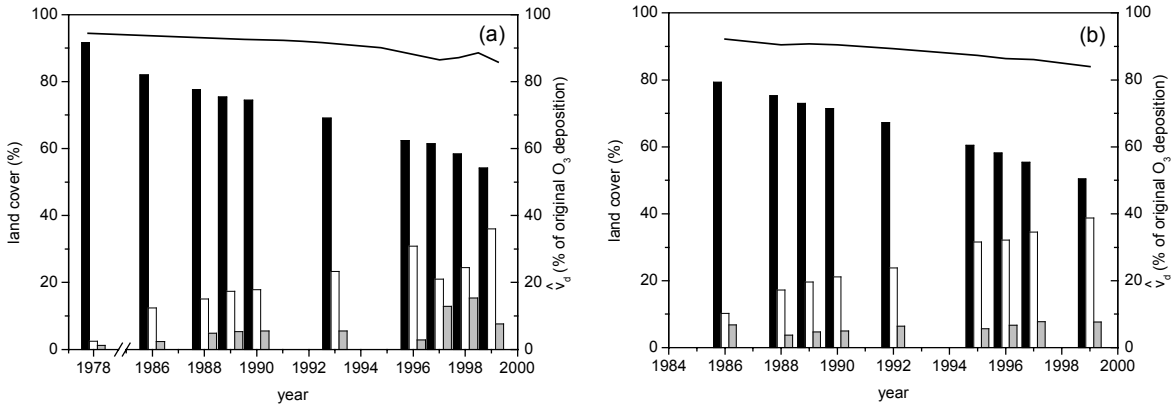

Fig. 18. Temporal evolution of the areal percentage of the three major land-cover classes (primary rain forest: black column, pasture: white column, and secondary growth: gray column) of two LANDSAT scenes: (a) Ji-Paraná (~26500 km^2) and (b) Luiza (~30000 km^2) in central Rondônia (Roberts et al., 2002). The black line indicates the corresponding change of the areal O_3 deposition average in relation to the original forest cover.

Fig. 18 displays the land cover history of the two scenes from 1978 and 1986 to 1999 for Ji-Paraná and Luiza, respectively (Roberts et al., 2002). Both areas show a similarly reduction of the tropical rain forest cover from 82% and 79% in the year 1986 to 54% and 50% in 1999. The calculated reduction of the area averaged O_3 deposition for the same time period is from 93% to 86% and from 92% to 84% of the original tropical rain forest value.

5 Summary and Conclusions

The eddy covariance flux measurements made above a primary rain forest in southwest Amazonia in two campaigns revealed new information about seasonal and diel behaviour of O_3 deposition to that tropical ecosystem type. Magnitude and diel variation of O_3 flux and deposition velocity at the end of the wet season during LBA-EUSTACH 1 were comparable to the findings of Fan et al. (1990), which carried out the only eddy covariance measurements of O_3 flux directly above an Amazonian rain forest so far (ABLE 2B, near Manaus, wet season). The RBJ data, with mean daytime maxima of -11.0 nmol m^{-2} s^{-1} and 2.3 cm s^{-1} for O_3 flux and deposition velocity, respectively, (i) confirm their results, and (ii) show that the tropical rain forest in the south western part of the Amazon basin is also an effective O_3 sink during the wet season.

The mean O_3 deposition determined during LBA-EUSTACH 2 (at the end of the local dry season) was generally lower than former integral boundary layer budget estimates e.g. by Gregory et al. (1988), where surface deposition was not specifically addressed. Beside the mean values, the results of LBA-EUSTACH 2 provide the very first information about the diel course of O_3 deposition to a rain forest under dry season conditions, i.e. under influence of substantial biomass burning activities. The daytime O_3 uptake of the canopy at the end of the local dry season was influenced by specific humidity deficit *SHD* and consequently controlled by stomatal aperture. Days characterized by moderate *SHD* values showed rather higher daytime O_3 fluxes than days with extreme specific humidity deficits, although systematically higher O_3 mixing ratios occurred during the latter period. This suggests that the occurrence of mixing ratios up to 80 ppb above the forest canopy might be also a consequence of limited daytime O_3 uptake (under extremely dry conditions), beside enhanced atmospheric O_3 production as a consequence of biomass burning.

In contrast to LBA-EUSTACH 1, the strongly reduced O_3 uptake during LBA-EUSTACH 2 was also visible in a substantial canopy storage, which in turn changed the characteristic diel variation of the measured flux under extremely dry conditions. Here, considerable non-stomatal O_3 deposition, i.e. to vegetation surfaces like leaf cuticle and bark, directly after sunset is one possible explanation for the strong decrease of O_3 mixing ratios in the first half of the night.

Branch cuvette measurements of O_3 exchange on a tropical deciduous tree species (*Hymenaea courbaril* L.) support the occurrence of cuticular deposition. But the obtained mean cuticula resistance for O_3 of ~ 4000 s m^{-1} to 5000 s m^{-1} might be to high to explain the fast O_3 depletion after sunset solely by dry deposition on plant surfaces.

The mean diel course of O_3 deposition to the canopy species inferred from cuvette measurements agreed extremely well with the results of the eddy covariance measurements. This suggests that the O_3 deposition to the rain forest at daytime is dominated by the stomatal uptake of the crown species, which as a functional group are similar in their stomatal behavior (see McWilliam et al., 1996; Roberts et al., 1990; 1993).

Comparison of O_3 deposition measurements, simultaneously performed at a 22 year old cattle pasture (FNS) and the primary rain forest site (RBJ) showed a ~ 35% lower mean deposition velocity at FNS at the end of the wet season. At the end of the dry season the mean deposition velocity at the pasture site was only ~ 25% lower compared to the forest. This smaller difference is mainly a consequence of enhanced canopy resistances at the forest as reaction on the high specific humidity deficits in the dry season.

Assuming both experiments to be representative for two equally long seasons the regional O_3 surface sink would be about 70% of the original value for a total rain forest to pasture conversion. Based on land cover information provided by LANDSAT images, the current regional O_3 deposition average for central Rondônia was estimated, to be ~ 85% of the original sink provided by the native rain forest cover.

Due to the pronounced dry season in Rondônia and the immediate neighbourhood to development areas with massive biomass burning activities, elevated surface O_3 mixing ratios (> 50 ppb, afternoon) are reached every day above the forest for periods of weeks. A regularly exposure of the tropical trees to such high mixing ratios might cause permanent plant damage. In a greenhouse experiment by Gut et al. (2002b) young tropical tree species showed substantial leaf damage (S. Rottenberger personal communication) after a few days of O_3 fumigation (daytime maximum values of ~60 ppb). On the other hand, it was recognized e.g. by Fuhrer et al. (1992) that the impact on plants might be more closely related to the internal O_3 dose or the flux of O_3 trough the stomata, than the exposure to high ambient O_3 mixing ratios. As the O_3 flux at RBJ was found to be reduced during periods of extreme O_3 mixing ratios (due to simultaneously occurring high specific humidity values), adverse consequences for the forest might be limited.

However, if considerable plant damage will be likely, it would additionally reduce the O_3 uptake capability of the remaining rain forest, especially in those areas where the O_3 surface sink strength is already reduced as a

consequence of deforestation and transformation to pastures.

Acknowledgements

This research is supported by the "Environmental and Climate Programme" (Project LBA-EUSTACH, ENV4-CT97-0566) of the European Union, and by the Max Planck Society. We would like to thank the staff at INCRA (Instituto Nacional de Colonização e Reforma Agrária), especially Jaõ Luis Esteves, Eduardo Conceição, and Claudionor Rodrigues. Further, Carlos Brãndao and the staff of IBAMA (Instituto Brasileiro do Meio Ambiente e dos Recursos Naturais Renováveis) in Ji- Paraná are gratefully acknowledged for their help in installing and maintaining the infrastructure at the forest. We are indebted to Beatriz E. Gomes (Universidade Federal de Rondônia, Ji-Paraná) for support concerning everything and to Sr. Afonso Pereira de Andrade for allowing us to measure at his Fazenda Nossa Senhora Aparecida. We are also grateful to Monika Scheibe, Michael Welling, and Wesley Saores da Silva for assisting us in the field. Special thanks to Hans Peter Schmid for use of his footprint model.

Appendix

The functional relationships of climatic variables used in the bulk stomatal resistance model Eq. (10) by Wright et al. (1996) are:

$$f(SHD) = e^{(-a_2 SHD)} \tag{A1}$$

$$f(T) = \frac{(T - T_l)(T_h - T)^{\frac{(T_h - a_3)}{(a_3 - T_l)}}}{(a_3 - T_l)(T_h - a_3)^{\frac{(T_h - a_3)}{(a_3 - T_l)}}} \tag{A2}$$

$$f(S_R) = \frac{S_R}{1000}\frac{1000 + a_4}{S_R + a_4} \tag{A3}$$

Because no dependence of the canopy transpiration on soil moisture content was found during their measurements at Jaru, this parameter is not included in Eq. (10). T_l and T_h are the lower and upper temperature limit to transpiration, they set to 0 °C and 45 °C respectively. The parameter group a_1 to a_4 was optimised for the calibration of Eq. (10). Here the first free parameter a_1 is the product $G_{s,max}$ LAI, which is why the original value of $a_1 = 65.2$ mm s^{-1} was not adapted to the LAI measured during LBA-EUSTACH experiments. As discussed by Wright et al. (1996) after the optimisation there is a strong interdependence between the parameters, which cannot be ignored by just adapting a single one. In the model the quantity $G_{s,max}$ LAI has to be seen as an "effective" parameter, disassociated from canopy structure and stomatal physiology. The values of the remaining parameters are $a_2 = 0.1064$ kg g^{-1}, $a_3 = 44.6$ °C, and $a_4 = 743$ W m^{-2}.

References

Ammann, C., 1999. On the aplicability of relaxed eddy accumulation and common methods for measuring trace gas fluxes. Dissertation Thesis, Universität Zürich, 229 pp.

Andreae, M.O., Browell, E.V., Garstang, M., Gregory, G.L., Harriss, R.C., Hill, G.F., Jacob, D.J., Pereira, M.C., Sachse, G.W., Setzer, A.W., Silva Dias, P.L., Talbot, R.W., Torres, A.L., Wofsy, S.C., 1988. Biomass-burning emissions and associated haze layers over Amazonia. Journal of Geophysical Research, 93 (D2), 1509-1527.

Andreae, M.O., Chapuis, A., Cros, B., Fontan, J., Helas, G., Justice, C., Kaufman, Y.J., Minga, A., Nganga, D., 1992. Ozone and Aitken nuclei over Equatorial Africa: Airborne observations during DECAFE 88. Journal of Geophysical Research, 97 (D6), 6137-6148.

Andreae, M.O., Artaxo, P., Brandao, C., Carswell, F.E., Ciccioli, P., da Costa, A.L., Culf, A., Esteves, J.L., Gash, J.H.C., Grace, J., Kabat, P., Lelieveld, J., Mahli, Y., Manzi, A.O., Meixner, F.X., Nobre, A.D., Nobre, C., Ruivo, M.d.L.P., Silva-Dias, M.A., P., S., Valentini, R., von Jouanne, J., Waterloo, M.J., 2002. Biogeochemical cycling of carbon, water, energy, trace gases, and aerosols in Amazonia. Journal of Geophysical Research, 107 (D20), 8066, doi: 10.1029/2001 JD000524.

Araujo, A.C., Nobre, A.D., Kruijt, B., Elbers, J., Dallarosa, R., Stefani, P., von Randow, C., Manzi, A.O., Culf, A., Gash, J.H.C., Valentini, R., Kabat, P., 2002. Comparative measurements of carbon dioxide fluxes from two nearby towers in a central Amazonian rainforest: the Manaus LBA site. Journal of Geophysical Research, 107 (D20), 8090, doi: 10.1029/2001 JD000676.

Aubinet, M., Grelle, A., Ibrom, A., Rannik, U., Moncrieff, J.B., Foken, T., Kowalski, A.S., Martin, P.H., Berbigier, P., Bernhofer, C., Clement, R., Elbers, J., Granier, A., Grünwald, T., Morgenstern, K., Pilegaard, K., Rebmann, C., Snijders, W., Valentini, R., Vesala, T., 2000. Estimation of annual net carbon and water exchange of forests: The EUROFLUX methodology. Advances in Ecological Research, 30, 113-175.

Baldocchi, D., 1988. A multi-layer model for estimating sulfur dioxide deposition to a deciduous oak forest canopy. Atmospheric Environment, 22 (5), 869-884.

Baldocchi, D., Finnigan, J., Wilson, K., Paw U, K.T., Falge, E., 2000. On measuring net ecosystem carbon exchange over tall vegetation on complex terrain. Boundary-Layer Meteorology, 96 (1-2), 257-291.

Baldocchi, D., Falge, E., Gu, L., Olson, R., Hollinger, d., Running, S., Anthoni, P., Bernhofer, C., Davis, K., Evans, R., Fuentes, J.D., Goldstein, A., Katul,

G.G., Law, B., Lee, X., Malhi, Y., Meyers, T.P., Munger, W., Oechel, W., Paw U, K.T., Pilegaard, K., Schmid, H.P., Valentini, R., Verma, S., Vesala, T., Wilson, K., Wofsy, S.C., 2001. FLUXNET: A new tool to study the temporal and spatial variability of ecosystem-scale carbon dioxide, water vapour, and energy flux densities. Bulletin of the American Meteorological Society, 82 (11), 2415-2434.

Baldocchi, D.D., Hicks, B.B., Camara, P., 1987. A canopy stomatal-resistance model for gaseous deposition to vegetated surfaces. Atmospheric Environment, 21 (1), 91-101.

Baldocchi, D.D., Luxmoore, R.J., Hatfield, J.L., 1991. Discerning the forest from the trees: an essay on scaling canopy stomatal conductance. Agricultural and Forest Meteorology, 54, 197-226.

Beier, N., Schneewind, R., 1991. Chemical reactions of gases in tubes of probing systems and their influence on measured concentrations. Annales Geophysicae, 9, 703-707.

Browell, E.V., Gregory, G.L., Harriss, R.C., Kirchhoff, V.W.J.H., 1990. Ozone and aerosol distributions over the amazon basin during the wet season. Journal of Geophysical Research, 95 (D10), 16887-16901.

Chamberlain, A.C., 1966. Transport of gases to and from grass and grass-like surfaces. Proc. Roy. Soc. A, 290, 236-265.

Chameides, A.L., Fehsenfeld, F.C., Rodgers, M.O., Cardelino, C., Martinez, J., Parrish, D.D., Lonneman, W., Lawson, D.R., Rasmussen, R.A., Zimmermann, P., Greenberg, J., Middleton, P., Wang, T., 1992. Ozone precursor relationships in ambient atmosphere. Journal of Geophysical Research, 97 (D5), 6037-6055.

Coppin, P.A., Raupach, M.R., Legg, B.J., 1986. Experiments on scalar dispersion within a model-plant canopy. 2. An elevated plane source. Boundary-Layer Meteorology, 35 (1-2), 167-191.

Cros, B., Delmas, R., Nganga, D., Clairac, B., Fontan, J., 1988. Seasonal trends of ozone in Equatorial Africa: experimental evidence of photochemical formation. Journal of Geophysical Research, 93 (D7), 8355-8366.

Cros, B., Fontan, J., Minga, A., Helas, G., Nganga, D., Delmas, R., Chapuis, A., Benech, B., Druilhet, A., Andreae, M.O., 1992. Vertical profiles of ozone between 0 and 400 meters in and above the African Equatorial forest. Journal of Geophysical Research, 97 (D12), 12877-12887.

Cros, B., Delon, C., Affre, C., Marion, T., Druilhet, A., Perros, P.E., Lopez, A.,

2000. Sources and sinks of ozone in savanna and forest areas during EXPRESSO: Airborne turbulent flux measurements. Journal of Geophysical Research, 105 (D24), 29347-29358.

Crutzen, P.J., 1979. The role of NO and NO_2 in the chemistry of the troposphere and the stratosphere. Annual Review of Earth and Planetary Sciences, 7, 443-472.

Crutzen, P.J., Delany, A.C., Greenberg, J., Haagenson, P., Heidt, L., Lueb, R., Pollock, W., Seiler, W., Wartburg, A., Zimmermann, P., 1985. Tropospheric chemical composition measurements in Brazil during the dry season. Journal of Atmospheric Chemistry, 2, 233-256.

Crutzen, P.J. (Editor), 1986. The role of the tropics in atmospheric chemistry. The Geophysiology of Amazomia. John Wiley, New York, 107-130 pp.

Crutzen, P.J., Andreae, M.O., 1990. Biomass burning in the tropics: impact on atmospheric chemistry and biogeochemical cycles. Science, 250, 1669-1678.

Culf, A., Esteves, J.L., Marques Filho, A.d.O., da Rocha, H.R., 1996. Radiation, temperature and humidity over forest and pasture in Amazonia. In: J.H.C. Gash, C.A. Nobre, J.M. Roberts and R.L. Victoria (Editors), Amazonian deforestation and climate. John Wiley & Sons, Chichester, pp. 175-191.

Delany, A.C., Haagenson, P., Walters, S., Wartburg, A., Crutzen, P.J., 1985. Photochemically produced ozone in the emission from large-scale tropical vegetation fires. Journal of Geophysical Research, 90 (D1), 2425-2429.

Dolman, A.J., Gash, J.H.C., Roberts, J., Shuttleworth, W.J., 1991. Stomatal and surface conductance of tropical rainforest. Agricultural and Forest Meteorology, 54, 303-318.

Fan, S.M., Wofsy, S.C., Bakwin, P.S., Jacob, D.J., Fitzjarrald, D.R., 1990. Atmosphere-biosphere exchange of CO_2 and O_3 in the central Amazon forest. Journal of Geophysical Research, 95 (D10), 16851-16864.

Fearnside, P.M., 1980. The effects of cattle pastures on soil fertility in the Brazilian Amazon:consequences for beef production sustainability. Tropical Ecology, 21, 125-137.

Finnigan, J., 1999. A comment on the paper by Lee (1998): "On micrometeorological observations of surface-air exchange over tall vegetation". Agricultural and Forest Meteorology, 97 (1), 55-64.

Finnigan, J., Clement, R., Mahli, Y., Leuning, R., Cleugh, H.A., 2003. A re-evaluation of long-term flux measurement techniques. Part 1: Averaging and coordinate rotation.

Boundary-Layer Meteorology, 107, 1-48.

Fitzjarrald, D.R., Stormwind, B.L., Fisch, G., Cabral, O.M.R., 1988. Turbulent transport observed just above the Amazon forest. Journal of Geophysical Research, 93 (D2), 1551-1563.

Foken, T., Wichura, B., 1996. Tools for quality assessment of surface-based flux measurements. Agricultural and Forest Meteorology, 78, 83-105.

Foken, T., 1998. Die scheinbar ungeschlossene Energiebilanz am Erdboden. 24, Leibnitz-Sozietät E.V., Berlin.

Foken, T., Göckede, M., Mauder, M., Mahrt, L., Amiro, B.D., Munger, J.W. (Editors), 2004. Post-field data quality control. Handbook of Micrometeorology: A Guide for Surface Flux Measurements. Kluwer, Dordrecht, 181-204 pp..

Fuhrer, J., Grandjean Grimm, A., Tschannen, W., Shariat-Madari, H., 1992. The response of spring wheat (*Triticum aestivum* L.) to ozone at higher elevations. 2 Changes in yield, yield components and grain quality in response to ozone flux. New Phytol., 13, 459-464.

Gash, J.H.C., Nobre, J.M., Roberts, J.M., Victoria, R.L., 1996. An overview of ABRACOS. In: J.H.C. Gash, J.M. Nobre, J.M. Roberts and R.L. Victoria (Editors), Amazonian deforestation and climate. John Wiley & Sons, Chichester, pp.1-14.

Gregory, G.L., Browell, E.V., Warren, L.S., 1988. Boundary-layer ozone - an airborne survey above the Amazon Basin. Journal of Geophysical Research, 93 (D2), 1452-1468.

Gregory, G.L., Browell, E.V., Warren, L.S., 1990. Amazon Basin ozone and aerosol: Wet season observations. Journal of Geophysical Research, 95 (D10), 16903-16912.

Güsten, H., Heinrich, G., Schmidt, R.W.H., Schurath, U., 1992. A novel ozone sensor for direct eddy flux measurements. Journal of Atmospheric Chemistry, 14, 73-84.

Güsten, H., Heinrich, G., Mönnich, E., Sprung, D., Weppner, J., Ramadan, A.B., Ezz El-Din, M.R.M., Ahmed, D.M., Hassan, G.K.Y., 1996. On-Line measurements of ozone surface fluxes: Part II. surface level ozone fluxes onto the Sahara desert. Atmospheric Environment, 30 (6), 911-918.

Gut, A., van Dijk, S.M., Scheibe, M., Rummel, U., Welling, M., Ammann, C., Meixner, F.X., Andreae, M.O., Lehmann, B.E., 2002a. NO emission from an Amazonian rain forest soil: Continuous measurements of NO flux and soil compensation concentration. Journal of Geophysical Research, 107

(D20), 8057, doi: 10.1029/2001 JD000521.

Gut, A., Scheibe, M., Rottenberger, S., Rummel, U., Welling, M., Ammann, C., Kirkman, G.A., Kuhn, U., Meixner, F.X., Kesselmeier, J., Lehmann, B.E., Schmidt, J., Müller, E., Piedade, M.T.F., 2002b. Exchange fluxes of NO_2 and O_3 at soil and leaf surfaces in an Amazonian rain-forest. Journal of Geophysical Research, 107 (D20), 8060, doi:10.1029/2001JD000654.

Harriss, R.C., Garstang, M., Wofsy, S.C., Beck, S.M., Bendura, R.J., Coelho, J.R.B., Drewry, J.W., Heoell Jr., J.M., Matson, P.A., McNeal, R.J., Molion, L.C.B., Navarro, J.W., Rabine, V., Snell, R.L., 1990. The Amazon boundary layer experiment: Wet season 1987. Journal of Geophysical Research, 95 (D10), 16721-16736.

Hicks, B.B., Baldocchi, D.D., Meyers, T.P., Hosker, R.P., Matt, D.R., 1987. A preliminary multiple resistance routine for deriving dry deposition velocities from measured quantities. Water Air and Soil Pollution, 36 (3-4), 311-330.

Horst, T.W., Weil, J.C., 1992. Footprint estimation for scalar flux measurements in the atmospheric surface layer. Boundary-Layer Meteorology, 59, 279-296.

Horst, T.W., 2000. On frequency response corrections for eddy covariance flux measurements. Boundary-Layer Meteorology, 94 (3), 517-520.

Jacob, D.J., Wofsy, S.C., 1988. Photo-chemistry of biogenic emissions over the Amazon forest. Journal of Geophysical Research, 93 (D2), 1477-1486.

Jacob, D.J., Wofsy, S.C., 1990. Budgets of reactive nitrogen, hydrocarbons, and ozone over the Amazon-Forest during the wet season. Journal of Geophysical Research, 95 (D10), 16737-16754.

Jarvis, P.G., 1976. The interpretation ovf the variations in leaf water potential and stomatal conductance found in canopies in the field. Philosophical Transactions of the Royal Society of London B, 373, 593-610.

Kaharabata, S.K., Schuepp, P.H., Ogunjemiyo, S., Shen, S., Leclerc, M.Y., Desjardins, R.L., MacPherson, J.I., 1997. Footprint considerations in BOREAS. Journal of Geophysical Research, 102 (D24), 29'113-29'124.

Kaimal, J.C., Wyngaard, J.C., Izumi, Y., Cote, O.R., 1972. Spectral characteristics of surface-layer turbulence. Quarterly Journal of the Royal Meteorological Society, 98, 563-589.

Kaplan, W.A., Wofsy, S.C., Keller, M., da Costa, J.M., 1988. Emission of NO and deposition of O_3 in a tropical forest system. Journal of Geophysical Research, 93 (D2), 1389-1395.

Kerstiens, G., Lendzian, K.J., 1989. Interactions between ozone and plant cuticles. 1. Ozone deposition and permeability. New Phytol., 112 (1), 13-19.

Kirchhoff, V.W.J.H., Browell, E.V., Gregory, G.L., 1988. Ozone measurements in the troposphere of an Amazonian rain forest environment. Journal of Geophysical Research, 93 (D12), 15850-15860.

Kirchhoff, V.W.J.H., 1988. Surface Ozone Measurements in Amazonia. Journal of Geophysical Research, 93 (D2), 1469-1476.

Kirchhoff, V.W.J.H., Dasilva, I.M.O., Browell, E.V., 1990. Ozone measurements in Amazonia - dry season versus wet season. Journal of Geophysical Research, 95 (D10), 16913-16926.

Kirchhoff, V.W.J.H., Alves, J.R., da Silva, F.R., Fishman, J., 1996. Observations of ozone concentratios in the Brazilian cerrado during the TRACE A field expedition. Journal of Geophysical Research, 101 (D19), 24029-24042.

Kirkman, G.A., Gut, A., Ammann, C., Gatti, L.V., Cordova, A.M., Moura, M.A.L., Andreae, M.O., Meixner, F.X., 2002. Surface exchange of nitric oxide, nitrogen dioxide, and ozone at a pasture in Rondonia, Brazil. Journal of Geophysical Research, 107 (D20), 8083, doi: 10.1029/2001JD000523.

Kramm, G., Müller, H., Dlugi, R., 1995. On the relationship between the roughness length of a scalar quantity and the corresponding sublayer-Stanton number. Meteorologische Zeitschrift, NF 4, 209-212.

Kramm, G., Dlugi, R., Mölders, N., 2002. Sublayer-Stanton numbers of heat and matter for aerodynamically smooth surfaces: basic consideratiobs and evaluation. Meteorol. Atmos. Phys., 79, 173-194.

Kristensen, L., 1998. Time series analysis. Dealing with imperfect data, Riso National Laboratory, Roskilde, Denmark.

Kruijt, B., Lloyd, J., Grace, J., McIntyre, J.A., Farquhar, G.D., Miranda, A.C., McCracken, P., 1996. Sources and sinks of CO2 in Rondonia tropical rainforest. In: J.H.C. Gash, C.A. Nobre, J.M. Roberts and R.L. Victoria (Editors), Amazonian deforestation and climate. John Wiley & Sons, Chichester, pp. 331-351.

Kuhn, U., Rottenberger, S., Biesenthal, T., Wolf, A., Schebeske, G., Ciccioli, P., Brancaleoni, E., Frattoni, M., Tavares, T.M., Kesselmeier, J., 2002a. Isoprene and monoterpene emission of Amazonian tree species during the wet season: Direct and indirect investigations of controlling functions. Journal of Geophysical Research, 107

(D20), 8071, doi:10.1029/2001 JD000978.

Kuhn, U., Rottenberger, S., Biesenthal, T., Ammann, C., Wolf, A., Schebeske, G., Oliva, S.T., Tavares, T.M., Kesselmeier, J., 2002b. Exchange of short-chain monocarboxylic acids by vegetation at a remote tropical forest site in Amazonia. Journal of Geophysical Research, 107 (D20), 8069, doi:10.1029/2001JD000303.

Laisk, A., Kull, O., Moldau, H., 1989. Ozone concentration in leaf intercellular air spaces is close to zero. Plant Physiol., 90, 1163-1167.

Lamaud, E., Carrara, A., Brunet, Y., Lopez, A., Druilhet, A., 2002. Ozone fluxes above and within a pine forest canopy in dry and wet conditions. Atmospheric Environment, 36, 77-88.

Lee, X., 1998. On micrometeorological observations of surface-air exchange over tall vegetation. Agricultural and Forest Meteorology, 91, 39-49.

Lenschow, D.H., Kristensen, L., 1985. Uncorrelated noise in turbulence measurements. Journal of Atmospheric and Oceanic Technology, 2, 68-81.

Lenschow, D.H., Raupach, M.R., 1991. The attenuation of fluctuations in scalar concentrations through sampling tubes. Journal of Geophysical Research, 96 (D8), 15259-15268.

Leuning, R., Judd, M.J., 1996. The relative merits of open- and closed-path analysers for measurement of eddy fluxes. Global change Biology, 2, 241-253.

Logan, J.A., Kirchhoff, V.W.J.H., 1986. Seasonal variations of tropospheric ozone at Natal, Brazil. Journal of Geophysical Research, 91 (D7), 7875-7881.

Malhi, Y., Nobre, A.D., Grace, J., Kruijt, B., Pereira, M.G.P., Culf, A., Scott, S.L., 1998. Carbon dioxide transfer over a central Amazonian rain forest. Journal of Geophysical Research, 103 (D24), 31593-31612.

Malhi, Y., Pegoraro, E., Nobre, A.D., Pereira, M.G.P., Grace, J., Culf, A., Clement, R., 2002. Energy and water dynamics of a central Amazonian rain forest. Journal of Geophysical Research, 107 (D20), 8061, doi: 10.1029/2001 JD000623.

McWilliam, A.-L.C., Cabral, O.M.R., Gomes, B.M., Esteves, J.L., Roberts, J.M., 1996. Forest and pasture leaf gas exchange in south-west Amazonia. In: J.H.C. Gash, C.A. Nobre, J.M. Roberts and R.L. Victoria (Editors), Amazonian deforestation and climate. John Wiley & Sons, Chichester, pp. 266-285.

Meixner, F.X., Fickinger, T., Marufu, L., Mukurumbira, L., Makina, E.,

Nathaus, F.J., Serca, D., Andreae, M.O., 1997. Preliminary results on nitric oxide emission from a southern African savanna ecosystem. Nutrient Cycling in Agroecosystems, 48, 123-138.

Moncrieff, J.B., Massheder, J.M., deBruin, H., Elbers, J., Friborg, T., Heusinkveld, B., Kabat, P., Scott, S., Soegaard, H., Verhoef, A., 1997. A system to measure surface fluxes of momentum, sensible heat, water vapour and carbon dioxide. Journal of Hydrology, 188-189, 589-611.

Monteith, J.L., Unsworth, M.H., 1990. Principles of environmental physics. Edward Arnold, London, 291 pp.

Moore, C.J., Fisch, G.F., 1986. Estimating heat storage in Amazonian tropical forest. Agricultural and Forest Meteorology, 38, 147-169.

Moore, C.J., 1986. Frequency response correction for eddy correlation systems. Boundary-Layer Meteorology, 37, 17-35.

Munger, W.J., Wofsy, S.C., Bakwin, P.S., Fan, S.M., Goulden, M.L., Daube, B.C., Goldstein, A.H., Moore, K.E., Fitzjarrald, D.R., 1996. Atmospheric deposition of reactive nitrogen oxides and ozone in a temperate decidous forest and subarctic woodland. 1. Measurements and mechanisms. Journal of Geophysical Research, 101 (D7), 12639 - 12657.

Nobre, C.A., Fisch, G., da Rocha, H.R., Lyra, R.F.d.F., da Rocha, E.P., da Costa, A.C.L., Ubarana, V.N., 1996. Observations of the atmospheric boundary layer in Rondônia. In: J.H.C. Gash, C.A. Nobre, J.M. Roberts and R.L. Victoria (Editors), Amazonian deforestation and climate. John Wiley & Sons, Chichester, pp. 413-423.

Owen, P.R., Thomson, W.R., 1963. Heat transfer across rough surfaces. Journal of Fluid Mechanics, 15, 321-334.

Paulson, C.A., 1970. The mathematical representation of wind speed and temperature profiles in the unstable atmospheric surface layer. Journal of Applied Meteorology, 9, 857-861.

Paw U, K.T., Baldocchi, D.D., Meyers, T.P., Wilson, K.B., 2000. Correction of eddy-covariance measurements incorporating both advective effects and density fluxes. Boundary-Layer Meteorology, 97, 487-511.

Rannik, Ü., Aubinet, M., Kurbanmuradov, O., Sabelfeld, K.K., Markkanen, T., Vesala, T., 2000. Footprint analysis for measurements over a heterogeneous forest. Boundary-Layer Meteorology, 97 (1), 137-166.

Rannik, Ü., Markkanen, T., Raittila, J., Hari, P., Vesala, T., 2003. Turbulence statistics inside and over forest:

Influence on footprint prediction. Boundary-Layer Meteorology, 109, 163-189.

Raupach, M., Shaw, R.H., 1982. Averaging procedures for flow within vegetation canopies. Boundary-Layer Meteorology, 22, 79-90.

Raupach, M.R., 1994. Simplified expressions for vegetation roughness length and zero-plane pisplacement as functions of canopy height and area index. Boundary-Layer Meteorology, 71 (1-2), 211-216.

Roberts, D.A., Numata, I., Holmes, K., Batista, G., Krug, T., Monteiro, A., Powell, B., Chadwick, O.A., 2002. Large scale mapping of land-cover change in Rondônia using multitemporal spectral mixture analysis and decision tree classifiers. Journal of Geophysical Research, 107 (D20), 8073, doi: 10.1029/2001JD000374.

Roberts, J., Cabral, O.M.R., Deaguiar, L.F., 1990. Stomatal and Boundary-Layer Conductances in an Amazonian Terra-Firme Rain-Forest. Journal of Applied Ecology, 27 (1), 336-353.

Roberts, J., Cabral, O.M.R., Fisch, G., Molion, L.C.B., Moore, C.J., Shuttleworth, W.J., 1993. Transpiration from an Amazonian rainforest calculated calculated from stomatal conductance measurements. Agricultural and Forest Meteorology, 65, 175-196.

Rondon, A., Johansson, C., Granat, L., 1993. dry deposition of nitrogen dioxide and ozone to coniferous forests. Journal of Geophysical Research, 98 (D3), 5159-5172.

Rottenberger, S., Kuhn, U., Wolf, A., Schebeske, G., Oliva, S.T., Tavares, T.M., Kesselmeier, J., 2004. Exchange of short-chain aldehydes between Amazonian vegetation and the atmosphere. Ecological Applications, 14 (4), 247-262.

Rottenberger, S., Kuhn, U., Wolf, A., Schebeske, G., Oliva, S.T., Tavares, T.M., Kesselmeier, J., 2005. Form-aldehyde and acetaldehyde exchange during leaf development of the Amazonian deciduous tree species *Hymeaea courbaril*. Atmospheric Environment, in press.

Rummel, U., Ammann, C., Gut, A., Meixner, F.X., Andreae, M.O., 2002. Eddy covariance measurements of nitric oxide flux within an Amazonian rainforest. Journal of Geophysical Research, 107(D20), 8050, doi: 10.1029/2001JD000520.

Rummel, U., Ammann, C., Foken, T., Andreae, M.O., Meixner, F.X., 2005. Application of a surface renewal model for the determination of heat, carbon dioxide, and ozone fluxes from a tropical rain forest in Amazonia. Atmos. Chem. Phys., for submission.

Sakai, R.K., Fitzjarrald, D.R., Moore, K.E., 2001. Importance of low frequency contributions to eddy fluxes observed over rough surfaces. Journal of Applied Meteorology, 40 (2178-2192).

Schmid, H.P., 1994. Source Areas for Scalars and Scalar Fluxes. Boundary-Layer Meteorology, 67, 293-318.

Schmid, H.P., 1997. Experimental design for flux measurements: matching scales for observations and fluxes. Agricultural and Forest Meteorology, 87, 179-200.

Shuttleworth, W.J., Gash, J.H.C., Lloyd, C.R., Moore, C.J., Roberts, J., Marques Filho, A.d.O., Fisch, G.F., de Paula Silva Filho, V., de Nazare Goes Rebeiro, M., Molion, L.C.B., de Abreu Sa, L.D., Nobre, J.C.A., Cabral, O.M.R., Patel, S.R., de Moraes, J.C., 1984. Eddy correlation measurements of energy partition for Amazonian forest. Quarterly Journal of the Royal Meteorological Society, 110, 1143-1162.

Sigler, J.M., Fuentes, J.D., Heitz, R.C., Garstang, M., Fisch, G., 2002. Ozone dynamics and deposition processes at a deforested site in the Amazon basin. Ambio, 31 (1), 21-27.

von Caemmerer, S., Farquhar, G.D., 1981. Some relationships between the biochemistry of photosynthesis and the gas exchange of leaves. Planta, 153, 1293-1304.

von Randow, C., Sa, L.D.A., Gannabathula, P.S.S.D., Manzi, A.O., Arlino, R.A., 2002. Scale variability of atmospheric surface fluxes of energy and carbon over a tropical rainforest in southwest Amazonia. I. Diurnal conditions. Journal of Geophysical Research, 107, 10.1029/2001JD000379.

Webb, E.K., Pearman, G.I., Leuning, R., 1980. Correction of flux measurements for density effects due to heat and water vapour transfer. Quarterly Journal of the Royal Meteorological Society, 106, 85-100.

Wienhold, F.G., Frahm, H., Harris, G.W., 1994. Measurements of N_2O fluxes from fertilized grassland using a fast response tunable diode laser spectrometer. Journal of Physical Oceanography, 99 (D8), 16557-16567.

Wilczak, J.M., Oncley, S.P., Stage, S.A., 2001. Sonic anemometer tilt correction algorithms. Boundary-Layer Meteorology, 99, 127-150.

Wilson, K., Goldstein, A., Falge, E., Aubinet, M., Baldocchi, D.D., Berbigier, P., Bernhofer, C., Ceulemans, R., Dolman, H., Field, C., Grelle, A., Ibrom, A., Law, B.E., Kowalski, A.S., Meyers, T.P., Moncrieff, J.B., Monson, R.K., Oechel, W., Tenhunen, J., Valentini, R., Verma, S., 2002.

Energy balance closure at FLUXNET sites. Agricultural and Forest Meteorology, 113, 223-243.

Wright, I.R., Gash, J.H.C., da Rocha, H.R., Roberts, J.M., 1996. Modelling surface conductance for Amazonian pasture and forest. In: J.H.C. Gash, C.A. Nobre, J.M. Roberts and R.L. Victoria (Editors), Amazonian deforestation and climate. John Wiley & Sons, Chichester, pp. 437-457.

Zeller, K., Massman, W., Stocker, D., Fox, D.G., Stedman, D., Hazlett, D., 1989. Initial Results from the Pawnee Eddy Correlation System for Dry Acid Deposition Research. RM-282, United States Department of Agriculture (USDA), Forest Service.

Appendix C

Eddy Covariance Measurements of Nitric Oxide Flux within an Amazonian Rain Forest

U. Rummel*, C. Ammann, A. Gut, F.X. Meixner, and M.O. Andreae

Max Planck Institute for Chemistry, Mainz, Germany

Journal of Geophysical Research 107 (D20), 8050, doi:10.1029/2001JD000520

Received 9 February 2001; revised 25 May 2001; accepted 30 May 2001; published 4 September 2002

NO flux measurements by the eddy covariance technique were performed within a tropical rain forest 1 m and 11 m above the forest floor. A fast-response chemiluminescence NO analyzer with a sampling tube of 25 m length was used for the gas measurements. Nighttime similarity between the cospectra of sensible heat and NO flux offered the possibility to quantify the high-frequency attenuation of the NO eddy covariance by spectral analysis. Integrated flux correction factors of about 21% for the system at 1 m and 5% for the one at 11 m above ground were calculated by transfer functions adopted from the literature and confirmed experimentally. For an independent validation, the results of the eddy covariance system were compared with the NO soil emissions obtained by dynamic chambers. For nighttime averages good agreement within 10% was found. The obtained NO fluxes were 3.5 ± 0.14 and 4.8 ± 0.39 ng N m^{-2} s^{-1} for the two investigated periods at 1 m and 11 m height, respectively. During the day, chemical reaction with ozone entrained from aloft reduced the fraction of the soil-emitted NO that reached the measuring height of the eddy covariance system. The average flux showed a reduction of 48% at 1 m and 92% at 11 m height compared to the corresponding soil emission measured by the chamber system.

INDEX TERMS: 0315 Atmospheric Composition and Structure: Biosphere/atmosphere interactions; 3322 Meteorology and Atmospheric Dynamics: Land/atmosphere interactions; 3394 Meteorology and Atmospheric Dynamics: Instruments and technics; 3379 Meteorology and Atmospheric Dynamics: Turbulence; 0322 Atmospheric Composition and Structure: Constituent sources and sinks; *KEYWORDS:* eddy covariance; nitric oxide flux; turbulence; Amazonian rain forest; cospectral similarity

*corresponding author

1 Introduction

The oxides of nitrogen NO_x ($NO + NO_2$) are important compounds for the regulation of atmospheric photochemical oxidants such as ozone O_3 and the hydroxyl radical OH [*Crutzen*, 1979]. Within the global tropospheric ozone budget, the low NO_x levels over large tropical ecosystems like Amazonia are assumed to be important potential counterparts to the high NO_x levels over industrialized areas. According to *Chameides et al.* [1992], NO_x mixing ratios found at remote sites in Amazonia are on the threshold required for net photochemical ozone formation. Therefore tropical tropospheric chemistry might be very sensitive to the ongoing deforestation and land-use change. Besides the direct impact of biomass burning on the tropospheric NO_x concentration, this man-made encroachment will also modify the biogenic NO emission from soil [*Gut et al.*, 2002b; *Kirkman et al.*, 2002; *van Dijk et al.*, 2002], which represents an important NO_x source, especially in remote areas [*Galbally*, 1985; *Davidson and Kingerlee*, 1997]. To assess the effect of this modified "source strength" of the soil on the composition of the tropical troposphere, one has to consider the influence of the forest canopy on the surface exchange of nitrogen oxides. Various chemical and physical processes affect the soil-emitted NO on its way through the canopy layer and may reduce the net NO_x emissions of the ecosystem [*Jacob and Wofsy*, 1990; *Meixner*, 1994; C. Ammann et al., unpublished manuscript, 2001].

Only a few results have been published on the biogenic NO emissions from soils in the Amazonian rain forest [*Kaplan et al.*, 1988; *Bakwin et al.*, 1990; *Verchot et al.*, 1999; *Gut et al.*, 2002b]. They were mainly obtained by enclosure methods, partly complemented by nighttime in-canopy NO budget estimations. Static and dynamic enclosure measurements represent the standard technique to determine soil emissions, because the mass budget principle is not too critical with respect to the accuracy and the temporal resolution of the trace gas analysers. The eddy covariance method is an alternative approach to determine the NO emissions, integrating over large source areas without the risk of chamber measurements to disturb local environment. Very few NO flux measurements using the eddy covariance technique have been reported up to now [*Delany et al.*, 1986; *Civerolo and Dickerson*, 1998; *Li et al.*, 1999], and all of them were performed above low vegetation canopies. Within forest canopies, some eddy covariance measurements have been made for other trace gases as H_2O, CO_2, O_3 and SO_2 [*Demnead*, 1984; *Baldocchi et al.*, 1986; *Baldocchi and Meyers*, 1991; *Lee and Black*, 1993; *Meyers and Baldocci*, 1993; *Baldocchi et al.*, 1997; *Blanken et al.*, 1997; 1998].

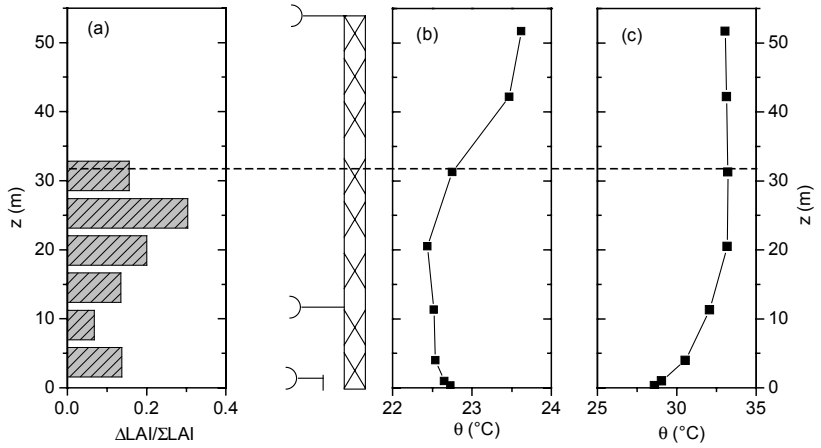

Figure 1. Vertical profiles of (a) the relative one-sided leaf area index (LAI), positions of the sonic anemometers, and the potential temperature (b) at night-time and (c) at daytime. The mean height of the closed canopy (32 m) is displayed by the horizontal line (dashed). The height of the eight profile measurement levels is indicated by the data points in (b) and (c).

The study presented here was performed as part of the EUSTACH–LBA experiment (EUropean Studies on Trace gases and Atmospheric CHemistry as a contribution to the Large scale Biosphere–Atmosphere experiment in Amazonia) [*Andreae et al.*, 2002]. The focus of this work was to measure NO fluxes within a tropical rain forest using the eddy covariance method, in order to investigate the expected flux reduction with height. Measurement results, an error analysis, and the comparison of the obtained fluxes with the results of a dynamic chamber system for validation purposes are presented in this paper.

2 Materials and Methods

2.1 Site Description

The measurements presented here were performed within the LBA-EUSTACH-2 campaign during the dry-to-wet season transition period from September to November 1999. The site is located in a biological reserve 90 km north of Ji-Paraná in the state of Rondônia, southwest Amazonia, Brazil (10°04′55′′ S, 61°55′48′′ W). The area is covered by a primary open rain forest with a closed canopy of about 32 m height. There are single jutting trees up to a height of 45 m. A palm-rich understory of only a few metres height exists under a relatively open stem space up to 20 m (Figure 1). Fairly uniform rain forest vegetation extends at least 1.5 km in the main wind direction sector from NW to SE. To the southwest, a river (Rio Machado) limits the fetch to about 400 m. For further information about the site and the campaign see [*Andreae et al.*, 2002].

2.2 Instrumentation

The main platform for the micro-meteorological and trace gas measurements was a scaffolding tower of 52 m height erected in 1991 [*Gash et al.*, 1996]. Most of the measurements close to the forest floor (0–4 m height) were made at 15 m distance northeast of the main tower, over a relatively undisturbed surface area. Eddy covariance systems were mounted most of the time at 53 m, 11 m and 1 m above the forest floor. In order to obtain additional information about the horizontal homogeneity of the soil emission, a second location for the 1 m system was chosen 15 m west of the tower. At all three levels, wind and temperature fluctuations were measured by three-dimensional sonic anemometers (Gill Instruments, Solent Research 1012 K55 and K125). The anemometers at 11m and at 1m were alternately combined with a nitric oxide chemiluminescence analyser (CLD 780 TR, ECO Physics, Switzerland) for ten-day periods. This commercial NO sensor is based on the reaction of NO with O_3, which forms electronically excited NO_2. Under reduced pressure, the excited NO_2 molecules decay to the ground state by emitting a photon. The total light intensity in the reaction chamber, detected by a photomultiplier tube (PMT), is proportional to the NO mixing ratio [*Fontijn et al.*, 1970].

The instrument was flushed by a high-vacuum scroll pump (ESD12, Edwards High Vacuum International, UK). A capillary (critical orifice) at the sample inlet restricts the flow to 3 L min^{-1} and creates a low pressure of 20 hPa in the reaction chamber with a volume of 0.75 L. Therefore the exchange rate of the sample air in this chamber is 4.5 times per second, limiting the temporal resolution of the NO measurement. In the present experiment the instrument was running in a continuous mode, integrating the photons over 0.1 s.

The NO analyser was housed in an air-conditioned shelter at the forest floor 10 m away from the tower base. The sample air was brought from the inlet positions at the different heights to the instrument through a 25 m long opaque TEFLON® tube with 4.3 mm inner diameter. In the rain forest environment, relative bulky inlets were necessary to keep off liquid water and insects from entering the tube. To avoid distortion of the turbulence near the sonic anemometer, the tube inlet was placed at a horizontal distance of 30 cm to the sonic head. The flow restricting capillary was installed close to the inlet, reducing the pressure and therefore the residence time of the sample air in the tube [*Wesely et al.*, 1982; *Delany*, 1993]. The resulting delay time between the vertical wind component and the NO signal was 3.6 s, determined via crosscorrelation analysis of the two time series. The crosscorrelation functions for the eddy covariance system at 1 m height can be seen in Figure 2.

Compared to the w-T-correlation, a peak broadening and amplitude reduction obviously occurs in the w-[NO]-correlation function due

to damping effects on high frequency fluctuations (see Section 2.4).

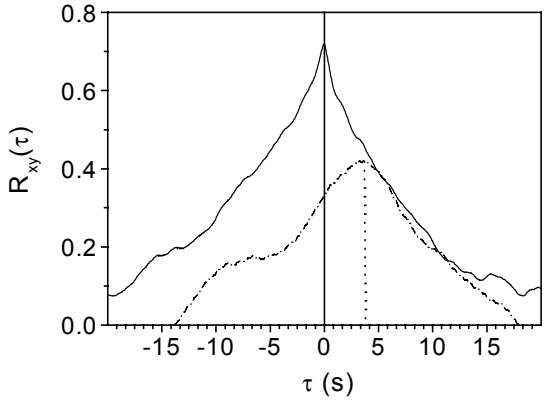

Figure 2. Cross correlation functions of the sensible heat flux (solid) and the NO flux (dashed).

Trace gas profile measurements of NO, NO_2, O_3, CO_2 and H_2O were also performed above and throughout the canopy [*C. Ammann et al.*, unpublished manuscript, 2001] The air sampling system consisted of TEFLON® tube inlets on 8 levels (0.3 m, 1.0 m, 4.0 m, 11.3 m, 20.5 m, 31.3 m, 42.2 m, 51.7 m). All heights were sequentially sampled by a TEFLON® valve distribution unit and continuously flushed through a purging pump. The NO_x concentrations were determined by a second analyser similar to the eddy covariance instrument. It was operated in combination with a photolytic converter (PLC 760, ECO Physics, Switzerland). Ozone was measured with a UV absorption analyser (Thermo Instruments, TE49C, USA). Temperature was determined at all levels by fine wire thermocouples. The profile NO analyser was calibrated regularly by a cylinder standard and was utilized as an online reference for the eddy covariance system.

To determine the soil emission of nitric oxide, dynamic chamber measurements were made 50 m north of the main tower. The system consisted of three measurement chambers and one blank chamber (closed against the soil) as reference. Soil NO emission was determined according to *Meixner et al*. [1997] including corrections for gas-phase-reactions and blank chamber effects. The gas analysers applied were of the same type as the profile instruments described above. For details about the soil emissions and the chamber system see *Gut et al*. [2002a; 2002b].

2.3 Data Acquisition

The eddy covariance signals were sampled with a portable desktop computer at a frequency of 20.8 Hz. The data from the sonic anemometer and the NO analyser were transferred digitally via serial interfaces. A Labview (National Instruments, US) program was used for real-time data acquisition and processing. First- and second-order statistical moments as well as eddy covariance fluxes were calculated online and displayed in charts on the screen. All raw data were stored on optical disks every few days. Another Labview program on a second laptop computer in combination with a data acquisition device (DAQPad-1200, National Instruments, US) was used to control the trace gas profile system. The temperature profile was recorded on a 21X data logger (Campbell, US).

2.4 Data Evaluation and Corrections

For the present evaluation, the raw data were used to recalculate the fluxes after an intensive peak and gap control. Half-hour fluxes were calculated with a linear detrending of the time series [*Ammann*, 1999]. The fluxes were aligned perpendicular to the mean air stream by a two-dimensional coordinate rotation that forces the means of v and w to zero [see *Aubinet et al.*, 2000]. For correction and validation purposes, cospectra of the sensible heat and NO flux were calculated for 1-hour time series and classified by wind speed and thermal stratification.

Correlating the outputs of different sensors, one has to deal with errors caused by the physical properties of the sensors, the system setup, and the data acquisition. These errors especially affect the high-frequency part of the turbulence spectrum contributing to the flux. The spatial separation of the sensors (i.e., the sonic probe and the gas inlet), the limited dynamic instrument response, and the path averaging of the anemometer were potential sources for high-frequency attenuation of the applied eddy covariance system. Additionally, the laminar flow (Reynolds number Re = 1091) within the long inlet tubing enforced the need to estimate the resulting damping effect [see *Lenschow and Raupach*, 1991]. All mentioned effects could be described quantitatively as spectral transfer functions according to *Moore* [1986], *Zeller* et al. [1989], and *Horst* [2000]. In the following, the application of this transfer functions will be referred to as the theoretical approach.

The sensible heat flux solely measured by the sonic anemometer is only affected by the averaging along the finite sensing path. To estimate this effect the measured cospectra of the sensible heat flux were multiplied by the corresponding inverse transfer function. The resulting integrated flux correction factors are $6.8 \pm 1.5\%$ for the anemometer at 1 m and $2.1 \pm 0.5\%$ for the one at 11 m height.

To quantify the NO flux attenuation, cospectral similarity of the NO flux and the sensible heat flux during night time was assumed. The transfer functions derived for the NO system were applied to the corrected heat flux cospectra, which were considered as undamped reference spectra. The resulting mean NO flux loss obtained by this theoretical approach was $20.9 \pm 4.6\%$ for 1 m and $5.2 \pm 1.5\%$ for 11 m. During the day, the sensible heat flux and the corresponding cospectra showed a large variability and often changed the sign. Therefore they were not suitable for estimating the high-frequency attenuation. As a simple approach, the average night-time flux loss value was used for the correction of all fluxes including the daytime cases.

A potential systematic error source for flux measurements of reactive trace gases are chemical reactions within the tubing between the sampling inlet and the analyser. In the case of NO, only the chemical loss by the reaction with ozone ($NO + O_3 \rightarrow NO_2 + O_2$) had to be

considered, because photochemical NO production ($NO_2 + h\nu \rightarrow NO + O$) was excluded by the use of opaque tubes. An estimation of the effect according to *Beier and Schneewind* [1992] resulted in concentration modifications below the detection limit of the sensor and therefore could be neglected.

Exchange of sensible heat and water vapour lead to fluctuations in the density of dry air. These can generate contributions to the measured flux of other atmospheric constituents. *Webb et al*. [1980] showed that, especially for a trace gas with small turbulent fluctuations compared to the average mole fraction (e.g., CO_2), this apparent flux can be significant. According to an estimation of *Wienhold et al*. [1994], the temperature fluctuations are totally damped out through the long inlet tube and therefore have no influence on the NO flux measurements in this case. The evaporation determined by the dynamic soil chamber system was used to estimate the magnitude of the water vapour influence on the NO flux. In 95% of the half-hour values the contribution was below 1% and was therefore generally neglected in the flux evaluation.

2.5 Error Estimation and Rejection Criteria

Compared to other micrometeorological methods, the eddy-covariance technique is the most direct physical approach to determine turbulent fluxes. Instrumental errors excluded and an appropriate detrending assumed, the result represents at least a local flux at the measuring height also in a forest canopy. To ensure that the measured fluxes are representative for the exchange rates of the underlying surface, several requirements based on the conservation budget of the quantity of interest have to be met [*Baldocchi and Meyers*, 1991]. This requirements were taken into account by excluding periods with insufficient homogenous upwind fetch [*Businger*, 1986] or unsteady conditions. A criterion similar to the one suggested by *Foken and Wichura* [1996] was used for the stationarity test. Data were rejected if the flux averaged over 30 minutes deviated more than 50% from the average of the fluxes obtained from 10 minute subintervals. The chosen rejection threshold considers the fact that the contribution of larger turbulence elements to the trace gas transport is rather distinct within tall vegetation canopies. On the other hand, if more than 50% of the total covariance is contributed by the very low-frequency fluctuations of the turbulence spectra, the value is rejected by this procedure suspecting a non-linear trend to be the reason for the large difference. The overall rejection rate was 48% of the original data set.

There are various error sources in the flux determination because of the high requirements of the eddy covariance method on the sensor properties and the environmental conditions [see *Businger*, 1986; *Ammann*, 1999]. Besides the high temporal resolution, the noise level of the trace gas analyser must be low enough to allow the detection of turbulent concentration fluctuations above the noise level [*Baldocchi and Meyers*, 1991]. The NO analyser has a 1σ-noise level (detection

limit) of 70 ppt at an integration interval of 0.1 s (the signal integration is equivalent to a low-pass filter which prevents alaising effects). The power spectrum (Figure 3) of the NO time series recorded at 1 m above the forest floor shows this distinct noise at frequencies higher than 0.6 Hz. A slope of +1 in the log–log plot as shown by the NO spectrum is indicative for ideal white noise [*Wesely and Hart*, 1985]. Such white noise makes no systematic contribution to the turbulent flux because it is not correlated to the fluctuations of the vertical wind component. The random effect according to *Lenschow and Kristensen* [1985] results in a minimum resolvable NO flux of 0.07 ng N m^{-2} s^{-1}.

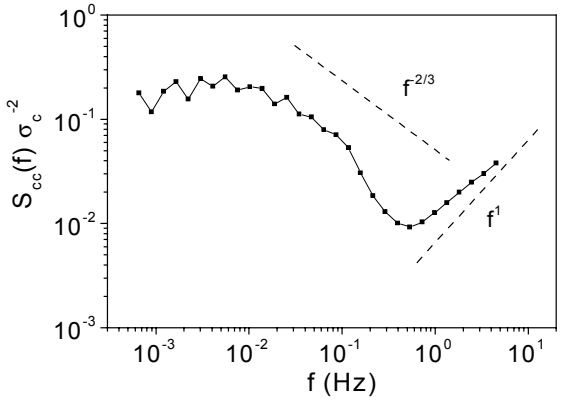

Figure 3. NO composite power spectrum, 1 m above the forest floor.

3 Results and Discussion

3.1 Stability Conditions and Cospectral Characteristics

Turbulent transport processes within tall canopies are not always directly related to the turbulence regime of the atmospheric boundary layer above the canopy. Especially on calm clear nights, the lower part of the canopy is often decoupled from the stable surface layer aloft and dominated by free convection. Detailed investigations on night-time in-canopy convection have been made by *Jacobs et al*. [1994] for maize and by *Bosveld et al*. [1999] for a Douglas fir forest. This phenomenon also occurred at the RBJ forest site, as previously observed by *Kruijt et al*. [2000].

A slightly unstable layer up to 20 m within the canopy can be seen on the typical night time profile of the potential temperature in Figure 1b. Responsible for this thermal stratification is a strong radiative cooling in the crown region between 20 m and 30 m where the biomass concentration has its maximum. The upward sensible heat flux from the relatively warm forest floor represents a comparable source situation for the sensible heat and the NO emitted from the soil, substantiating the cospectral similarity assumed for the high-frequency correction in Section 2.4. Figure 4a and b show composite cospectra of the sensible heat flux and the NO flux as observed for unstable conditions and moderate wind speeds at 11 m and 1 m height, respectively. Also displayed are the cospectra of the sensible heat flux damped by the theoretical transfer functions (Figure 4c and d). Despite the fact that some of these transfer functions are derived on the basis of isotropic turbulence (which probably can not be assumed to be present within the canopy), the

agreement with the high-frequency behaviour of the NO system is remarkably good.

For a quantitative validation of the high-frequency correction applied, the integral damping factor was also determined from a direct comparison of the measured cospectra of the NO and the sensible heat flux by empirical fitting of a transfer function of the following form

$$Tr(f) = \exp\left(-0.347\left(\frac{f}{f_c}\right)^{\frac{3}{2}}\right) \quad (1)$$

Here, f denotes the frequency (Hz) and f_c is the cut-off frequency which was determined for typical wind speed conditions to be 5.9×10^{-2} Hz and 2.7×10^{-2} Hz for 11 m and 1 m height, respectively. Only small differences between the fitted and the theoretical transfer functions are visible for the cases shown in Figure 4c and d. The resulting mean flux reduction was $20.9 \pm 2.8\%$ and $5.4 \pm 1.2\%$. These values are practically identical to the ones derived by the theoretical approach referenced in Section 2.4.

Due to the low horizontal wind speeds within the canopy, the total spectral attenuation at both heights was generally dominated by the spatial separation between the sample inlet and the sonic anemometer (Figure 4c and d). The effect is more pronounced for the system at 1m because of the smaller size of flux contributing eddies close to the ground. In accordance with the cospectra shown by *Meyers* and *Baldocchi* [1993] for several trace gases within a deciduous forest, only a minimal part of the covariance occurs at frequencies higher than 1 Hz. The pronounced flux contributions of larger structures that can be seen in the cospectra show that the use of a relatively long averaging interval of 30 minutes is necessary even within a forest canopy.

During night time the conditions within the lowest 20 m of the forest did not vary significantly with respect to wind speed and thermal stratification. Thus, the application of a constant average correction factor is not problematic. During the day the similarity between the sensible heat flux and the NO flux is not valid. A completely different source/sink distribution for both quantities leads to a lack of reference cospectra for the NO flux correction.

The flux loss determined solely for unstable night time conditions probably represents a lower limit for the real flux loss between 0800 LT and 1800 LT. Owing to the stable stratification (see Figure 1c) at this time of the day, the covariance portion of the high frequencies is probably higher.

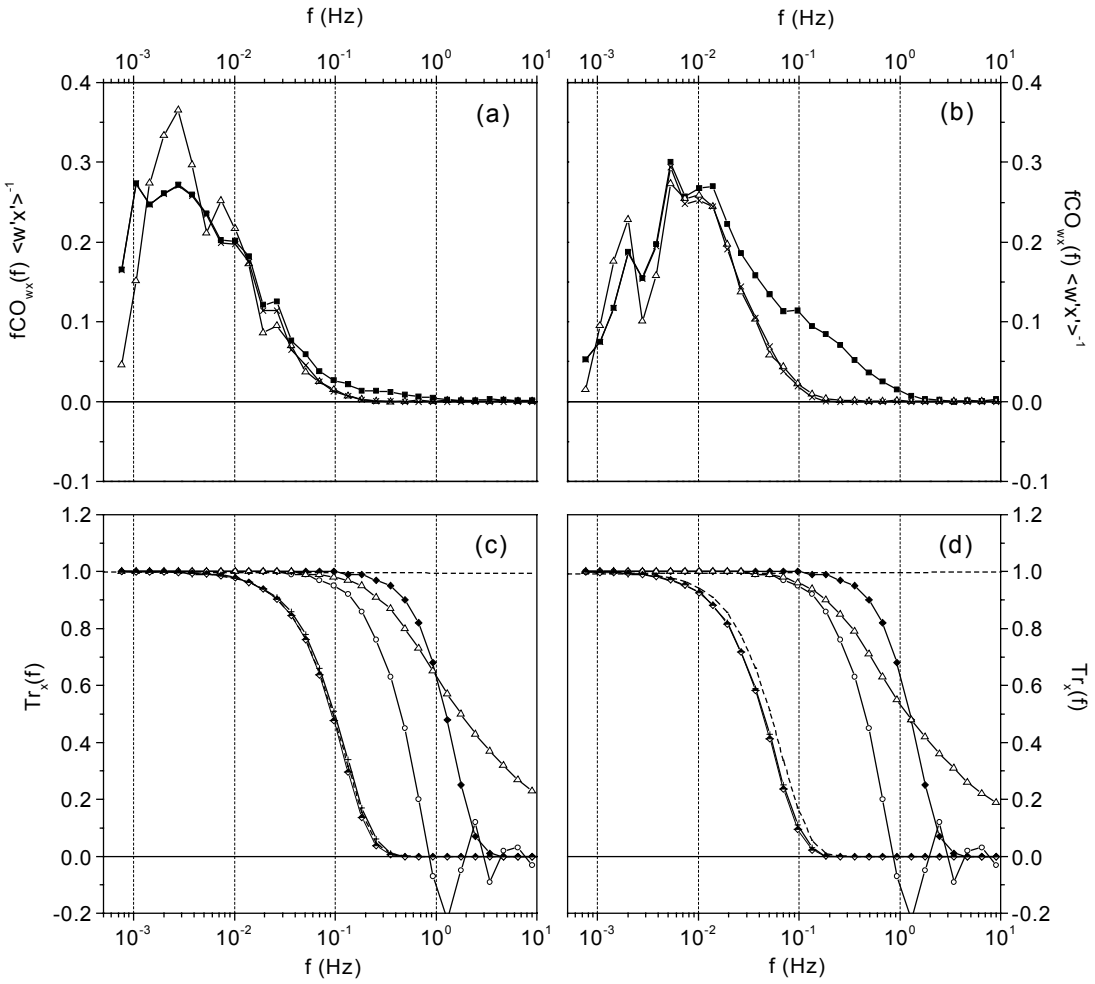

Figure 4. Normalised cospectra of the corrected sensible heat flux (solid squares), damped with the theoretical transfer function (crosses) and the measured NO flux (open triangles) (a) at 11 m height and (b) at 1 m height. Transfer functions of instrument response (open circles), tube damping (solid diamonds), sonic path averaging (open triangles), sensor separation (cross), total (half solid diamonds), and the one fitted to the measured cospectra ratio (dashed line); (c) at 11 m height, (d) at 1 m height (negative values of transfer functions is a result of the numerical approximation and not relevant here).

3.2 Comparison of Eddy Covariance and Chamber Fluxes

For validation and interpretation of the NO flux measurements by the eddy covariance technique, the results are compared to the soil NO emission simultaneously measured by the dynamic chambers. The fact that the chamber system was 50 m away from the micrometeorological setup makes a direct comparison problematic. The probability to have the chamber array within the main source

area of the eddy covariance system is not very high. *Baldocchi* [1997] investigated the spatial characteristics of 'flux footprints' under a forest canopy with a Lagrangian random walk model. Transferring his results to the situation in a tropical rain forest, the main source area, especially for the system at 1 m above ground, is relatively small and close to the probe. Typical ratios between the mean horizontal wind velocity $\overline{u}$ and the standard deviation of the vertical wind component σ_w of about 3 result in a peak of the 'footprint' function at a distance of only 2 to 5 m for the lower system and 22 to 55 m for the higher one. Inhomogeneous distribution of incoming radiation and precipitation may produce long- and short-term spatial variations of parameters as soil temperature or soil moisture which have direct influence on the NO emissions [*van Dijk and Meixner*, 2001]. Thus a direct matching of individual flux measurements by the eddy covariance and the soil chamber method may not be expected.

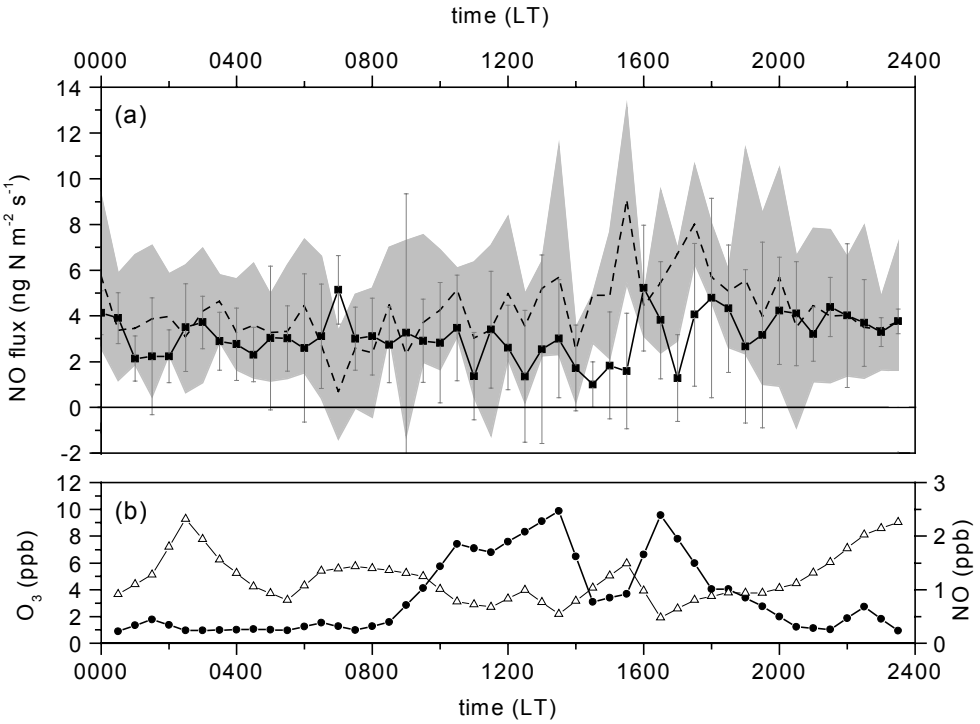

Figure 5. Mean diurnal course from 23 October to 01 November of (a) the NO flux measured by the eddy covariance system at 1 m height (full squares), NO soil emissions measured by the dynamic chambers (mean: dashed line; range: grey shaded area) and (b) NO (open triangles) and O3 (solid circles) mixing ratio at 1 m height . The vertical bars indicate the variability of the eddy covariance results over the averaging period.

Table 1. Average values for the period from 23 OCT to 01 NOV 1999[a].

Quantity	Total average	Average night	Average day
NO, ppb	1.7 ± 0.11	2.0 ± 0.17	1.2 ± 0.13
O3, ppb	5.2 ± 0.37	3.4 ± 0.39	7.7 ± 0.67
NO flux EC, ng N m^{-2} s^{-1}	3.4 ± 0.14	3.5 ± 0.14	2.9 ± 0.27
Soil emmission chambers, ng N m^{-2} s^{-1}	4.5 ± 0.20	3.9 ± 0.14	5.5 ± 0.36

[a]Mixing ratios and eddy covariance (EC) results are measured at 1 m height. The night-time and daytime averages represent the measurements from 2000 LT to 0800 LT and 0930 LT to 1800 LT, respectively.

For the comparison of the two methods, it seems to be more appropriate to use the mean diurnal course. It represents a spatially averaged NO emission behaviour of the forest soil, because the local short-term variability is smoothed out. In Figure 5a the diurnal pattern of the NO emission for a 10-day period from 23 October to 1 November 1999 is displayed as half-hour means (the average values for this period are compiled in Table 1). In order to reduce the impact of non-representative outliers on the diurnal course, the median is generally used for the averaging over this period. The flux results of the chamber measurements show a relative wide range with values up to 12 ng N m^{-2} s^{-1}, reflecting the small-scale spatial heterogeneity of the soil with respect to NO emissions. The mean value of all three chambers shows only a weak diurnal variation with highest values in the afternoon and an overall average of 4.5 ± 0.20 ng N m^{-2} s^{-1}. The displayed eddy covariance fluxes include the results of the 1 m system installed at the two sensing locations, since no systematic difference was found between them The NO concentration at the measurement height was generally high with averages of 1.2 ppb for daytime and 2.0 ppb for night time (Figure 5b). The average NO flux derived by eddy covariance is 3.4 ± 0.14 ng N m^{-2} s^{-1} and therefore 23% lower than the overall average of the chamber measurements. During the night from 2000 LT to 0800 LT the measured fluxes of both methods match quite well. With a night-time average of 3.9 ± 0.14 ng N m^{-2} s^{-1} and 3.5 ± 0.14 ng N m^{-2} s^{-1} for the NO fluxes measured by the chambers and eddy covariance, respectively, the difference is only 9%. In the late morning the results of the two systems start to diverge. The daytime eddy covariance flux is generally on the lower limit of the individual chamber results. The difference for the average fluxes measured during the day amount to 48%. The main part of this deviation may be attributed to the

chemical reaction of nitric oxide with ozone. Above the canopy, ozone is photochemically produced or transported downwards from the residual layer because of the increasing vertical mixing after sunrise. Intermittently, turbulence events [*Gao et al.*, 1989; *Raupach et al.*, 1996] are penetrating down into the canopy transporting the whole bunch of atmospheric constituents into the stem space. As a result of this entrainment from aloft, the mean ozone mixing ratio at 1 m height reaches up to 10 ppb during daytime and consequently the NO concentration is reduced to 1.2 ppb (Figure 5b). A slight underestimation of the real flux during the day might be introduced by an inadequate correction of the high-frequency damping effects. For the stable stratification during the day, the attenuation might be somewhat higher than estimated. But this error is presumably small compared to the chemical effect. In contrast to the daytime situation, there are ideal conditions during the night for the comparison of the soil emissions and the fluxes measured at some height above. Almost no chemical reaction can occur between the surface and the measuring height of the eddy covariance, because the ozone concentration is very low and a well-developed vertical mixing prevents a significant storage within this layer.

Figure 6a shows the corresponding results for an earlier 9-day period from 23 September to 1 October 1999, when the eddy covariance system was installed at 11 m (Table 2). The range of the individual chamber fluxes was higher during this period with values up to 18 ng N m^{-2} s^{-1}. The mean soil emission shows also a slightly different diurnal course with the highest values occurring between 1100 LT and 1500 LT. The overall average for these 9 days is 5.8 ± 0.25 ng N m^{-2} s^{-1}. The equivalent value of the eddy covariance results is 2.8 ± 0.25 ng N m^{-2} s^{-1} and therefore 51% lower. This discrepancy is mainly caused by differences in the daytime values. High ozone mixing ratios with a maximum of 31 ppb at 11 m (Figure 6b) led to a strong chemical loss of NO in the lower part of the canopy. As a consequence, nearly no NO was able to reach the measuring height between 0930 LT and 1800 LT, leading to a very low average daytime concentration of 0.07 ppb. The average daytime NO flux measured at 11 m height was 0.6 ± 0.12 ng N m^{-2} s^{-1} and therefore 92% lower than the corresponding soil emission. At night, the lack of chemical sinks in the lowest 11 m and the effective mixing within the stem space led to much higher NO concentrations averaging 1.9 ppb; and the magnitude of the mean flux measured by eddy covariance (4.8 ± 0.39 ng N m^{-2} s^{-1}) agrees quite well with the mean soil emission (5.2 ± 0.31 ng N m^{-2} s^{-1}) obtained by the dynamic chamber system.

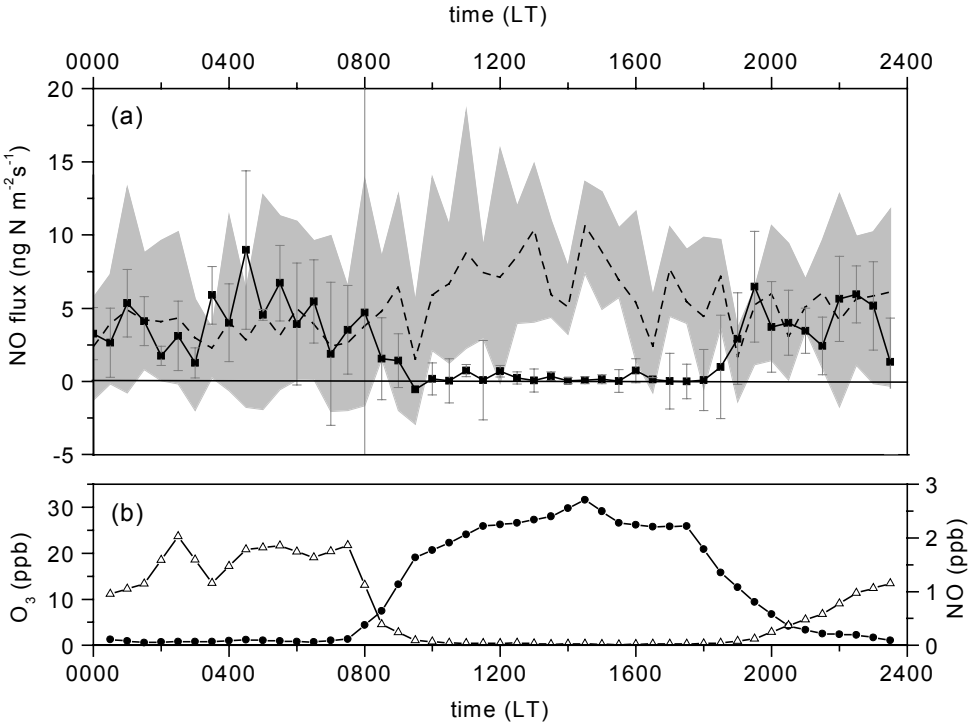

Figure 6. Mean diurnal course from 23 September to 01 October of (a) the NO flux measured by the eddy covariance system at 11 m height (full squares), NO soil emissions measured by the dynamic chambers (mean: dashed line; range: grey shaded area) and (b) NO (open triangles) and O3 (solid circles) mixing ratio at 11.3 m height . The vertical bars indicate the variability of the eddy covariance results over the averaging period.

Table 2. Average values for the period from 23 SEP to 01 OCT 1999.

Quantity	Total average	Average night	Average day
NO, ppb	1.0 ± 0.12	1.9 ± 0.21	0.07 ± 0.02
O3, ppb	13.2 ± 0.86	3.5 ± 0.52	26.2 ± 0.93
NO flux EC, ng N m^{-2} s^{-1}	2.8 ± 0.25	4.8 ± 0.39	0.6 ± 0.12
Soil emission chambers, ng N m^{-2} s^{-1}	5.8 ± 0.25	5.2 ± 0.31	6.8 ± 0.47

[a]Mixing ratios are measured at 11.3 m, eddy covariance (EC) results at 11 m height. The averaging intervals are identical to Table 1

As mentioned before, the relatively large range of the soil emissions obtained by the dynamic chamber measurements is an indication for small-scale inhomogeneities. They can be caused by variations in soil temperature, soil moisture, leaf litter cover, or the vicinity of trees [*Pilegaard et al.*, 1999]. This makes clear that it is necessary to choose well-distributed spots for the array of chambers to get a representative picture of the mean forest soil emission. In contrast, the eddy covariance method directly yields fluxes averaging over a large source area of several hundreds to thousands of square metres, which is a distinct advantage of this method.

4 Conclusions

Eddy covariance measurements of the turbulent NO flux were performed at two different heights within a tropical rain forest. The specifications of the NO analyser applied were found to be sufficient to meet the high requirements of this method. The residence time in the 25 m sampling tube could be kept low by the flow regulating capillary installed close to the inlet. In this way, a significant reduction of NO owing to the reaction with ozone within the tubing was prevented. Night time similarity between the cospectra of the sensible heat flux and the NO flux offered the possibility to correct the high-frequency attenuation of the NO eddy covariance measurements. Integrated flux correction factors of 20.9 ± 4.6% for the system at 1 m and 5.2 ± 1.5% for the one at 11 m above ground were estimated by transfer functions adopted from the literature and confirmed empirically by comparing the measured cospectra.

At night, the NO fluxes measured by eddy covariance were generally in good agreement with the mean NO soil emission rates obtained by a dynamic chamber system. During daytime, ozone entrained from above into the canopy created a local sink of NO within the layer between the surface and the measuring height of the flux system. Therefore the NO flux as measured by the eddy covariance method was significantly reduced. At 11 m height the daytime NO flux was generally close to zero, indicating that nearly all soil emitted NO was reacting with ozone forming NO_2 within the lowest few meters of the forest canopy.

The good agreement between the two independent flux measurement techniques under suitable night time conditions indicates that the eddy covariance method can be used to make reliable NO flux measurements within a forest canopy. These results encourage the use of the eddy covariance method as a promising tool for the investigation of in-canopy processes relevant to the NO transport.

Acknowledgements

This research is supported by the "Environmental and Climate Programm" (ENV4-CT97-0566) of the European Union and the Max Planck Society. The authors thank Thomas Foken for the helpful discussion and

Carol Strametz for improving the language of the manuscript. We would also like to thank the staff at INCRA (Instituto Nacional de Colonização e Reforma Agrária) and IBAMA (Instituto Brasileiro do Meio Ambiente e dos Recursos Naturais Renováveis) in Ji-Paraná for the help in installing and maintaining the infrastructure. We are indebted to Beatrize E. Gomes (Universidade Federal de Rondônia, Ji-Paraná) for support concerning everything. We are also grateful to Monika Scheibe and Wesley Saores da Silva for assisting us in the field.

References*

Ammann, C., On the aplicability of relaxed eddy accumulation and common methods for measuring trace gas fluxes, Dissertation thesis, Universität Zürich, 229 pp., 1999.

Andreae, M. O., P. Artaxo, C. Brandao, F. E. Carswell, P. Ciccioli, A. L. da Costa, A. Culf, J. L. Esteves, J. H. C. Gash, J. Grace, P. Kabat, J. Lelieveld, Y. Mahli, A. O. Manzi, F. X. Meixner, A. D. Nobre, C. Nobre, M. d. L. P. Ruivo, M. A. Silva-Dias, S. P., R. Valentini, J. von Jouanne, and M. J. Waterloo, Biogeochemical cycling of carbon, water, energy, trace gases, and aerosols in Amazonia, *Journal of Geophysical Research*, *107* (D20), 8066, doi: 10.1029/2001JD000524, 2002.

Aubinet, M., A. Grelle, A. Ibrom, U. Rannik, J. B. Moncrieff, T. Foken, A. S. Kowalski, P. H. Martin, P. Berbigier, C. Bernhofer, R. Clement, J. Elbers, A. Granier, T. Grünwald, K. Morgenstern, K. Pilegaard, C. Rebmann, W. Snijders, R. Valentini, and T. Vesala, Estimation of annual net carbon and water exchange of forests: The EUROFLUX methodology, *Advances in Ecological Research*, *30*, 113-175, 2000.

Bakwin, P. S., S. C. Wofsy, and S. M. Fan, Measurements of Reactive Nitrogen-Oxides (NO_y) within and above a Tropical Forest Canopy in the Wet Season, *Journal of Geophysical Research-Atmospheres*, *95* (D10), 16765-16772, 1990.

Baldocchi, D., Flux footprints within and over forest canopies, *Boundary-Layer Meteorology*, *85* (2), 273-292, 1997.

Baldocchi, D. D., and T. P. Meyers, Trace gas exchange above the floor of a deciduous forest, 1. Evaporation and CO2 flux, *Journal of Geophysical Research*, *96*, 7271-7285, 1991.

Baldocchi, D. D., S. B. Verma, D. R. Matt, and D. E. Anderson, Eddy correlation measurements of carbon dioxide efflux from the floor of a deciduous forest, *Journal of Applied Ecology*, *23*, 967-975, 1986.

* References in press were actualized in comparison to the original manuscript

Baldocchi, D. D., C. A. Vogel, and B. Hall, Seasonal variation of energy and water vapor exchange rates above and below a boreal jack pine forest canopy, *Journal of Geophysical Research*, *102* (D24), 28939-28951, 1997.

Beier, N., and M. Weber, Turbulente Austauschprozesse in der Grenz-schicht, Meteorologisches Institut der Universität München, München, 1992.

Blanken, P. D., T. A. Black, H. H. Neumann, G. Den Hartog, P. C. Yang, Z. Nesic, R. Staebler, W. Chen, and M. D. Novak, Turbulent flux measurements above and below the overstory of a boreal aspen forest, *Boundary-Layer Meteorology*, *89* (1), 109-140, 1998.

Blanken, P. D., T. A. Black, P. C. Yang, H. H. Neumann, Z. Nesic, R. Staebler, G. den Hartog, M. D. Novak, and X. Lee, Energy balance and canopy conductance of a boreal aspen forest: partitioning overstory and understory components, *JGR*, *102* (D24), 28915 - 28927, 1997.

Bosveld, F. C., A. A. M. Holtslag, and B. Van den Hurk, Nighttime convection in the interior of a dense douglas fir forest, *Boundary-Layer Meteorology*, *93*, 171-195, 1999.

Businger, J. A., Evaluation of the accuracy with which dry deposition can be measured with current micrometeo-rological techniques, *Journal of Climate and Applied Meteorology*, *25*, 1100-1124, 1986.

Chameides, A. L., F. C. Fehsenfeld, M. O. Rodgers, C. Cardelino, J. Martinez, D. D. Parrish, W. Lonneman, D. R. Lawson, R. A. Rasmussen, P. Zimmermann, J. Greenberg, P. Middleton, and T. Wang, Ozone precursor relationships in ambient atmosphere, *Journal of Geophysical Research*, *97* (D5), 6037-6055, 1992.

Civerolo, K. L., and R. R. Dickerson, Nitric oxide soil emissions from tilled and untilled cornfields, *Agricultural and Forest Meteorology*, *90* (4), 307-311, 1998.

Crutzen, P. J., The role of NO and NO_2 in the chemistry of the troposphere and the stratosphere, *Annual Review of Earth and Planetary Sciences*, *7*, 443-472, 1979.

Davidson, E. A., and W. Kingerlee, A global inventory of nitric oxide emissions from soils, *Nutrient Cycling in Agroeecosystems*, *48*, 37-50, 1997.

Delany, A. C., Fast-response chemical sensors used for eddy correlation flux measurements, in *Measurement Challenges in Atmospheric Chemistry*, pp. 91-100, American Chemical Society, 1993.

Delany, A. C., D. R. Fitzjarrald, D. H. Lenschow, R. Pearson, G. J. Wendel, and B. Woodruff, Direct measuremants

of nitrogen oxides and ozone over grassland, *Journal of Atmospheric Chemistry*, *4*, 429-444, 1986.

Demnead, O. T., Plant physiological methods for studying evapotranspiration problems of telling the forest from the trees, *Agr. Water Manage.*, *8*, 167-189, 1984.

Foken, T., and B. Wichura, Tools for quality assessment of surface-based flux measurements, *Agricultural and Forest Meteorology*, *78*, 83-105, 1996.

Fontijn, A., A. J. Sabadell, and R. J. Ronco, Homogenous chemiluminescent measurement of nitric oxide with ozon, *Analythical Chemistry*, *42* (6), 575 - 579, 1970.

Galbally, I. E., Emission of fixed nitrogen compounds to the atmosphere in remote areas, in *Biogeochemical Cycling of Sulfur and Sitrogen in Remote Areas*, edited by J.N. Galloway, D. Reidel, Norwell, Mass., 1985.

Gao, W., R. H. Shaw, and K. T. Paw U, Observation of organized structure in turbulent flow within and above a forest canopy, *Boundary-Layer Meteorology*, *47*, 349-377, 1989.

Gash, J. H. C., J. M. Nobre, J. M. Roberts, and R. L. Victoria, An overview of ABRACOS, in *Amazonian Deforestation and Climate*, edited by J.H.C. Gash, J.M. Nobre, J.M. Roberts, and R.L. Victoria, John Wiley, New York, 1996.

Gut, A., M. Scheibe, S. Rottenberger, U. Rummel, M. Welling, C. Ammann, G. A. Kirkman, U. Kuhn, F. X. Meixner, J. Kesselmeier, B. E. Lehmann, J. Schmidt, E. Müller, and M. T. F. Piedade, Exchange fluxes of NO_2 and O_3 at soil and leaf surfaces in an Amazonian rain-forest, *Journal of Geophysical Research*, *107* (D20), 8060, doi:10.1029/2001JD000654, 2002a.

Gut, A., S. M. van Dijk, M. Scheibe, U. Rummel, M. Welling, C. Ammann, F. X. Meixner, M. O. Andreae, and B. E. Lehmann, NO emission from an Amazonian rain forest soil: Continuous measurements of NO flux and soil compensation concentration, *Journal of Geophysical Research*, *107* (D20), 8057, doi: 10.1029/2001JD000521, 2002b.

Horst, T. W., On frequency response corrections for eddy covariance flux measurements, *Boundary-Layer Meteorology*, *94* (3), 517-520, 2000.

Jacob, D. J., and S. C. Wofsy, Budgets of reactive nitrogen, hydrocarbons, and ozone over the Amazon-Forest during the wet season, *Journal of Geophysical Research*, *95* (D10), 16737-16754, 1990.

Jacobs, A. F. G., J. H. van Boxel, and R. M. M. Elkilani, Nighttime free-convection characteristics within a clant canopy, *Boundary-Layer Meteorology*, *71* (4), 375-391, 1994.

Kaplan, W. A., S. C. Wofsy, M. Keller, and J. M. da Costa, Emission of NO and deposition of O_3 in a tropical forest system, *Journal of Geophysical Research*, *93* (D2), 1389-1395, 1988.

Kirkman, G. A., A. Gut, C. Ammann, L. V. Gatti, A. M. Cordova, M. A. L. Moura, M. O. Andreae, and F. X. Meixner, Surface exchange of nitric oxide, nitrogen dioxide, and ozone at a pasture in Rondonia, Brazil, *Journal of Geophysical Research*, *107* (D20), 8083, doi: 10.1029/2001JD000523, 2002.

Kruijt, B., Y. Malhi, J. Lloyd, A. D. Nobre, A. C. Miranda, M. G. P. Pereira, A. Culf, and J. Grace, Turbulence statistics above and within two Amazon rain forest canopies, *Boundary-Layer Meteorology*, *94*, 287-331, 2000.

Lee, X., and A. Black, Atmospheric turbulence within and above a Douglas-Fir stand. Part 2: Eddy fluxes of sensible heat and water vapour, *Boundary Layer Meteorology*, *64*, 369-389, 1993.

Lenschow, D. H., and L. Kristensen, Uncorrelated noise in turbulence measurements, *Journal of Atmospheric and Oceanic Technology*, *2*, 68-81, 1985.

Lenschow, D. H., and M. R. Raupach, The attenuation of fluctuations in scalar concentrations through sampling tubes, *Journal of Geophysical Research*, *96* (D8), 15259-15268, 1991.

Li, Y., V. P. Aneja, S. P. Arya, J. Rickman, J. Brittig, P. Roelle, and D. S. Kim, Nitric oxide emission from intensively managed agricultural soil in North Carolina, *JGR*, *104* (D21), 26115 - 26123, 1999.

Meixner, F. X., Surface exchange of odd nitrogen oxides, *Nova Acta Leopoldina*, *70* (288), 299-348, 1994.

Meixner, F. X., T. Fickinger, L. Marufu, L. Mukurumbira, E. Makina, F. J. Nathaus, D. Serca, and M. O. Andreae, Preliminary results on nitric oxide emission from a southern African savanna ecosystem, *Nutrient Cycling in Agroecosystems*, *48*, 123-138, 1997.

Meyers, T. P., and D. D. Baldocci, Trace gas exchange above the floor of a deciduous forest 2. SO_2 and O_3 deposition, *JGR*, *98* (D7), 12631 - 12638, 1993.

Moore, C. J., Frequency response correction for eddy correlation systems, *Boundary-Layer Meteorology*, *37*, 17-35, 1986.

Pilegaard, K., P. Hummelshoj, and N. O. Jensen, Nitric oxide emission from a

Norway spruce forest floor, *Journal of Geophysical Research*, *104* (D3), 3433-3445, 1999.

Raupach, M. R., J. J. Finnigan, and Y. Brunet, Coherent eddies and turbulence In vegetation canopies - the mixing-layer analogy, *Boundary Layer Meteorology*, *78*, 351-382, 1996.

van Dijk, S. M., A. Gut, G. A. Kirkman, B. M. Gomes, F. X. Meixner, and M. O. Andreae, Biogenic NO emissions from forest and pasture soils: relating laboratory studies to field measurements, *Journal of Geophysical Research*, *107* (D20), 8050, doi:10.1029/2001JD000358, 2002.

van Dijk, S. M., and F. X. Meixner, Production and consumption of NO in forest and pasture soils from the Amazonian basin: A laboratory study, *Water Air and Soil Pollution*, *Focus:1*, 119-130, 2001.

Verchot, L. V., E. A. Davidson, J. H. Cattanio, I. L. Ackermann, H. E. Erickson, and M. Keller, Land use change and biogechemical controls of nitrogen oxide emissions from soils in eastern Amazonia, *Global Biogeochemical Cycles*, *13*, 31-46, 1999.

Webb, E. K., G. I. Pearman, and R. Leuning, Correction of flux measurements for density effects due to heat and water vapour transfer, *Quarterly Journal of the Royal Meteorological Society*, *106*, 85-100, 1980.

Wesely, M. L., J. A. Eastman, D. H. Stedman, and E. D. Yalvac, An eddy-correlation measurement of NO_2 flux to vegetation and comparison to O_3 fluxs, *Atmospheric Environment*, *16*, 1982.

Wesely, M. L., and R. L. Hart, Variability of short term eddy-correlation estimates of mass exchange, in *The Forest Atmosphere Interaction*, edited by B.A. Hutchison, and B.B. Hicks, pp. 591-612, D. Reidel Publishing Company, Oak Ridge, Tennesee, 1985.

Wienhold, F. G., H. Frahm, and G. W. Harris, Measurements of N_2O fluxes from fertilized grassland using a fast response tunable diode laser spectrometer, *Journal of Physical Oceanography*, *99* (D8), 16557-16567, 1994.

Zeller, K., W. Massman, D. Stocker, D. G. Fox, D. Stedman, and D. Hazlett, Initial results from the pawnee eddy correlation system for dry acid deposition research, United States Department of Agriculture (USDA), Forest Service, 1989.

Appendix D

Characterization of Turbulent Air Motion within and above a Tropical Rain Forest in Amazonia

U. RUMMEL[1*], C. AMMANN[3], T. FOKEN[2], and F.X. MEIXNER[1]

[1]Max Planck Institute for Chemistry, Biogeochemistry Dept., D-55020 Mainz, Germany, [2]Universität Bayreuth, Abt. Mikrometeorologie, D-95440 Bayreuth, Germany, [3]Air Pollution - Climate group (TP 11.3), FAL-Reckenholz,P.O.Box, CH-8046 Zürich, Switzerland

for submission in **Boundary Layer Meteorology**

Abstract. The turbulence structure within and above a tropical rain forest was investigated in southwest Amazonia. The results confirm the findings of a former experiment which indicated that compared to the extremely dense rain forest of central Amazonia, during daytime a larger volume of the more open canopy is directly coupled to the atmosphere above. Especially under windy conditions with wind speeds above 2 m s^{-1}, high values of skewness and kurtosis indicate the occurrence of large scale eddies which penetrate deep into the forest. The mean vertical distribution of turbulent TKE (turbulent kinetic energy) transport shows, that during daytime only a relative shallow layer above the forest floor is not included in the direct air exchange with regions above the vegetation stand. At night, the sub-canopy was mostly decoupled from the nocturnal boundary layer by a temperature inversion throughout the forest crown. The vertical turbulence structure in the unstably stratified nocturnal rain forest stem space was found to be similar to that of the atmospheric mixing layer and could be closely described by an analogous convective velocity scale w_* (on the basis of the inversion base height and a internal sub-canopy heat flux).

Keywords: Tropical forest, Turbulent kinetic energy, Statistical moments, Night time convection

1 Introduction

Vegetation-atmosphere exchange of momentum, heat and trace gases is largely dependent on the coupling of the canopy to the boundary layer above. The way in which turbulent transport is established determines the temporal and spatial framework for all air-surface interactions and chemical reactions within the canopy space. Therefore, particularly to understand the exchange of reactive trace gases like nitrogen oxides and ozone, detailed information about the turbulent wind field

*corresponding author

characteristics and transport mechanisms is valuable. The architecture of rain forests with high LAI and huge canopy space as well as the environmental conditions in the tropics, characterized by high humidity and radiative input, are very specific. Beside wind tunnel experiments, most intensive field studies on forest turbulence were carried out in temperate and boreal canopies (for reviews see Kaimal and Finnigan, 1994; Raupach et al., 1996; Finnigan, 2000). The investigations which were focusing on turbulence characteristics of tropical rain forest canopies are scarce (Fitzjarrald et al., 1988; Pinker and Holland, 1988; Fitzjarrald and Moore, 1990; Fitzjarrald et al., 1990; Kruijt et al., 2000). The most extensive measurements from 5 simultaneously operated sonic anemometers were presented by Kruijt et al. (2000) at a forest site in central Amazonia. One of their main results was that during typical daytime conditions only the upper third of this tropical vegetation layer is coupled to the atmosphere above. Additionally presented mean daytime profiles of turbulent velocity statistics from a site in southwest Amazonia suggested less pronounced decoupling of the rain forest canopy in that region.

The present study was part of the LBA-EUSTACH program (EUropean Studies on Trace gases and Atmospheric CHemistry as a contribution to Large-scale Biosphere–atmosphere experiment in Amazonia; LBA) (Andreae et al., 2002). Although the LBA-EUSTACH field studies were not designed specifically as turbulence experiments, the obtained data set provides information about the turbulence structure at the rain forest site in southwest Amazonia, complementary to the results of Kruijt et al. (2000). Beside classified mean profiles of statistical velocity moments and turbulent kinetic energy budget terms, air motion within the nocturnal stem space is particularly addressed.

2 Experimental Information

The experimental site (10°04´55´´ S, 61°55´48´´ W, 147 m a.s.l.), a former ABRACOS site (Gash et al., 1996) is located in the Reserva Biológica Jarú (RBJ), a forest reserve 90 km north of the city Ji-Paraná in the state of Rondônia (southwest Amazonia), Brazil. An aluminum scaffolding tower of 52 m height erected in 1991 (Gash et al., 1996) was the main platform for the measurements conducted at the RBJ site. The vegetation cover of RBJ, owned by the Brazilian Environmental Protection Agency IBAMA (Instituto Brasileiro de Meio Ambiente e Recursos Renováveis) is a primary (terra firme) open rain forest with a closed canopy of about 32 m height (h_c). Single jutting trees reach heights up to 45 m. Due to their relevance for turbulence, an effective canopy layer height of 40 m (h) was defined for the analysis following Kruijt et al. (1996). The understory consists mainly of palms. The total LAI (leaf area index) was measured (LI-COR LAI 2000, USA) to be about 5.6. The horizontal extent of the forest is partly limited. Within the west-northwest to southeast sector primary rain forest exists for several tens of km. In the remaining sector a river (Rio Machado)

interrupts the vegetation. The minimum distance to the river (in the southwest direction) is about 400 m.

The LBA-EUSTACH measurements were performed in two experiments in 1999. The first experiment (LBA-EUSTACH 1) took place during the wet-to-dry season transition in April/May, the second one (LBA-EUSTACH 2) in September/October during the reverse transition from dry-to-wet season (see Andreae et al., 2002).

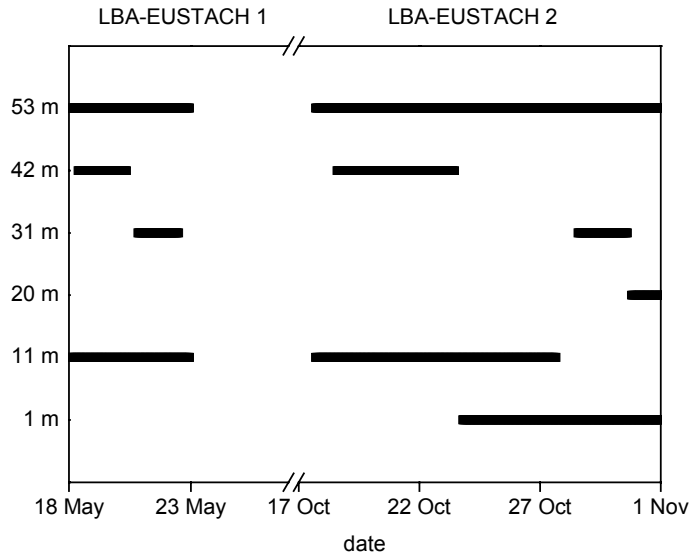

Figure 1. Time-height assignement for the sonic anemometers at the RBJ tower during LBA-EUSTACH 1 and 2 campaigns.

Fluctuations of the three wind velocity components (u, v, w) and virtual temperature (T_v) were almost continuously measured at heights of 53 m (= 1.33 h) and 11 m (= 0.28 h) by sonic anemometers (Gill Instruments, Solent Research 1012 K55, UK) mounted on booms extending 4 m horizontally. In order to characterize turbulent transport mechanisms within and above the canopy, experimental effort was intensified during temporally limited periods of each LBA-EUSTACH campaign. From 18 May to 22 May (LBA-EUSTACH 1) a third sonic anemometer (Gill Instruments, Research HS, UK) was operated alternately at 42 m (1.05 h) and 31 m (0.78 h) throughout the canopy to complement those at 53 m and 11 m height. From 17 October to 1 November (LBA-EUSTACH 2) two additional levels at 20 m (0.5 h) and 1 m (0.03 h) were included in the alternation of the third sonic anemometer (see Figure 1 for the time-height assignement of the sonic anemometers). Therefore, simultaneously acquired high frequency data from three levels are available during these time periods. The higher number of alternately measured levels during LBA-EUSTACH 2 was decisive for focusing the spatial analysis of single-point turbulence statistics on the time interval from

17 October to 1 November. On the other hand, the sensitivity of the fast trace gas probes above the canopy, specifically the ozone sensor, was higher during May. Because the canopy-atmosphere exchange of ozone is a crucial point of the LBA-EUSTACH project, the investigation of daytime scalar transport characteristics in Rummel et al. (2005c; 2005b) is confined on 18 May to 22 May.

3 Methods

3.1 TKE-Budget and Higher Statistical Moments

3.1.1 Mean Turbulent Kinetic Energy Budget

The relative importance of processes which control turbulent fluid motion is illustrated by the turbulent kinetic energy (TKE) budget. Within vegetation canopies additional terms in the surface layer TKE budget arise from flow interaction with plant elements. This flow-vegetation interaction, like aerodynamic drag, together with spatial variability imposed by plant elements cause a necessity of volume averaging the budget equation (Wilson and Shaw, 1977; Raupach and Shaw, 1982; Finnigan, 1985). The mean turbulent kinetic energy (TKE) $e = 0.5\left(\overline{u'^2} + \overline{v'^2} + \overline{w'^2}\right)$ budget equation for stationary and horizontally homogeneous (at spatial scales larger than the horizontal volume dimensions) conditions in a vegetation canopy is (e.g. Raupach et al., 1986; Finnigan, 2000):

$$\frac{\partial\langle e\rangle}{\partial t} = 0 = \underbrace{-\langle\overline{u'w'}\rangle\frac{\partial\langle\bar{u}\rangle}{\partial z}}_{P_s} \underbrace{-\langle\bar{u}\rangle f_D}_{P_w} + \underbrace{\frac{g}{\overline{\theta}_v}\langle\overline{w'\theta_v'}\rangle}_{P_b} \underbrace{-\frac{\partial\langle\overline{w'e}\rangle}{\partial z}}_{T_t}$$

$$\underbrace{-\frac{1}{\rho}\frac{\partial\langle\overline{w'p'}\rangle}{\partial z}}_{T_p} \underbrace{-\frac{\partial\langle\overline{w}''\overline{e}''\rangle}{\partial z}}_{T_d} + \underbrace{\upsilon\frac{\partial^2}{\partial z^2}\langle e\rangle}_{T_m} - \underbrace{\langle\varepsilon\rangle}_{D_e} \qquad (1)$$

Here overbar and single prime represent a temporal average and the departure from it, respectively. $\langle\ \rangle$ represents the volume average and the double prime the corresponding departure therefrom. Beside the wind velocity components u, v, and w, g is the gravitational acceleration, ρ is the air density, θ_v is the virtual potential temperature, and f_D is the effective aerodynamic drag (force per unit mass). The first three terms of the right side describe production/loss processes. The shear production P_s is usually transferring kinetic energy from the mean flow to the turbulent component. The buoyant production P_b converts potential energy to turbulent kinetic energy in unstable conditions. T_t and T_p represent the turbulent transport and the pressure transport of TKE, respectively. They are usually the

main non-local contributions to the TKE budget. The molecular transport term T_m is negligible. The last term at the right side D_e is the viscous dissipation ε. Two additional canopy specific terms in Eq. (1) (compared to the TKE surface layer budget) are P_w and T_d. A third term, namely the waving production is not listed in Eq. (1). It is associated with plant motion (leaf fluttering, etc.) and represents mainly a transfer of TKE from larger turbulent eddies to resonant frequencies of various plant elements. The effect of this transfer across the turbulence spectrum may cancel out for the integral (summing up all frequencies) TKE (Kaimal and Finnigan, 1994). Like P_s, the wake production term P_w represents a conversion rate of mean kinetic energy to turbulent kinetic energy. But as a consequence of the work done by the mean flow against the canopy elements the TKE arises at characteristic wake scales of those elements. Terms like the dispersive transport T_d arise from correlations in departures from spatial averages. Beside the fact, that dispersive terms can not be assessed from single tower measurements like the LBA-EUSTACH data set, they seem to be small in relation to other TKE budget terms, as suggested by wind tunnel experiments (see, e.g., Raupach et al., 1986). Because the LBA-EUSTACH experiments are mainly addressing the exchange of trace gases, the focus here is specifically on profiles of the turbulent transport T_t and the production terms P_s, P_w, and P_b. In order to asses these TKE budget terms, the single point measurements at each height are assumed to be representative for the local volume average. Hereby T_t, P_s, and P_b can be determined directly. The wake production was calculated by the approximation proposed by Raupach et al. (1986):

$$P_w = -\left\langle \overline{u} \right\rangle f_D = -\left\langle \overline{u'_i u'_j}'' \frac{\partial u_i''}{\partial x_j} \right\rangle \approx -\left\langle \overline{u} \right\rangle \frac{\partial \left\langle \overline{u'w'} \right\rangle}{\partial z} \qquad (2)$$

The approximation requires also dispersive contributions to be negligible.

3.1.2 Higher Statistical Moments

Skewness, the normalized third-order central statistical moment, is a measure for the asymmetry of the probability distribution. Defined as :

$$Sk_x = \frac{\overline{x'^3}}{\sigma_x^3}. \qquad (3)$$

A positive skewed distribution is characterized by a mean which is larger than the modus. A greater probability of large positive deviations from the mean than large negative one. For negative skewed data it is vice versa. The skewness of velocity components in the surface layer is usually close to zero equivalent to a Gaussian distribution.

Kurtosis expresses the peakedness or flatness of the probability density distribution and is the normalized fourth-order statistical moment.

$$K_x = \frac{\overline{x'^4}}{\sigma_x^4} \tag{4}$$

A value of 3 is for a normally (Gaussian) distributed variable is also characteristic for the velocity components in the surface layer.

3.2 DATA PROCESSING AND REJECTION CRITERIA

As motioned before, three ultrasonic anemometers were available at the same time. Therefore turbulence statistics for different measuring levels in the analysis here are not based on simultaneously acquired data. Data coverage is also varying for the different levels. Figure 2 shows the sample size of half hour averages for each measuring height during both intensive measuring periods after application of the rejection criteria specified below. Especially the measurements at 20 m and 31 m have small sample sizes. Measurements at 53 m, the top level of the tower, were made continuously throughout both periods. With reference to above canopy conditions, the turbulence data at each level were classified and ensemble averaged.

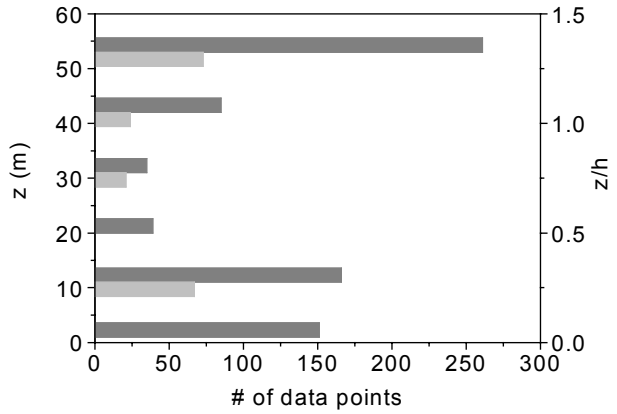

Figure 2. Number of half hour values at different measuring levels available for the turbulence profile analysis during both periods (18 to 21 May 1999: light gray; 17 October to 1 November 1999: gray).

Wind speed above the canopy and separating day and night time situations (implicit consideration of stability) turned out to be a suitable classification criterion to reveal the main regimes controlling turbulence also within the canopy. Four cases have been established:

- daytime: 1000 LT to 1500 LT
- night time: 2100 LT to 0400 LT
- low wind condition: wind speed < 2 m s^{-1}
- high wind condition: wind speed ≥ 2 m s^{-1}

The given time windows exclude transition periods to focus on stationary daytime and night time conditions. For example the roughness sublayer partly starts to stabilize again at 1600 LT (not shown).

Some of the turbulence parameters analyzed in the following are normalized by appropriate scales. As a canopy specific length scale, a defined effective forest height h of 40 m (preset) is used. Following the suggestion of Kruijt et al. (2000) this height represents an average between the mean canopy height (closed up at 32 m) and single trees jutting up to 45 m (which are important for turbulence). Friction velocity measured at the top level $u_{*,\,top}$ is the velocity scale used for normalizing (e.g. standard deviations of wind vector components). In order to avoid artifacts caused by normalizing with very low $u_{*,\,top}$ values, cases with $u_{*,\,top} \leq 0.05$ m s^{-1}are disregarded in the turbulence analysis. This relatively low threshold was necessary to get representative turbulence statistics especially for calm night time conditions. Beside low $u_{*,\,top}$ situations half hour intervals which include rain events were also rejected. The resulting relative rejection rate for each measuring level is specified in Table 1.

Whereas it was only sporadically raining from 18 May to 22 May, the last days of the second intensive measuring period were frequently interrupted by heavy rain events. During these days the measurements at $z/h = 0.78$ were conducted resulting in the maximum relative rejection rate of 20.5%. The second criteria caused much higher rejection rates within the first period. Mainly owing to the high stability during night (see Section 4.1) up to 22% of the half hourly data were rejected.

TABLE 1

Rejection rates (% of individual sample size at each height, see Figure 2) of both intensive measuring periods because of rain events and low friction velocity

		z/h					
Period	Criteria	1.33	1.05	0.78	0.50	0.28	0.03
18 May to 22 May	rain	1.6	2.3	2.4	-	1.7	-
	$u_{*top} \leq 0.05$ ms^{-1}	19.7	15.9	22.0	-	20.7	-
17Oct to 1 Nov	rain	4.5	0.0	20.5	4.5	1.1	7.6
	$u_{*top} \leq 0.05$ ms^{-1}	6.2	8.6	0.0	0.0	9.2	4.7

Data processing for the single point turbulence statistics is the same as for the eddy covariance calculations described in Rummel et al. (2005a). Half hour averages were calculated. Long term variations and turbulent fluctuations were separated by linear detrending. All turbulence statistics were calculated by using these fluctuating terms.

The coordinate system on each level is oriented, that $\overline{u}$ is aligned with the mean horizontal flow direction. Tilt correction to force $\overline{w}$ to zero was just applied at the two uppermost levels.

3.3 Error Estimation for Statistical Moments in a Forest Canopy

3.3.1 Statistical Errors

Due to the high precision of sonic anemometers (± 1.5%; manufacturer specification for wind speed) within most atmospheric conditions, instrumental noise is not the limitation for the determination of turbulent velocity moments. Main statistical uncertainty, however arises from averaging over time periods of finite length T_a instead of using ideal ensemble averages to describe turbulence properties. All field experiments using fixed sensors base on the "ergodic" hypothesis which assumes time average and ensemble average to be equivalent under stationary conditions (Lumley and Panofsky, 1964). In other words, for $T_a \rightarrow \infty$ the time average converges towards the ensemble average. In the surface layer however, averaging times between 30 min and 1 h are usually long enough to include the main variance or flux contributions of the spectrum of turbulent eddies. The use of much longer averaging times is usually not in the interest of most studies due to the loss of information about temporal evolution of velocity statistics (for a discussion of T_a, see also Rummel et al. (2005a)). Therefore, individual time averages of a statistical moment will be distributed around their ensemble average ($\langle\ \rangle_e$). As shown by Lumley and Panofsky (1964) the normalized error variance $\sigma^2(\mu_n(x))$ and consequently the statistical uncertainty of the nth moment (order n) $\mu_n(x)$ of a Gaussian distributed quantity x is a function of the ratio between the integral timescale Γ_n and the averaging time T_a (for $T_a >> \Gamma_n$) and the order n.

$$\frac{\sigma^2(\mu_n(x))}{\langle\mu_n(x)\rangle_e^2} = \frac{\langle\mu_n(x) - \langle\mu_n(x)\rangle_e\rangle_e^2}{\langle\mu_n(x)\rangle_e^2}\frac{2\Gamma_n}{T_a} \tag{5}$$

Here the integral timescale Γ_n is defined as:

$$\Gamma_n = \int_0^\infty R_{xx}^n(\tau)d\tau \tag{6}$$

$R_{xx}^n(\tau)$ is the auto-correlation function of the corresponding nth moment of x. The normalized ensemble

variance (first fraction on the right side of Eq. (5)) is determined by the relations between the moments of a Gaussian distribution and therefore by the order n.

As a rather conservative estimate Lumley and Panofsky (1964) suggested the usage of Γ_1 also for estimating the uncertainty of higher order moments. As a result they got a five times higher uncertainty for a 4th-order moment compared to a 2nd-order one. Sreenivasan et al. (1978) also showed in their analysis of surface layer data that $\Gamma_1 > \Gamma_n$ (n>1).

The approach of Lumley and Panofsky (1964) was also used in the few forest turbulence studies in which the theoretical uncertainty of presented higher order moments was stated (e.g. Baldocchi and Meyers, 1988; Leclerc et al., 1990a; Meyers and Baldocchi, 1991). There, in a rather optimistic way, the uncertainty was determined for measurements above the canopy. Within the canopy the highly non-Gaussian nature of turbulence (skewed and kurtotic; see Sections 4.2.3 and 4.2.4) has to be considered in order to get a realistic estimate of the uncertainty for higher order moments compared in average profiles. Lenschow et al. (1994) derived approximated formulations for the statistical uncertainty of moments in skewed and kurtotic turbulence. Their comparison with measurements from the convective boundary layer shows that their theoretical formulations describes the non-Gaussian effects quite well. In contrast to Lumley and Panofsky (1964) they really use Γ_n approximated by a exponential auto-correlation function. One of their main findings is that the statistical uncertainty of higher order moments seems to be more affected by non-Gaussian effects than lower order moments. In a skewed process (Sk ≈ 1.1) a 4th-order moment shows a 10 times higher error variance than a 2nd order one, compared to the factor 5 between them in a Gaussian process like mentioned above.

TABLE 2:
Maximum relative uncertainty (%) for2ndand 4th-order moments (u,w) of all four classes at each measuring height.

		z/h					
Component	Moment	1.33	1.05	0.78	0.50	0.28	0.03
u	2nd	31	35	26	28	29	26
	4th	68	75	72	68	62	68
w	2nd	15	15	14	18	24	13
	4th	32	31	38	47	65	36

The formulations given in Table 6 of Lenschow et al. (1994) were used to estimate the statistical uncertainty of second and fourth order moments of the presented profiles for the used averaging time T_a of 1800 s. According to the average skewness at a height the uncertainty was determined by the corresponding formulation. The integral timescales were calculated by integrating the auto-correlation function over a time lag until the first zero-crossing. Table 2 shows the maximum statistical uncertainty for 2nd and 4th-order moments of the classified profiles. Due to its larger timescale the uncertainty for the moments of streamwise wind component is almost double the uncertainty for the corresponding moments of the vertical component. This is in agreement with findings of Sreenivasan et al. (1978) in the marine surface layer. It should be emphasized, that the values shown in Table 2 are a conservative estimate for the uncertainties, because they state the "worst case" on each height. Above the canopy the highest uncertainties for moments of *w* occur during extremely unstable daytime situations (see also Wyngaard, 1973; Ammann, 1999) because slowly moving large scale eddies are increasing the timescale. For the moments of *u* the timescales during extremely stable night time conditions are even larger probably due to gravity wave formation in the upper part of the canopy and above. Uncertainties of 4th-order moments for typical daytime situations are about 25% and 50% for *w* and *u* respectively. In the crown layer the highest uncertainty occurs during daytime periods with the highest skewness and kurtosis values (see Sections 4.2.3 and 4.2.4). Within the stem space of the forest the maximum uncertainties were obtained in night time conditions with unstable stratification in that part of the canopy. Here uncertainties of 4th-order moments for typical daytime situations are about 30% and 55% for *w* and *u* respectively.

Compared to the mentioned forest turbulence studies the obtained theoretical uncertainties are quite high. This shows the influence of rather large timescales above the tropical canopy within typical convective situations during daytime and the influence of non-Gaussian turbulence on the statistical error especially of higher moments within the forest. The uncertainties for 3rd-order moments in non-Gaussian turbulence are comparable to the ones for 4th-order moments stated here. Mixed third order moments like in the turbulent transport term in the budget of turbulent kinetic energy or variances (see Eqs. (1) and (10)), are likely to have a rather high statistical error comparable to the moments of *u* (Wyngaard, 1973; Sreenivasan et al., 1978).

3.3.2 Systematic Errors

According to Lenschow et al. (1994) beside the statistic error, a systematic underestimation of statistical moments is caused by the use of averaging intervals of finite length. In contrast to the statistic uncertainty, the systematic error shows only a weak growth with increasing skewness. With increasing ratio T_a/Γ_1 the systematic error decreases much faster than the statistic uncertainty. For the

velocity moments here, the systematic underestimation is below 4% (10%) and 10% (20%) for 2nd and 4th-order moments of w (u) respectively.

An additional systematic effect has the high frequency damping due to the path averaging of the sonic anemometers (Moore, 1986). According to the used spectral model of Kaimal et al. (1972) the effect was generally below 10% for 2nd order moments above the canopy. Within the canopy the effect is likely to be smaller because of lower wind speeds and the domination of relative large scales. Due to the lack of a corresponding spectral model within the canopy the damping effect was not corrected.

The statistical error caused by finite averaging intervals is dominating the general uncertainty of the velocity moments. Owing to this considerable uncertainty no correction of the rather small systematic effects was applied.

4 Results and Discussion

4.1 General Characterization of the Intensive Measuring Periods

Frequency distributions of environmental conditions during both periods are compared in Figure 3. In principle, temperature distributions of both periods are quite similar. The second period (during LBA-EUSTACH 2) was warmer on average, corresponding to the higher net radiation (maximum of 843 W m^{-2} compared to 713 W m^{-2}) at the end of the dry season and in agreement to the findings of Culf et al. (1996). The average temperature determined for end of May was 24.2 °C compared to 25.8 °C for the second half of October. The maximum temperatures differ by 6 °C while the minimum temperatures measured are closer (19.4 °C and 20.9 °C; first and second intensive investigation period, respectively).

Frequency distributions of relative humidity show a high degree of similarity due to the fact, that frequently the air is at least close to saturation (rh > 95%) from around 2100 LT till 0700 LT (one hour after sunrise). Therefore nearly 50% of all observed data show a relative humidity greater than 95%. Daytime values reflect pretty much the temperature distribution, with minimum values of 53% in the first and 35% in the second intensive measuring period.

A higher percentage of very stable ((z-d)/L > 0.5) half hour intervals occurred during nights of the first intensive measuring period. This is reflected by the relative differences in the corresponding frequency distributions of friction velocity (Figure 3 (d)) and horizontal wind speed (Figure 4 (a)) at he lower end of the displayed data range. Despite the fact, that on average the relative contribution of calm ($u \leq$ 0.5 m s^{-1}) half hour periods is tree times lower in the first period, the percentage of half hour intervals with $u_* \leq$ 0.1 m s^{-1} is higher by a factor of 1.6. During daytime hours of the first period the stability of the roughness sublayer was mainly in the near neutral to slightly unstable (-0.3 <

(z-d)/$L \leq$ 0.0) range. The second period shows a higher ratio of unstable situations ((z-d)/$L \leq$ -0.3). This corresponds to higher daytime average values of horizontal wind speed and friction velocity in the first period. Average values are 2.7 m s^{-1} compared to 1.6 m s^{-1} for wind speed and 0.46 m $s^{-1}$and 0.35 m s^{-1} for friction velocity during the first and second intensive measuring period, respectively.

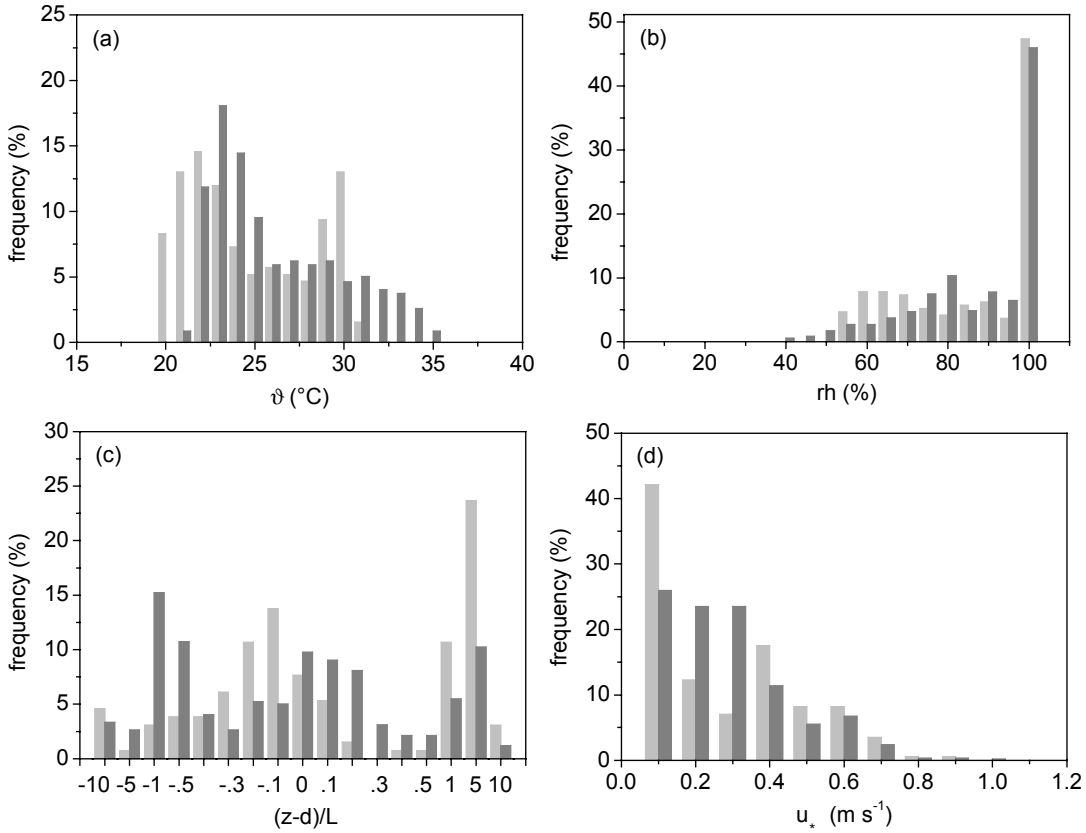

Figure 3. Half hour frequency distributions of temperature ϑ (a), relative humidity (b), stability (c), and friction velocity (d) measured at 53 m for both intensive measuring periods (18 to 21 May 1999: light gray; 17 October to 1 November 1999: gray).

Figure 4 (b) shows the absolute frequency distribution of the wind direction for both periods. Obviously during both time periods south-south east was the predominating wind direction. During the first intensive measuring period the air originated nearly exclusively from the sector 145°-190°, while also a lot of situations with north-easterly wind direction have been measured during the second period. For a description of climate variables and a discussion of fetch-footprint ratios during LBA-EUSTACH 1 and 2 see Rummel et al. (2005a).

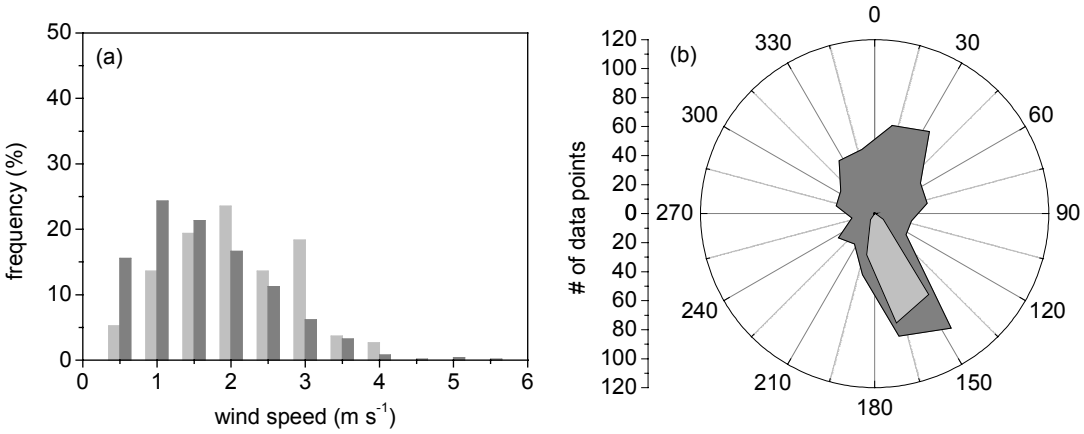

Figure 4. Half hour frequency distributions of (a) horizontal wind speed and (b) wind direction for both intensive measuring periods (18 to 21 May 1999: light gray; 17 October to 1 November 1999: gray).

4.2 PROFILES OF STATISTICAL VELOCITY MOMENTS

Understanding of turbulence regimes governing the exchange of energy, momentum, and mass between the forest and the atmosphere is facilitated by analyzing single point statistics of wind velocity components at different heights. Possible coupling of air motion above and within the canopy, as well as structurization and intermittency of turbulence becomes visible through the combined information about vertical distributions of velocity moments of different order. Profiles of normalized standard deviations, Reynolds stress, and higher order moments (skewness and kurtosis) were investigated for the RBJ rain forest canopy.

4.2.1 Standard Deviations

The vertical profiles of the normalized velocity standard deviations (Figure 5) $\sigma_u/u_{*,top}$ and $\sigma_w/u_{*,top}$ display distinct differences during night and day. For high wind conditions during daytime both quantities are monotonically decreasing from canopy top (where shear production has its maximum) down to the forest floor. The vertical distributions of normalized velocity standard deviations under these conditions are comparable to the well known profiles under neutral stability, presented e.g. in the review of Kaimal and Finnigan (1994). Only the streamwise wind fluctuations show a weak maximum within the canopy during low wind conditions. This indicates that, during daytime turbulence within the large canopy space is on average not produced locally (but originating from above).

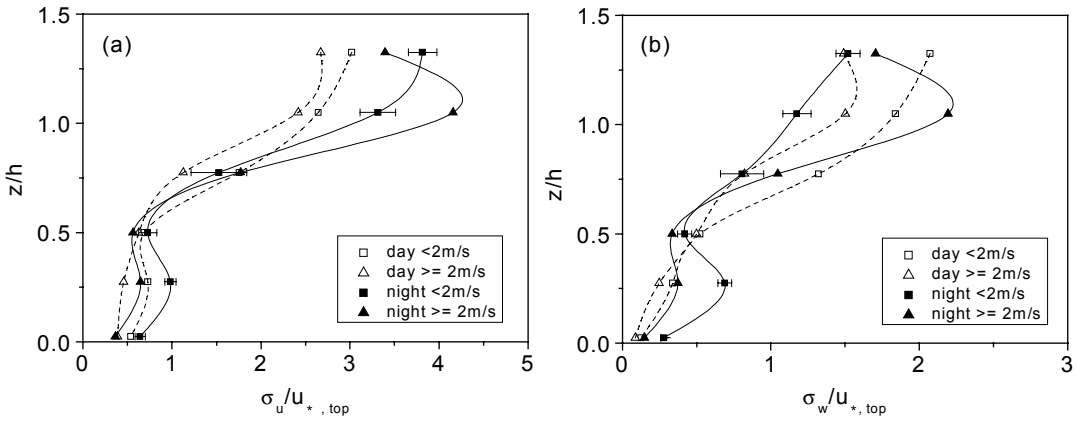

Figure 5. Vertical profiles of the standard deviation of streamwise σ_u (a) and vertical wind speed σ_w (b) normalized with the friction velocity measured at 53 m ($u_{*,top}$). Two wind speed classes are distinguished for daytime (1000 LT to 1500 LT; open symbols) and night time (2100 LT to 0400 LT; full symbols) values (implicit consideration of stability). Shown are mean profiles (17 October to 1 November 1999). Error bars represent standard errors which are just shown for one class for the sake of clarity.

The night time profiles of $\sigma_u/u_{*,top}$ and $\sigma_w/u_{*,top}$ are more structured. All of them show a more or less pronounced local maximum within the stem space (0.28 h) of the forest. This local maximum is most clearly visible in the profile of the vertical component in low wind night time conditions (Figure 5 (b)).

Due to the unstable thermal stratification from the forest floor up to the crown region (see Rummel et al., 2002) especially during calm nights, it seems reasonable to assume that turbulence within the lower part of the canopy is mainly buoyancy driven in that case. Therefore the structure of these night time profiles may be caused by a superposition of (i) shear driven turbulence in the crown region and above the canopy and (ii) buoyancy produced turbulence in the lower part of the canopy. The minimum at 0.5 h (which is the height of the nocturnal temperature inversion base) separates both spheres of influence. Especially the profiles of $\sigma_w/u_{*,top}$ indicate that during nights with relative high wind speed the shear production at the canopy top is obviously large whereas in calm nights the buoyancy production in the lower part the canopy is more pronounced. This nocturnal situation will be specifically addressed in Section 4.4.4.

A possible contribution to the absolute magnitude of $\sigma_u/u_{*,top}$ and $\sigma_w/u_{*,top}$ within the canopy during calm nights could arise from the division by very low $u_{*,top}$ values which is also increasing the normalized standard deviations. This artifact was tried to restrict by introducing a lower threshold of 0.05 m s^{-1} for $u_{*,top}$.

4.2.2 Reynolds Stress

The classified profiles of normalized Reynolds stress $\overline{u'w'}/u_{*,top}^2$ are presented in Figure 6. Reynolds stress decreases sharply in magnitude with depth into the canopy due to the absorption of momentum by foliage and other canopy elements. The main stress fraction is absorbed in the uppermost quarter of the forest were the concentration of foliage is high. The penetration depth D_{p50} (defined by Shaw et al. (1988) as the average height at which 50% of the momentum at $z = h$ is absorbed) is $D_{p50}/h \approx 0.87$ for daytime and about 0.91 for night time conditions. Shaw et al. (1988) showed that the depth of the canopy layer were the momentum absorption mainly occurs decreases with increasing foliar density. For the highest leaf area index of LAI = 4.9 they got $D_{p50}/h \approx 0.86$, which is very close to the results measured in the rainforest with a somewhat higher total LAI = 5.6. That the architecture of the canopy (i.e. the vertical leaf area distribution) is also important in that context is shown by the results of Meyers and Baldocchi (1991). They measured nearly 80% momentum reduction already in the upper 10% of a dense deciduous forest (LAI = 5) with 75% of the leaf area concentrated at the highest 20% of the canopy .

An unexpected feature of the profiles in Figure 6, is that in three of the shown classes the Reynolds stress at $z/h = 1.05$ is larger than at the highest measuring level. In the roughness sublayer above most of the various canopies compiled in the "family portrait" of Raupach et al. (1996) a vertically almost constant Reynolds stress was measured for near neutral stability conditions. Due to the assumed lack of additional momentum sources or sinks above the canopy one would expect a constant stress layer. Nevertheless this increasing normalized Reynolds stress towards the canopy top is a relative frequently observed phenomena above forests (e.g. Baldocchi and Meyers, 1988; Shaw et al., 1988; Lee and Black, 1993; Kruijt et al., 2000).

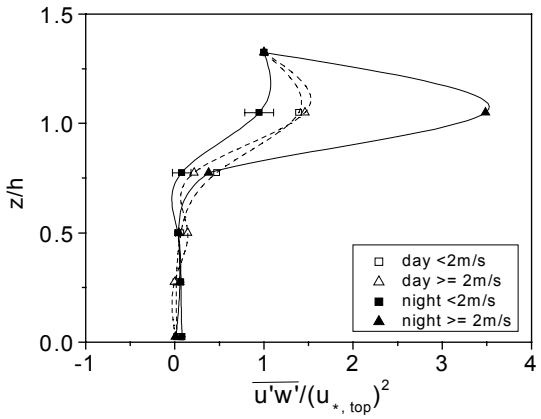

Figure 6. Vertical profile of $\overline{u'w'}/u_{*,top}^2$. Classification and averaging like Figure 5.

At RBJ, the extreme value of $\overline{u'w'}/u_{*,top}^2$ = 3.5 at z/h = 1.05 for windy night time conditions is most striking. Like for their extreme value which Kruijt et al. (2000) obtained at the rainforest site Cuieiras near Manaus, this case is also associated by a very large standard error of 0.9 compared to a maximum standard error of 0.2 for the other cases. It is suspected that this very large scatter may have two different reasons.

Firstly, especially for the Reynolds stress (which is directly connected to stability) the chosen profile classification might not be strict enough to construct ensemble averages. Hence, it may be likely that different stability ranges may contribute to the obtained scatter. Applying a classification based on stability alone (see Table 3) shows that for all classes in the range $|(z\text{-}d)/L| \leq 1$ the average values of $\overline{u'w'}/u_{*,top}^2$ at z/h = 1.05 are between 1.0 and 1.2 with a maximum standard error of 0.2 (not shown here). The larger ratios occur under extremely unstable or stable conditions and are therefore connected to partly very small values of $u_{*,top}$. As a consequence the ratio of small Reynolds stresses measured at z/h = 1.05 and 1.33 is only poorly determined.

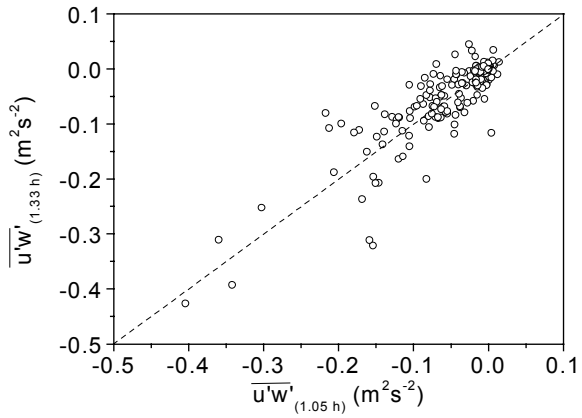

Figure 7. Scatter diagram of Reynolds stress measured at 1.33 *h* versus 1.05 *h*. The dashed line marks the 1:1 ratio.

Secondly, another reason for enhanced $\overline{u'w'}$ values at canopy height (as given by Baldocchi and Meyers (1988)) might be particularly apply to the rough rainforest canopy surface. Local wakes and vortices downwind of single trees jutting out from the mean effective canopy height may lead to larger $\overline{u'w'}$ values at the canopy-atmosphere interface. Additionally, the run to run variability for the streamline orientation sensitive Reynolds stress is relatively large just above the rough canopy surface. This is supported by Figure 7 which compares single half hour Reynolds stress values at 1.33 *h* with measurements at 1.05 *h* including all stability classes (and the few positive $\overline{u'w'}$ values under weak conditions are most likely a consequence of flow distortion from the supporting units of the sonic

anemometer (see Foken, 1990; Ammann, 1999). The values show considerable scatter. But generally the scatter is around the one-to-one line indicative for a constant stress layer above the canopy.

4.2.3 Skewness

Figure 8 shows the skewness profiles of streamwise (Sk_u) and vertical (Sk_w) wind speed. The profiles resemble the general characteristics measured in other forest canopies (e.g. Amiro and Davis, 1988; Baldocchi and Meyers, 1988; Amiro, 1990; Lee and Black, 1993). Above the canopy horizontal and vertical velocity fluctuations are more or less normal distributed with a skewness value close to zero. A high degree of symmetry is visible in the upper half of the canopy: in this upper part of the forest the profiles of all classes show a positive skewness maximum for streamwise wind speed and the most negative skewness values for the vertical wind component. These arises from intermittent downdrafts penetrating the canopy with velocities and turbulence activities much higher than the local mean values (Shaw and Seginer, 1987). On the other side in the canopy interior there is a lack of corresponding sources creating equivalent large updrafts with lower horizontal velocities.

Due to the limited vertical transport during night time (see also TKE analysis in Section 4.4.2) the maximum and minimum skewness values for u and w, respectively, occur at 0.78 h in the upper part of the crown layer. Due to the suppression of vertical motion the absolute magnitude of skewness for the fluctuations of u is on average larger than for w, although the values show distinct scattering. During daytime the extremes are about the same magnitude for u and w. For higher wind speeds owing to the enhanced transport these extremes are also at lower heights (z/h = 0.5).

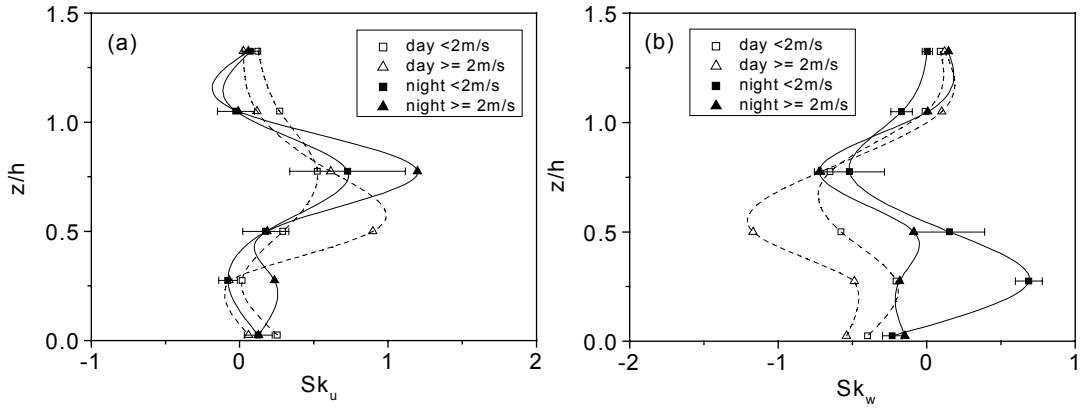

Figure 8. Vertical profiles of skewness of streamwise (a) and vertical wind fluctuations (b). Classification and averaging like Figure 5.

Below z = 0.5 h considerable differences are visible in the skewness profiles of streamwise and vertical wind speed. During day, Sk_u is close to zero in the lower half of the canopy. In contrast, Sk_w is

especially during windy periods with values of about -0.5 below $z = 0.5\ h$ still significantly different from zero. In contrast to measurements in artificial canopies where relative high values of Sk_u were also measured close to the canopy floor (e.g. Raupach et al., 1986; Brunet et al., 1994) a lot of investigations in different natural forest canopies show a nearly Gaussian probability density distribution of u' in the stem space (e.g. Baldocchi and Meyers, 1988; Amiro, 1990; Lee and Black, 1993; Kruijt et al., 2000).

During the four days of the intensive turbulence investigation period of LBA-EUSTACH 1 (see Section 2) the difference obtained between Sk_u and Sk_w in the lower canopy was even higher. From similar magnitude in the crown layer the average daytime skewness values (for $wind\ speed_{top} \geq 2\ m\ s^{-1}$) diverge with decreasing height to values 0.3 for u' and -1.3 for w' in the stem space at 0.28 h. Like shown in Section 4.1 this period is characterized by relative constant environmental conditions. Wind speed at the tower top exceeded 2 m s^{-1} quite frequently during daytime and the wind direction was nearly exclusively from south-southeast. Figure 9 shows Sk_u and Sk_w at 0.28 h from this first period as a function of stability $|(z-d)/L_{top}|$. Displayed are day- and night time values for the same times used for the ensemble averages in the profiles. In agreement with the results of Leclerc et al. (1990b) for daytime conditions one can see a relative clear dependence of Sk_w on stability in Figure 9. The most negative values are reached for near neutral conditions. On the other hand a very weak stability dependence of Sk_u with significantly lower values can only be suspected for daytime conditions. This uncertainty does also resemble the results of Leclerc et al. (1990b) who got no clear stability dependence of Sk_u at their lowest measuring height ($z/h = 0.327$). This discrepancy is suspected to have two reasons which will be discussed in connection with the kurtosis analysis in the following Section.

The night time values of Sk_u and Sk_w show also systematic differences at 0.28 h. Whereas Sk_u scatters around zero, Sk_w shows a systematic offset towards positive values (Figure 9). In the profile of Sk_w in Figure 8 this can be seen for low wind night time conditions. The most positive value is reached at the half height of the stem space. This is most likely caused by updrafts in the convective layer of the lower canopy which was already suggested in connection with the nocturnal profiles of standard deviations (Section 4.2.1). The updraft motion is obviously exceeding the compensating downward air motion in magnitude.

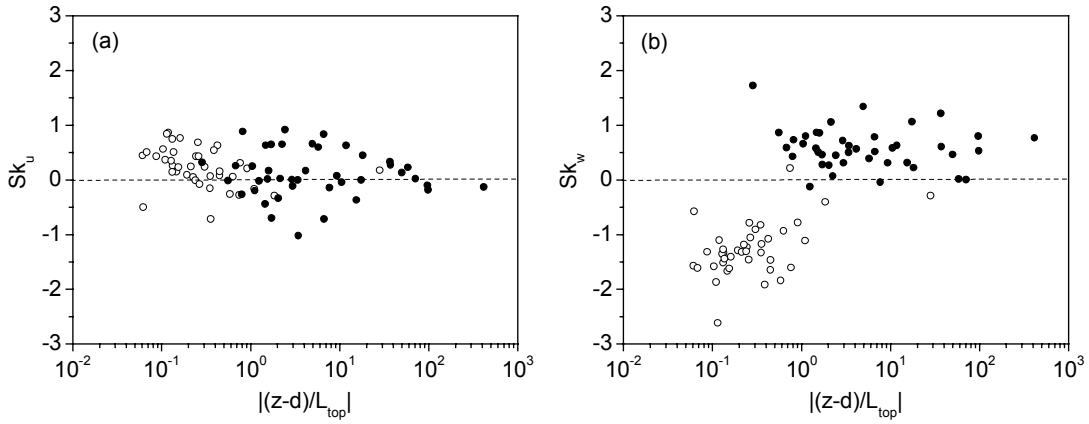

Figure 9. Skewness of (a) streamwise and (b) vertical wind fluctuations at 11 m (0.28 *h*) as a function of $|(z\text{-}d)/L_{top}|$. Shown are daytime (open circles; unstable stability) and night time (full circles; stable stability) data for the time intervals considered for the profiles. The data are measured during the first investigation period (18 May to 21 May 1999).

4.2.4 Kurtosis

The profiles of the kurtosis in Figure 10 show characteristics corresponding to the skewness profiles. With values between 3 and 4 above the canopy the kurtosis for streamwise (K_u) and vertical (K_w) wind speed is also close to 3, characteristic for a normally distributed quantity. In the upper half of the canopy the kurtosis of both wind components show a high degree of correspondence with maximum values up to 6 and 7. Also in accordance with the skewness, the profiles of K_u and K_w peak at $z/h = 0.5$ for windy daytime conditions, and therefore at significantly lower heights than during night.

Systematic differences between K_u and K_w appear also within the stem space below $z/h = 0.5$. Here K_u is with values between 3 and 4 just slightly higher than the Gaussian value of 3 measured above the canopy. The kurtosis of the vertical wind component is significantly higher in the lower canopy. Again during windy daytime conditions the kurtosis at the lower heights is relative constant with values slightly above 6. This is again in accordance to the results of other turbulence investigations in forest canopies (e.g. Baldocchi and Meyers, 1988; Amiro, 1990; Kruijt et al., 2000). The relative high peakedness of w' in the sub canopy space during periods with high wind speed suggests that air motion there is dominated by large scale eddies that have sufficient energy to penetrate deep enough (Baldocchi and Meyers, 1988). Relative high standard errors up to 0.9 at the lowest heights are also a sign for the high variability of turbulent motion deep in the canopy.

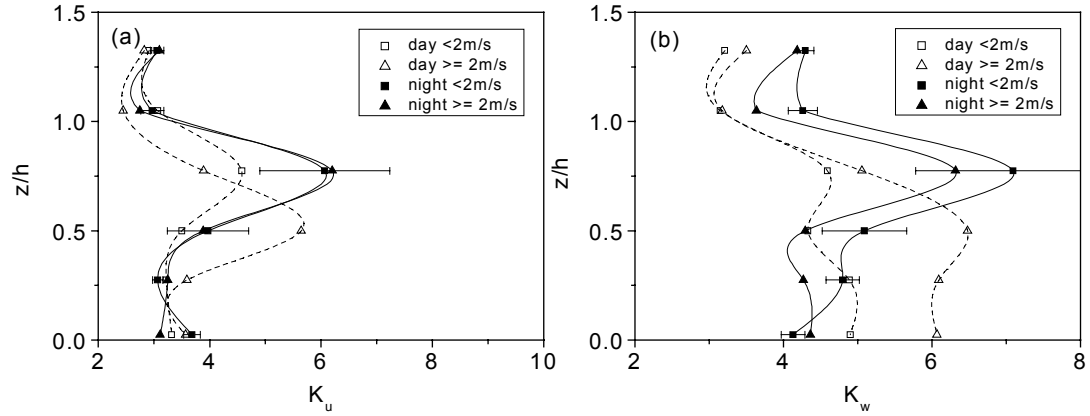

Figure 10. Vertical profiles of kurtosis of the streamwise (a) and vertical wind fluctuations (b). Classification and averaging like Figure 5.

Figure 11 shows the kurtosis of both velocity components at 11 m (0.28 *h*) for the same investigation period as shown in Figure 9. During the relative constant daytime wind conditions K_w within the stem space is obviously also dependent on stability, again with the highest values for near neutral conditions. Like the skewness, the kurtosis of the streamwise velocity component K_u shows also no stability dependence. Like mentioned above, here two reasons are suspected to cause the differences in skewness and kurtosis of both velocity components below the crown layer.

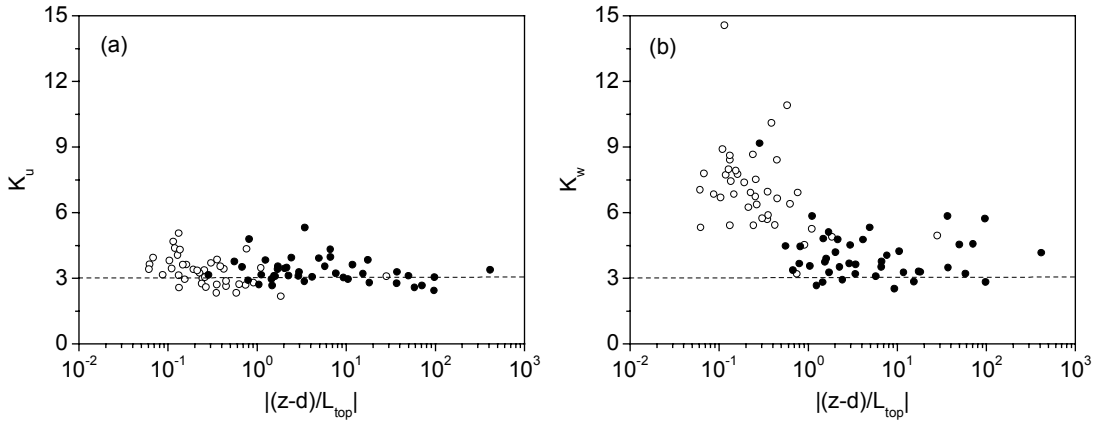

Figure 11. Kurtosis of (a) streamwise and (b) vertical wind fluctuations at 11 m (0.28 *h*) as a function of $|(z\text{-}d)/L_{top}|$. Shown are daytime (open circles; unstable stability) and night time (full circles; stable stability) data for the time intervals considered for the profiles. The data are measured during the first investigation period (18 May to 21 May 1999).

Firstly, the large scale intermittent eddies that have enough energy to penetrate deep into the canopy are of course also visible in the time series of u'. But the fact, that stream wise horizontal air motion is more affected by the aerodynamic drag of canopy elements, contributes to a stronger amplitude reduction of u' compared to w' when the gust passes the canopy crown. The eddies produced by canopy element scale wake motion are much smaller than the original eddies. This contributes to a relative reduction of K_u.

Secondly, according to Shaw and Zhang (1992) pressure perturbations imposed on the canopy layer are responsible for much of the wind fluctuations in the lowest layers of a canopy. Due to the stable stratified lower canopy, surface layer pressure fluctuations (e.g. associated with large scale eddies (Shaw et al., 1990)) will affect horizontal and vertical air motion in a different way. The weak upward directed vertical air motion will be strongly damped in amplitude by the buoyancy forces whereas the fast downward moving air is affected to a smaller extend. Due to the lack of a buoyancy equivalent force the horizontal air motion is accelerated or decelerated by corresponding pressure gradients in a more balanced way. Shaw and Zhang (1992) suspect the pressure effects at higher layers of the canopy to be weak compared to the much stronger turbulent fluctuations. Therefore skewness values of both velocity components show a higher degree of symmetry in the upper half of the canopy.

Up to this point, the depicted profiles suggest, depending on the time of day, clearly different regimes governing above and in-canopy turbulence. Now these control regimes and possible dependencies are directly addressed by comparison with different scaling approaches. Additionally, determination of specific TKE budget terms provides complementary information about forest-atmosphere coupling and the relative importance different turbulence production mechanisms.

4.3 CONTROL REGIMES OF ABOVE-CANOPY TURBULENCE

According to similarity theory of Obukhov (1960) in the surface layer the normalized standard deviations of turbulent velocity components of a steady flow over homogeneous terrain are fully described as a function of the stability parameter z/L or $(z\text{-}d)/L$. According to de Bruin et al. (1991) and Foken and Wichura (1996) the functional relation over ideal terrain, if known with certainty, can be used to test the turbulent wind field over complex terrain (like here, in the roughness sublayer above a forest canopy). In this way, it can be seen whether the surface is aerodynamically homogeneous or whether e.g. obstacles are disturbing the equilibrium wind field by additional mechanical turbulence.

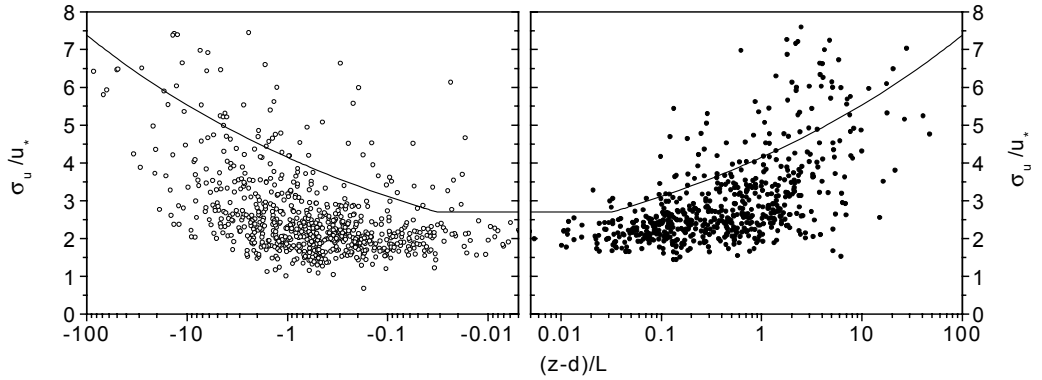

Figure 12. Standard deviation of streamwise wind speed normalized with friction velocity measured at 1.33 *z/h* as function of stability (*z-d*)/*L* (unstable: open circles; stable: full circles). The solid line represents surface layer similarity according to Foken et al. (1997) (Eq. (7)).

Figure 12 and Figure 13 show the normalized standard deviations of the streamwise and the vertical wind components versus (*z-d*)/*L*. All quantities were measured during the intensive measuring period of LBA-EUSTACH 2 (see Section 2) at 1.33 *h*, the top level of the tower. The results obtained in May are similar and therefore not explicitly shown here. The solid line in Figure 12 represents the parameterization according to surface layer similarity found by Foken et al. (1997):

$$\frac{\sigma_u}{u_*} = \Phi_u\left(\frac{z-d}{L}\right) = \begin{cases} 2.7 & for -0.032 < \dfrac{z-d}{L} < 0 \\ 4.15\left(\left|\dfrac{z-d}{L}\right|\right)^{\frac{1}{8}} & for \dfrac{z-d}{L} < -0.032 \end{cases} \tag{7}$$

Despite the fact that this parameterization is only validated for neutral and unstable conditions it is also plotted in the stable range ((*z-d*)/*L* > 0) for orientation purposes. The measured values of σ_u/u_* show a considerable scatter. There is hardly any scaling with the stability parameter. However, in the unstable range the values seem to increase with increasing instability from about (*z-d*)/*L* ≈ -0.5 on. This is one order of magnitude further in the unstable range than postulated by the parameterization after Foken et al. (1997). On the stable side just a broadening of the range of values can be seen with increasing stability. Generally the measured values are significantly lower than the shown parameterization. For near neutral conditions (|(*z-d*)/*L*| ≤ 0.032) the average of the measured σ_u/u_* values is 2.2 ± 0.4 compared to 2.7 from the parameterization. Asymptotic constants of σ_u/u_* of other investigations (near neutral stability) over relative ideal terrain are for example 2.2 (McBean, 1971; Beljaars and Holtslag, 1991; de Bruin et al., 1993) or 2.39 as a result of analyzing several data sets by Panofsky and Dutton (1984). Therefore the value of σ_u/u_* obtained from the measurements (near

neutral stability) above a rough rain forest canopy here, is within the range of uncertainty which could be expected from literature for measurements above aerodynamically smoother surfaces. In this context, it should be mentioned that there is considerable uncertainty about the right scaling parameters of σ_u/u_* under non-neutral stability conditions. The results of Foken et al. (1991) and Foken et al. (1997) indicate that σ_u/u_* scales with stability. In contrast there is evidence that σ_u/u_* does not follow surface layer similarity according to Obukhov (1960) and is therefore not a universal function of $(z\text{-}d)/L$ (McBean, 1971; Panofsky et al., 1977; Panofsky and Dutton, 1984; de Bruin et al., 1993). This seems to be also suggested by the large scatter of the data here. Similar results with no clear dependence of σ_u/u_* on stability together with systematically lower values compared to the parameterization of Foken et al. (1997) were obtained over a spruce canopy by Mangold (1999).

Due to the fact that large boundary layer size eddies do not contribute to the momentum flux but affect the fluctuations of the horizontal wind components in the surface layer, Panofsky et al. (1977) suggested z_i/L that should be the appropriate non dimensional scaling parameter (z_i is the boundary layer height). Other studies indicate σ_u/u_* to scale with $\ln(z\text{-}d)f/u_*$ (f is the Coriolis parameter) (e.g. Högström, 1990). Beside the fact that z_i was not measured, testing all the different scaling approaches is beyond the scope of this study. A comparison of several scaling approaches on different data sets is given by Thomas (2001).

In view of the high uncertainty concerning a potentially scaling of σ_u/u_* with stability above ideal surfaces it seems not to be an appropriate test for the quality assessment of the horizontal wind field above the forest canopy here. However, various surface layer experiments gave evidence that surface layer similarity prediction holds for the normalized standard deviation of vertical wind speed σ_w/u_*. Figure 13 shows the observed values for σ_w/u_* together with two different empirical parameterizations according to Wesely (1988):

$$\frac{\sigma_w}{u_*} = \varphi_w\left(\frac{z-d}{L}\right) = \begin{cases} 1.3 & for \dfrac{z-d}{L} \geq 0 \\ 1.3\left(1-2\dfrac{z-d}{L}\right)^{\frac{1}{3}} & for \dfrac{z-d}{L} < 0 \end{cases} \tag{8}$$

and Kaimal and Finnigan (1994):

$$\frac{\sigma_w}{u_*} = \varphi_w\left(\frac{z-d}{L}\right) = \begin{cases} 1.25\left(1+0.2\dfrac{z-d}{L}\right)^{\frac{1}{3}} & for \dfrac{z-d}{L} \geq 0 \\ 1.25\left(1+3\left|\dfrac{z-d}{L}\right|\right)^{\frac{1}{3}} & for \dfrac{z-d}{L} \leq 0 \end{cases} \tag{9}$$

Apart from slightly different constants for $(z\text{-}d)/L \leq 0$ the main difference between the parameterizations is the course of the function under stable conditions. There, the functional relation between σ_w/u_* and $(z\text{-}d)/L$ is according to Wesely (1988) the same constant value asymptotically reached for $(z\text{-}d)/L \rightarrow 0$ while Kaimal and Finnigan (1994) suggest that σ_w/u_* rises with increasing stability.

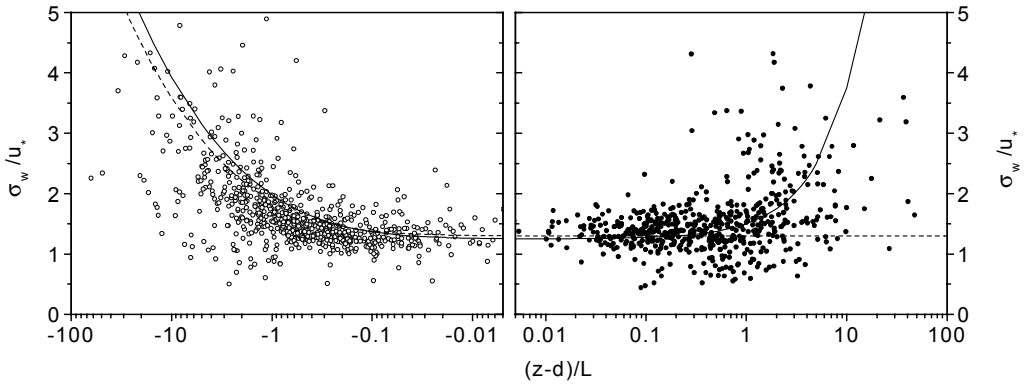

Figure 13. Standard deviation of vertical wind speed normalized with friction velocity measured at 1.33 *z/h* as function of stability $(z\text{-}d)/L$ (unstable: open circles; stable: full circles). The solid and the dashed lines represent surface layer similarity according to Wesely (1988) and Kaimal and Finnigan (1994) (Eqs.(8) and (9)), respectively.

Despite the considerable scatter, for unstable conditions σ_w/u_* scales clearly with stability. In the near neutral stability range σ_w/u_* levels out to an average value of 1.3 ± 0.25. Without disregarding the relative large standard deviation this agrees well with the asymptotic values 1.3 and 1.25 of both parameterizations for $(z\text{-}d)/L \rightarrow 0$. The enhancement with increasing instability is somewhat less steep compared to similarity relations of Wesely (1988) and Kaimal and Finnigan (1994), which were derived from measurements above smooth uniform terrain. For positive $(z\text{-}d)/L$ the picture is less clear. Again like the tendency of σ_u/u_* just the scatter seems to grow with increasing stability. Most likely, the higher values at very stable conditions originate also from increasing uncertainty. Both σ_w and u_* are very small in this stability range so that their ratio σ_w/u_* is poorly determined. Therefore, it is not possible to identify any clear tendency σ_w/u_* under extremely stable conditions ($(z\text{-}d)/L > 1$) over the canopy at RBJ.

As mentioned before above uniform smooth terrain the functional relation between σ_w/u_* and $(z\text{-}d)/L$ is quite well determined. Therefore a comparison between the measured values and the corresponding parameterization is a suitable tool to asses the characteristics of the vertical wind field within the roughness layer of the forest site. After Foken and Wichura (1996) a deviation from the

parameterization (Foken et al., 1991) exceeding 30% is indicative for a systematically disturbed vertical wind field. Here, the parameterization after Wesely (1988) was used for that purpose. It is only slightly different from the formulation according to Foken et al. (1991) for $0 > (z\text{-}d)/L \geq -4$.

Because no clear increase of σ_w/u_* under very stable conditions is visible in Figure 13 the constant near-neutral value was taken for σ_w/u_* in agreement with the recommendation by Panofsky and Dutton (1984). In Table 3 the percentages of half hour values deviating more than ±30% from the parameterization are given for both experiments. No explicit break down into wind direction sections is made because no systematic differences were found except the tower caused flow distortion which was excluded in the analysis.

TABLE 3

Percentage of half hour σ_w/u_* values with a deviation from the parameterisation (Wesely, 1988) exceeding 30% for both intensive measuring periods. The values in brackets are the absolute sample sizes in the corresponding stability ranges.

	Unstable		neutral $(z\text{-}d)/L$	Stable	
	< -1.0	< -0.032 and ≥ -1.0	≤ 0.032 and ≥ -0.032	≤ 1.0 and > 0.032	> 1.0
Period 1	25 (88)	9.1 (241)	0.0 (18)	12.2 (156)	51.7 (120)
Period 2	26.2 (172)	11.7 (367)	9.8 (51)	9.1 (297)	44.9 (136)

Within the stability interval of $|(z\text{-}d)/L| \leq 1$ a constant percentage of about 90% of the half hour values show deviations below the threshold proposed by Foken and Wichura (1996). This is a nice result in consideration of the rough surface structure of this tropical forest. The high surface roughness is most likely one of the main reasons for the considerable scatter in the data. For example within $-1 \leq (z\text{-}d)/L < -0.032$ the average deviation from the parameterization is 13.2% ± 14.8% (15.5% ± 14.2%) within the first (second) intensive measuring period. This are typical results for the vertical wind field at this site, a large standard deviation but significantly within the 30% range.

According to Holtslag and Nieuwstadt (1986) the validity of surface layer similarity is restricted to $|(z\text{-}d)/L| \leq 1$. Other studies suggest that the scaling laws hold for unstable stratification down to $(z\text{-}d)/L = -5$ or even further (e.g. de Bruin et al., 1993; Katul et al., 1995). At stabilities with $|(z\text{-}d)/L| > 1$ the amount of σ_w/u_* values which differ more than 30% from the parameterization is much

higher but again fairly consistent in intensive measuring periods (Table 3). Whereas under very unstable conditions (local free convection) the percentage is about 25%, it is between 44% and 52% for extremely stable cases. Under convective conditions the turbulence production is more and more buoyancy driven. The friction velocity is less important for fluctuations of the vertical wind velocity and can get relatively small. Hence with increasing instability the determination of σ_w/u_* gets more and more uncertain. For extreme stable cases like mentioned above turbulent vertical air motion is almost totally suppressed making the determination of σ_w/u_* even worse or meaningless.

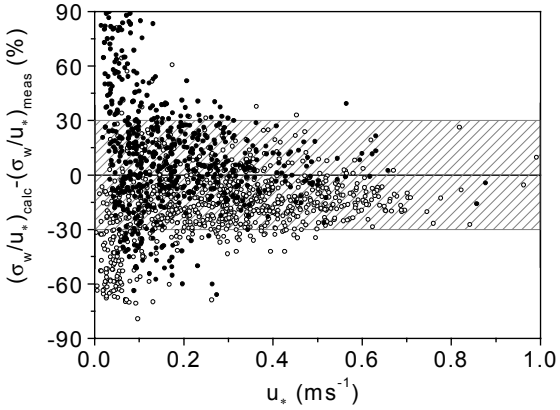

Figure 14. Deviation between parameterization according to Wesely (1988) $(\sigma_w/u_*)_{calc}$ and the measured values $(\sigma_w/u_*)_{meas}$ versus u_* for the second intensive measuring period; ($(z\text{-}d)/L \leq 0$: open circles; $(z\text{-}d)/L > 0$: full circles).The hatched area marks the ± 30% range.

This is clearly confirmed by Figure 14. Displayed is the difference between the calculated values of σ_w/u_* based on the parameterization after Wesely (1988) and the measured values of the second intensive measuring period as function of the friction velocity u_*. In stable as well as in unstable conditions the bulk of the deviations larger than 30% occurs almost exclusively in periods with low friction velocity and therefore weak mechanical turbulence. Above $u_* \approx 0.1$ m s^{-1} the difference between the parameterization and the measured values is only sporadically larger than 30% even if the scatter within this 30% range is considerable. So, despite the small numerical differences of the applied parameterization (Wesely, 1988) compared to the original formulation which was used by Foken and Wichura (1996), their suggested 30% range seems also to be reasonable for the evaluation of the vertical wind field above the aerodynamical rough terrain. Reversely the results indicate a well developed turbulent vertical wind field above the canopy for the RBJ forest site. In both experiments together 14% (24%) of all cases with $(z\text{-}d)/L \leq 0$ (> 0) σ_w/u_* show deviations from the parameterization beyond 30%. Nearly all of them occur under extremely stable or unstable stability conditions with low friction velocity.

4.4 CONTROL REGIMES OF IN-CANOPY TURBULENCE

4.4.1 Coupling of Canopy and Roughness-Sublayer

The profiles of σ_u/u_* and σ_w/u_* (Figure 5) gave already a hint at the mechanisms controlling the wind velocity fluctuations within this tropical forest canopy. The intention of this paragraph is to investigate explicitly to which extend the turbulent air motion in the lower part of the forest depends on different parameters above and within the canopy. Because the emphasize of this study is the exchange of scalars which is mainly connected to vertical air motion the focus of the following analysis is on the fluctuations of the vertical wind component. The results shown here base also on the intensive measuring period of LBA-EUSTACH 2. The findings of the intensive measuring period during LBA-EUSTACH 1 are equivalent and therefore not shown here.

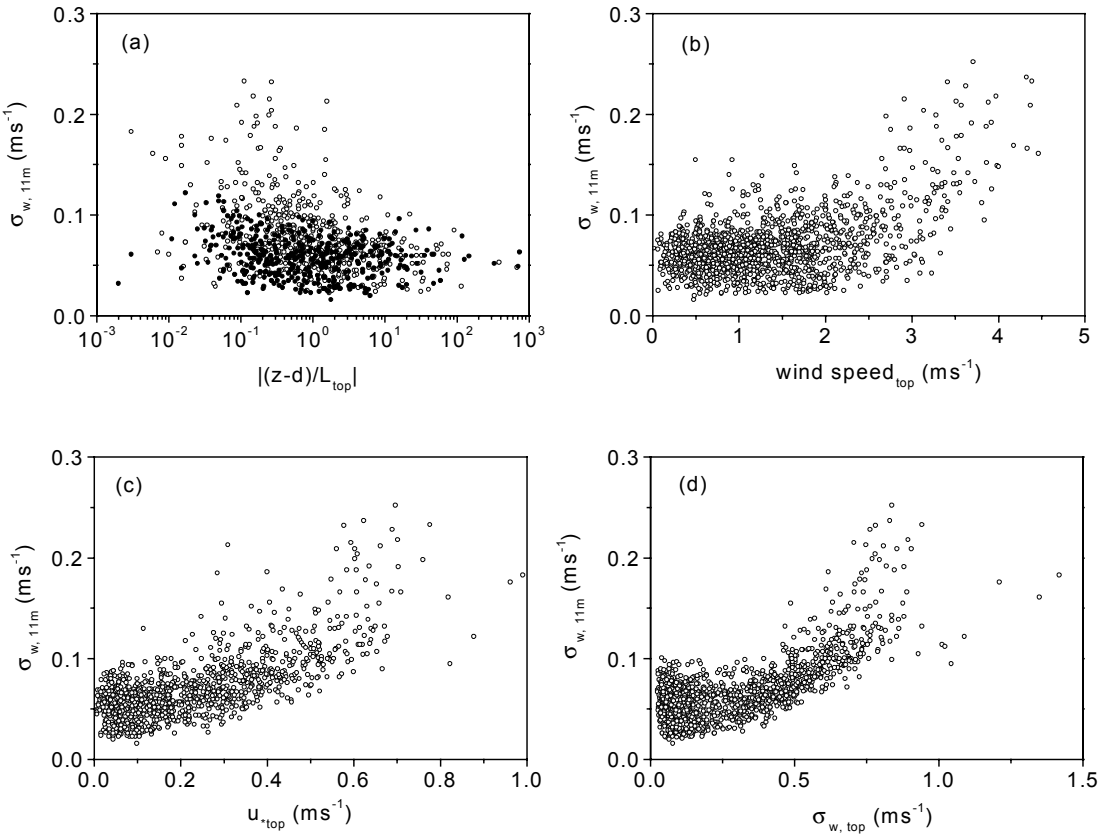

Figure 15. Standard deviation of vertical wind speed σ_w at 11 m (0.28 *h*) as function of (a) stability (*z-d*)/*L* (open circles: (*z-d*)/*L* $\leq$ 0; solid circles: (*z-d*)/*L* > 0), (b) wind speed, (c) friction velocity u_*, and (d) standard deviation of the vertical wind speed σ_w above the canopy (1.33 *h*).

In Figure 15 the standard deviation of the vertical wind speed in the stem space of the forest at 11 m (0.28 *h*) is shown as function of stability, wind speed, friction velocity, and the standard deviation of the vertical wind speed above the canopy (1.33 *h*). The data displayed here include day and night time periods. The in canopy σ_w data show a distinct dependency on *wind speed*$_{top}$, $u_{*,top}$, and $\sigma_{w,top}$. No clear dependency on above canopy stability is visible. The range of σ_w values is clearly increasing towards neutral stratification. This enhancement is of course higher in unstable stratified air during the day. As function of horizontal wind speed σ_w reveals a partitioning in two groups. Up to approximately 2 m s^{-1} there seems to be no functional relation between the two quantities. The bulk of the night time values is contained in this group. However, for wind speeds higher than 2 m s^{-1}, σ_w shows a clear increase (although with distinct scatter). Due to this obvious division in two parts with different characteristics, the horizontal wind speed was chosen as one criterion for the classification of the turbulence profiles.

A clear scaling with reduced scatter of σ_w at 11 m height can be seen with $u_{*,top}$ and $\sigma_{w,top}$. The correlation between σ_w above and within the canopy shows the smallest scatter. Especially this fact is supporting the assumption that during daytime most of the turbulence inside of this dense tropical forest is originating from aloft and therefore that the stem space is coupled to the atmosphere above the canopy. The dependence of σ_u at 11m (0.28 *h*) height on $u_{*,top}$ and $\sigma_{u,top}$ (not shown here) is even more distinct.

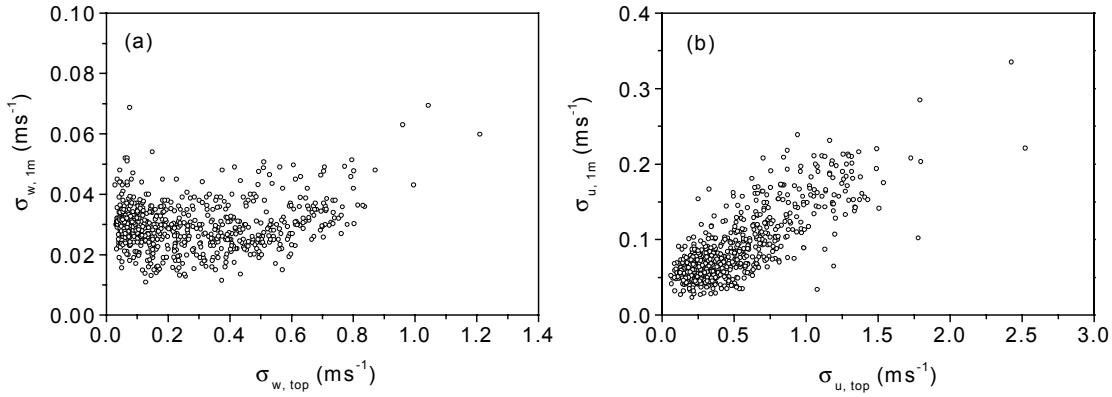

Figure 16. Standard deviation of (a) vertical and (b) streamwise wind speed at 1 m (0.03 *h*) as function of the same quantity measured at 1.33 *h*.

In the lowest part of the canopy the situation is slightly different. Figure 16 shows σ_u and σ_w measured 1 m (0.03 *h*) above the forest floor as function of the corresponding standard deviations above the canopy ($\sigma_{w,top}$; $\sigma_{u,top}$). Whereas σ_w seems to be nearly independent from $\sigma_{w,top}$, σ_u shows again a distinct relation to the turbulence state above. Two reasons are conceivable. Firstly, at such a low height, the soil surface might already deflect downward moving air into horizontal motion like

Raupach et al. (1986) noticed in their wind tunnel experiment. Secondly, the turbulent transport might not reach down to the lowest meter above the forest floor. The connection between fluctuations of the horizontal wind speed at 53 m and 1 m height might then be caused by velocity-pressure interaction (e.g. Shaw and Zhang, 1992). This means that horizontal motion in the lowest part of the canopy is rather originating from high frequent pressure gradients than from direct turbulent exchange with the air flow above.

4.4.2 Variance and TKE Budget

Estimating the magnitude of transport term T_t (Eq. (10)) as a non local contribution to the mean turbulent kinetic energy (TKE) budget (Eq. (1)) at different heights, gives additional information concerning the extent to which the canopy space is coupled to the layer above. The fact that the estimated terms base on not simultaneously measured turbulence data contributes to the uncertainty which is anyway considerable for higher order statistical moments (see Section 3.3). However, the derived ensemble averaged profiles interpreted in a rather qualitative way show some interesting and systematic effects concerning the turbulence regimes within the canopy. For consistency, all gradients and mean values were calculated for an average height between the corresponding measuring levels. The resulting value characterizes therefore the whole layer between these measuring heights. Figure 17 shows the turbulent transport term T_t for the variance of streamwise and vertical wind speed. It is defined as:

$$T_t\left(i'^2\right) = \frac{\partial \overline{w' i'^2}}{\partial z} \qquad i = u,\, w\,. \tag{10}$$

The profiles show a characteristic form well-known from measurements in other forest types, wind tunnel and model studies (e.g. Wilson and Shaw, 1977; Meyers and Baldocchi, 1991; Raupach et al., 1996). Above the canopy and in the upper part of the crown region the transport term acts as a sink for horizontal and vertical variance whereas it represents a source below that layer. The turbulent transport profiles of both components show similar differences between the classes. For day and night time conditions a clear dependence on the wind velocity is visible concerning the absolute magnitude of the term. This is caused by the different variance production in the upper part of the canopy as shown below for the TKE budget. The difference between the streamwise and vertical variance transport concerning the uppermost level will also be discussed in that context.

Both components show a considerable smaller penetration depth during night due to the stable stratification in the crown region. Whereas at night time the turbulent transport approaches zero below 0.5 h, the base of the crown layer, it is only negligible below 0.28 h for daytime conditions. This is in agreement with the relation shown in Figure 15, confirming that during daytime this height is directly coupled to the air motion above. On the other hand the profile for the streamwise component indicates

that on average the correlation between the measurements of σ_u above the canopy and 1 m above the forest floor (0.03 h) is not due to direct turbulent transport. This supports the second explanation attempt mentioned above, that the connection of this lowest part of the canopy to the upper layers is mainly indirect via pressure transport.

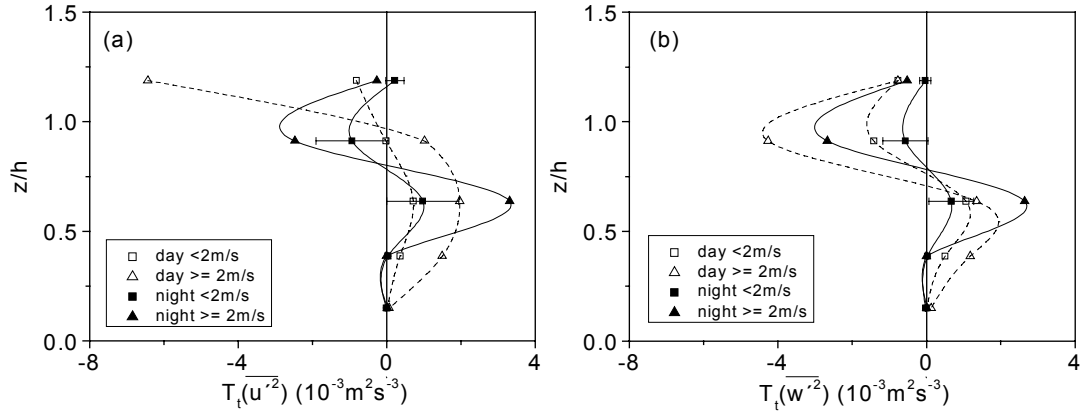

Figure 17. Turbulent transport term of the variance budget for (a) streamwise and (b) vertical wind speed. Classification and averaging like Figure 5.

The turbulent transport T_t of the mean turbulent kinetic energy TKE is shown in Figure 18 for the most representative stability ranges (daytime: $-1 \leq (z\text{-}d)/L_{top} < -0.032$; nighttime: $0.032 < (z\text{-}d)/L_{top} \leq 1$). In addition the main production processes, namely shear production P_s, wake production P_w, and buoyant production P_b within and above the canopy are displayed (see Section 3.1).

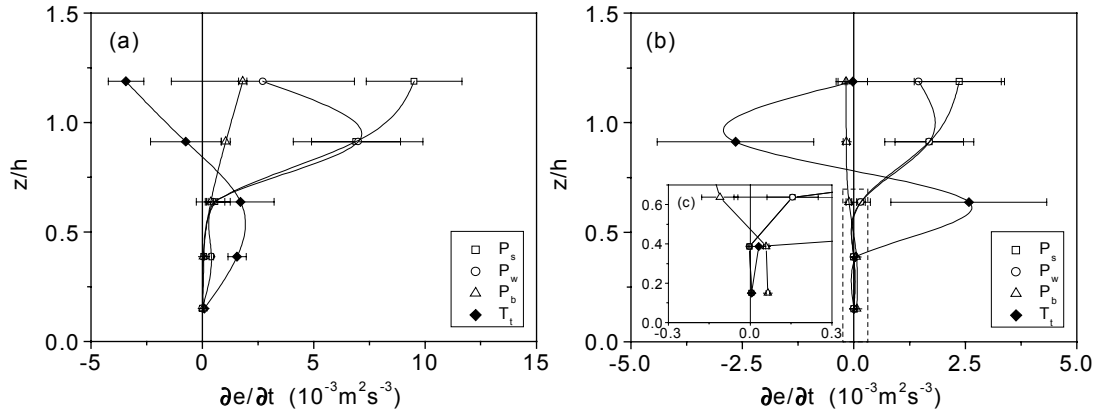

Figure 18. Turbulent transport Tt and production terms (Ps, Pw, Pb) of the turbulent energy budget (e = TKE; Eq. (1)) for (a) unstable daytime ($-1 \leq (z\text{-}d)/L_{top} < -0.032$) and (b) stable night time ($0.032 < (z\text{-}d)/L_{top} \leq 1$) conditions. The dashed box in the stable case marks the focus area (c).

In both stability cases the dominating source of TKE above the canopy is shear production P_s. The absolute value of P_s is about 4 times higher within the unstable conditions mainly due to a factor of 3.6 between the average momentum fluxes. The average wake production terms P_w are also not zero at that height. This is probably caused by the single jutting trees resulting in a relative high scatter for the vertical gradient of the momentum flux (see Figure 6). The uncertainty of P_w above the canopy with relative standard errors above 100% indicates that the average difference from zero is statistically not significant. Since the dimensions of turbulent eddies produced at the wake scale of plant elements are rather small, turbulent air motion which is mainly responsible for scalar transport is produced by P_s and P_b. The buoyancy term P_b acts as a TKE source in unstable conditions and is on average 5 times smaller than the dominating sheer production at the height of 1.19 *h*. Correspondingly P_b is a sink in stable stratified air nearly a factor -14 lower than P_s. Under extreme stable or unstable conditions ($|(z\text{-}d)/L_{top}| > 1$) the ratio P_s/P_b at the highest level changes significantly. In very stable conditions the influence of P_W shrinks drastically ($P_s/P_b \approx$ 3) due to low momentum fluxes. The convective case is in addition to the reduced vertical wind shear characterized by high sensible heat fluxes ensuring that P_b exceeds P_s resulting in a ratio of 0.4 (these two cases are not shown). Fitzjarrald et al. (1988) also found buoyancy to be a very important production process in the daytime variance budget for the vertical wind component over a rain forest canopy in central Amazonia (Reserva Ducke).

In both cases shown in Figure 18 wake and shear production have the same magnitude trough the crown layer and are the dominating TKE production processes down to 0.7 *h*. This behavior is in agreement with results from other relative dense forest canopies published by Meyers and Baldocchi (1991) or Novak et al. (2000). At $z/h = 0.65$ P_w decreases below 10% of its value at canopy height for both stability ranges shown here. Dwyer et al. (1997) got exact the same height for the 10% value in their large eddy simulation (LES) of the TKE budget in a dense forest. This reduction is closely related to the canopy architecture. The tropical forest investigated in this study has its LAI maximum at $z/h \approx 0.6$, like their dense model canopy (LAI = 5.0).

Below that height the bulk of turbulent kinetic energy during daytime is imported from above except a small fraction originating from wake production. At the lowest average height (0.15 *h*) displayed in Figure 18 (a), the magnitude of all production processes shown here is very small. Nevertheless the turbulent transport there is also exceeding the other processes at least by a factor of 2. But in view of the small magnitude it seems likely that, as mentioned above, turbulent transport is not the main process establishing the connection between TKE close to the forest floor and the layer above the canopy. A result of the LES by Dwyer et al. (1997) in that context is, that the pressure transport which was explicitly calculated in their simulations, plays a major role for the TKE budget within the lower canopy. They found that especially for dense canopies in unstable conditions like in the case of the RBJ rain forest, it seems to be important.

Above the canopy, during daytime the increasing negative value of T_t suggests a relative thick layer form which TKE is withdrawn by turbulent transport. This seems to be largely connected to the streamwise wind component if one compares Figure 17 (a) and (b). The main shear production term containing the large vertical gradient of the mean streamwise wind speed above the canopy is solely contributing to the budget of $\overline{u'^2}$. The shear production is extremely large in this typical daytime stability class, still increasing at $z/h = 1.19$. This fact is probably one reason for the different form of the T_t profiles for the streamwise and vertical variance budget during daytime situations.

For stable night time conditions the turbulent transport of TKE is obviously vertically limited to the layer between $z/h = 1.19$ and 0.39. The vertical limitation of T_t in both directions within stable stratification agrees qualitatively with the results of Leclerc et al. (1990a) for a deciduous forest. They obtained a height of about $z/h \approx 1.85$ where T_t change its sign from negative to positive, which is higher than $z/h \approx 1.2$ in the present study. This might partly due to the higher stability included in the case presented here.

Therefore, at night the TKE in the crown region seems to be also imported from above. Below that layer at $z/h \leq 0.39$, the magnitude of all shown terms is small. Figure 18 (c) focuses on that part of the nocturnal TKE budget. It turns out that due to the unstable night time stratification within the stem space buoyancy production is the process dominating turbulence in the lower part of the canopy. At $z/h = 0.15$, P_b exceeds all other production terms calculated here at least by a factor 10 indicative for a free convection state.

Here, convective air motion arises as an effective mechanism to compensate for the nocturnal energy loss in the upper part of the canopy (Jacobs et al., 1994). The maximum radiative cooling in a dense forest canopy occurs in the crown layer were the bulk of the biomass surface is exposed to the atmosphere above. On average, the stable stratification above this elevated temperature minimum is restricting or even suppressing turbulent exchange between the lower canopy and the roughness layer as seen in the TKE budget. As shown by Fitzjarrald (1990) this nocturnal decoupling between the lower canopy and the atmosphere is only occasionally broken up. This can be caused by suddenly enhanced wind speeds or an abrupt onset of shadowing (by clouds) reducing the radiative cooling.

Summarizing, especially during calm and clear nights the turbulence within the canopy is in contrast to the daytime situation driven by internal processes. Therefore it seems likely to see whether nocturnal turbulence in the lower part of the rainforest scales with local parameters.

4.4.3 Local Surface Layer Scaling of Nocturnal Turbulence just above the Forest Floor

Figure 19 (a) shows normalized night time σ_w/u_* values measured 1 m above the forest floor (0.03 h) as function of the local stability. Since hardly ever stable stratification occurred at night, only

data for $-z/L$ are displayed. Like above the canopy during day, the main fraction of the nocturnal stability values lie between $z/L = -0.1$ and -10. Also shown is the surface layer scaling according to Wesely (1988) (Eq. (8)) and a non linear least squares fit based on Eq. (8) as well. The exponent was fixed on the expected 1/3 value for the asymptotic behaviour of σ_w/u_* for $z/L \rightarrow -\infty$ caused by the decreasing influence of u_* (Wyngaard et al., 1971).

The measured values show significantly lower values than predicted by the surface layer scaling. The least squares fit results in 0.81 ± 0.03 and 2.7 ± 0.3 ($R^2 = 0.96$, $\alpha_p = 0.05$), respectively, for the first and the second coefficient in Eq. (8). The most significant difference is in the near neutral stability range, where values between 1.25 and 1.3 are expected for the surface layer. On the other hand, Rotach (1991) obtained an average value of 0.94 in the roughness layer of an urban canopy. Despite the fact that in the urban environment stability was in the range $0 > (z-d)/L > -1$ and turbulence was more dominated by mechanical production (which is clearly not the case here) he got this similar low value.

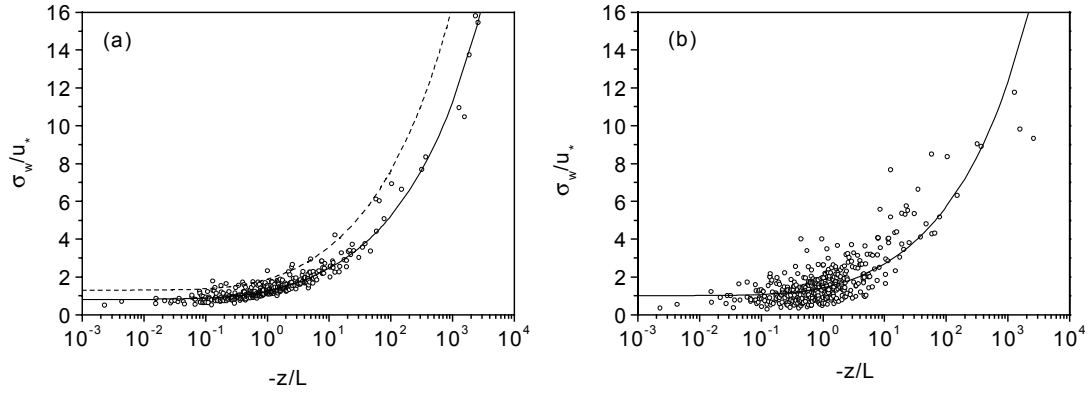

Figure 19. Nocturnal standard deviation of vertical wind speed σ_w at 1 m normalized by the local friction velocity u_* as function of the local stability $-z/L$. Open circles indicate measured σ_w values in (a) and random σ_w values in (b). The dashed line represents the surface layer similarity according to Wesely (1988) (Eq. (8)). The solid lines are fitted, also on the basis of Eq. (8).

The ratio of two small values (with corresponding sample errors) one would expect to be poorly determined with large scatter. Bearing this in mind the functional relation obtained in Figure 19 is quite clear. The high R^2 value for the fit is of course also largely caused by the values beyond $z/L = -10$. But the rather small scatter and the clear dependence on local stability of night time turbulence data deep within a tropical rainforest could not be expected.

However, the proportionality of dimensionless turbulence variables like σ_w/u_* with respect to $(z/L)^{1/3}$ is implicitly contained by sharing u_* in both variables as showed by Hicks (1981). By combining a set of random variables he obtained similar results for the dependencies of σ_x/x_* on (z/L)

which result from surface layer data (see also Gerstmann (1988) for a critical discussion of his results). To see whether the relationship obtained for the in canopy data differ significantly from random data a similar test was carried out. The dataset of σ_w was exchanged by random numbers with a probability distribution having the same average and standard deviation as the original data. All other variables involved in the calculation were left original. The result is shown in Figure 19 (b). The similar course of the non linear fit ($R^2 = 0.77$, $\alpha_p = 0.05$) shows the result of the implicit dependence. The obtained values of 1.01 ± 0.08 and 1.8 ± 0.5 are even closer to the surface layer coefficients in Eq. (8). The missing physical connection between σ_w and the other quantities is expressed in the considerable higher scatter. Calculating the correlation coefficient r_{uw} shows the poor determination by including random numbers clearly. In the stability range of $0 > z/L \geq -1$ the average correlation coefficient for the measured values agrees with $r_{uw} = -0.35 \pm 0.13$ well with the expected surface layer value of -0.35 (Kaimal and Finnigan, 1994) although the standard deviation is rather large. Contrastingly the correlation coefficient is $r_{uw} = -0.71 \pm 1.41$ for the random datasets for σ_u and σ_w within the same stability range. Here, the large value of r_{uw} together with its huge uncertainty reveals the incoherent random character of its data basis. The results suggest, that the scaling of σ_w/u_* with respect to $(z/L)^{1/3}$ within the lowest part of the nocturnal canopy is not just based on the implicit functional relation of both quantities. Although the obtained ratio σ_w/u_* is clearly lower than typically found in the surface layer.

During a lot of the nocturnal periods shown in Figure 19 the local Obukhov length L is clearly smaller than the measuring height z (1 m above the forest floor). This indicates that the influence of a very small local u_* on turbulence might be negligible due to convective conditions. At higher levels within the nocturnal stem space this effect is even stronger due to a larger z.

4.4.4 Mixed Layer Scaling within the Nocturnal Stem Space

Within convective conditions like the daytime mixed layer the governing parameters are in contrast to MO surface layer similarity just the kinematic virtual temperature (or buoyancy) surface flux $\left(\overline{w'T_v'}\right)_0$, the buoyancy parameter g/T_v, and the height z (Wyngaard et al., 1971). Therefore a different scaling was introduced by Deardorff (1970) for the convective situation in the mixed layer. The corresponding velocity scale is:

$$w_* = \left(\frac{g}{T_v} z_i \left(\overline{w'T_v'}\right)_0 \right). \tag{11}$$

Here z_i is the height of the convective layer, vertically limited by the base of the temperature inversion aloft.

In a few studies the mixed layer scaling was also applied to the convective night time situation within plant canopies. Jacobs et al. (1994) showed that nocturnal wind speed and temperature profiles within a maize canopy nicely collapse if normalised with corresponding mixed layer scales. In addition they could demonstrate that during calm nights the heat flux within the canopy was largely driven by convection (see also Simon, 1999). As a criterion characterizing periods with free convection dominating air motion throughout the canopy they used $w_* > u_{*,top}$. That means if the convective velocity scale within the canopy exceeds the friction velocity above the canopy the air motion within the canopy is decoupled from above. In agreement Bosveld et al. (1999) suggest that the ratio of w_* and $u_{*,top}$ is one of the main factors governing to which extent the nocturnal radiative surface temperature and the energy exchange in the crown layer of a Douglas Fir forest is influenced by the convective air motion in the stem space. Instead of the soil heat flux like Jacobs et al. (1994) they used a modelled storage heat flux to determine w_* taking into account the large canopy space and the massive cooling in the crown layer of the dense forest compared to the maize canopy.

The nocturnal enhancement of in canopy turbulence has also direct influence on the exchange and vertical distribution of trace gases. This fact was considered by parameterisations for the nocturnal σ_w profiles within the rainforest canopy by Kruijt et al. (1996) and a crop canopy by Simon (1999). In order to model the CO_2 exchange of these canopies they used with height linearly decreasing or vertically constant σ_w profiles for the rainforest and crop canopy respectively .

In the following it is to be clarified whether the measured nocturnal profiles of turbulent velocity fluctuations within the rain forest interior show characteristics similar to the daytime convective boundary layer. In accordance to Bosveld et al. (1999) w_* was calculated with the buoyancy flux $\left(\overline{w'T_v'}\right)_{11}$ measured at 11 m (0.28 *h*) instead of the soil heat flux or the flux measured at 1 m (0.03 *h*). $\left(\overline{w'T_v'}\right)_{11}$ was considered to be more representative for the stem space than corresponding surface fluxes. The reason is, that in contrast to the mixed layer also the warmer biomass from the lower part of the canopy is contributing to the temperature difference between the stem space and the crown region which drives the convective air motion. As the characteristic length scale z_i the height is used, where in most of the nocturnal cases the base of the temperature inversion was observed. This height is 20.5 m (0.51 *h*) and within the lower part of the crown region of the forest.

In Figure 20 the ratio $u_{*,top}/w_*$ is displayed for night time conditions as function of *wind speed*$_{top}$ measured above the canopy. During most of the night time periods (77.3%) w_* is larger than $u_{*,top}$. This supports the results from the TKE budget estimates above, which suggested convection to be the dominating nocturnal production process of turbulent air motion below the crown layer of the forest. Because w_* is relative constant between the transition periods of dawn and dusk, the main part of the variability of $u_{*,top}/w_*$ is caused by the time evolution of the friction velocity $u_{*,\ top}$. The influence of

wind speed$_{top}$ on $u_{*,top}/w_*$ can therefore be mainly attributed to the connection between *wind speed*$_{top}$ and $u_{*,top}$. During daytime conditions (Figure 15 (b)) a *wind speed*$_{top}$ of about 2 m s^{-1} marks approximately the threshold beyond which the lower canopy is directly coupled with the air flow above. At night again 2 m s^{-1} is a good estimate for a wind speed limit below which w_* is usually larger than $u_{*,top}$ and vice versa at higher wind speeds. The failure percentage of 23% (*wind speed*$_{top} \geq$ 2 m s^{-1} and $u_{*,top}/w_* < 1$) and 25% (*wind speed*$_{top} <$ 2 m s^{-1} and $u_{*,top}/w_* \geq 1$) above and below the wind speed threshold are quite similar. Therefore the applied profile classification seems also to be appropriate to distinguish nighttime conditions where canopy space turbulent air motion is more or less independent from above from situations were a distinct coupling is apparent.

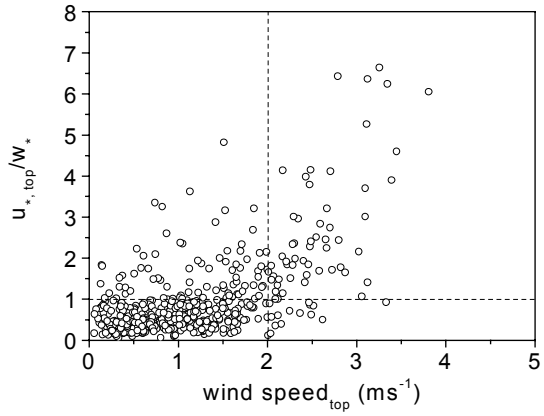

Figure 20. Ratio of friction velocity $u_{*,top}$ measured above the canopy and in canopy free convection velocity scale w_* as function of wind speed during night time conditions.

Normalized night time profiles of streamwise and vertical velocity variance measured at three heights (1 m, 11 m, and 20 m) within the canopy are displayed in Figure 21. The average profiles include half hour intervals with $w_* > u_{*,top}$. For comparison, corresponding mean profiles from laboratory convection chamber experiments (Willis and Deardorff, 1974) and convective boundary layer measurements, published in Caughey and Palmer (1979), are shown additionally in Figure 21.

The average values of the σ_u^2/w_*^2 data are within the range of Caughey and Palmer's (1979) boundary layer data (Figure 21 (a)). Like the boundary layer data, the in-canopy profile shows only a weak vertical structure. In the boundary layer data one might identify two variance maxima, a near-surface one and one at ~ 0.8 z_i. Contrastingly, the data within the forest indicate a local maximum at 0.54 z_i. In a convective boundary layer, large scale convective motion extending over the whole layer depth is usually providing a near uniform vertical distribution of the mean potential temperature, horizontal wind speed, and horizontal velocity variances. Analogously, convective cells horizontally limited by the gaps between plants are assumed to be responsible for the in-canopy well mixed layer (up to z_i). On the other hand, a weak but distinct horizontal sub-canopy flow occurs especially during

those calm nights which have been averaged for the profiles shown in Figure 21. Due to the higher drag in the crown region and close to the forest floor (where the LAI is higher than in the middle of the stem space), a local wind speed maximum appears at 0.54 z_i. In combination with the vertical structure of σ_w^2/w_*^2 this might be an explanation for the additional local maximum shown by the σ_u^2/w_*^2 data.

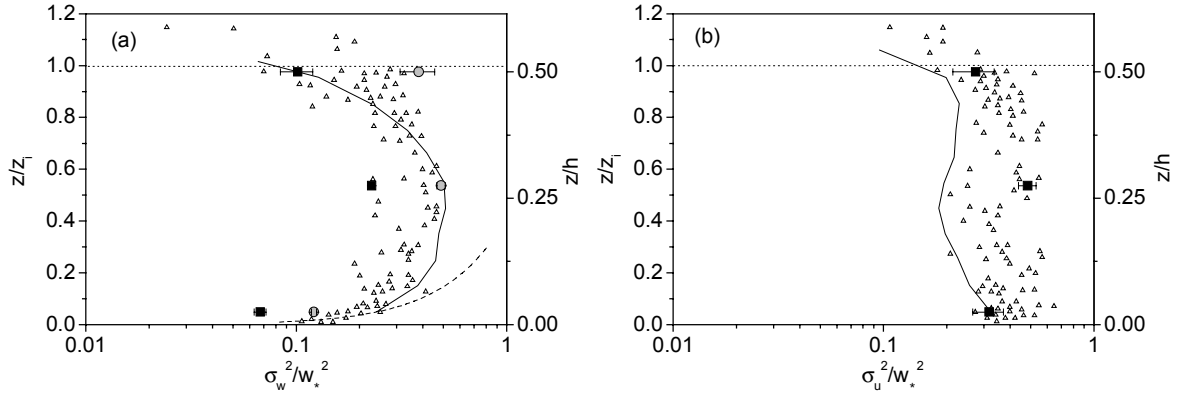

Figure 21. Average night time profiles of vertical (a) and streamwise (b) velocity variance measured at three heights (1 m, 11 m, and 20 m), normalized by the squared convective velocity scale (calculated with buoyancy flux at 11 m: black squares; and in (a) at 1 m:grey circles). Error bars represent standard errors. Height z is normalized by the assumed convective boundary layer height z_i (left axis) or the canopy height h (right axis).The lower dashed curve indicates the local free convection surface layer scaling after Kaimal et al. (1976). The solid line shows the average convective layer results of laboratory model experiments carried out by Willis and Deardorff (1974). Mixed layer data of two field experiments presented in Caughey and Palmer (1979) are displayed as open triangles.

The structure of σ_w^2/w_*^2 profiles is more evident than it is in the variance profiles of the horizontal component. All shown data, namely the boundary layer data, the data from the convection chamber experiment, and the in canopy profile data of σ_w^2/w_*^2 exhibit a maximum between 0.5 and 0.6 z_i. Near the surface and just below of the inversion base (at z_i), the vertical variance is smaller. This can be explained by the maximum vertical velocity which thermals have at around half height of the convective layer, after their initial acceleration near the surface and before decelerated again due to increasing dilution with environmental air towards the top of the layer. Other numerical (Deardorff, 1974) and experimental (Lenschow et al., 1980) studies obtain the maximum of the vertical velocity variance at somewhat lower heights at $z/z_i \approx 0.3$. The general structure and the absolute value of the maximum σ_w^2/w_*^2 between 0.45 and 0.5 are very similar in most of the convective boundary layer studies. The maximum value for σ_w^2/w_*^2, 0.23 ± 0.01 (s.e.) in the forest canopy at $z/z_i = 0.54$ is at the lower limit of the data range obtained in the boundary layer at that height. Furthermore, the normalized vertical variance values in the nocturnal forest canopy seem to be systematically lower

than the corresponding values from the investigations carried out in the convective boundary layer. Several reasons for this discrepancy are conceivable. Due to a finite spacing between trees in the forest the drag caused by canopy elements could limit the vertical air motion compared to the free boundary layer. The fact that within the canopy the heat (or buoyancy) flux is not monotonically decreasing with height is another fundamental difference to the boundary layer. As already mentioned, all vegetation elements of the lower canopy might act as elevated heat sources during night. Therefore, it might be still questionable whether the buoyancy flux at 11 m (0.54 z_i) used for the calculation of the velocity scale w_* is representative for all heights within the canopy. This would be of importance especially at the lowest height, where in fact the largest relative deviations from the surface layer σ_w^2/w_*^2 values occur. The gray circles in Figure 21 (b) show the profile of σ_w^2/w_*^2 when the buoyancy flux measured at 1 m (0.05 z_i) is used for the calculation of w_*. As expected the deviation from the boundary layer and laboratory data is then reduced for the lowest height. Unlike the deviation at the lower layers the difference to the boundary layer values is enlarged at 20 m (0.98 z_i). At that height as indicated by the turbulent transport term in Figure 17 (a), σ_w^2 might be enhanced by entrainment from above. This effect would mask a difference to the boundary layer values existent in reality. That would explain the inverse behavior compared to the lower heights depending on the buoyancy flux used for the calculation of w_*.

Even if the absolute values of σ_u^2/w_*^2 and σ_w^2/w_*^2 do not fully agree with results from boundary layer experiments, the agreement is much better than an order of magnitude. In addition, especially the profile of the vertical velocity variance shows a structure which is characteristic for the convective boundary layer.

5 Summary and Conclusions

The turbulent vertical wind field above the RBJ rain forest was found to be quite well developed. Despite the high roughness of the canopy surface, over a wide range of stability conditions σ_w/u_* is well described by the universal functions $\varphi_w(z\text{-}d)/L$ on the basis of surface layer similarity according to Obukhov (1960) for horizontally homogeneous conditions. Contrastingly, in agreement with many former studies on surface layer turbulence, the streamwise component σ_u/u_* is not scaling with $(z\text{-}d)/L$.

The turbulent air motion within the rain forest canopy is subject to clearly different regimes under day and night time conditions.

During daytime direct turbulent transport is coupling the main part of the canopy to the atmosphere above. Especially in windy conditions with wind speeds above 2 m s^{-1}, large scale eddies have sufficient energy to penetrate deep into the stably stratified lower part of the forest. This is indicated by high kurtosis and negative skewness of the vertical wind fluctuations in the stem space. In

agreement to the findings of Kruijt et al. (2000) the lower part of the canopy is most of the time not included in the direct exchange with the atmosphere above the vegetation layer. But this layer is mostly limited to the first meters above the forest floor and much shallower than in the forest canopy in central Amazonia.

Contrastingly, to the daytime situation, at night the whole sub-canopy space is mostly decoupled from the atmosphere above the forest. A strong inversion throughout the upper crown layer and above it isolates the stem space below most of the time. Unstable stratification in the isolated stem space initiates an internal convective air motion. The resulting sub-canopy vertical turbulence structure is similar to that of the atmospheric mixing layer and can be closely described by the corresponding scaling approach. Here, the convective velocity scale w_* was calculated on the basis of the layer depth and the internal heat flux.

As a consequence of this night time convection soil emitted NO is mixed up to the lower crown region (see Rummel et al. (2002)). Therefore occasionally occurring nocturnal turbulence enhancements, which break up the inversion layer may be able to effectively transfer accumulated NO to the atmosphere above the forest.

Acknowledgements

This research is supported by the “Environmental and Climate Programme” (Project LBA-EUSTACH, ENV4-CT97-0566) of the European Union, and by the Max Planck Society. We would like to thank the staff at INCRA (Instituto Nacional de Colonização e Reforma Agrária), especially Jaõ Luis Esteves, Eduardo Conceição, and Claudionor Rodrigues. Further, Carlos Brãndao and the staff of IBAMA (Instituto Brasileiro do Meio Ambiente e dos Recursos Naturais Renováveis) in Ji-Parana are gratefully acknowledged for their help in installing and maintaining the infrastructure at the forest. We are indebted to Beatriz E. Gomes (Universidade Federal de Rondonia, Ji Parana) for support concerning everything. We are also grateful to Monika Scheibe, Michael Welling, and Wesley Saores da Silva for assisting us in the field.

References

Amiro, B. D., and Davis, P. A.: 1988, 'Statistics of Atmospheric Turbulence within a Natural Black Spruce Forest Canopy', *Boundary-Layer Met.* **44**, 267-283.

Amiro, B. D.: 1990, 'Comparison of Turbulence Statistics within 3 Boreal Forest Canopies', *Boundary-Layer Met.* **51**, 99-121.

Ammann, C., 1999, *On the Aplicability of Relaxed Eddy Accumulation and Common Methods for Measuring Trace Gas Fluxes*. Dissertation Thesis, Universität Zürich, 229 pp.

Andreae, M. O., Artaxo, P., Brandao, C., Carswell, F. E., Ciccioli, P., da Costa, A. L., Culf, A., Esteves, J. L., Gash, J. H. C., Grace, J., Kabat, P., Lelieveld, J., Mahli, Y., Manzi, A. O., Meixner, F. X., Nobre, A. D., Nobre, C., Ruivo, M. d. L. P., Silva-Dias, M. A., P., S., Valentini, R., von Jouanne, J., and Waterloo, M. J.: 2002, 'Biogeochemical Cycling of Carbon, Water, Energy, Trace Gases, and Aerosols in Amazonia', *J. Geophys. Res.* **107**, 8066, doi: 10.1029/2001JD000524.

Baldocchi, D. D., and Meyers, T. P.: 1988, 'Turbulence Structure in a Deciduous Forest', *Boundary-Layer Met.* **43**, 345-364.

Beljaars, A. C. M., and Holtslag, A. A. M.: 1991, 'Flux Parametrization over Land Surfaces for Atmospheric Models', *J. Appl. Met.* **30**, 327-341.

Bosveld, F. C., Holtslag, A. A. M., and Van den Hurk, B.: 1999, 'Nighttime Convection in the Interior of a Dense Douglas Fir Forest', *Boundary-Layer Met.* **93**, 171-195.

Brunet, Y., Finnigan, J. J., and Raupach, M. R.: 1994, 'A Wind-Tunnel Study of Wir-Flow in Waving Wheat - Single-Point Velocity Statistics', *Boundary-Layer Met.* **70**, 95-132.

Caughey, S. J., and Palmer, S. G.: 1979, 'Some Aspects of Turbulence Structure through the Depth of the Convective Boundary Layer', *Quart. J. Roy. Met. Soc.* **105**, 811-827.

Culf, A., Esteves, J. L., Marques Filho, A. d. O., and da Rocha, H. R.: 1996, 'Radiation, Temperature and Humidity over Forest and Pasture in Amazonia', in J. H. C. Gash, C. A. Nobre, J. M. Roberts and R. L. Victoria (ed.), *Amazonian Deforestation and Climate*, John Wiley and Sons, Chichester, pp. 175-191.

de Bruin, H. A. R., Bink, N. J., and Kroon, L. J. M.: 1991, 'Fluxes in the Surface Layer under Advective Conditions', in T. J. Schmugge and A. J. C. (ed.), *Workshop on Land Surface Evaporation, Measurement and Parameterization*, Springer Verlag, New York, pp. 157-169.

de Bruin, H. A. R., Kohsiek, W., and Van den Hurk, B.: 1993, 'A Verification of Some Methods to Determine the Fluxes of Momentum, Sensible Heat, and Water-Vapor Using Standard- Deviation and Structure Parameter of Scalar Meteorological Quantities', *Boundary-Layer Met.* **63**, 231-257.

Deardorff, J. W.: 1970, 'Convective Velocity and Temperature Scales for the Unstable Planetary Boundary Layer', *Journal of Atmospheric Science* **27**, 1211-1213.

Deardorff, J. W.: 1974, 'Three-Dimensional Numerical Study of Turbulence in an Entraining Mixed Layer', *Boundary-Layer Met.* **7**, 199-206.

Dwyer, M. J., Patton, E. G., and Shaw, R. H.: 1997, 'Turbulent Kinetic Energy Budgets from a Large-Eddy Simulation of Airflow above and within a Forest Canopy', *Boundary-Layer Met.* **84**, 23-43.

Finnigan, J.: 2000, 'Turbulence in Plant Canopies', *Annual Review of Fluid Mechanics* **32**, 519-571.

Finnigan, J. J.: 1985, 'Turbulent Transport in Flexible Plant Canopies', in B. A. Hutchison and B. B. Hicks (ed.), *The Forest-Atmosphere Interaction*, D. Reidel Publishing Company, Oak Ridge, Tennesee, pp. 443-480.

Fitzjarrald, D. R., Stormwind, B. L., Fisch, G., and Cabral, O. M. R.: 1988, 'Turbulent Transport Observed Just above the Amazon Forest', *J. Geophys. Res.* **93**, 1551-1563.

Fitzjarrald, D. R., Moore, K. E., Cabral, O. M. R., Scolar, J., Manzi, A. O., and Sa, L. D. D.: 1990, 'Daytime Turbulent Exchange between the Amazon Forest and the Atmosphere', *J. Geophys. Res.-Atmos.* **95**, 16825-16838.

Fitzjarrald, D. R., and Moore, K. E.: 1990, 'Mechanisms of Nocturnal Exchange between the Rain Forest and the Atmosphere', *J. Geophys. Res.* **95**, 16839-16850.

Foken, T., 1990, 'Turbulenter Energieaustausch Zwischen Atmosphäre Und Unterlage - Methoden, Messtechnische Realisierung, Sowie Ihre Grenzen Der Anwendungsmöglichkeit', Berichte des Deutschen Wetterdienstes **180**, Offenbach am Main.

Foken, T., Skeib, G., and Richter, S. H.: 1991, 'Dependence of the Integral Turbulence Characteristics on the Stability of Stratification and Their Use for Doppler-Sodar Measurements', *Z. Meteorol.* **41**, 311-315.

Foken, T., and Wichura, B.: 1996, 'Tools for Quality Assessment of Surface-Based Flux Measurements', *Agric. For. Met.* **78**, 83-105.

Foken, T., Jegede, O. O., Weisensee, U., Richter, S. H., Handorf, D., Görsdorf, U., Vogel, G., Schubert, U., Kirzel, H.-J., and Thiermann, V., 1997, 'Results of the Linex 96/2 Experiment', Deutscher Wetterdienst, Geschäftsbereich Forschung und Entwicklung, Arbeitsergebnisse 48, pp.75.

Gash, J. H. C., Nobre, J. M., Roberts, J. M., and Victoria, R. L.: 1996, 'An Overview of Abracos', in J. H. C. Gash, J. M. Nobre, J. M. Roberts and R. L. Victoria (ed.), *Amazonian Deforestation and Climate*, John Wiley, New York, pp.

Gerstmann, W.: 1988, 'An Evaluation of Turbulence Statistics in the Surface Boundary Layer', *Boundary-Layer Met.* **43**, 91-92.

Hicks, B. B.: 1981, 'An Examination of Turbulence Statistics in the Surface Boundary Layer', *Boundary-Layer Met.* **21**, 389-402.

Högström, U.: 1990, 'Analysis of Turbulence Structure in Rhe Surface Layer with a Modified Similarity Formulation for near Neutral Conditions', *Journal of Atmospheric Science* **47**, 1949-1972.

Holtslag, A. A. M., and Nieuwstadt, F. T. M.: 1986, 'Scaling the Atmospheric Boundary Layer', *Boundary-Layer Meteorlogy* **36**, 201-209.

Jacobs, A. F. G., van Boxel, J. H., and Elkilani, R. M. M.: 1994, 'Nighttime Free-Convection Characteristics within a Clant Canopy', *Boundary-Layer Met.* **71**, 375-391.

Kaimal, J. C., Wyngaard, J. C., Izumi, Y., and Cote, O. R.: 1972, 'Spectral Characteristics of Surface-Layer Turbulence', *Quart. J. Roy. Met. Soc.* **98**, 563-589.

Kaimal, J. C., Wyngaard, J. C., Haugen, D. A., Cote, O. R., Izumi, Y., Caughey, S. J., and Readings, C. J.: 1976, 'Turbulence Structure in the Convective Boundary Layer', *Journal of Atmospheric Science* **33**, 2152-2169.

Kaimal, J. C., and Finnigan, J. J.: 1994, *Atmospheric Boundary Layer Flows*, Oxford University Press, New York, Oxford, 280 pp.

Katul, G., Goltz, S. M., Hsieh, C. I., Cheng, Y., Mowry, F., and Sigmon, J.: 1995, 'Estimation of Surface Heat and Momentum Fluxes Using the Flux- Variance Method above Uniform and Nonuniform Terrain', *Boundary-Layer Met.* **74**, 237-260.

Kruijt, B., Lloyd, J., Grace, J., McIntyre, J. A., Farquhar, G. D., Miranda, A. C., and McCracken, P.: 1996, 'Sources and Sinks of Co2 in Rondonia Tropical Rainforest', in J. H. C. Gash, C. A. Nobre, J. M. Roberts and R. L. Victoria (ed.), *Amazonian Deforestation and Climate*, John Wiley & Sons, Chichester, pp. 331-351.

Kruijt, B., Malhi, Y., Lloyd, J., Nobre, A. D., Miranda, A. C., Pereira, M. G. P., Culf, A., and Grace, J.: 2000, 'Turbulence Statistics above and within Two Amazon Rain Forest Canopies', *Boundary-Layer Met.* **94**, 287-331.

Leclerc, M. Y., C., B. K., Shaw, R. H., den Hartog, G., and Neumann, H. H.: 1990a, 'The Influence of Atmospheric Stability on Budgets of Reynolds Stress and Turbulent Kinetic Energy within and above a Deciduous Forest', *J. Appl. Met.* **29**, 916-933.

Leclerc, M. Y., Beissner, K. C., Shaw, R. H., den Hartog, G., and Neumann, H. H.: 1990b, 'The Influence of Buoyacy on Third-Order Velocity Statistics within a Deciduous Forest', *Boundary-Layer Met.* **55**, 109-123.

Lee, X., and Black, A.: 1993, 'Atmospheric Turbulence within and above a Douglas-Fir Stand. Part 1: Statistical Properties of the Velocity Field', *Boundary Layer Meteorology* **64**, 149-174.

Lenschow, D. H., Wyngaard, J. C., and Pennell, W. T.: 1980, 'Mean Field and Second Moment Budgets in a Baroclinic, Convective Boundary Layer', *Journal of Atmospheric Science* **37**, 1313-1326.

Lenschow, D. H., Mann, J., and Kristensen, L.: 1994, 'How Long Is Long Enough When Measuring Fluxes and Other Turbulent Statistics', *J. Atmos. Oceanic Technol.* **11**, 661-673.

Lumley, J. L., and Panofsky, H. A.: 1964, *The Structure of Atmospheric Turbulence*, Interscience-Wiley, New York, 239 pp.

Mangold, A., 1999, *Untersuchung Der Lokalen Einflüsse Auf Turbulenzmessungen Der Station Weidenbrunnen*. Diploma Thesis, University of Bayreuth, Bayreuth, 175 pp.

McBean, G. A.: 1971, 'The Variations of the Statistics of Wind, Temperature and Humidity Fluctuations with Stability', *Boundary-Layer Met.* **1**, 438-457.

Meyers, T. P., and Baldocchi, D. D.: 1991, 'The Budgets of Turbulent Kinetic Energy and Reynolds Stress within and above a Deciduous Forest', *Agric. For. Met.* **53**, 207-222.

Moore, C. J.: 1986, 'Frequency Response Correction for Eddy Correlation Systems', *Boundary-Layer Met.* **37**, 17-35.

Novak, M. D., Warland, J. S., Orchansky, A. L., Ketler, R., and Green, S. R.: 2000, 'Wind Tunnel and Field Measurements of Turbulent Flow in Forests. Part1: Uniformly Thinned Stands', *Boundary-Layer Met.* **95**, 475-495.

Obukhov, A. M.: 1960, 'O Strukture Temperaturnogo Polja I Polja Skorostej V Uslovijach Konvecii', *Izv AN SSSR, ser Geofiz*, 1392-1396.

Panofsky, H. A., Tennekes, H., Lenschow, D. H., and Wyngaard, J. C.: 1977, 'The Characteristics of Turbulent Velocity Components in the Surface Layer under Convective Conditions', *Boundary-Layer Met.* **11**, 355-361.

Panofsky, H. A., and Dutton, J. A.: 1984, *Atmospheric Turbulence, Models and Methods for Engineering Applications*, John Wiley & Sons, New York, Chichester, Brisbane, Toronto, Singapore, pp.

Pinker, R. T., and Holland, J. Z.: 1988, 'Turbulence Structure of Tropical Forest', *Boundary-Layer Met.* **43**, 43-63.

Raupach, M., and Shaw, R. H.: 1982, 'Averaging Procedures for Flow within Vegetation Canopies', *Boundary-Layer Met.* **22**, 79-90.

Raupach, M. R., Coppin, P. A., and Legg, B. J.: 1986, 'Experiments on Scalar Dispersion within a Model-Plant Canopy .1. The Turbulence Structure', *Boundary-Layer Met.* **35**, 21-52.

Raupach, M. R., Finnigan, J. J., and Brunet, Y.: 1996, 'Coherent Eddies and Turbulence in Vegetation Canopies - the Mixing-Layer Analogy', *Boundary Layer Meteorology* **78**, 351-382.

Rotach, M. W., 1991, *Turbulence within and above an Urban Canopy*. Dissertation Thesis, Universität Zürich, 245 pp.

Rummel, U., Ammann, C., Gut, A., Meixner, F. X., and Andreae, M. O.: 2002, 'Eddy Covariance Measurements of Nitric Oxide Flux within an Amazonian Rainforest', *J. Geophys. Res.* **107(D20)**, 8050, doi:10.1029/2001JD000520.

Rummel, U., Ammann, C., Kirkman, G. A., Moura, M. A. L., Rottenberger, S., Kuhn, U., Kesselmeier, J., Foken, T., Andreae, M. O., and Meixner, F. X.: 2005a, 'Seasonal Variation of Ozone Deposition to a Tropical Rain Forest in Southwest Amazonia', *Agric. For. Met.* **for submission**

Rummel, U., Ammann, C., Foken, T., Andreae, M. O., and Meixner, F. X.: 2005b, 'Application of a Surface Renewal Model for the Determination of Heat, Carbon Dioxide, and Ozone Fluxes from a Tropical Rain Forest in Amazonia', *Atmos. Chem. Phys.* **for submission**

Rummel, U., Ammann, C., Andreae, M. O., and Meixner, F. X.: 2005c, 'Wet Season NO_x Exchange between an Amazonian Rain Forest and the Atmosphere-Implication from Time Scale Analysis', *Atmos. Environ.* **for submission**

Shaw, R. H., and Seginer, I.: 1987, 'Calculation of Velocity Skewness in Real and Articicial Plant Canopies', *Boundary-Layer Met.* **39**, 315-332.

Shaw, R. H., Denhartog, G., and Neumann, H. H.: 1988, 'Influence of Foliar Density and Thermal Stability on Profiles of Reynolds Stress and Turbulence Intensity in a Deciduous Forest', *Boundary-Layer Met.* **45**, 391-409.

Shaw, R. H., Paw U, K. T., Zhang, X. J., Gao, W., den Hartog, G., and Neumann, H. H.: 1990, 'Retrievel of Turbulent Pressure Fluctuations at the Ground Surface beneath a Forest', *Boundary-Layer Met.* **50**, 319-338.

Shaw, R. H., and Zhang, X. J.: 1992, 'Evidence of Pressure-Forced Turbulent Flow in a Forest', *Boundary-Layer Met.* **58**, 273-288.

Simon, E., 1999, *Quellsenkenverteilung Von Energie und Spurengasen in einem seneszenten Getreidefeld: Modellierung und Vergleich mit Meßdaten*. Diploma Thesis, Johannes Gutenberg Universität, Mainz,, 149 pp.

Sreenivasan, K. R., Chambers, A. J., and Antonia, R. A.: 1978, 'Accuracy of Moments of Velocity and Scalar Fluctuations in the Atmospheric Surface Layer', *Boundary-Layer Met.* **14**, 341-359.

Thomas, C., 2001, *Integral Turbulence Characteristics and Their Parameterisations*. Diploma Thesis, University of Bayreuth, Bayreuth, 101 pp.

Wesely, M. L.: 1988, 'Use of Variance Techniques to Measure Dry Air-Surface Exchange- Rates', *Boundary-Layer Met.* **44**, 13-31.

Willis, G. E., and Deardorff, J. W.: 1974, 'A Laboratory Model of the Unstable Planetary Boundary Layer', *Journal of Atmospheric Science* **31**, 1297-1307.

Wilson, N. R., and Shaw, R. H.: 1977, 'A Higher Order Closure Model for Canopy Flow', *J. Appl. Met.* **16**, 1197-1205.

Wyngaard, J. C., Cote, O. R., and Izumi, Y.: 1971, 'Local Free Convection, Similarity, and the Budgets of Shear Stress and Heat Flux', *Journal of Atmospheric Science* **28**, 1171-1182.

Wyngaard, J. C.: 1973, 'On Surface-Layer Turbulence', in D. A. Haugen (ed.), *Workshop on Micrometeorology*, American Meteorological Society, Boston, pp. 101-149.

Appendix E

Application of a Surface Renewal Model for the Determination of Heat, Carbon Dioxide, and Ozone Fluxes from a Tropical Rain Forest in Amazonia

U. Rummel[1*], C. Ammann[2], T. Foken[3], M.O. Andreae[1], and F.X. Meixner[1]

[1]Max Planck Institute for Chemistry, Biogeochemistry Dept., D-55020 Mainz, Germany,

[2]Air Pollution - Climate group (TP 11.3), FAL-Reckenholz,P.O.Box, CH-8046 Zürich, Switzerland

[3]University of Bayreuth,. Mikrometeorology Dept., D-95440 Bayreuth, Germany

for submission in **Atmospheric Chemistry and Physics**

Abstract.

A surface renewal model was used to determine the turbulent fluxes of four different scalar quantities above a tall tropical rain forest in southwest Amazonia. To extract the ramp pattern information (the 'fingerprint' of coherent eddy motion) from high-frequency scalar time series of temperature, water vapor, carbon dioxide, and ozone, a combined two-level detection and filtering scheme on the basis of continuous wavelet transform was applied. A mean time interval of ~1.6 h/u_* (h being the canopy height and u_* the friction velocity) between consecutive ramps was found. Comparison of the obtained fluxes with results from eddy covariance measurements showed good agreement for all the scalar quantities. For the specific rain forest canopy in our study, the model calibration factor α that accounts for the vertical distribution of the scalar sources/sinks was determined. Only slightly different α values, between 0.37 and 0.44, were obtained for the investigated scalar quantities. The effect of instrumental noise on an artificial time series was simulated. A systematic overestimation (up to 15%) of the surface renewal derived flux was predicted for high signal-to-noise ratios, increasing with higher ramp occurrence frequencies.

1 Introduction

Turbulent air motions above permeable surfaces such as vegetation canopies show peculiarities that distinguish them from boundary layer flows over impervious surfaces (Raupach and Thom, 1981). Large-scale turbulent structures, which are highly

*corresponding author

intermittent and spatially organized (coherent), are a prominent feature of flows within and above vegetation canopies (Gao et al., 1989; Gao et al., 1992; Paw U et al., 1992; Raupach et al., 1989; Raupach et al., 1996; Shaw et al., 1989). Mass, heat, and momentum exchange between the canopy and the atmosphere occurs to a large extent during these strong turbulent events (see, e.g., Bergström and Högström, 1989; Lu and Fitzjarrald, 1994; Qiu et al., 1995) which appear as ramp pattern in high-resolution time series of temperature and trace gases. Wavelet transform, used since the early nineties in laboratory and atmospheric turbulence studies (see, e.g., Farge, 1992; Gamage and Hagelberg, 1993; Hagelberg and Gamage, 1994; Handorf and Foken, 1997; Katul and Vidacovic, 1996; Mahrt and Gibson, 1992; Yamada and Ohkitani, 1990) is an appropriate tool for detailed structure analysis. The time localization of wavelet base functions matches the intermittent nature of coherent structures within and above vegetation canopies; and wavelet transform has been successfully used to determine the scales of the dominant turbulent structures and to estimate their flux contribution by, e.g., conditional averaging or using filter characteristics of wavelets (Brunet and Irvine, 2000; Collineau and Brunet, 1993a; 1993b; Gao and Li, 1993; Lu and Fitzjarrald, 1994; Qiu et al., 1995; Rummel et al., 2002a; Wichura et al., 2000). Characteristic time scales of exchange-relevant structures and therefore residence times of air within plant canopies are key variables especially for the transfer of heat and trace gases. The residence time is the temporal frame for in-canopy processes such as surface and stomatal exchange or chemical reaction.

The surface renewal method (Paw U et al., 1995) is a model approach to estimate scalar fluxes. This method assumes the canopy air to be instantaneously exchanged only during the strong coherent events. Various modifications of this model approach were used to determine the sensible and latent heat fluxes from different vegetation covers (Chen et al., 1997a; 1997b; Katul et al., 1996; Paw U et al., 1995; Snyder et al., 1996; Spano et al., 1997a; 2000b). To our knowledge the only study in which the surface renewal approach was used for the flux estimate of further quantities is the work of Spano et al. (2000a) who determined CO_2 fluxes from a coniferous forest canopy.

The above studies focus on the forest–atmosphere exchange at temperate and boreal vegetation. As stated by Kruijt et al. (2000), only a few studies investigated specifically the turbulence structure and transport mechanisms within tropical rain forests (Fitzjarrald et al., 1988; Fitzjarrald et al., 1990; Fitzjarrald and Moore, 1990; Kruijt et al., 2000; Pinker and Holland, 1988), although the area of tropical forests amount to about 52% of the world's total forest cover (FAO, 2001). The rain forest of the Amazon Basin alone contributes about 14% to this area and plays a considerable role in the global carbon cycle (Grace, 1995; Phillips, 1998) and tropospheric chemistry (Crutzen, 1995). The in-canopy transport is most relevant for the atmospheric input of soil-

emitted reactive constituents. A prominent example is the net emission of biogenic NO_x ($NO + NO_2$) from the ecosystem. Although Amazonian forest soils were found to be significant sources of NO (e.g., Bakwin et al., 1990; Gut et al., 2002a; Kaplan et al., 1988), chemical transformation to NO_2 and uptake by the vegetation or deposition back to the soil surface can considerably reduce the NO_x fraction actually released to the atmosphere (Gut et al., 2002b; Jacob and Wofsy, 1990; Jacob and Bakwin, 1992; Rummel et al., 2002b). A model study by Ganzeveld et al. (2002) on the role of canopy processes in global biogenic NO_x emissions has shown that, especially in pristine areas like the tropics, the exchange is most sensitive to these in-canopy processes.

Recently within the framework of the LBA program (Large-scale Biosphere–atmosphere experiment in Amazonia), a scale analysis of energy and CO_2 fluxes above the rainforest was made by von Randow et al. (2002).

The present study, part of the LBA-EUSTACH program (EUropean Studies on Trace gases and Atmospheric CHemistry as a contribution to LBA) (Andreae et al., 2002), addresses the coupling of the canopy space and the atmosphere above an Amazonian rainforest and the derivation of characteristic transport time scales within the canopy during daytime. On the basis of the time scales determined by wavelet analysis, fluxes of sensible heat, latent heat, CO_2, and O_3 were estimated by a surface renewal approach. Up to now this approach has not been used to determine the flux of a reactive constituent like O_3.

2 Methodical and Theoretical Framework

2.1 Surface Renewal Approach

Surface renewal models (Chen et al., 1997b; Katul et al., 1996; Paw U et al., 1995; Snyder et al., 1996) assume that the ramp patterns occurring in scalar time series, measured with sufficient temporal resolution, arise from an idealized air parcel motion which is illustrated in Fig. 1. An air parcel of volume V_0 is assumed to originate above the forest and to instantaneously penetrate the canopy. During a certain residence time the parcel stays in contact with leaves and other canopy elements, exchanging heat and mass. Small-scale diffusive exchange together with chemical production (or loss) for reactive species results in a gradual enrichment (e.g., for temperature with a warmer canopy) or gradual depletion (e.g., for deposited quantities like ozone) of a scalar X within the parcel, until the parcel leaves the canopy and is replaced (renewed) by another one from aloft. The measured time series of X shows a correspondingly slow, nearly constant, temporal increase or decrease dX/dt throughout the residence time, which is concluded by a step-like change back to the initial level when the parcel is exchanged by a coherent structure.

Assuming that (i) the canopy–atmosphere exchange of X occurs exclusively through

these instantaneous replacements and (ii) the loss/gain of X at the parcel top during the entire residence time is negligible, one can derive the surface flux density F_X. It is the mean storage change in the corresponding air volume associated with all coherent structures throughout the averaging period T_a.

$$\begin{aligned} F_x &= \frac{V_0}{A}\frac{1}{z_m}\int_0^{z_m}\left[\frac{dX(z)}{dt}\right]_{+/-} dz \\ &= \frac{V_0}{A}\left[\left\langle\frac{dX(z)}{dt}\right\rangle_z\right]_{+/-} \\ &\approx z_m\alpha\left[\frac{dX^S(z_m)}{dt}\right]_{+/-} \end{aligned} \quad (1)$$

$$\left[\frac{dX}{dt}\right]_{+/-} = \frac{1}{T_a}\int_0^{T_a}\frac{dX}{dt}\Lambda\left(\frac{dX}{dt}, F_x\right)dt \quad (2)$$

$$\Lambda\left(\frac{dX}{dt}, F_x\right) = \begin{cases} 1 & sign\left(\frac{dX}{dt}\right) = sign(F_x) \\ 0 & else \end{cases} \quad (3)$$

dX/dt is the temporal derivative of the measured scalar and $[\ ]_{+/-}$ is a conditional temporal average of dX/dt depending on the direction of the flux (see Section 2.2). V_0 and A are the air parcel volume and ground area. V_0/A can be approximated by the height of the correspondent air parcel. In the original work of Paw U et al. (1995) (see also Katul et al. (1996)), the canopy height h (equivalent to their measuring height z_m) was considered as the air parcel top, assuming the whole canopy depth to be involved in the renewal process (Fig. 1 (b)).

For a (approximately) horizontally uniform canopy, the average change of storage is described by the depth-averaged mean of dX/dt below the measuring height in Eq. (1). The depth average in Eq. (1) is indicated by $\langle\ \rangle_z$. With assumptions (i) and (ii) mentioned above, the weighting coefficient α accounts for the dX/dt profile due to the vertical distribution of sources and sinks within the considered air volume V_0 and relates therefore the average temporal change in X of the whole volume to the temporal change at the measuring height z_m. Paw U et al. (1995) proposed $\alpha = 0.5$ which approximates the real vertical gradient of dX/dt in the air volume by a linear increase of dX/dt with height from zero at the ground to a maximum dX/dt measured at $z_m = h$. Despite the differences in the vertical source/sink distribution of heat and water vapor in plant canopies, with this value of α good agreement with the corresponding eddy covariance fluxes was achieved for sensible and latent heat exchange at forest canopies (Katul et al., 1996; Paw U et al., 1995). Well above shorter canopies like grass or wheat, α was found to be close to unity for the sensible heat flux, most likely because the main part of the air parcel influenced by the mean temperature change remains above the canopy and is therefore relatively independent of the uneven source distribution within the canopy below (Anandakumar, 1999; Snyder et al., 1996; Spano et al., 1997a).

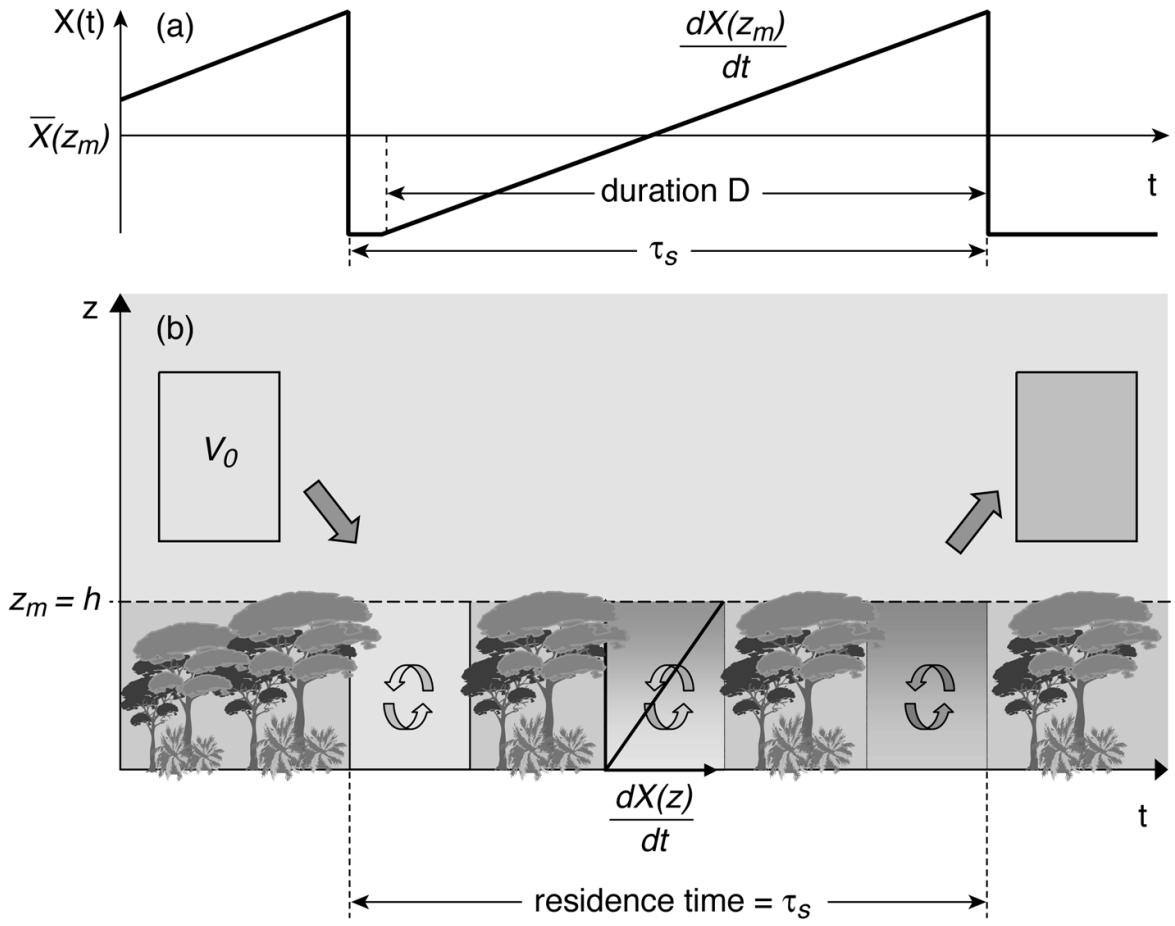

Fig. 1. Conceptual scheme of the air parcel motion on which the surface renewal approach is based *(Paw U et al., 1995)*. During the residence time τ_s, the volume V_0 is in contact with the canopy surface, and the scalar property X is exchanged. The mean duration D of the turbulent structures is directly related to the peak of the corresponding wavelet variance spectrum (scale a_0; for details see text). The exchange results in a gradual increase (here for an emitted scalar quantity) in the time series $X(t)$ measured at z_m until the parcel is replaced by another one. Small-scale turbulence and the source/sink distribution within V_0 control the vertical profile of the temporal change $dX(z)/dt$ (the profile suggested by Paw U et al. (1995) is indicated by the black curve in the middle volume).

Triggered by the fact that ramp patterns were frequently observed in scalar time series measured well above the forest top (Fig. 3; see also, e.g., Gao et al. (1989)), a slightly different conceptual picture is proposed in Fig. 2 for the forest–atmosphere exchange of scalars. It is a combination of the concepts for tall canopies by Paw U et al. (1995) and lower vegetation by Snyder et al. (1996) and Spano et al. (1997a). Due to the large canopy space of the rain forest, the average storage change of the volume V_0 must be clearly influenced by the vertical source/sink distributions of X within the forest. The fact, however, that pronounced ramp patterns occur at 1.33 h without clear amplitude reduction compared to

1.05 *h* (see Fig. 3) indicates that the top of the relevant air volume may be above the canopy height. Between the renewal events, the top of the air volume is characterized by negligible vertical exchange. But the temporal change of *X* (ramp slope) above the canopy must be a result of upward transport (if *X* is an emitted scalar), since no direct surface exchange is possible there. Therefore it seems very likely, as indicated in Fig. 2, that a considerable part of the air parcel that is enriched or depleted by surface exchange is sitting above the canopy. Fig. 2 also shows the supposed vertical profile of $dX(z)/dt$. It has a maximum in a broad band around the canopy top and declines towards the ground owing to decreasing surface exchange.

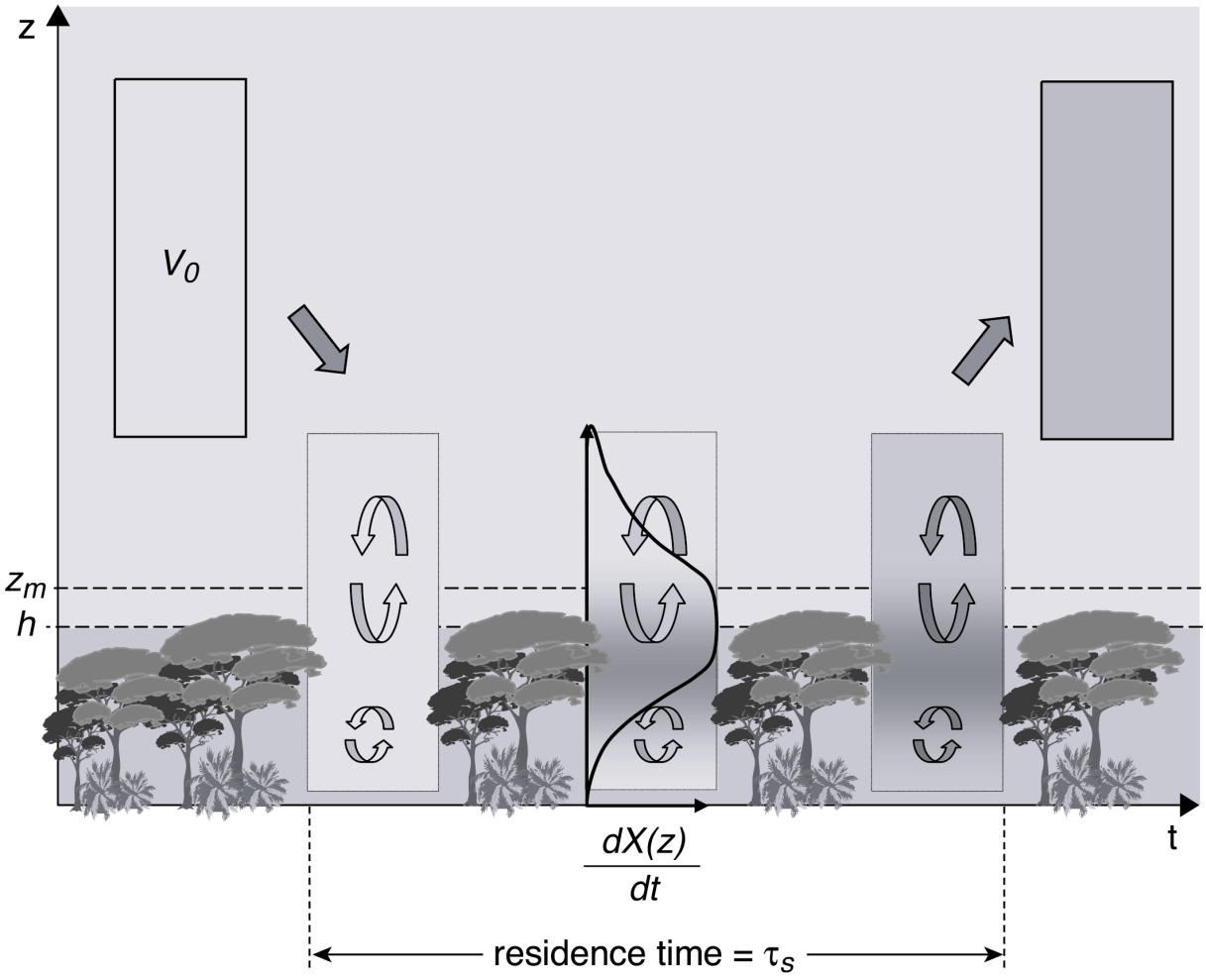

Fig. 2. Conceptual scheme as in Fig. 1 (b) with a modified vertical extent of the air parcel. In between consecutive renewal events, considerable small-scale exchange is assumed to occur at canopy height. This exchange is responsible for the pronounced ramp pattern registered above the canopy (the black curve in the middle volume indicates the corresponding profile of $dX(z)/dt$).

Towards larger heights above the canopy, $dX(z)/dt$ is also expected to decline because of decreasing internal transport and the consequently reduced ramp amplitude. The top of the air volume is characterized by a negligible ramp amplitude. Because the volume height is most likely variable and not detectable, it is only possible to use a local spatial scale like z_m and the corresponding $dX(z_m)/dt$ in the surface renewal approach. Here z_m marks not the top of the whole renewed air parcel but the top of the volume which is considered in the analysis. The weighting factor α is therefore not just accounting for the vertical distribution of $dX(z)/dt$ (for $z \leq z_m$) but also for the reduction or enhancement of the average storage change caused by the internal small-scale transport through the top of the considered volume at the measuring height z_m. For forest canopies such a local approach has only been applied by Chen et al. (1997b), throughout a Douglas-fir canopy for sensible heat, resulting in a height constant α of also about 0.5.

The application of Eq. (1) requires the temporal change $dX^S(z_m)/dt$ associated with the ramp slope in between consecutive renewal events. These events (expressed by the step-like change at the end of each single ramp) are separated by a characteristic time τ_s (Fig. 1 (a)). Although fluctuations of X arising from volume-internal small-scale transport make no contribution to the depth-averaged temporal change in Eq. (1), the measured temporal change $dX(z_m)/dt$ is influenced by them. It is therefore necessary to separate the contributions to the time series X associated with the ramp slopes from those associated with small-scale turbulence and instrumental noise. Due to the fact that these contributions occur mainly on different time scales (Paw U et al., 1995), filtering schemes can be employed for this separation. For a filtered scalar time series $X^f(t)$, the time derivative is $dX^f(z_m)/dt \approx dX^S(z_m)/dt$. In former studies several methods were used to achieve the separation. A Butterworth band-pass filter was used by Paw U et al. (1995) and in combination with an orthonormal wavelet thresholding scheme by Katul et al. (1996). Another method to extract the mean ramp characteristics from small-scale turbulence employs structure functions of the scalar time series (e.g., Snyder et al., 1996; Spano et al., 1997a; 2000b). All studies in which structure functions were applied for surface renewal analysis are on the basis of the results of van Atta (1977), except for Chen at al. (1997a; 1997b), who used a modified approach. In the present study a combined detection and filtering scheme on the basis of continuous wavelet transform was applied to extract the ramp pattern in the time series.

2.2 Structure Detection and Filtering Scheme

Beside their intermittent nature, coherent structures have a sharp localization in the time domain which is evident in the step-like changes in the scalar time series. Therefore wavelets as time-localized base functions are an appropriate tool to detect and extract the

'fingerprints' of coherent eddy motion in these time series. The wavelet transform in Eq. (4) is a convolution between the scalar time series $X(t)$ and a wavelet $g_{p,a,b}(t)$ for each scale a. It decomposes the signal $X(t)$ into a theoretically infinite series of dilated (scale a) and translated (time localization b) versions of a base or 'mother wavelet' $g_{p,1,0}(t)$ (see, e.g., Grossmann et al., 1989; Torrence and Compo, 1998). The resulting wavelet coefficients $T_p(a, b)$ contain the degree of similarity between $X(t)$ and $g_{p,a,b}(t)$ for each value of a and b. The power coefficient p just influences the amplitude of the wavelet.

$$T_p(a,b) = \int_{-\infty}^{\infty} X(t)\, g_{p,a,b}(t)\, dt \qquad (4)$$

$$g_{p,a,b}(t) = \frac{1}{a^p}\left[1 - \left(\frac{t-b}{a}\right)^2\right] e^{\frac{-\left(\frac{t-b}{a}\right)^2}{2}} \qquad (5)$$

For a detailed description of the mathematical requirements that have to be met by a wavelet function, in addition to its limited temporal extent, see, e.g., Young (1993). In the present paper the 'Mexican Hat' (MHAT) wavelet Eq. (5) was used for all calculations with p set to 1 following Collineau and Brunet (1993a). As a second derivative of a Gaussian function, the MHAT wavelet has some characteristics that are of great benefit for the purpose here.

The coefficients $T_p(a, b)$ of the axis-symmetric MHAT wavelet show zero-crossing (changing sign) at a time b_0 when a step-like change (jump) occurs in $X(t)$, avoiding the definition of an empirical threshold (necessary if point symmetric wavelets like the HAAR wavelet are used which peak at jumps in $X(t)$) (Collineau and Brunet, 1993a). The orientation of the zero-crossing depends on the jump direction in the time series. Because the extreme jumps in scalar time series are frequently connected to coherent structures, an objective method is offered to determine the time period τ_s separating the consecutive structures. The value $a_{0,}$ corresponding to the peak of the wavelet variance spectrum $W_p(a)$, is an appropriate scale to determine an optimum detection function from $T_p(a, b)$, which is neither picking up small-scale fluctuations of $X(t)$ nor missing a lot of real ramp structures (Collineau and Brunet, 1993a). $W_p(a)$ is defined as

$$W_p(a) = \frac{1}{T_a}\int_0^{T_a} \left|T_p(a,b)\right|^2 db \qquad (6)$$

the square modulus of the wavelet coefficients integrated over all translations b. Its maximum occurs at the scale where covariance between the wavelet and the dominating structures in $X(t)$ is the highest. It was found that a_0 (times a wavelet dependent form factor which is $\pi\sqrt{2}$ for MHAT) corresponds to the time duration D of dominant ramps in the analyzed time series (see, e.g., Collineau and Brunet, 1993b) (note that D here is the duration of the whole ramp and therefore 2 times the duration defined by Collineau et al. (1993b)). The mean duration D of the ramps within a measuring period is a fraction of the average separation time τ_s, due to quiescent periods embedded from time to

time in between consecutive events (Fig. 1 (a)).

Large-scale events penetrating the main part of the canopy are spatially coherent and therefore visible in the simultaneously acquired time series from different measuring levels throughout the forest (Gao et al., 1989; 1992). In order to reduce the number of erroneous detections caused by background turbulence, a two-level detection scheme was used, including data from the uppermost measuring height (1.33 h) and the stem space of the forest (0.28 h). This scheme to determine the time interval τ_s consists of the following steps. After calculating the wavelet transform of the scalar time series measured at $z_{m1} = 1.33\ h$ and $z_{m2} = 0.28\ h$, the wavelet variance spectrum at each height provides a scale $a_0(z_{mi})$ corresponding to its peak. With these values individual detection functions $T_p(a_0(z_{mi})\ ,\ b)$ can be determined. The mean time delay τ_{del} between the measurements caused by the vertical distance is considered by calculating the time shift of maximum lag cross-correlation $R^X{}_{z_{m1}z_{m2}}(\tau_{del})$ between z_{m1} and z_{m2}.

$$R^X{}_{z_{m1}z_{m2}}(\tau) = \frac{\overline{X'_{z_{m1}}(t)\ X'_{z_{m2}}(t+\tau)}}{\sqrt{\overline{X'_{z_{m1}}(t)^2}\ \overline{X'_{z_{m2}}(t)^2}}} \qquad (7)$$

A zero-crossing in $T_p(a_0(z_{mi})\ ,\ b)$ at 1.33 h was only accepted as valid if the detection function at 0.28 h also changed its sign within a tolerance time interval of ±10 s. The mean separation interval between coherent events τ_s is then the averaging time T_a (here 1800 s) divided by the number of detections.

Fig. 3 shows 10-min examples of temperature time series which were mainly used for the detection scheme together with the individual detection functions $T_p(a_0(z_{mi}),\ b)$. An additional measuring level at 1.05 h available at that time is also displayed. Please note that due to the mean thermal stratification, the heat flux was negative in the lower canopy so that inverted ramps are displayed in T' at 0.28 h. It is obvious that not all events that were detected at both upper heights, are reaching down to the level in the stem space of the canopy (e.g., at t ≈ 370 s). One can also see that at the expense of an excellent localization in the frequency domain, the time localization of MHAT shows a higher uncertainty than point symmetrical wavelets do. Owing to the uncertainty principle, an arbitrarily high precision in both domains cannot be achieved (see Kumar and Foufoula-Georgiou, 1994). However it was shown by Collineau and Brunet (1993a; 1993b) that despite the higher uncertainty, good agreement was achieved between τ_s values obtained with MHAT and point symmetric wavelets.

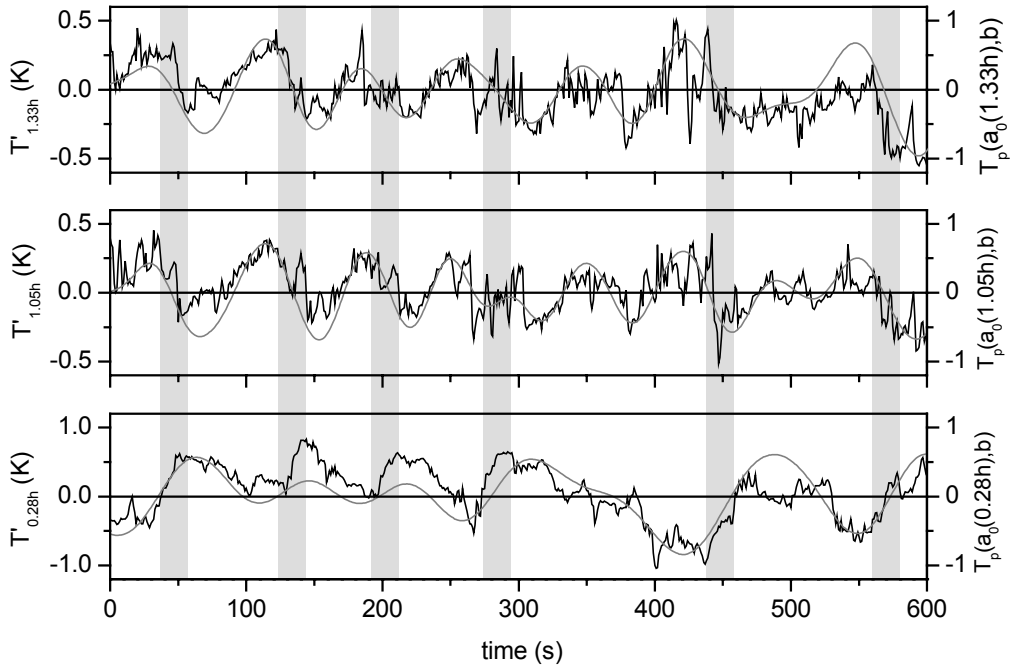

Fig. 3. Temperature time series measured simultaneously at three heights (black curves). The gray curves are the corresponding wavelet transforms $T_p(a_0(z_{mi}), b)$ at the peak scales a_0 of the wavelet variance spectra $W_p(a)$. The wavelet transforms $T_p(a_0(z_{mi}), b)$ are displayed in normalized form. The vertical gray shaded rectangles mark the tolerance windows of the two-level detection scheme for structures simultaneously detected at 1.33 h and 0.28 h (details in the text).

Its good frequency localization makes the MHAT wavelet an appropriate choice to extract the ramp information from the measured scalar time series. At each layer included in the jump detection procedure, the ratio between the mean structure duration D and the time separation interval τ_s between the structures was found to be around 0.94. Similar fractions (keeping in mind the factor 2 by definition of D, as mentioned above) were found by Collineau and Brunet (1993b) and Lu and Fitzjarrald (1994) applying several different wavelets. $D \approx \tau_s$ was used to derive a corresponding wavelet scale a_f (or duration D_f) for the separation interval τ_s obtained from the two-level detection. The scale $a_f \approx \tau_s \left(\pi\sqrt{2}\right)^{-1}$ is then assumed to be characteristic for the structures penetrating deep into the canopy. In the scale domain the wavelet transform of the scalar time series is weighted (Eq. (8)) with a one-decade wide rectangular filter window (Eq. (9)) centered around a_f with $a_f = \sqrt{a_S a_L}$ (comparable to the Butterworth filter width applied by Paw U et al. (1995)). The wavelet coefficients $T_p(a,b)$ are set to zero for scales $a < a_S$ and $a > a_L$ before the inverse wavelet transform (Eq. (10)) is applied on $T_p^f(a,b)$.

$$T_p{}^f(a,b) = T_p(a,b)\,\delta(a_S, a_L) \tag{8}$$

$$\delta(a_S, a_L) = \begin{cases} 1 & a_S < a < a_L \\ 0 & else \end{cases} \tag{9}$$

$$X^f(t) = \frac{1}{C_g}\int_{-\infty}^{\infty}\int_{0}^{\infty} T_p{}^f(a,b)\, g_{p,a,b}(t)\,\frac{da\,db}{a^{3-2p}}$$
$$C_g = 2\pi\int_{-\infty}^{\infty}\frac{\left|\hat{g}_{p,1,0}(\omega)\right|^2}{\omega}\,d\omega \tag{10}$$

An example of the filter procedure can be seen in Fig. 4 (c). Displayed are a 1-s block-averaged ozone time series before ($X(t)$) and after ($X^f(t)$) the application of the filter. It can be seen that high-frequency noise and fluctuations are removed by the scheme. Fig. 4 (a) and (b) show the corresponding wavelet variance spectrum $W_p(a)$ (with the filter window) and the wavelet transform $T_p(a,b)$, respectively.

In order to make the obtained filter principally transferable to other time periods (e.g., when only one measuring height is available) or to make the results comparable for other canopies, a functional relation to environmental parameters is necessary. The frequency of coherent structures occurrence $1/\tau_s$ at the vegetation–atmosphere interface was found to scale with horizontal wind shear at $z = h$ (Paw U et al., 1992; Raupach et al., 1989). Raupach et al. (1989; 1996) proposed a plane mixing-layer analogy to describe canopy turbulence characteristics like the development of coherent eddies. A necessary condition for the occurrence of hydrodynamic instabilities (the origin of coherent structure development) is an inflection in the vertical wind profile of the mean velocity. The spatial separation of the structures in flow direction was found to be a function of a canopy related shear length scale (see also Brunet and Irvine, 2000; Katul et al., 1998).

Owing to the lack of a continuously measured horizontal wind velocity at the canopy height, a suggestion of Chen et al. (1997b) was taken up, that u_*/h can be used analogously to a mean wind shear measure like $\overline{u}(h)/h$. The separation time interval τ_s between coherent structures is assumed to scale with h/u_*:

$$\tau_s = \begin{cases} m\dfrac{h}{u_*} & u_* \geq u_{*L} \\ m\dfrac{h}{u_{*L}} & u_* < u_{*L} \end{cases} \tag{11}$$

Here m is an empirical coefficient. For friction velocities below u_{*L} = 0.1 m s^{-1}, a constant value for τ_s was assumed due to the pole at u_* = 0 m s^{-1}. This parameterization was used in the filtering scheme and applied on 1-s block-averaged scalar time series. The value of $\left[dX^S(z_m)/dt\right]_{+/-}$ in Eq. (1) was then calculated by averaging solely the instantaneous positive or negative temporal changes in $X^f(t)$ depending on the flux direction determined by third-order structure functions (Chen et al., 1997a).

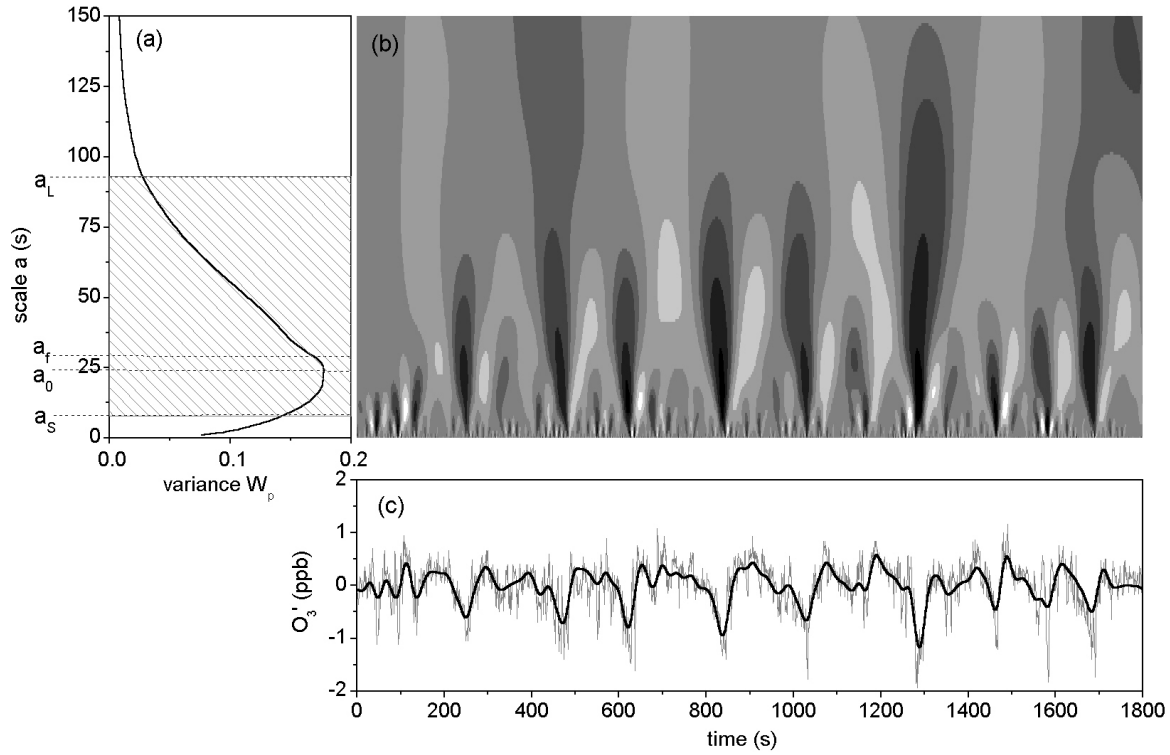

Fig. 4. Wavelet transform $T_p(a,b)$ (b) of an ozone time series ((c); gray curve). The white areas display scales of high correlation. Integrating $T_p(a,b)$ over time results in the variance spectrum W_p (a) which shows a distinct maximum at scale a_0. The gray-shaded area in (a) marks the width (between a_S and a_L) and af the center of the applied scale filter. The filter procedure results here in the time series (black curve (c)), which is used in the surface renewal approach.

3 Experiment

3.1 Site and Experimental Period

The measurements were carried out during the LBA-EUSTACH-1 campaign in the wet-to-dry season transition period from April to May 1999. The analysis focuses on four days between 18 and 22 May at the end of the experiment. The experimental site (10°04´55´´ S, 61°55´48´´ W, 147 m a.s.l.), a former ABRACOS site (Gash et al., 1996) is located in the Reserva Biológica Jarú (RBJ), a forest reserve 90 km north of the city Ji-Paraná in the state of Rondônia (southwest Amazonia), Brazil. The vegetation cover of RBJ, owned by the Brazilian Environmental Protection Agency IBAMA (Instituto Brasileiro de Meio Ambiente e Recursos Renováveis) is a primary (terra firme) open rain forest with a closed canopy of about 32 m height (h_c). Single jutting trees reach heights up to 45 m. Due to their relevance for turbulence, an effective canopy layer height of 40 m (h) was defined for the analysis following Kruijt et al. (1996). The understory consists mainly of palms. The vertical LAI (leaf area

index) distribution is shown in Fig. 6. The total LAI was measured (LI-COR LAI 2000, USA) to be about 5.6. The horizontal extent of the forest is partly limited. Within the west-northwest to southeast sector primary rain forest exists for several tens of km. In the remaining sector a river (Rio Machado) interrupts the vegetation. The minimum distance to the river (in the southwest direction) is about 400 m. Further information about the site and the campaign is given by Andreae et al. (2002).

3.2 Instrumental Setup

An aluminum scaffolding tower of 52 m height erected in 1991 (Gash et al., 1996) was the main platform for the measurements conducted at the RBJ site.

3.2.1 Turbulence and Fast Trace Gas Measurements

Fluctuations of the three wind velocity components (u, v, w) and virtual temperature (T_v) were continuously measured at heights of 53 m (= 1.33 h) and 11 m (= 0.28 h) by sonic anemometers (Gill Instruments, Solent Research 1012 K55, UK) mounted on booms extending 4 m horizontally. During the four-day period investigated here, the measurements at these two heights were complemented using a third sonic anemometer (Gill Instruments, Research HS, UK), which was alternately employed at 42 m (= 1.05 h) and 31 m (= 0.78 h) for a period of about 24 h each.

High-frequency measurements of H_2O, CO_2, and O_3 mixing ratios were continuously performed at the uppermost level at 1.33 h and another fast O_3 system was located at 0.28 h. For the H_2O and CO_2 measurements, a closed-path differential infrared absorption analyzer (LI-COR LI-6262, USA) with a nominal response time of 0.1 s was used (e.g., Ammann, 1999; Aubinet et al., 2000; Moncrieff et al., 1997). The inlet of the air sampling system, consisting of a small funnel to keep out liquid water, was attached to the horizontal boom 20 cm from the head of the sonic anemometer. A 6.4 mm TEFLON® tube (inner diameter: 4.35 mm) of 8 m length connected the inlet through a 1 µm pore size filter (Gelman Acro 50) to the LI-6262 located in a ventilated housing 2 m below. A constant flow rate of about 7 L min^{-1} (turbulent flow) was provided by a combination of a mass flow meter (MKS 358C, Germany) and a rotation pump (Brey G12/07-N, Germany) downstream of the analyzer. The resulting lower pressure in the measuring cell of the analyzer was recorded by a piezoresistive pressure transducer (Data Instruments XT, USA) and considered for the calculation of CO_2 and H_2O mixing ratios together with the internal LI-6262 cell temperature. The analyzer was operated in the absolute mode with the reference cell connected to a closed air circuit containing a scrubber column (soda lime + $Mg(ClO_4)_2$).

The analytical basis of the fast O_3 analyzers is a surface chemiluminescence reaction of O_3 with a marin dye layer on aluminum plates in

the sample air stream. One of the analyzers is custom built (IMK Karlsruhe, Germany) and the other one is a commercial reproduction of it (GFAS, Germany). The analyzing principle is described by Güsten et al. (1992), Güsten and Heinrich (1996) and Ammann (1999). Both sensors were directly attached under the booms of the sonic anemometers. The sampling air was led to the O_3 analyzers by tubes of 0.5 m length and an inner diameter of 0.02 m. To prevent flow distortion by the tubes, the inlets were separated by 0.30 m from the heads of the sonic anemometers. Turbulent flow in the tubing was ensured by micro fans of the O_3 analyzers, maintaining flow rates of ~100 L min^{-1}. Response times of the O_3 analyzers are well below 0.1 s (Ammann, 1999). The instrumental sensitivity of the chemiluminescence analyzers was relative low from time to time, most likely caused by the extremely humid tropical environment. The effect of low sensitivity will be discussed in Section 4.3.1.

All high-frequency data were sampled at 20.8 Hz. The trace gas signals were fed into the built-in analogue-to-digital converter of the sonic anemometer. The data were transferred via serial interfaces to laptop computers in an air-conditioned shelter at the tower base.

For calibration purposes, the fast H_2O, CO_2, and O_3 measurements were referenced to their corresponding mixing ratios measured by the profile system at the same height.

3.2.2 Profile Measurements

Vertical profiles of H_2O, CO_2, O_3, NO, and NO_2 mixing ratios were measured above and throughout the canopy. The air sampling system consisted of eight 6.4 mm TEFLON® tubes connecting the inlets at 0.3 m, 1.0 m, 4.0 m, 11.3 m, 20.5 m, 31.3 m, 42.2 m, and 51.7 m to the analyzers in the shelter at the tower base. The individual tubes were bundled up in two opaque insulated main pipes, which were heated just above environmental air temperature to prevent condensation in the tubing system. All inlets at heights up to 4 m above ground were attached to a separate tripod located 15 m northeast of the tower, where the surrounding area was closed off to minimize soil disturbance. All tubes were continuously flushed through a purging pump and air from all heights was sequentially sampled by a TEFLON®valve manifold. Past the manifold, the inlets to each trace gas analyzer were branched off from the main sampling stream. H_2O and CO_2 were sampled by a second LI-6262 analyzer, which was regularly calibrated by a dew point generator (LI-COR LI-610, USA) and gas standard cylinders in the case of CO_2. O_3 mixing ratios were measured with a UV absorption analyzer (Thermo Instruments TE49C, USA). For NO and NO_2 a gas phase chemiluminescence analyzer (ECO Physics CLD 780 TR, Switzerland) combined with a photolytic converter (ECO Physics PLC 760, Switzerland) was employed (see Rummel et al., 2002b). A gas-phase titration unit, which

contains a UV lamp as O_3 source (ANSYCO SYCOS K/GPT, Germany) was used together with zero air and NO cylinder standards for combined O_3, NO, and NO_2 calibrations.

Two complete cycles of sequentially sampled profile data were averaged to obtain corresponding half-hour data sets of vertically resolved H_2O, CO_2, O_3, NO, and NO_2 mixing ratios. Within one cycle, the dwell time at each height was 1.5 min with 30 s rejected because of adaptation processes. Due to different tubing length the delay times within the sample lines varied from ~1 s up to ~8 s from the lowest to the highest level. Mixing ratios of O_3, NO, and NO_2 were corrected for the gas-phase reaction $NO + O_3 \rightarrow NO_2 + O_2$ occurring within the tubes, depending on the corresponding delay time (Beier and Schneewind, 1991). For data recording and controlling of the trace gas profile system, a laptop computer, equipped with a data acquisition device (National Instruments DAQPad-1200, USA) was used.

Air temperature profiles were determined by fine wire thermocouples (Omega, USA) recorded by a data logger / multiplexer system (Campbell 21X and AM25T, USA).

3.3 Eddy Covariance Data Processing

After an intensive spike and error control of the raw data, half-hour averages of heat and trace gas fluxes were calculated. Time lags between the signals from sonic anemometers and trace gas analyzers were estimated by determining the maxima of the covariance functions within preset time lag intervals. A linear detrending was applied to the time series. A two-axis rotation was applied on the wind field coordinates such that the average values of lateral and vertical wind speed equaled zero (e.g., Aubinet et al., 2000). The correction according to Webb et al. (1980) was applied to account for trace gas flux contributions caused by air density fluctuations from sensible and latent heat exchange. Because temperature fluctuations are damped out within the long inlet tubing of the LI-6262 (Leuning and Judd, 1996; Wienhold et al., 1994), only the humidity correction was necessary for CO_2. The short inlet system of the O_3 analyzers is just damping a certain fraction of the temperature fluctuations (Ammann, 1999), so that a corresponding correction is necessary. High-frequency flux loss caused by physical properties of sensors, setup, and data acquisition where corrected according to Moore (1986), Zeller et al. (1989), Lenschow and Raupach (1991), and Horst (2000), using the semiempirical spectral formulations of Kaimal et al. (1972). The linear detrending was used to keep the related flux loss at low frequencies limited. This loss, estimated with a transfer function after Kristensen (1998) (see Aubinet et al., 2000), was about 6% during daytime. But the model spectra for typical unstable daytime situations are, in contrast to the high-frequency end, rather poorly determined at the low-frequency end. Therefore the calculated fluxes were not corrected for that effect.

The presented analysis focuses on daytime situations. To avoid the influence of rapidly changing environmental conditions on the analysis, a stationarity test slightly modified from Foken and Wichura (1996) was applied to all derived variances and covariances. Data were rejected if the (co)variance averaged over 30 minutes deviated more than 50% from the average of the fluxes obtained from 10-min subintervals (instead of 5-min subintervals proposed by Foken and Wichura (1996)). The unstable stratification within the tropical boundary layer and the occurrence of large coherent structures are taken into account by the longer subintervals. The obtained rejection rate was 6% of the dataset for daytime conditions.

4 Results and Discussion

4.1 Source Area Estimate

Because during the investigation period southerly winds were prevailing where the river was limiting the fetch of the site, a source area analysis for the flux measurements at RBJ was indispensable. For this purpose the scalar Flux-Source Area Model (FSAM) after Schmid (1994; 1997) was used. This model determines numerically the upwind source area of a percentage P defined as the smallest possible area responsible for the contribution P to the flux measured by the sensors (projected area of the fraction P of the total integrated source weight function). Like many Eulerian approaches, this model is also based on atmospheric surface layer similarity assumptions (K-theory) and is therefore not intended for application in the roughness sublayer of forest canopies. Rannik et al. (2000) determined footprint (source weight) functions above a forest canopy with a Lagrangian stochastic model driven by parameterizations for turbulent flow within and above the canopy. According to their results for neutral stratification, the use of canopy turbulence parameterization and a leaf area weighted vertical source/sink distribution smears out the footprint function compared to surface layer flow above a source/sink level at displacement height. The effect decreases with increasing measuring height. Unfortunately no equivalent comparison was made for unstable stratification, the prevailing daytime condition above the tropical forest. In a recent study (Rannik et al., 2003) the effect of stability on footprint functions was only discussed for a substance released from the forest ground

In contrast to these results, a comparison by Kaharabata et al. (1997) showed approximate agreement between the obtained source area dimensions after Schmid (1994) and the corresponding results from a modified surface layer approach according to Horst and Weil (1992). The approach of Horst and Weil (1992) was adjusted to tracer experiments conducted in the roughness sublayer of three boreal forests. Compared to this approach, the formulation according to Schmid (1994) seems to be a rather conservative one, which especially under unstable conditions tends to overestimate the source area dimensions.

Considering the uncertainty of such tracer experiments and the results of the comparison by Rannik et al. (2000), the FSAM estimates might represent lower limits of the actual source area dimensions.

Bearing this in mind, the FSAM model was used to calculate the 80% flux source areas for daytime conditions (0900 LT – 1600 LT). The two-dimensional frequency distribution in Fig. 5 shows how often each point in the tower surrounding terrain contributed to the corresponding 80% source areas of any flux measured on the RBJ tower at 53 m within these time intervals. During daytime, the unstable stratification ensured rather small source areas. Therefore, despite the unfortunate wind direction, about 95% of the investigated daytime cases seemed to be not or barely influenced by the river. On the other hand, during the stably stratified periods and during nighttime hours (not shown), the 80% flux source area frequently included parts of the river. In spite of this fact, no systematic influence on the measured fluxes was noticed. This is most likely related to the relatively small magnitude of the fluxes and a higher relative uncertainty within calm and stable stratified nighttime and transition periods.

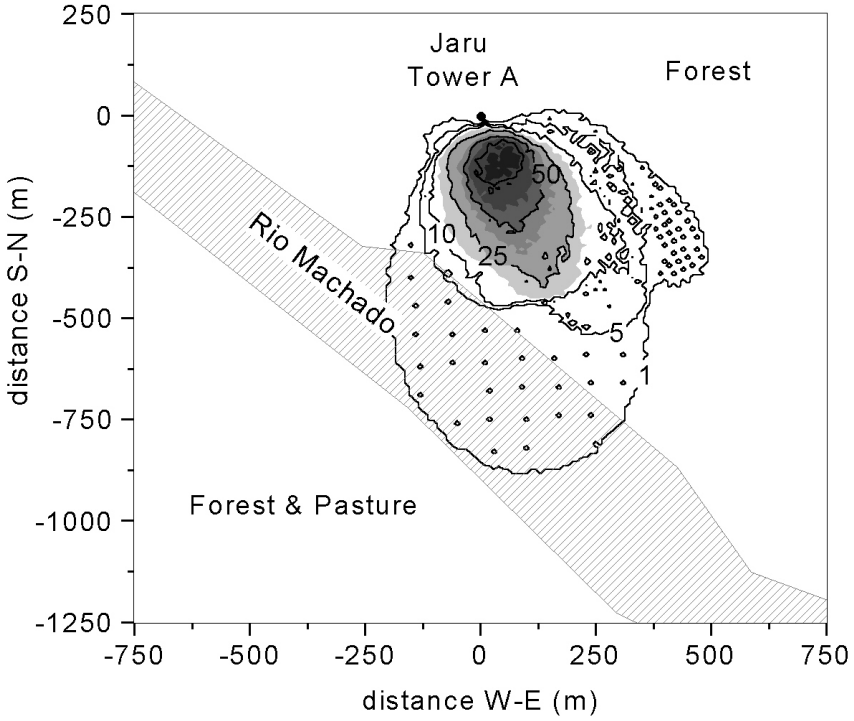

Fig. 5. Two-dimensional frequency distribution in percent which shows how often each point in the terrain surrounding the tower has contributed to the 80%-flux source areas of any flux measured on the RBJ tower at 53 m between 0900 LT and 1600 LT. The river (Rio Machado) coordinates are from a Landsat TM image from August 1999 [G. A. Kirkman, personal communication].

4.2 Vertical Mixing Ratio Profiles

The profiles of potential temperature in Fig. 6 indicate totally different turbulent regimes during night and day. At night a slightly unstable stratification can be observed in the stem space up to 20 m, because radiative cooling is largest in the crown layer. This thermal situation drives a nocturnal convection within the canopy, a well-known effect in tall vegetation (e.g., Baumgartner, 1956), which is clearly developed in the huge stem space of a tropical forest (Kruijt et al., 2000; Rummel et al., 2002b). The internal air motion causes almost vertically constant mixing ratios of H_2O and CO_2 in stem space (Fig. 6). Nocturnal O_3 mixing ratios were close to the detection limit (0.5 ppb) of the analyzer because within the fairly isolated stem space, O_3 is almost totally titrated by soil-emitted NO.

During day at 1300 LT the stratification of the upper canopy and the roughness sublayer above is unstable, whereas the lower canopy is stably stratified. The difference in the O_3 mixing ratios at 51.7 m and 11.2 m was typically small, only 2 ppb in the example shown . The H_2O profile presents a similar picture but mirror-imaged. CO_2 mixing ratios are relatively constant down to 4 m, at about 360 ppm. These small vertical trace gas gradients are indicative of effective turbulent transport mechanisms such as coherent structures that couple the main part of the forest layer with the atmosphere above. In the lower canopy towards the forest floor, increasing vertical trace gas mixing ratio gradients are caused by a combination of different processes.

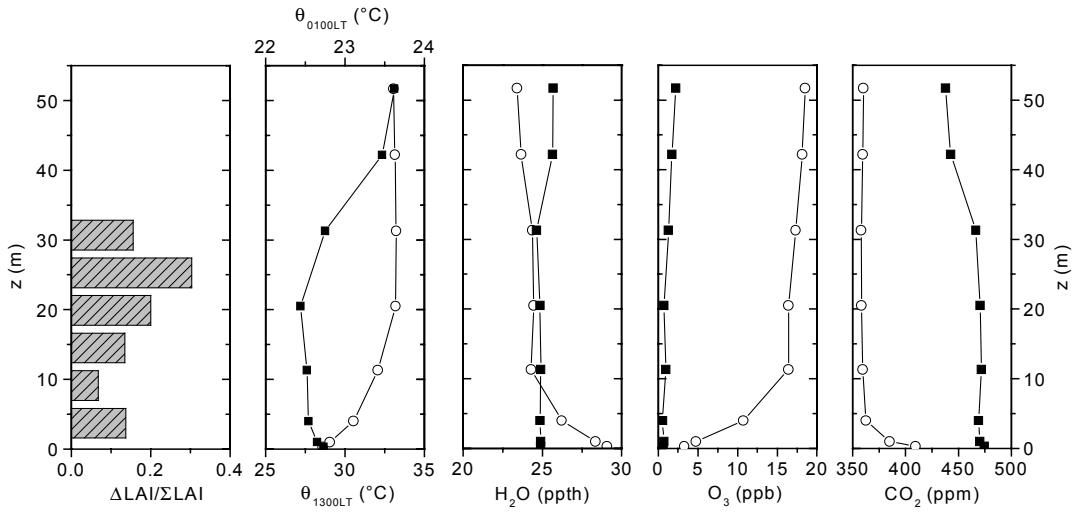

Fig. 6. Vertical distribution of the one-sided leaf area index (LAI) and profiles of potential temperature θ and the mixing ratios of H_2O, O_3, and CO_2 at 0100 LT (full squares) and 1300 LT (open circles) on 21 May 1999.

For O_3, beside vegetation uptake, the reaction with soil-emitted NO without compensation from photolysis is reducing the mixing ratio near the ground. Higher CO_2 values are caused by soil respiration. But a strongly reduced turbulent transport in the lowest layer (see Section 4.4.2) is the most likely cause for the steeper gradients near the ground as compared to the higher canopy layers.

4.3 Application of the Surface Renewal Approach

Before the obtained fluxes will be discussed, an estimation of the influence of instrumental noise on the fluxes and the determination of the coefficient m in the parameterization of τ_s (Eq. (11)) is presented in the following paragraphs.

4.3.1 The Effect of Instrumental Noise on Surface Renewal Flux Estimates

Atmospheric flux measurements are always affected by instrumental noise. Measurements of trace gas fluxes by eddy covariance are usually more influenced by the noise level of the gas sensor than by the noise of the corresponding sonic anemometer. Due to the fact that instrumental noise is usually characterized as " ideal white noise" that does not correlate with the vertical velocity fluctuations, it has no systematic effect on the trace gas flux. But the associated statistical error directly affects the magnitude of the minimal resolvable flux. According to an estimation of Lenschow and Kristensen (1985), an effective flux detection limit of ~0.45 nmol m^{-2} s^{-1} was obtained for O_3, considering the worst case sensitivity mentioned above. The corresponding limits for latent heat and CO_2 fluxes were 0.2 W m^{-2} and 0.18 μmol m^{-2} s^{-1}, respectively.

It is expected that flux determination by the surface renewal approach is not affected systematically by instrumental noise, because application of a band-pass scale filter should exclude high-frequency fluctuations. But the decreasing sensitivity of the fast ozone sensor, raising the noise-to-signal ratio from time to time, was reason enough to test the influence of instrumental noise on flux estimates using a simulation. For this purpose an artificial scalar time series showing regular ramp structures was generated. The separation interval τ_s of consecutive ramps was calculated according to Eq. (11) with varying values of u_* and with $m = 1.62$ as determined below. Random noise with a gradually increasing standard deviation σ_n was superimposed on the generated time series. For each combination of $\tau_s(u_*)$ and σ_n, the flux F_x^{noise} was determined by application of Eq. (1) with the temporal derivative of the filtered time series dX^f/dt, as an average of 25 realizations. Equivalently, as a measure of noise amplitude, the average ratio $W_p(a_n)/W_p(a_o)$ was calculated. These are the values of the wavelet variance spectrum corresponding to the superimposed noise (smallest scale a_n) and the ramp structures (a_0).

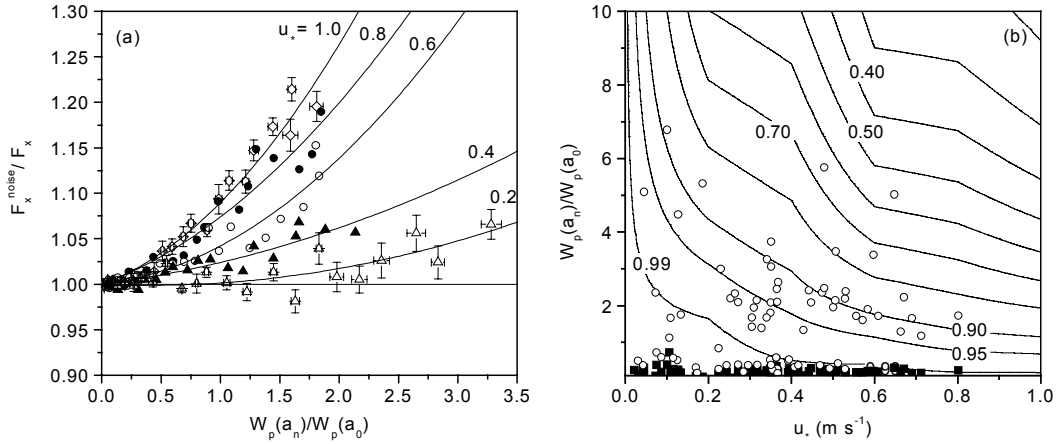

Fig. 7. (a) Simulated flux overestimation F_x^{noise} / F_x (symbols) as a function of $W_p(a_n) / W_p(a_o)$ for different values of u_*. Error bars show standard errors of the ensemble average (details in the text). The solid lines show second-order polynomials fitted for each u_* step. (b) Interpolated correction matrix F_x / F_x^{noise} (u_*, $W_p(a_n) / W_p(a_o)$) represented by the isolines. Open circles and full squares show the corresponding localization of measured half-hour values for ozone and water vapor respectively.

Fig. 7 (a) shows the ratio of F_x^{noise} and F_x (the calculated flux without noise contamination) as a function of $W_p(a_n)/W_p(a_o)$ for different values of u_*. A clear and systematic behavior can be seen. With increasing noise-to-signal ratio and with increasing u_* (shorter duration of ramp structures), dX^f/dt and therefore the resulting flux is more and more overestimated. For each friction velocity value (0.1m s^{-1} steps), the flux overestimation was approximated by second-order polynomial functions forced through $F_x^{noise}/F_x = 1$ at $W_p(a_n)/W_p(a_o) = 0$ (also displayed in Fig. 7 (a)). With linear interpolation between these polynomials, a correction matrix F_x/F_x^{noise} (u_*, $W_p(a_n)/W_p(a_o)$) was calculated which is shown in Fig. 7 (b).

The effect on the surface renewal flux estimates of each half-hour time interval was then estimated using the average values of u_* and the $W_p(a_n)/W_p(a_o)$ ratio. As shown in Fig. 7 (b), an effect is visible for ozone. Except for a few outliers just before the dye-coated plate of the analyzer was replaced, the flux overestimation due to low analyzer sensitivity was below 15%. This overestimation was corrected in the calculation of the ozone flux. For the fast water vapor measurements with higher signal-to-noise ratio, also representative for T and CO_2, the effect was mainly below 1% and therefore neglected (Fig. 7 (b)).

4.3.2 Parameterization of the time interval τ_s

The time interval τ_s separating consecutive ramp events was determined by two-level detection during daytime hours (0700 LT to 1700 LT) as described in Section 2.2. Fig. 8

shows τ_s as function of the time scale h/u_*. Assuming the functional relation in Eq. (11) between the time scales, the coefficient m was determined by linear regression forced through the origin. The narrow data range and considerable scatter provide a rather poor determination of m with $R^2 = 0.28$. Owing to this low R^2 value, it is necessary to consider the influence of this uncertainty on the fluxes obtained by the surface renewal model. For this, the scale filter was also calculated for the confidence interval (0.95) limits of m. The value obtained for the slope is $m = 1.62 \pm 0.24$. Two other studies over forest canopies have related the separation interval τ_s (or the reciprocal frequency of occurrence) of temperature ramp structures to a scale employing u_* instead of $\overline{u}(h)$. Despite the totally different canopy architectures and environmental conditions, the derived coefficients m are of a similar magnitude, suggesting that similar mechanisms cause the ramp structures in scalar time series. Collineau and Brunet (1993b) got $m = 1.8$ at a pine forest site with 13.5 m canopy height and a LAI of 2.8. Over a 16.7 m high Douglas-fir forest with a LAI of 5.4, Chen at al. (1997b) derived a value of 1.41 for m. Both results are within the confidence interval for the slope in Fig. 8.

Due to the pole of mh/u_* for $u_* \rightarrow 0$, the time interval τ_s was set constant in Eq. (11) for friction velocities smaller than 0.1 m s^{-1}. This is no limitation because, for h/u_{*L}, structures with separation times τ_s up to the average interval T_a of half an hour are already included by the filter.

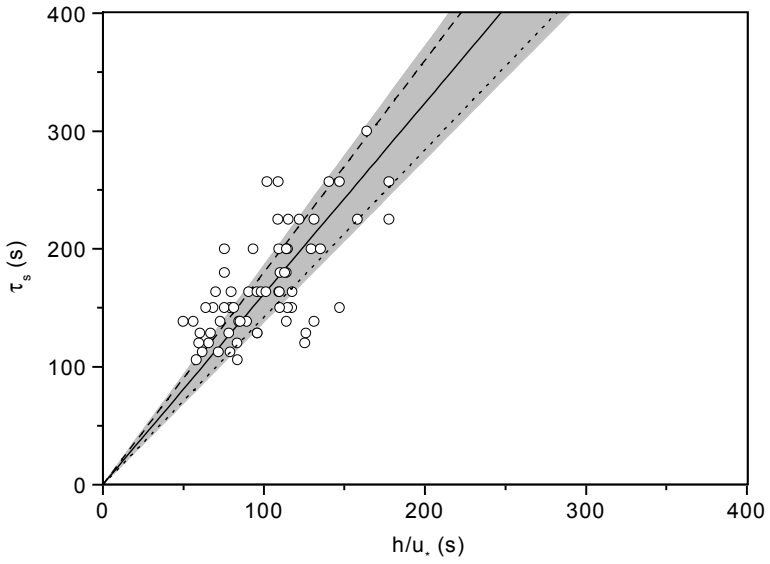

Fig. 8. Linear regression between the time scales h/u_* and τ_s (Eq. (11)) in the RBJ rain forest. The regression curve (solid line) was forced through zero. The gray-shaded area displays the 0.95 confidence interval of the regression model. In addition relations after Collineau and Brunet (1993b) (dashed line; pine forest) and Chen et al. (1997b) (dotted line; Douglas-fir forest) are shown.

During daytime hours (0700 LT to 1700 LT), for which Eq. (11) was derived, u_* was above this lower limit (u_{*L}) in 95% of the half-hour intervals. On calm nights, which were predominating in the investigation period, the vertical turbulent transport at the canopy top is restricted or breaks down (for $u_* < 0.05$), due to large thermodynamic stability. On the other hand, transport-relevant events at night are assumed to increase the friction velocity above the threshold and shift the filter window towards shorter time scales. Examples for such intermittently occurring nighttime situations with intensify turbulence above an Amazonian rainforest were investigated by Fitzjarrald and Moore (1990).

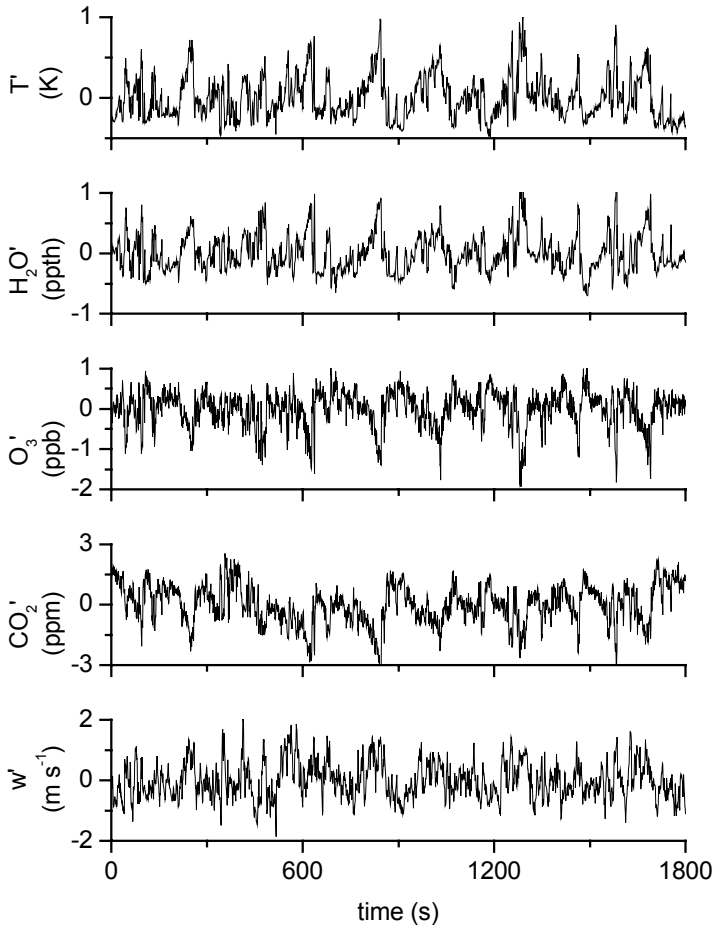

Fig. 9. Half-hour time series of different scalars and vertical wind velocity measured at 1130 LT on 21 May 1999 above the canopy at 1.3 *h* (Rummel et al., 2002a).

4.3.3 Comparison with Scalar Fluxes Measured by Eddy Covariance

An example of half-hour scalar fluctuation time series measured at 1.33 *h* is shown in Fig. 9. A distinct ramp pattern is visible in the traces of all measured scalars. The ramp orientation depends on the direction of the corresponding scalar flux. The time series of the vertical wind velocity fluctuations w' also shows the pattern, although with a less pronounced ramp shape. The high degree of similarity between the measured scalars is typical for daytime situations like here at 1130 LT. Correlation coefficients between the 1-s block-averaged time series of the different scalars were frequently in the range from 0.8 to 0.95 at this time of day (between 0.5 and 0.8 for O_3 during the periods of lower analyzer sensitivity).

The procedure described in Sections 2.1 and 2.2 was identically applied on all measured scalars to estimate their above-canopy fluxes. The average value of $\left[dX^S(z_m)/dt\right]_{+/-}$ in Eq. (1) was determined for each filtered half-hour time series and multiplied by the measuring height z_m, assuming the entire volume to be included in the exchange process. The weighting coefficient α was then obtained from linear regression of the results from the surface renewal method against the fluxes measured by eddy covariance as reference. The slope of the regression line (forced through the origin) corresponds to $1/\alpha$. The results for sensible and latent heat flux can be seen in Fig. 10.

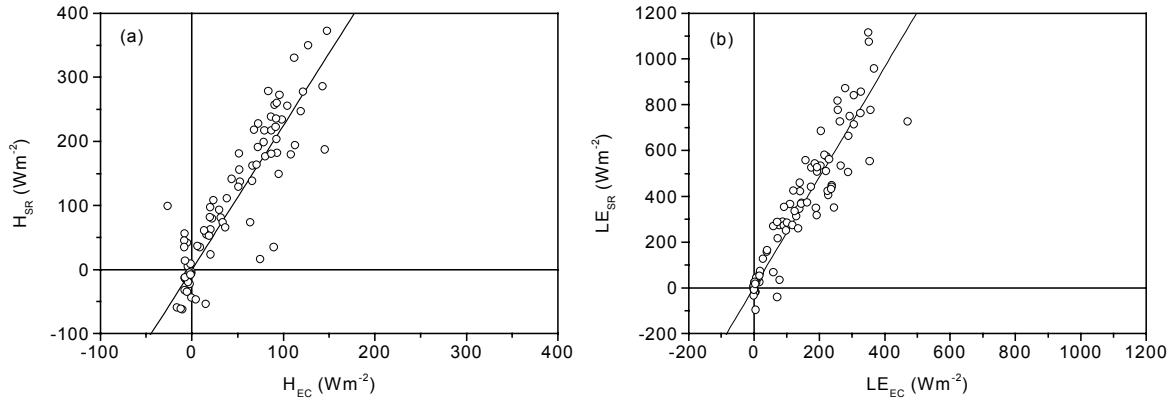

Fig. 10. Daytime sensible heat (a) and latent heat (b) flux at 1.33 *h* determined by the surface renewal (subscript SR) approach (with α =1 in Eq. (1)) versus correspondent fluxes measured by eddy covariance (subscript EC). For details of the linear regression (solid line), see Table 1.

Fig. 11 shows the comparison for O_3 and CO_2 fluxes. Regression statistics are summarized in Table 1. For the heat fluxes and the flux of ozone, high coefficients of determination R^2 between 0.80 and 0.85 were achieved by the linear regression model. With $R^2 = 0.54$, the determination for CO_2 is somewhat lower. Standard errors of estimate (SEE) relative to the corresponding flux range are below 16% for all scalar quantities. The nonstationary transition from respiration to uptake of CO_2 due to the beginning of photosynthesis in early morning hours was excluded from the regression analysis.

Fig. 12 displays time series of half-hour O_3 and CO_2 fluxes derived by the surface renewal approach (already weighted by the obtained α values) and determined by eddy covariance. Due to the high R^2 values of the linear regression, the daytime course of the fluxes is well-described.

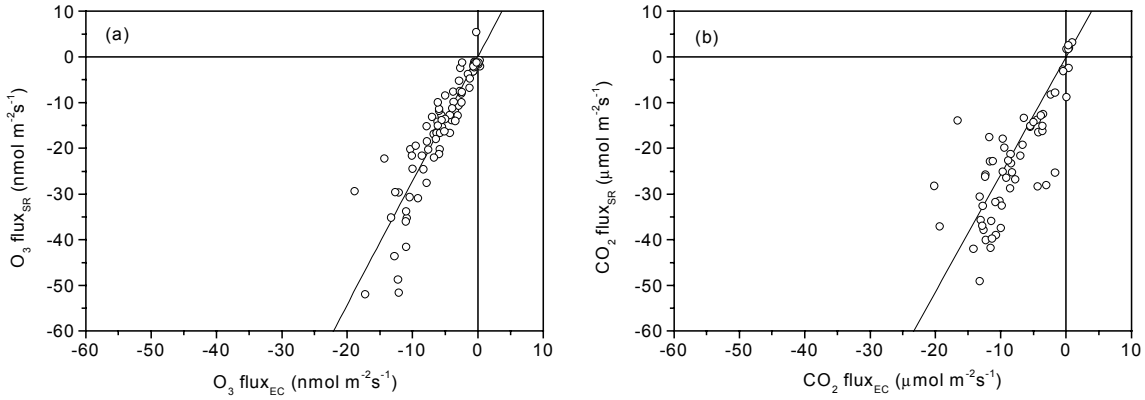

Fig. 11. Same as Fig. 10 for O_3 (a) and CO_2 (b) flux.

Table 1. Weighting factor α (slope -1), coefficient of determination R^2, standard error of estimate SEE, and number n of half-hour values from the linear regression (forced through the origin) between the fluxes determined by the surface renewal approach and eddy covariance (0600 LT - 1800 LT).

	α[a]	R^2	SEE [b]	n
sensible heat flux (Wm^{-2})	0.44 (± 0.068)	0.80	21(11.9)	88
latent heat flux (Wm^{-2})	0.42 (± 0.058)	0.85	45 (9.5)	88
O_3 flux (nmol m^{-2} s^{-1})	0.37 (± 0.064)	0.81	1.9 (10.1)	82
CO_2 flux[c] (µmol m^{-2} s^{-1})	0.39 (± 0.061)	0.54	3.2 (15.1)	60

[a] The α range in brackets results from the slope confidence interval (0.95) of the $\tau_s - h/u_*$ regression in Fig. 8.
[b] Absolute SEE is in flux units. Relative SEE in percent of the corresponding flux range is displayed in brackets.
[c] CO_2 fluxes were just compared for daytime values after 1000 LT

At nighttime the relative deviation between the two sets of fluxes is considerably larger. This is especially evident in the time series of the CO_2 flux because the ratio of nighttime to daytime fluxes is relatively large (compared to the other three scalars). This nocturnal effect is not surprising recalling the Lagrangian character of the air parcel motion assumed in the surface renewal approach. During nights with weak mechanical turbulence and high stability above the canopy, coherent structures occur only sporadically. If a ramp pattern is visible, it is vertically limited to a shallow layer near the canopy top. This layer is far from the vertical extent of the air parcels considered for daytime conditions in Eq. (1). A separate nighttime value of the coefficient α would reduce the overestimation to a certain degree. However no significant correlation between the obtained fluxes was found during nighttime.

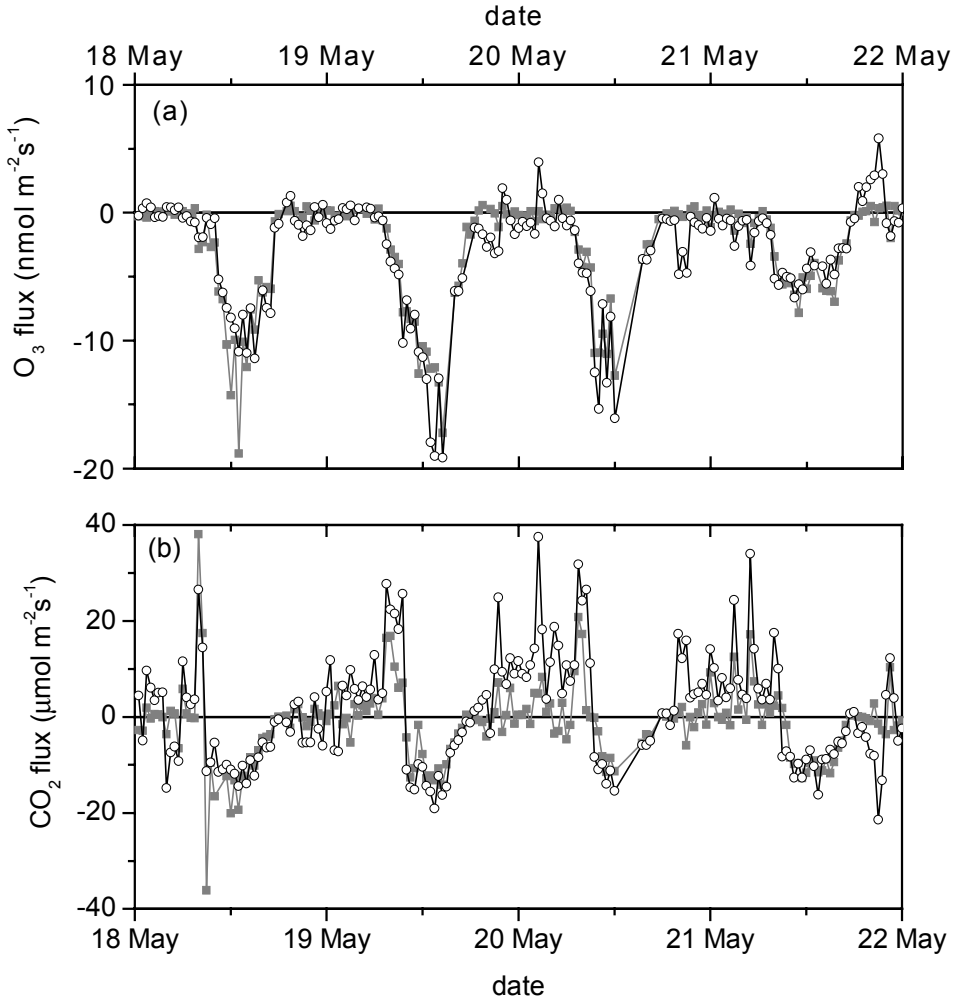

Fig. 12. Comparison of O_3 (a) and CO_2 (b) fluxes measured by eddy covariance (gray squares) and obtained by surface renewal approach (open circles) with (a) $\alpha = 0.37$ and (b) $\alpha = 0.39$. The nighttime comparison is questionable (for details see text).

4.4 Discussion of Influencing Parameters

4.4.1 The Coefficient α

As mentioned above, the weighting coefficient α accounts not only for a vertically different temporal change of the scalar X below z_m, but also for small-scale transport through the top of the considered volume at the measuring height z_m. Paw U et al. (1995) postulated $\alpha = 0.5$ for tall vegetation canopies as a reasonable approximation, assuming a linearly decreasing surface exchange of X from the top of the canopy down to a negligible exchange at the ground. This was confirmed by the findings of Katul et al. (1996). The coefficients for the tropical rainforest obtained by linear regression were found to be somewhat lower than 0.5 (Table 1). The coefficients for sensible and latent heat fluxes (0.44 and 0.42) are slightly larger than for the O_3 and CO_2 fluxes (0.37 and 0.39).

Spano et al. (1997a; 1997b; 2000b) obtained vertically decreasing α coefficients mainly above short or sparse canopies like grass, wheat, or grapevine plants. But also above a relatively dense avocado tree canopy, they found a steady decrease of α with increasing measuring height above the canopy top. A measuring height z_m exceeding the mean vertical dimension of the air parcels involved in the renewal process would result in an overestimation of the flux of X by using z_m in Eq. (1). As pointed out by Spano et al. (1997a), a consequence is a lower value of α, if no vertical decrease of $\left[dX^S(z_m)/dt\right]_{+/-}$ is compensating for it. For the conceptual picture proposed in Fig. 2, which assumes the measuring height z_m to be within the renewed air parcel, a similar behavior of α is expected with changing z_m. In the zone with vertically nearly constant $\left[dX^S(z_m)/dt\right]_{+/-}$, a higher α should result at $z_m = h$ than at 1.33 h, due to the smaller volume which is considered in Eq. (1). In fact, the RBJ data set was acquired at a height considerably above the estimated canopy height, in contrast to the data used in the analysis of Paw U et al. (1995) and Katul et al. (1996). This imposes the question whether the lower values of α, found here arises partially from this difference.

Fig. 13 shows results from the one and a half day period when an additional sonic anemometer was operated close to canopy height. Presented is also the linear regression of the sensible heat flux obtained by the surface renewal approach against the results determined by eddy covariance measurements, but at $z_m = 1.05\ h$. A value of 0.47 was found for α at this height, due to no significant vertical reduction of $\left[dX^S(z_m)/dt\right]_{+/-}$ above the canopy. With $R^2 = 0.90$ and a relative SEE of 11.6%, the determination of the estimate is comparable to the results at 1.33 h.

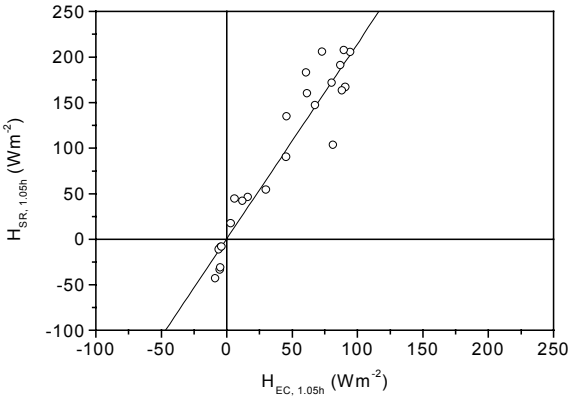

Fig. 13. Same as Fig. 10 for the sensible heat flux measured at $z = 1.05\ h$.

The obtained vertical difference of 7% in α is smaller than expected from the corresponding volume difference according to Eq. (1). A reason for this is a 17% smaller sensible heat flux measured by eddy covariance at 1.05 h compared to 1.33 h. Small-scale inhomogeneities in roughness and/or thermal characteristics of the canopy surface might be responsible for this slight flux difference. A potential influence of the river water surface on the daytime measurements at 1.33 h should be small, according to the source area estimates presented in Section 4.1. On the other hand, the source area for $z_m = 1.33\ h$ should be large enough to make flux estimates less biased by small-scale inhomogeneities than for the height just above the canopy top (1.05 h). Relating the flux estimates from the surface renewal approach in Eq. (1) at 1.05 h to the fluxes from the eddy covariance measurements at 1.33 h results in $\alpha = 0.57$. If the α values for the other scalars increase in a similar way as for sensible heat towards 1.05 h, they are in fact distributed around the findings of Paw U et al. (1995), Katul et al. (1996),and Chen et al. (1997b) at the forest canopy top. Chen et al. (1997b), the sole study in which the surface renewal approach was also applied above the forest canopy, obtained vertically constant α values. Unfortunately they did not comment on the reason for that constancy, whether the increasing volume considered in Eq. (1) is balanced by a reduction of $\left[dX^S(z_m)/dt\right]_{+/-}$ (their ramp slope M/τ) or by a strong vertical divergence of the fluxes measured by eddy covariance. Moreover, α is influenced by the following points:

(i) The range of α specified in Table 1 corresponds to the confidence interval of the slope m in Fig. 8. This means that the uncertainty in the parameterization of τ_s alone (equivalent to the position of the filter window center in the scale domain) could explain, for example, an α for sensible heat up to 0.51 at 1.33 h. In this context a comment on the results of Paw U et al. (1995) for the deciduous forest has to be made. They used a semiempirical

approach to adapt their frequency filter window position to a data subset. The resulting factor of proportionality (Strouhal number) between the frequency of ramp occurrence $1/\tau_s$ and the mean canopy shear scale they used for their filtering scheme was roughly 2.5 times lower than what they found from the functional relation between the two quantities in Paw U et al. (1992). Using the direct functional relation as done here (Fig. 8) would considerably reduce the value for α that they found for the deciduous forest.

(ii) In the present work only structures that penetrate the canopy down to $0.28\,h$ are considered in parameterization (Eq. (11)) by the usage of a two-level detection scheme. Therefore, the filter window position is shifted towards larger scales than in a single-layer detection (see Fig. 4 (a), position of a_f compared to a_0). Consequently α would be somewhat smaller, if a single-level detection scheme had been used as in other studies.

(iii) The mean ratio of about 1.0 between the structure duration D and the time separation interval τ_s between the structures is rather an upper limit for values found above different canopy types, for example, in Qiu et al. (1995). A lower value of D/τ_s would also affect the position of the filter window by shifting it towards larger scales, which would also lead to slightly smaller values of α.

(iv) The average depth to which the coherent turbulent structures actually penetrate the canopy is also affecting the weighting coefficient α in the surface renewal approach. Calculation with the corresponding measuring height z_m implies an upper limit for the volume that is actually renewed by the coherent structures below z_m. Therefore in contrast to the preceding points, a systematically larger α would result from using the actual penetration depth instead of z_m.

4.4.2 Penetration Depth of Coherent Structures

An exact determination of the mean penetration depth is not possible because high time resolution data were only measured at a few particular heights during the experiment. But the uncertainty can be narrowed to a shallow layer in the lowest part of the canopy. Fig. 14 shows the mean diurnal course of the maximum time lag cross-correlation (Eq. (7)) between high-resolution measurements of temperature, ozone, and the vertical wind velocity at $1.33\,h$ and $0.28\,h$. An absolute maximum (minimum in the case of temperature) was searched within a time lag of 100 s. If the absolute maximum (minimum) occurred at the interval limits, the cross-correlation was set to zero, assuming no direct turbulent coupling between the heights to exist. A distinct coupling occurs during daytime from 0700 LT to 1800 LT. Average cross-correlation coefficients with absolute values between 0.2 and 0.4 are reasonable, considering the vertical distance of more than 40 m with the dense crown layer in between. Maximal cross-correlation coefficients within this period were about ±0.65.

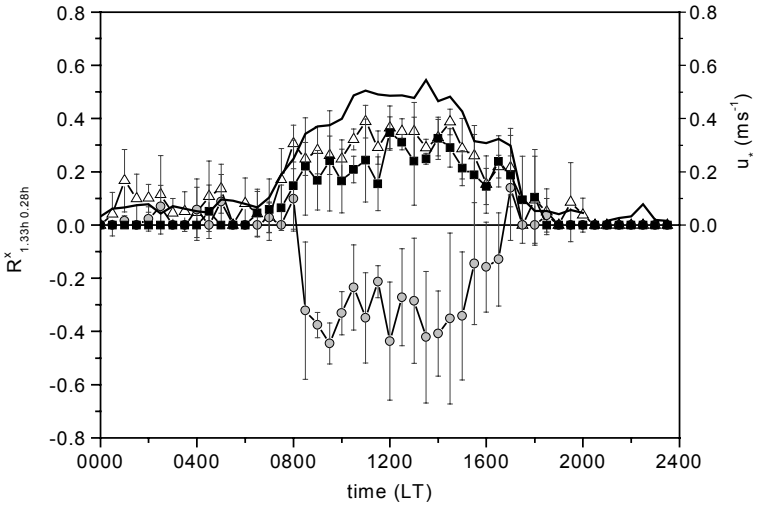

Fig. 14. Mean diurnal course of maximum lag cross-correlation between 1.33 *h* and 0.28 *h* for vertical wind velocity (open triangles), ozone (full squares), and temperature (gray-filled circles). The solid line indicates the mean course of the friction velocity.

Symptomatic for a distinct coupling of the stem space to the atmosphere above the canopy are large values for single-point statistical moments of wind velocity. For the vertical wind velocity *w* at 0.28 *h*, daytime average values for kurtosis and skewness are about 7 and -1.2, respectively. These values are typical for fast downdrafts penetrating the canopy during the day. Kruijt et al. (2000) found somewhat lower values at the RBJ site, indicative of lower mechanical turbulence during their investigation period. At nighttime only sporadic correlation can be seen in Fig. 14. Due to stable thermal stratification and low mechanical turbulence above and within the crown region, the stem space of the canopy is decoupled from the region aloft. This supports the explanation for the large relative differences between the scalar fluxes determined by eddy covariance and by the surface renewal approach at nighttime. During nighttime situations with enhanced turbulence and weakened stability, occasional coupling can be observed (Fitzjarrald and Moore, 1990).

A sonic anemometer was operated 1 m above the forest floor for a short-time period during a second experiment in October 1999 (see Rummel et al., 2002b). These measurements indicate that the lowest layer of the canopy is not directly included in the instantaneous exchange by large structures. This is also indicated by the trace gas profiles in Fig. 6 (see also Kruijt et al., 1996; 2000). The mean penetration depth (given here as height above ground) of large-scale structures is therefore in between 11 m (0.28 *h*) and 1 m (0.03 *h*). Due to the high skewness and kurtosis values for *w* at 11 m, the lower decoupled layer is assumed to be about 4 to 5 m thick. Excluding this shallow layer from the considered air volume up to 1.33 *h* (53 m) would increase α by about 10%.

4.4.3 Origin Height of Penetrating Air

For daytime conditions a rough estimate was made for the height from which the freshly renewed air within the stem space is originating. Similar to Gao et al. (1989), information from high-resolution scalar time series measured within the canopy was combined with the corresponding mean vertical profiles. Here, O_3 was used for this purpose. The average amplitude $\overline{A_{O_3}}$ of the detected ramp structures for each half-hour time series at 0.28 *h* was determined and added to the average O_3 mixing ratio at that height. Comparing this sum with the O_3 mixing ratios measured at the heights above 0.28 *h* leads to the height determination. Using O_3 as a tracer for the estimates, potential effects of chemical reactions and surface uptake on the mixing ratio of penetrating air have to be taken into account. Due to the high daytime average O_3 / NO_x ratio (~200) above and in the upper part of the canopy, the net effect of chemical reactions on the O_3 mixing ratio during the downward transport of air should be small. The surface uptake through the crown layer has, as a first-order process (proportional to the high O_3 mixing ratio), a higher potential to reduce the amplitude of ramp structures in the O_3 time series measured in the stem space below. Therefore the actual origin of penetrating air might be even higher than estimated here. In Fig. 15 this sum is shown as a function of the O_3 mixing ratio measured at h_c, the height up to which the canopy coverage is closed. The data points located above the 1:1 line therefore indicate half-hour intervals with an average height of origin above the closed canopy. Additionally, the regression line for the corresponding mixing ratios at the uppermost measuring level is displayed. In 73% of the daytime periods the average origin height is above the canopy crown and in 46% above the highest measuring level.

These results show that, during most of the daytime cases of the investigated period, a direct exchange between the stem space and the atmosphere above the forest occurs during the detected events. This, together with the good agreement between the results of the surface renewal approach and the fluxes measured by eddy covariance for all measured scalars, indicates that the assumed idealized air parcel motion might be a reasonable approximation of reality. So for the main part of the canopy, the separation time τ_s between consecutive ramps corresponds to the residence time of air within the canopy, which is a key quantity for uptake processes and chemical reactions. Due to the fact that not all turbulent events occurring above the forest are penetrating down into the lower canopy (see, e.g., Fig. 3), different average residence times were obtained for the crown region (including the layer above) and the canopy stem space. The average residence times were about 110 ± 49 s (±s.d.) for the crown layer and 155 ± 32 s for the stem space of the forest, respectively.

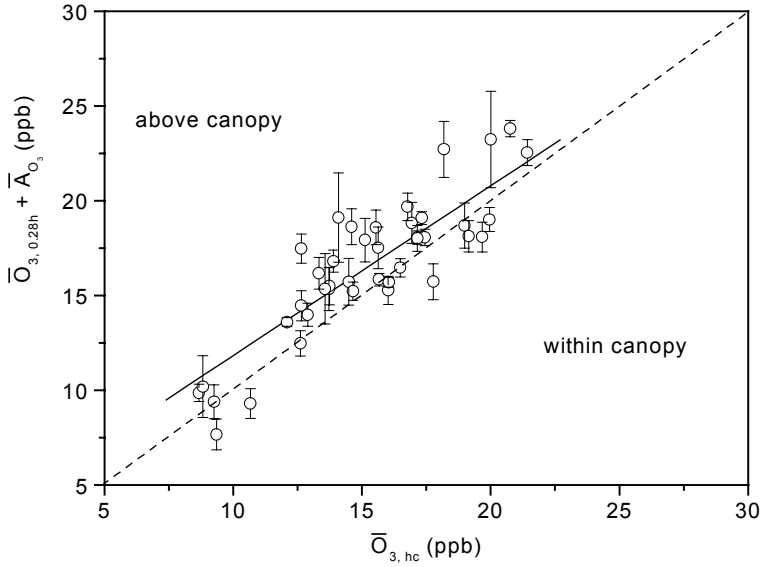

Fig. 15. The sum of the mean ozone mixing ratio and the average ramp amplitude at 0.28 h as a function of the ozone mixing ratio at h_c. The dashed line indicates the 1:1 ratio, and the solid line the corresponding ozone mixing ratios at the uppermost measuring level (1.33 h). For details see text.

5 Summary and Conclusions

Characteristics of the turbulent heat and trace gas exchange at a dense tropical rain forest canopy were investigated in this study. While during daytime, coherent structures establish direct coupling between the main part of the deep forest layer and the atmosphere above, the nocturnal canopy is mostly decoupled.

On average, consecutive exchange events were separated by a dimensionless time interval $(\tau_s\, u_*) / h$ of about 1.6, which is in the same range found in earlier studies for temperate and boreal forests. Typically, the characteristic ramp pattern was also pronounced in scalar time series measured well above the forest canopy. This was the trigger to develop a conceptual picture for the surface renewal approach for tall dense canopies, in which a considerable part of the exchanged air parcels is located above the canopy. The weighting factor α then relates the average storage change within these air parcels of unknown vertical extent to the storage change within the considered air volume below the sensor height z_m. The latter is approximated by the mean temporal exchange of the scalar at z_m between the renewal events.

During daytime hours the fluxes of the four measured scalars (including ozone) determined by the surface renewal approach agreed reasonably well with the corresponding results obtained by the eddy covariance method. Differences in the vertical source/sink distributions of the measured scalars had

obviously no pronounced effect on the corresponding weighting factors α. Values of α obtained at the measuring height of 1.33 h were between 0.37 and 0.44. For the sensible heat flux at $z \approx h$, α was within the range of 0.47 to 0.57, which is close to the value of 0.5 suggested originally by Paw U et al. (1995) for tall canopies. The vertical variation in α was almost exclusively a consequence of the different volumes considered in the surface renewal estimate. The sensitivity of the magnitude of α on the different parameters discussed shows the need to calibrate the surface renewal model for the specific canopies.

The influence of instrumental noise on flux estimates derived from the surface renewal approach was simulated using artificial time series. Except for periods of very low sensitivity of the fast O_3 sensor, during which an overestimation up to 15% was obtained, the effect was negligible.

In contrast to the main part of the canopy that is directly linked to the atmosphere during daytime by coherent structures, a relative shallow layer close to the forest floor was found to be mostly decoupled from this direct exchange. The long residence times in the lowest canopy layer might be particularly important for the fate of reactive trace gases such as NO, which are emitted from the forest soils. Comparing the time scales of transport mechanisms and chemical reactions between the measured trace gases is subject of a subsequent paper (Rummel et al., 2005).

Acknowledgements

This research is supported by the "Environmental and Climate Programme" (Project LBA-EUSTACH, ENV4-CT97-0566) of the European Union, and by the Max Planck Society. The authors thank Carol Strametz for improving the language of the manuscript. We would like to thank the staff at INCRA (Instituto Nacional de Colonização e Reforma Agrária), especially Jaõ Luis Esteves, Eduardo Conceição, and Claudionor Rodrigues. Further, Carlos Brãndao and the staff of IBAMA (Instituto Brasileiro do Meio Ambiente e dos Recursos Naturais Renováveis) in Ji-Parana are gratefully acknowledged for their help in installing and maintaining the infrastructure at the forest. We are indebted to Beatriz E. Gomes (Universidade Federal de Rondonia, Ji Parana) for support concerning everything. We are also grateful to Monika Scheibe, Michael Welling, and Wesley Saores da Silva for assisting us in the field. Special thanks to our GIS specialist Grant A. Kirkman and to Hans Peter Schmid for use of his footprint model.

References

Ammann, C.: On the aplicability of relaxed eddy accumulation and common methods for measuring trace gas fluxes, Dissertation Thesis, Universität Zürich, 229 pp., 1999.

Anandakumar, K.: Sensible heat flux over a wheat canopy: optical scintillometer measurements and surface renewal analysis estimations, Agricultural and Forest Meteorology, 96, 145-156, 1999.

Andreae, M. O., Artaxo, P., Brandao, C., Carswell, F. E., Ciccioli, P., da Costa, A. L., Culf, A., Esteves, J. L., Gash, J. H. C., Grace, J., Kabat, P., Lelieveld, J., Mahli, Y., Manzi, A. O., Meixner, F. X., Nobre, A. D., Nobre, C., Ruivo, M. d. L. P., Silva-Dias, M. A., P., S., Valentini, R., von Jouanne, J., and Waterloo, M. J.: Biogeochemical cycling of carbon, water, energy, trace gases, and aerosols in Amazonia, Journal of Geophysical Research, 107 (D20), 8066, doi: 10.1029/2001JD000524, 2002.

Aubinet, M., Grelle, A., Ibrom, A., Rannik, U., Moncrieff, J. B., Foken, T., Kowalski, A. S., Martin, P. H., Berbigier, P., Bernhofer, C., Clement, R., Elbers, J., Granier, A., Grünwald, T., Morgenstern, K., Pilegaard, K., Rebmann, C., Snijders, W., Valentini, R., and Vesala, T.: Estimation of annual net carbon and water exchange of forests: The EUROFLUX methodology, Advances in Ecological Research, 30, 113-175, 2000.

Bakwin, P. S., Wofsy, S. C., Fan, S.-M., Keller, M., Trumbore, S., and da Costa, J. M.: Emission of nitric oxide (NO) from tropical forest soils and exchange of NO between the forest canopy and atmospheric bounday layers, Journal of Geophysical Research, 95 (D10), 16'755-16'764, 1990.

Baumgartner, A.: Untersuchungen über den Wärme- und Wasserhaushalt eines jungen Waldes, Berichte des Deutschen Wetterdienstes, 28, Offenbach am Main, pp. 53, 1956.

Beier, N., and Schneewind, R.: Chemical reactions of gases in tubes of probing systems and their influence on measured concentrations, Annales Geophysicae, 9, 703-707, 1991.

Bergström, H., and Högström, U.: Turbulent Exchange above a Pine Forest .2. Organized Structures, Boundary-Layer Meteorology, 49 (3), 231-263, 1989.

Brunet, Y., and Irvine, M. R.: The control of coherent eddies in vegetation canopies: streamwise structure spacing, canopy shear scale and atmospheric stability, Boundary-Layer Meteorology, 94, 139-163, 2000.

Chen, W., Novak, M. D., Black, T. A., and Lee, X.: Coherent eddies and temperature structure functions for three contrasting surfaces. Part 1: Ramp model with finite microfront time, Boundary-Layer Meteorology, 84, 99-123, 1997a.

Chen, W., Novak, M. D., Black, T. A., and Lee, X.: Coherent eddies and temperature structure functions for three contrasting surfaces. Part 2: Renewal model for sensible heat flux, Boundary-Layer Meteorology, 84, 125-147, 1997b.

Collineau, S., and Brunet, Y.: Detection of Turbulent Coherent Motions in a Forest canopy Part 1: Wavelet analysis, Boundary-Layer Meteorology, 65, 357-379, 1993a.

Collineau, S., and Brunet, Y.: Detection of Turbulent Coherent Motions in a Forest canopy Part 2: Time-scales and conditional averages, Boundary-Layer Meteorology (66), 49-73, 1993b.

Crutzen, P. J.: Overview of tropospheric chemistry: Developments during the past quarter century and a look ahead, Faraday Discuss., 100, 1-21, 1995.

FAO: Global forest ressources assessment 2000, FAO Forestry Pap. No. 140, UN Food Agric. Org., Rome, 2001.

Farge, M.: Wavelet Transforms and their applications to turbulence, Annual Review of Fluid Mechanics, 24, 395-457, 1992.

Fitzjarrald, D. R., Stormwind, B. L., Fisch, G., and Cabral, O. M. R.: Turbulent transport observed just above the Amazon forest, Journal of Geophysical Research, 93 (D2), 1551-1563, 1988.

Fitzjarrald, D. R., Moore, K. E., Cabral, O. M. R., Scolar, J., Manzi, A. O., and Sa, L. D. D.: Daytime turbulent exchange between the Amazon forest and the atmosphere, Journal of Geophysical Research-Atmospheres, 95 (D10), 16825-16838, 1990.

Fitzjarrald, D. R., and Moore, K. E.: Mechanisms of nocturnal exchange between the rain forest and the atmosphere, Journal of Geophysical Research, 95 (D10), 16839-16850, 1990.

Foken, T., and Wichura, B.: Tools for quality assessment of surface-based flux measurements, Agricultural and Forest Meteorology, 78, 83-105, 1996.

Gamage, N. K. K., and Hagelberg, C. R.: Detection and analysis of microfronts and associated coherent events using localized transform, Journal of Atmospheric Science, 50 (5), 750-756, 1993.

Ganzeveld, L. N., Lilieveld, J., Dentener, F. J., Krol, M. C., Bouwman, A. J., and Roelofs, G.-J.: Global soil-biogenic NO_x emissions and the role of canopy processes, Journal of Geophysical Research, 107, 10.1029/2001JD001289, 2002.

Gao, W., Shaw, R. H., and Paw U, K. T.: Observation of organized structure in turbulent flow within and above a forest canopy, Boundary-Layer Meteorology, 47, 349-377, 1989.

Gao, W., Shaw, R. H., and Paw, K. T.: Conditional analysis of temperature and humidity microfronts and ejection sweep motions within and above a deciduous forest, Boundary-Layer Meteorology, 59 (1-2), 35-57, 1992.

Gao, W., and Li, B. L.: Wavelet analysis of coherent structures at the atmosphere-forest interface, Journal of Applied Meteorology, 32, 1717-1725, 1993.

Gash, J. H. C., Nobre, J. M., Roberts, J. M., and Victoria, R. L.: An overview of ABRACOS, in *Amazonian Deforestation and Climate*, edited by J. H. C. Gash, J. M. Nobre, J. M. Roberts and R. L. Victoria, John Wiley, New York, 1996.

Grace, J., et al.: Carbon dioxide uptake by an undisturbed tropical rain forest in southwest Amazonia, Science, 270, 778-780, 1995.

Grossmann, A., Kronland-Martinet, R., and Morlet, J.: Reading and understanding continuous wavelet transform, in *Wavelets*, edited by J. M. Combes, A. Grossmann and P. Tchamitchian, Springer Verlag, Berlin, 1989.

Güsten, H., Heinrich, G., Schmidt, R. W. H., and Schurath, U.: A novel ozone sensor for direct eddy flux measurements, Journal of Atmospheric Chemistry, 14, 73-84, 1992.

Güsten, H., Heinrich, G., Mönnich, E., Sprung, D., Weppner, J., Ramadan, A. B., Ezz El-Din, M. R. M., Ahmed, D. M., and Hassan, G. K. Y.: On-Line measurements of ozone surface fluxes: Part II. surface level ozone fluxes onto the Sahara desert, Atmospheric Environment, 30 (6), 911-918, 1996.

Gut, A., van Dijk, S. M., Scheibe, M., Rummel, U., Welling, M., Ammann, C., Meixner, F. X., Andreae, M. O., and Lehmann, B. E.: NO emission from an Amazonian rain forest soil: Continuous measurements of NO flux and soil compensation concentration, Journal of Geophysical Research, 107 (D20), 8057, doi: 10.1029/2001JD000521, 2002a.

Gut, A., Scheibe, M., Rottenberger, S., Rummel, U., Welling, M., Ammann, C., Kirkman, G. A., Kuhn, U., Meixner, F. X., Kesselmeier, J., Lehmann, B. E., Schmidt, J., Müller, E., and Piedade, M. T. F.: Exchange fluxes of NO_2 and O_3 at soil and leaf surfaces in an Amazonian rain-forest, Journal of Geophysical Research, 107 (D20), 8060, doi:10.1029/2001JD000654, 2002b.

Hagelberg, C. R., and Gamage, N. K. K.: Structure-preserving wavelet decompositions of intermittent turbulence, Boundary-Layer Meteorology, 70, 217-246, 1994.

Handorf, D., and Foken, T.: Struktuanalyse der atmosphärischen Turbulenz mittels Wavelet-Verfahren zur Bestimmung der Austauschprozesse über dem antarktischen Schelfeis, Deutscher Wetterdienst, Geschäftsbereich Forschung und Entwicklung, Arbeitsergebnisse 47, pp.49, Arbeitsergebnisse 47, 1997.

Horst, T. W., and Weil, J. C.: Footprint estimation for scalar flux measurements in the atmospheric surface layer, Boundary-Layer Meteorology, 59, 279-296, 1992.

Horst, T. W.: On frequency response corrections for eddy covariance flux measurements, Boundary-Layer Meteorology, 94 (3), 517-520, 2000.

Jacob, D. J., and Wofsy, S. C.: Budgets of reactive nitrogen, hydrocarbons, and ozone over the Amazon-Forest during the wet season, Journal of Geophysical Research, 95 (D10), 16737-16754, 1990.

Jacob, D. J., and Bakwin, P. S.: Cycling of NO_x in tropical forest canopies, in *Microbial Production and Consumption of Greenhouse Gases*, edited by W. B. Whitman, pp. 237-253, American Society of Microbiology, Washington, D.C., 1992.

Kaharabata, S. K., Schuepp, P. H., Ogunjemiyo, S., Shen, S., Leclerc, M. Y., Desjardins, R. L., and MacPherson, J. I.: Footprint considerations in BOREAS, Journal of Geophysical Research, 102 (D24), 29'113-29'124, 1997.

Kaimal, J. C., Wyngaard, J. C., Izumi, Y., and Cote, O. R.: Spectral characteristics of surface-layer turbulence, Quarterly Journal of the Royal Meteorological Society, 98, 563-589, 1972.

Kaplan, W. A., Wofsy, S. C., Keller, M., and da Costa, J. M.: Emission of NO and deposition of O_3 in a tropical forest system, Journal of Geophysical Research, 93 (D2), 1389-1395, 1988.

Katul, G. G., and Vidacovic, B.: The partitioning of attached and deattached eddy motion in the atmospheric surface layer using Lorentz wavelet filtering, Boundary-Layer Meteorology, 77, 153-172, 1996.

Katul, G. G., Hsieh, G.-I., Oren, R., Ellsworth, D., and Phillips, N.: Latent and Sensible Heat Flux From a Uniform Pine Forest using Surface Renewal and Flux Variance Technique, Boundary-Layer Meteorology, 80, 249-282, 1996.

Katul, G. G., Geron, G. D., Hsieh, C. I., Vidacovic, B., and Guenther, A. B.: Active turbulence and scalar transport near forest-atmosphere interface, Journal of Applied Meteorology, 37, 1533-1546, 1998.

Kristensen, L.: Time series analysis. Dealing with imperfect data, Riso National Laboratory, Roskilde, Denmark, 1998.

Kruijt, B., Lloyd, J., Grace, J., McIntyre, J. A., Farquhar, G. D., Miranda, A. C., and McCracken, P.: Sources and sinks of CO2 in Rondonia tropical rainforest, in *Amazonian deforestation and climate*,

edited by J. H. C. Gash, C. A. Nobre, J. M. Roberts and R. L. Victoria, pp. 331-351, John Wiley & Sons, Chichester, 1996.

Kruijt, B., Malhi, Y., Lloyd, J., Nobre, A. D., Miranda, A. C., Pereira, M. G. P., Culf, A., and Grace, J.: Turbulence statistics above and within two amazon rain forest canopies, Boundary-Layer Meteorology, 94, 287-331, 2000.

Kumar, P., and Foufoula-Georgiou, E.: Wavelets in geophysics: An introduction, in *Wavelets in Geophysics*, edited by E. Foufoula-Georgiou and K. P., pp. 373, Academic Press, San Diego, 1994.

Lenschow, D. H., and Kristensen, L.: Uncorrelated noise in turbulence measurements, Journal of Atmospheric and Oceanic Technology, 2, 68-81, 1985.

Lenschow, D. H., and Raupach, M. R.: The attenuation of fluctuations in scalar concentrations through sampling tubes, Journal of Geophysical Research, 96 (D8), 15259-15268, 1991.

Leuning, R., and Judd, M. J.: The relative merits of open- and closed-path analysers for measurement of eddy fluxes, Global change Biology, 2, 241-253, 1996.

Lu, C. H., and Fitzjarrald, D. R.: Seasonal and diurnal variations of coherent structures over a deciduous forest, Boundary-Layer Meteorology, 69, 43-69, 1994.

Mahrt, L., and Gibson, W.: Flux decomposition into cohorent structures, Boundary-Layer Meteorology, 60, 143-168, 1992.

Moncrieff, J. B., Massheder, J. M., deBruin, H., Elbers, J., Friborg, T., Heusinkveld, B., Kabat, P., Scott, S., Soegaard, H., and Verhoef, A.: A system to measure surface fluxes of momentum, sensible heat, water vapour and carbon dioxide, Journal of Hydrology, 188-189, 589-611, 1997.

Moore, C. J.: Frequency response correction for eddy correlation systems, Boundary-Layer Meteorology, 37, 17-35, 1986.

Paw U, K. T., Brunet, Y., Collineau, S., Shaw, R. H., Maitani, T., Qiu, J., and Hipps, L.: On coherent structures in turbulence above and within agricultural plant canopies, Agricultural and Forest Meteorology, 61, 55-68, 1992.

Paw U, K. T., Qiu, J., Su, H. B., Watnabe, T., and Brunet, Y.: Surface renewal analysis: a new method to obtain scalar fluxes, Agricultural and Forest Meteorology, 74, 119-137, 1995.

Phillips, O. L., et al.: Changes in the carbon balance of tropical forests: Evidence from long-term plots, Science, 282, 439-442, 1998.

Pinker, R. T., and Holland, J. Z.: Turbulence structure of tropical forest, Boundary-Layer Meteorology, 43, 43-63, 1988.

Qiu, J., Paw U, K. T., and Shaw, R. H.: Pseudo-wavelet analysis of turbulence patterns in three vegetation layers, Boundary-Layer Meteorology, 72, 177-204, 1995.

Rannik, Ü., Aubinet, M., Kurbanmuradov, O., Sabelfeld, K. K., Markkanen, T., and Vesala, T.: Footprint analysis for measurements over a heterogeneous forest, Boundary-Layer Meteorology, 97 (1), 137-166, 2000.

Rannik, Ü., Markkanen, T., Raittila, J., Hari, P., and Vesala, T.: Turbulence statistics inside and over forest: Influence on footprint prediction, Boundary-Layer Meteorology, 109, 163-189, 2003.

Raupach, M. R., and Thom, A. S.: Turbulence in and above Plant Canopies, Annual Review of Fluid Mechanics, 13, 97-129, 1981.

Raupach, M. R., Finnigan, J. J., and Brunet, Y., Coherent eddies in vegetation canopies, in *Australian Conference on Heat and Mass Transfer*, pp. 75-90, University of Canterbury, 1989.

Raupach, M. R., Finnigan, J. J., and Brunet, Y.: Coherent eddies and turbulence In vegetation canopies - the mixing-layer analogy, Boundary Layer Meteorology, 78, 351-382, 1996.

Rummel, U., Ammann, C., and Meixner, F. X., Characterizing turbulent trace gas exchange above a dense tropical rain forest using wavelet and surface renewal analysis, in *15th AMS Symposium on Boundary Layer and Turbulence*, pp. 602-605, Wageningen, NL, 2002a.

Rummel, U., Ammann, C., Gut, A., Meixner, F. X., and Andreae, M. O.: Eddy covariance measurements of nitric oxide flux within an Amazonian rainforest, Journal of Geophysical Research, 107(D20), 8050, doi:10.1029/2001JD000520, 2002b.

Rummel, U., Ammann, C., Andreae, M. O., and Meixner, F. X.: Wet season NO_x exchange between an Amazonian rain forest and the atmosphere-implication from time scale analysis, Atmospheric Environment, for submission, 2005.

Schmid, H. P.: Source Areas for Scalars and Scalar Fluxes, Boundary-Layer Meteorology, 67, 293-318, 1994.

Schmid, H. P.: Experimental design for flux measurements: matching scales for observations and fluxes, Agricultural and Forest Meteorology, 87, 179-200, 1997.

Shaw, R. H., Paw U, K. T., and Gao, W.: Detection of temperature ramps and flow structures at a deciduous forest site, Agricultural and Forest Meteorology, 47, 123-138, 1989.

Snyder, R. L., Spano, D., and Paw U, K. T.: Surface renewal analysis for sensible and latent heat flux density, Boundary-Layer Meteorology, 77, 249-266, 1996.

Spano, D., Snyder, R. L., Duce, P., and Paw U, K. T.: Surface renewal analysis for sensible heat flux density using structure functions, Agricultural and Forest Meteorology, 86, 259-271, 1997a.

Spano, D., Duce, P., Snyder, R. L., and Paw U, K. T., Surface renewal estimates of evapotranspiration. Tall canopies, in *2nd Int. Sym. on Irrigation of Hort. Crops*, edited by K. S. Chartzoulakis, pp. 63-68, 1997b.

Spano, D., Snyder, R. L., Duce, P., Paw U, K. T., and Falk, M., Determining scalar fluxes over an old-growth forest using surface renewal, in *24th Conference on Agricultural and Forest Meteorology*, pp. 80-81, Davis, CA, 2000a.

Spano, D., Snyder, R. L., Duce, P., and Paw U, K. T.: Estimating sensible and latent heat flux densities from grapevine canopies using surface renewal, Agricultural and Forest Meteorology, 104, 171-183, 2000b.

Torrence, C., and Compo, G. P.: A practical guide to wavelet analysis, Bulletin of the American Meteorological Society, 79, 61-78, 1998.

van Atta, C. W.: Effect of coherent structures on structure functions of temperature in the atmospheric boundary layer, Archives of Mechanics, 29 (1), 161-171, 1977.

von Randow, C., Sa, L. D. A., Gannabathula, P. S. S. D., Manzi, A. O., and Arlino, R. A.: Scale variability of atmospheric surface fluxes of energy and carbon over a tropical rainforest in southwest Amazonia. I. Diurnal conditions, Journal of Geophysical Research, 107, 10.1029/2001JD000379, 2002.

Webb, E. K., Pearman, G. I., and Leuning, R.: Correction of Flux Measurements for Density Effects Due to Heat and Water Vapour Transfer, Quarterly Journal of the Royal Meteorological Society, 106, 85-100, 1980.

Wichura, B., Buchmann, N., and Foken, T., Fluxes of stable carbon isotope 13C above a spruce forest measured by hyperbolic relaxed eddy accumulation method, in *14th AMS Symposium on Boundary Layer and Turbulence*, pp. 559-562, Boston, Aspen, CO., 2000.

Wienhold, F. G., Frahm, H., and Harris, G. W.: Measurements of N2O Fluxes from Fertilized Grassland Using a Fast Response Tunable Diode Laser Spectrometer, Journal of Physical Oceanography, 99 (D8), 16557-16567, 1994.

Yamada, M., and Ohkitani, K.: Orthonormal wavelet expansion and its application to turbulence, Prograss of Theoretical Physics, Progress Letters, 83 (5), 819-823, 1990.

Young, R. K.: Wavelet theory and its applications, 221 pp., Kluwer Academic Publishers, Norwell, Massachusetts, 1993.

Zeller, K., Massman, W., Stocker, D., Fox, D. G., Stedman, D., and Hazlett, D.: Initial Results from the Pawnee Eddy Correlation System for Dry Acid Deposition Research, United States Department of Agriculture (USDA), Forest Service, RM-282, 1989.

Appendix F

Wet Season NO_x Exchange between an Amazonian Rain Forest and the Atmosphere - Implication from Time Scale Analysis

U. Rummel[a], C. Ammann[b], M.O. Andreae[a], and F.X. Meixner[a]

[a]*Max Planck Institute for Chemistry, Biogeochemistry Dept., D-55020 Mainz, Germany,*

[b]*Air Pollution - Climate group (TP 11.3), FAL-Reckenholz,P.O.Box, CH-8046 Zürich, Switzerland*

for submission in **Atmospheric Environment**

Abstract

Mixing ratio profiles of the triad NO-NO_2-O_3 were measured at a tropical rain forest in southwest Amazonia the end of the wet season. In order to identify the processes, which are crucial for the vegetation-atmosphere exchange of O_3 and NO_x, these data, complemented by information obtained from various leaf- and canopy-scale measurements, were used to determine characteristic time scales of turbulent transport, uptake by plants, soil deposition, and chemical reactions within the forest. In the lowest part of the canopy the transport time scale (or mean residence time of air) was considerably larger than the chemical time scale of NO oxidation by O_3 imported from aloft. This in concurrence with a negligible NO_2 photolysis rate close to the ground ensured that during daytime nearly all soil emitted NO was transformed into NO_2 within the lowest 4 m of the canopy and is available for uptake by vegetation through the whole canopy depth. At night time a reversed ratio of transport and chemical ($NO + O_3$) time scales within the canopy enabled NO to reach higher regions of the forest. Potential emission of NO_x as NO is therefore more likely during night. For the first time measured NO_2 profiles from tropical rain forest canopy were available to determine the reduction of soil-emitted NO_x by the vegetation layer. The reduction obtained by a canopy budget approach is with up to 25% of the soil emission considerably smaller than corresponding results of previous model studies.

Keywords: Tropical forest; NO_x exchange, Canopy reduction, Time scales

*corresponding author

1 Introduction

Despite the fact, that only 10% of atmospheric ozone O_3 is present in the troposphere it is of great environmental relevance in that part of the atmosphere. Due to its radiative properties tropospheric O_3 is a very important greenhouse gas (e.g. IPCC, 2001; Portmann et al., 1997). Moreover, it is highly phytotoxic and detrimental to human health (McKee, 1993). On the other hand, O_3 is also the main precursor of the hydroxyl radical OH, the primary oxidant in the troposphere which controls the atmospheric lifetime of many gases like methane CH_4 or carbon monoxide CO (Levy, 1971). Most oxidation of trace gases occurs in the tropical troposphere, where high UV intensities and water vapor concentrations favor the formation of OH by O_3 photolysis (Crutzen, 1986). The photochemical production of tropospheric O_3 is largely controlled by the abundance of nitrogen oxides NO_x ($NO+NO_2$), the key catalyst in the formation process (Crutzen, 1979). In contrast to the industrialized regions of the northern hemisphere, the tropospheric chemistry in remote tropical areas is still controlled mainly by natural NO_x sources like lightning production (e.g. Labrador et al., 2004; Stockwell et al., 1999) and soil emission over continents (Gut et al., 2002a; Kaplan et al., 1988; Verchot et al., 1999). Because the large tropical ecosystems like the Amazonian rain forest undergo rapid changes by development for e.g. agricultural use (between 1990 and 2000 an area of about 23000 km^2 per year was deforested and burned, only in Brazil (FAO, 2001)), the soil emission of NO is directly affected by these activities (cf. Gut et al., 2002a; Keller et al., 1993; Kirkman et al., 2002; Neff et al., 1995). To asses the effect of land use change on the net NO_x input to the tropical troposphere, it is important to consider the impact of the forest layer on the NO emissions from soil (e.g. Jacob and Wofsy, 1990).

Within a forest canopy turbulent transport interferes with exchange processes at soil and plant surfaces and, in case of reactive constituents like NO_x, also with chemical transformations. Extremely difficult is the quantification of processes like leaf-air exchange of NO_2, which might be bi-directional. Leaf level enclosure measurements on various temperate plant species like coniferous trees and seeds (Hari et al., 2003; Johansson, 1987; Rondon et al., 1993; Rondon and Granat, 1994; Thoene et al., 1991; Thoene et al., 1996) and wheat (Ludwig et al., 1992; Weber and Rennenberg, 1996) showed the existence of a compensation point for NO_2, which is that ambient mixing ratio below which NO_2 is emitted by the plant. Recently Sparks et al. (2001) found a range of compensation points between 0.53 ppb and 1.6 ppb for 25 tropical tree species in Panama, clearly demonstrating NO_2 emissions below these mixing ratios. Especially these results from tropical tree species emphasize the basic controversy ("the NO_2 flux conundrum") as pointed out by Lerdau et al. (2000):

On the one hand the majority of lately published global inventories of NO_x emissions which consider the effect of vegetation cover on the net NO_x release to the atmosphere (e.g.Davidson and Kingerlee, 1997; Lee et al., 1997; Yienger and Levy, 1995) use the canopy reduction factor (CRF) concept according to Yienger and Levy (1995). The CRF is an empirical coefficient (ecosystem and LAI dependent) accounting for NO_2 scavenging within the vegetation. It bases on model results of Jacob and Wofsy (1990) which in term are deduced from one experiment, namely ABLE 2B (Harriss et al., 1990) during the wet season in the Amazonian rain forest. Jacob and Wofsy (1990) postulate a considerable vegetation uptake (24 h average: 80% of the soil NO emission) which is necessary to reconcile the experimental findings on NO soil emissions (Bakwin et al., 1990a) and NO_y mixing ratios (Bakwin et al., 1990b) just above the canopy.

On the other hand the ambient NO_2 mixing ratios postulated by Jacob and Wofsy (1990) are within a range (40-150 ppt) where NO_2 emission rather than NO_2 uptake would be expected if reference is made to the compensation points of the mentioned enclosure measurements. Ganzeveld et al. (2002) estimated the role of canopy processes on global soil-biogenic NO emission by implementing a multi-layer trace gas model into a chemistry-general circulation model. The introduction of a hypothetical NO_2 compensation mixing ratio of about 1 ppb resulted in a corresponding NO_2 emission from vegetation, which in turn reduced the overall NO_2 deposition velocity for July up to 80% (compared to results were only NO_2 uptake was considered) especially for remote ecosystems like boreal and tropical forests. Sparks et al. (2001) also made budget estimations of the vegetation effect by assuming NO_2 mixing ratios within the canopy, which are above and below the compensation point. They obtained a NO_2 emission/uptake by vegetation up to 19% of the soil NO emissions for NO_2 mixing ratios below/above the compensation point.

All these estimations for tropical forest sites lack in a considerable set of measured ambient NO_2 mixing ratio values, one of the most relevant quantities to assess the ecosystem exchange of NO_x.

In the present study as part of the LBA-EUSTACH campaigns (EUropean Studies on Trace gases and Atmospheric CHemistry as a contribution to Large-scale Biosphere–atmosphere experiment in Amazonia; LBA) (Andreae et al., 2002), closely oriented at the experimental data, the relevance of competing processes within a rain forest in southwest Amazonia will be assessed by their characteristic timescales. Further, based on the NO_2 mixing ratios measured at 8 levels throughout the rain forest canopy and the results of several other measurements at leaf and canopy scale, a tentative quantification of the forest impact on biogenic NO_x exchange is given and discussed in the second part of this paper.

2 Experiment

2.1 Site and Experimental Period

The measurements were carried out during the LBA-EUSTACH-1 campaign in the wet-to-dry season transition period from April to May 1999. The analysis focuses on a four day intensive measuring period between 18 and 22 May at the end of the experiment. A time period characterized by fairly constant environmental conditions (for further information, see Rummel et al. (2005b)) and no significant external influence of biomass burning, which is essential for investigating the fate of NO_x (originating from biogenic NO sources) within the vegetation.

The experimental site (10°04′55′′ S, 61°55′48′′ W, 147 m a.s.l.), a former ABRACOS site (Gash et al., 1996) is located in the Reserva Biológica Jarú (RBJ), a forest reserve 90 km north of the city Ji-Paraná in the state of Rondônia (southwest Amazonia), Brazil. The vegetation cover of RBJ, owned by the Brazilian Environmental Protection Agency IBAMA (Instituto Brasileiro de Meio Ambiente e Recursos Renováveis) is a primary (terra firme) open rain forest with a closed canopy of about 32 m height (h_c). Single jutting trees reach heights up to 45 m. The understory consists mainly of palms. The vertical LAI (leaf area index) distribution is shown in Fig. 6. The total LAI was measured (LI-COR LAI 2000, USA) to be about 5.6. The horizontal extent of the forest is partly limited. Within the west-northwest to southeast sector primary rain forest exists for several tens of km. In the remaining sector a river (Rio Machado) interrupts the vegetation. The minimum distance to the river (in the southwest direction) is about 400 m. Further information about the site and the campaign is given by Andreae et al. (2002).

2.2 Measurements

The main experimental platform was a scaffolding tower of 52 m height erected in 1991 (Gash et al., 1996). Measurements close to the forest floor (0–4 m height) were made at a tripod 15 m northeast of the main tower, over a relatively undisturbed surface area. H_2O, CO_2, O_3, NO, and NO_2 mixing ratios were measured above and throughout the canopy. The air sampling system consisted of eight 6.4 mm TEFLON® tubes connecting the inlets at 0.3 m, 1.0 m, 4.0 m, 11.3 m, 20.5 m, 31.3 m, 42.2 m, and 51.7 m to the analyzers in the shelter at the tower base. The individual tubes were bundled up in two opaque insulated main pipes, which were heated just above environmental air temperature to prevent condensation in the tubing system. All tubes were continuously flushed through a purging pump and air from all heights was sequentially sampled by a TEFLON®valve manifold. Past the manifold, the inlets to each trace gas analyzer were branched off from the main sampling stream. H_2O and CO_2 were sampled by a LI-6262 analyzer, which was regularly calibrated by a dew point generator (LI-COR LI-610, USA) and gas standard cylinders in the case of CO_2. O_3 mixing ratios were measured

with a UV absorption analyzer (Thermo Instruments TE49C, USA). For NO and NO_2 a gas phase chemiluminescence analyzer (ECO Physics CLD 780 TR, Switzerland) combined with a photolytic converter (ECO Physics PLC 760, Switzerland) was employed (see Rummel et al., 2002). A gas-phase titration unit, which contains a UV lamp as O_3 source (ANSYCO SYCOS K/GPT, Germany) was used together with zero air and NO cylinder standards for combined O_3, NO, and NO_2 calibrations.

Two complete cycles of sequentially sampled profile data were averaged to obtain corresponding half-hour data sets of vertically resolved H_2O, CO_2, O_3, NO, and NO_2 mixing ratios. Within one cycle, the dwell time at each height was 1.5 min with 30 s rejected because of adaptation processes. Due to different tubing length the delay times within the sample lines varied from ~1 s up to ~8 s from the lowest to the highest level. Mixing ratios of O_3, NO, and NO_2 were corrected for the gas-phase reaction $NO + O_3 \rightarrow NO_2 + O_2$ occurring within the tubes, depending on the corresponding delay time (Beier and Schneewind, 1991). For data recording and controlling of the trace gas profile system, a laptop computer, equipped with a data acquisition device (National Instruments DAQPad-1200, USA) was used.

Air temperature profiles were determined by fine wire thermocouples (Omega, USA) recorded by a data logger / multiplexer system (Campbell 21X and AM25T, USA).

NO_2 photolysis frequency j_{NO2} was alternately measured for about 2 day periods at 51.7 m, 22 m, and 1 m height by a selective radiation sensor (Meteorologie Consult, Germany).

Fluctuations of the three wind velocity components (u, v, w) were continuously measured at heights of 53 m and 11 m by sonic anemometers (Gill Instruments, Solent Research 1012 K55, UK) mounted on booms extending 4 m horizontally. During the four-day period investigated here, the measurements at these two heights were complemented using a third sonic anemometer (Gill Instruments, Research HS, UK), which was alternately employed at 42 m and 31 m for a period of about 24 h each.

3 Methods

To investigate the canopy processes, the air column between the uppermost measuring level and the forest floor was divided into four layers. Three layers were located throughout the canopy and one above. The layer above the canopy (i = 4) covers a vertical distance of about 21 m, from the top of the tower down to h_c = 32 m, the average height of the closed canopy. Position and depth of the three other layers (i = 1, 2, 3) within the forest were mainly oriented at the vertical distribution of the leaf area index (LAI). The upper one from h_c down to 20 m includes the main LAI fraction and is that part of the canopy through which the bulk of the incoming short wave radiation is attenuated (see Fig. 6). The middle

canopy layer extends from 20 m down to 4 m containing the lower part of the forest crown and a relative free stem space. Below that the LAI is increasing again due to understory vegetation ($i = 1$, 0-4 m). The relative LAI fractions of the layers $i = 1, 2, 3$ were 0.14, 0.4, 0.46, while the absolute accumulated LAI was about 5.6.

3.1 Chemistry

Based on the concentration measurements the focus is specifically on the photochemical triad of nitric oxide, nitrogen dioxide, and ozone, which interact according:

$$NO_2 + h\upsilon \xrightarrow{j_{NO2}} NO + O \quad (1)$$

$$O + O_2 \xrightarrow{k_1} O_3 \quad (2)$$

$$NO + O_3 \xrightarrow{k_2} NO_2 + O_2 \quad (3)$$

The reaction (2) is very fast and can be considered as immediate. Therefore in this simplified system O_3 is formed as a direct result of NO_2 photolysis by solar radiation ($\lambda \leq 420$ nm). The oxidation of NO by O_3 is reforming NO_2. Under clear sky conditions around noon the measured photolysis frequency j_{NO2} average to 8.3×10^{-3} s^{-1} above the forest. The average j_{NO2} values of the canopy layers $i = 1, 2, 3$ were determined on the basis of an exponential decay function fitted to the average daytime values obtained at the measurement heights (see Fig. 6). The reaction rate of (2) was calculated as $k_2 = 17/T \times \exp(-1450/T)$ in units of ppb^{-1} s^{-1}. The corresponding chemical time scales, which characterize the time necessary to reduce the constituents in layer i on the fraction 1/e of their initial mixing ratios, are then $\tau_{c,i,NO_2} = (j_{NO2,i})^{-1}$, $\tau_{c,i,NO} = (k_2 [O_3]_i)^{-1}$, and $\tau_{c,i,O_3} = (k_2 [NO]_i)^{-1}$. In this context $[O_3]_i$ and $[NO]_i$ represent the half hour average mixing ratios of layer i.

Chemical interaction with decomposition products of biogenic hydrocarbons are not taken into account, although daytime concentrations of e.g. isoprene and monoterpenes were quite high at crown level of the forest (Kesselmeier et al., 2002; Kuhn et al., 2002a). Therefore the contribution of peroxy radicals RO_2 to the oxidation of NO might be substantial in the upper part of the canopy but does not affect the budget of total NO_x. On the other hand the formation of PAN by the reaction of NO_2 and peroxyacetyl radicals was found to have only a small effect on NO_x in a tropical forest (Jacob and Bakwin, 1992).

3.2 Surface Exchange

Time scales for exchange processes at vegetation and soil surfaces were determined at the base of a multi-layer resistance model according to Baldocchi (1988) and Meyers (1987). Here the uptake of a constituent X by the vegetation is described by leaf level resistances for each canopy layer $i = 1, 2, 3$:

$$r_{L,i,X} = \left(\frac{1}{r_{b,i,X} + \frac{D_{H_2O}}{D_X} r_{s,i} + r_{m,X}} + \frac{2}{r_{b,i,X} + r_{ct,X}} \right)^{-1} \quad (4)$$

It is composed of a leaf boundary layer resistance $r_{b,i,X}$, a mesophyll resistance $r_{m,X}$, a cuticula resistance $r_{ct,X}$, and a stomatal resistance $r_{s,i}$ which is scaled by the ratio of molecular diffusivity of H_2O and that of the constituent X (here NO_2 and O_3, since the uptake of NO is negligible). All resistances are related to unit leaf area and assumed to be height dependent (subscript i) and/or constituent specific (subscript X). The resistance to diffusion through the quasi-laminar leaf boundary layer $r_{b,i,X}$ can be described as:

$$r_{b,i,X} = \frac{l}{D_x \, Sh_i} \quad (5)$$

Here l is a characteristic leaf length and Sh_i the Sherwood number at layer i. Because of the great variety of tropical plant species with a large spectrum of different leaves, a constant average $l = 0.2 \pm 0.1$ m was set without considering a height dependence in Eq. (5). The leaf length was determined as average of all plant species in the vicinity of the Jaru tower listed in McWilliam et al. (1996). Information about the characteristic leaf sizes of the species was taken from Ribero and Berg (1999). Expressions for the Sherwood number have been originally derived for rigid, flow parallel thin plates in model experiments. For a laminar boundary layer flow follows:

$$Sh_i = 0.66 \, \mathrm{Re}_i^{\frac{1}{2}} \, Sc_X^{\frac{1}{3}} \quad (6)$$

Re is the Reynolds number related to leaf length l and the average wind velocity u_i at layer i. Sc_X is the Schmidt number, defined as the ratio of the kinematic viscosity of air and the molecular diffusivity of X. If, in more realistic conditions, leaf inclination to the flow direction and leaf fluttering are considered, the boundary layer resistance was found to be lower by a factor of 2-2.5 compared to the usage of Eq. (6) (e.g. Chen et al., 1988; Grace and Wilson, 1976; Schuepp, 1971). To account for that discrepancy, following a suggestion of Finnigan and Raupach (1987) (see also Baldocchi (1988)), a constant of 1.32 instead of 0.66 was used in Eq. (6) resulting in:

$$r_{b,i,X} = \frac{\nu^{\frac{1}{6}}}{1.32 \, D_X^{\frac{2}{3}}} \left(\frac{l}{u_i} \right)^{\frac{1}{2}} \quad (7)$$

with the kinematic viscosity of air υ As described in Section 2.2, during the intensive measuring period of LBA-EUSTACH 1 continuous wind speed measurements were only made at 53 m and 11 m height. These data together with the wind velocity data of the alternately measured heights were averaged (1000 LT to 1400 LT) and spline interpolated to obtain a mean daytime wind profile which was used in Eq. (7).

A major factor regulating the exchange of gaseous constituents between the atmosphere and the leaf internal tissues is stomatal opening. Functioning of stomata is controlled by plant physiological processes and environmental factors (Hosker and Lindberg,

1982). The stomatal resistances $r_{s,i}$ for each canopy layer used here are average values which are based on measurements made at the RBJ site during the ABRACOS experiment in 1993 (Gash et al., 1996). Approximately during the same time of the year (beginning of June, M5 experiment) as the intensive measuring period (end of May), porometer measurements were made by McWilliam et al. (1996) on several plant species at different heights and days. For days with comparable environmental conditions (see Section 4.1) these data were averaged depending on canopy layer and time of day. The stomatal resistances determined by transpiration measurements were in accordance with Eq. (4) scaled by the corresponding molecular diffusivity ratio. For O_3 and NO_2 here a ratio $D_{H_2O}/D_X = 1.6$ was used for both constituents (Hicks et al., 1987). Half hour values between the porometer measuring times were linearly interpolated.

The assumptions of leaf internal mesophyll resistances $r_{m,X}$ rely on the results of Gut et al. (2002b). Greenhouse branch enclosure measurements on two plant species typical for the Amazon rain forest showed a negligible mesophyll resistance for O_3 in accordance with specifications for temperate vegetation types by Wesely (1989). For NO_2 Gut et al. (2002b) found the stomatal resistance to account just for 55% of the total leaf resistance, which is a clear indication for a considerable mesophyll resistance r_{m,NO_2} for these tropical tree species. The existence of a mesophyll resistance for NO_2 is also suggested by the results of Sparks et al. (2001) from enclosure measurements on various tropical tree species in Panama. Consequently, here the magnitude of the mesophyll resistance for NO_2 was set to 300 s m^{-1}, that the ratio of stomatal resistance and total leaf resistance is $\left(\left(D_{H_2O}/D_{NO_2}\right)r_{s,i}\right)/r_{L,i,NO_2} = 0.55$, in accordance with the results of Gut et al. (2002b). The corresponding cuticula resistance for NO_2, characterizing the parallel pathway to stomatal uptake, was set to 20000 m s^{-1}. This bases on the formulation suggested by Wesely (1989) which considers the solubility and reactivity of NO_2. The cuticula resistance for O_3 was set to 4000 m s^{-1}, following the results of the leaf level O_3 exchange cuvette measurements of Rummel et al. (2005a). The factor 2 in Eq. (4) accounts for the fact that cuticular uptake is generally possible at both sides of the leaf, while deciduous tropical trees, like many deciduous temperate species are mainly hypo-stomatous (stomata are concentrated at one side of the leaf).

Assuming a first order process, the time scale $\tau_{u,i,X}$ characteristic for the uptake of X at canopy layer i can be determined by:

$$\left(\frac{dX_i}{dt}\right)_u = -\frac{1}{r_{L,i,X}}\frac{\Delta LAI_i}{\Delta z_i}X_i \qquad (8)$$

Integrating of Eq. (8) results in:

$$X_i = X_{0,i}e^{-\frac{t}{\tau_{u,i,X}}} \qquad (9)$$

with:

$$\tau_{u,i,X} = \left(\frac{1}{r_{L,i,X}} \frac{\Delta LAI_i}{\Delta z_i} \right)^{-1} \quad (10)$$

Here $(dX_i/dt)_u$ is the temporal mixing ratio change at layer i caused by surface uptake. ΔLAI_i and Δz_i are the corresponding leaf area fraction and layer depth respectively.

The time scale for soil uptake from the lowest canopy layer is calculated by $\tau_{g,1,X} = r_{g,1,X} \Delta z_1$. Soil resistances $r_{g,1,X}$ have been determined by dynamic soil chamber measurements of Gut et al. (2002b).

The turbulent transport time scales for the lowest canopy layer were determined by spline interpolation between the aerodynamic resistances for the lowest meter determined by Gut et al. (2002b) and a corresponding aerodynamic resistance of the canopy layer $i = 2$ above. The resulting equidistant resistance values were averaged and multiplied by the layer depth Δz_1 to obtain the corresponding time scale. For daytime conditions the resistance for layer 2 (the upper fix point of the interpolation) was the mean residence time of air between consecutive exchange events (taken from Rummel et al. (2005c)) devided by Δz_2. During night time the stem space was mostly isolated from the nocturnal surface layer above the canopy. A characteristic aerodynamic resistance for the internal air motion of layer 2 was determined by the quotient of the temperature difference within the stem space between 4 m and 20.5 m and the sensible heat flux measured at 11 m height.

4 Results and Discussion

4.1 Canopy Resistances

The boundary layer resistances for water vapor r_{b,i,H_2O} obtained from Eq. (7) are shown in Fig. 1. The average r_{b,i,H_2O} increases from about 32 s m^{-1} in the upper crown layer to 154 s m^{-1} near the forest floor, reflecting the strong reduction of wind speed with increasing canopy depth. Also displayed in Fig. 1 is the vertical boundary layer resistance profile averaged for three canopy layers from Roberts et al. (1990). These data were measured within a terra firme rain forest in central Amazonia (Reserva Ducke, 25 km from Manaus). The forest has a comparable architecture (trees up to 40 m; with a somewhat higher LAI (Shuttleworth et al., 1984)). Roberts et al. (1990) determined the r_{b,i,H_2O} values by potential evaporation experiments. They measured weight loss of wetted blotting paper replicas of several tree species at different heights within the canopy. The average r_{b,i,H_2O} values show excellent agreement with the data obtained from Eq. (7) for the Jaru forest. This supports the suggestion of Finnigan and Raupach (1987) to include a factor 2 (in Eq (6)) in order to account for leaf fluttering and inclination effects.

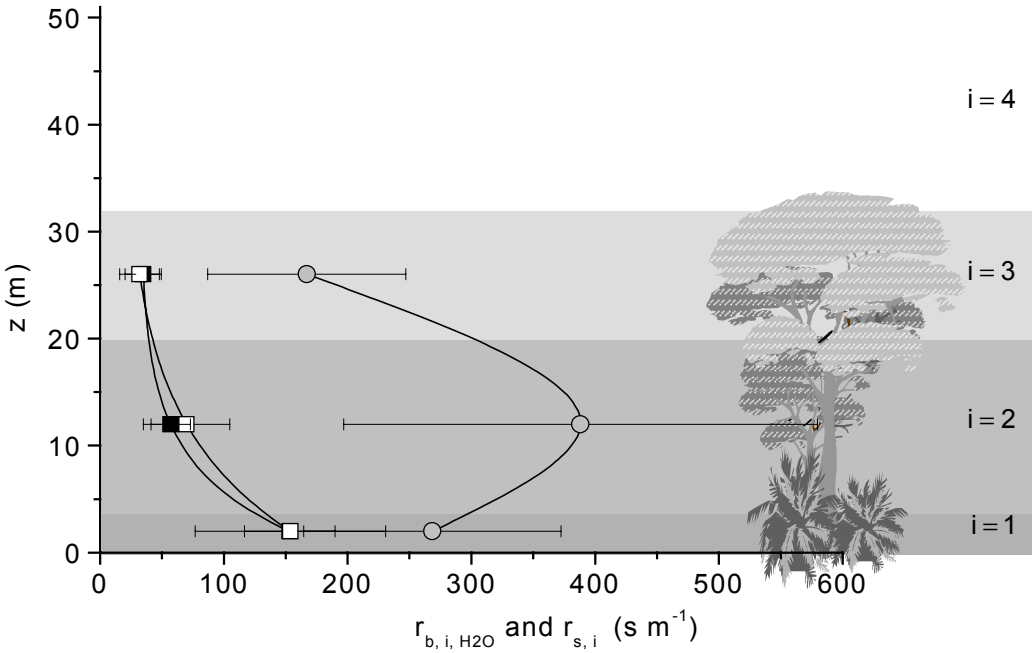

Fig. 1. Vertical profiles of average water vapor boundary layer resistances determined from (open squares) weight loss measurements of blotting paper leave replicas within an central Amazonian rain forest (near Manaus, for details see text) by Roberts et al. (1990) and by Eq. (7) for the RBJ site (full squares). The gray circles represent the stomatal resistances determined from the porometer data of McWilliam et al. (1996).

Additionally the vertical profile of average stomatal resistances $r_{s,i}$ for water vapor, which base on the porometer measurements by McWilliam et al. (1996) are shown in Fig. 1. The lowest stomatal resistances were found in the uppermost canopy layer ($i = 3$), that part of the crown which is to a large extent exposed to direct incoming short wave radiation. The average value is 167 ± 80 s m^{-1} (s.d.). The largest value for $r_{s,i}$ was found for the middle layer ($i = 2$). The higher trees of this layer show characteristics of crown species with low stomatal resistances, but the bulk of the probed species at that part of the canopy has considerably higher resistances than the ground layer species. The average stomatal resistances are 388 ± 192 s m^{-1} and 269 ± 104 s m^{-1} for layer $i = 2$ and 1 respectively. The high standard deviation of $r_{s,2}$ is mainly reflecting the wide spectrum of species included in layer 2.

Comparing the magnitude of average boundary layer and stomatal resistances shows that the vegetation exchange of the two upper layers is clearly controlled by stomatal activity. Stomatal resistances are more than five times the corresponding boundary layer resistances. In the only sporadically ventilated ground layer the ratio of the average resistances is only 1.7, with overlapping uncertainty ranges. Consequently, the scalar exchange at the vegetation-air interface in this lowest sub-canopy layer is also limited by molecular diffusion through the leaf boundary layer.

Direct usage of average stomatal resistances which originate from data, measured during an other experiment, requires comparable environmental conditions. Fig. 2 shows the average stomatal resistances obtained at the uppermost canopy layer for the daytime interval from 0900 LT to 1700 LT, for which porometer data were available. These values are compared to stomatal resistances determined by branch cuvette measurements at the IBAMA camp site (Andreae et al., 2002), at two secondary growth deciduous tree species (*Apeiba tibourbou* and *Hymenaea courbaril*), both commonly distributed in secondary and primary Amazonian forests. From both trees sunlit as well as shade leaves where enclosed by the cuvettes in the crown layer of the canopy. The corresponding sampling periods where earlier in May 1999 (for details see Kuhn et al., 2002b; Rottenberger et al., 2004) than the measurements reported here.

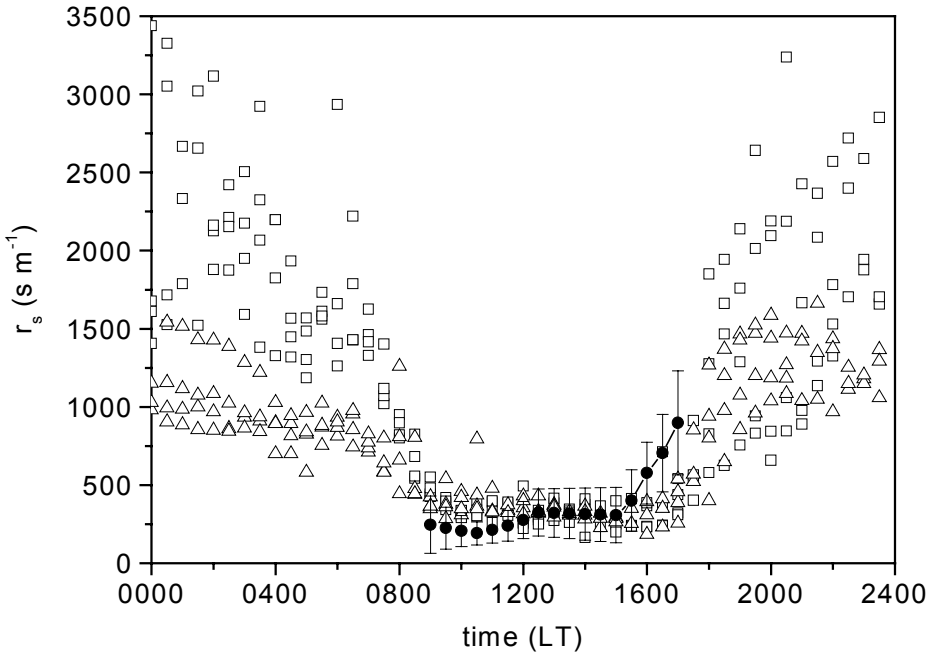

Fig. 2. Diel course of stomatal resistance measured by branch cuvettes at the IBAMA site (open triangles: Apeiba tibourbou; open squares: Hymenaea courbaril) (see Kuhn et al., 2002b; Rottenberger et al., 2004) from two typical Amazonian tree species during May 1999. Average stomatal resistance for the uppermost canopy layer at the Jaru site (full circles, data estimated from daytime porometer measurements by McWilliam et al. (1996) at June1993). Error bars represent standard deviations from the ensemble average.

Table 1

Incoming short wave radiation S_R, air temperature T, specific humidity deficit *SHD*, and soil moisture for the different periods. Average, maximum, and minimum are displayed for each quantity.

	EUST[a]	EUST[b]	EUST[c]	ABR[d]
S_R (W m^{-2})	607.9 881.2 172.4	488.9 935.1 59.9	482.1 883.9 60.8	509.2 841.9 153.2
T (°C)	27.6 30.1 22.0	27.2 30.8 23.2	26.7 30.1 21.7	27.0 30.6 19.2
SHD (g kg^{-1})	8.1 13.0 0.7	4.8 10.9 0.7	4.7 9.5 0.1	6.5 10.9 0.1
Soil moisture (m^3 m^{-3})[e]	0.148 0.192 0.113			0.215 0.260 0.170

[a] Investigation period 18 May to 22 May 99 (primary rain forest, RBJ)
[b] Investigation period 08 May to 12 May 99 (secondary growth Jatoba, IBAMA camp)
[c] Investigation period 02 May to 06 May 99 (secondary growth Pente, IBAMA camp)
[d] ABRACOS investigation period 04, 13, 14 June 93 (primary rain forest, RBJ)
[e] LBA-EUSTACH soil moisture represents the upper 5 cm, ABRACOS soil moisture represents the upper 1 m

The agreement between the average stomatal resistances from the Jaru site and the IBAMA camp site is reasonable. Just the values after 1530 LT from Jaru show an earlier increase of the stomatal resistance. Table 1 shows environmental variables, which are potentially influencing the stomatal aperture. If available, incoming short wave radiation (S_R), air temperature, water vapor deficit (*SHD*), and soil moisture values are shown for all four periods. Air temperature is very similar during all experimental periods. The periods in which the cuvette measurements were made show the lowest values concerning the averages of S_R and *SHD*, followed by the ABRACOS period and the experimental period investigated here. The differences in *SHD* might be responsible for the earlier increase of stomatal resistance compared to the cuvette measurements. The largest water vapor deficits were normally reached around 1500 LT or even later. This coincides with the time when the divergence starts in Fig. 2. *SHD* during the experimental period here was again somewhat higher than during the ABRACOS experiment. Considering this difference together with the somewhat lower soil moisture values compared to the ABRACOS experimental period, the used stomatal resistances for the highest canopy layer represent most likely a lower limit for the actual ones. However, the following time scale analysis is concentrating on the time interval between 1000 LT and 1400 LT, in which, despite the *SHD*

differences, the stomatal resistances determined from the cuvette measurements agree well with those obtained from the porometer measurements (ABRACOS) (Fig. 2). Therefore, the differences between stomatal resistances of the upper canopy layer during ABRACOS and the actual ones during the investigation period here are most likely also not substantial. In lower canopy layers the stomatal resistances of the investigation period here are assumed to be even better represented by values from the ABRACOS experiment, since the stomatal resistances of the sub-canopy plants showed, compared to crown species, a weaker or even no dependence on *SHD* (McWilliam et al., 1996).

4.2 Ozone Exchange Relevant Time Scales (Daytime Situation)

Fig. 3 compares time scales of processes which are relevant for the forest-atmosphere exchange of O_3. Here the vertical profile of the transport time scales reflects findings of Rummel et al. (2005c). The occurrence of coherent structures couples the upper canopy layers $i = 2$, 3 directly to the boundary layer above the forest. Mean time scales or residence times below 200 s are characteristic for daytime conditions. Towards the forest floor the transport is strongly reduced. The average time scale of about 1200 s represents typical daytime exchange times between the ground canopy layer and layer 2 directly above it. In contrast to that, the timescale of layer 2 is already characteristic for the direct exchange with the atmosphere above the forest.

During the daytime situation here, the chemical O_3 sink via reaction with NO plays a minor role in the upper part of the canopy and above. The chemical time scales in the layers $i = 2$ to 4 are almost three orders of magnitude larger than the characteristic transport times. This shows clearly, that the chemically caused O_3 flux divergence in the roughness sublayer is negligible during daytime. Therefore, for flux measurements at the tower top, O_3 can be handled approximately like a flux of an inert trace gas. Towards the ground the chemical sink gains importance. Caused by the reduced transport and increasing NO mixing ratios close to the soil source, both processes have timescales of about the same magnitude.

The time scales of O_3 uptake by vegetation in the upper two canopy layers are considerably shorter than the corresponding time scales of the reaction with NO. They are only one order of magnitude longer than the turbulent transport time scales. In the lowest layer the timescales of all processes, which taken into account, are about the same order of magnitude. Here O_3 soil deposition is somewhat faster compared to the other sink processes. Like mentioned in Section 3.2 the timescale shown here relies just on the ground surface resistance. As shown by Gut et al. (2002b) the relative high aerodynamic resistance within the lowest meters of the canopy has also to be considered for estimation of O_3 soil deposition. This makes the time scale for soil deposition comparable to the time scales of vegetation uptake and chemical loss

via reaction with NO. All three timescales here are about 2000 s.

Fig. 3 shows also a timescale which is characteristic for the O_3 sink strength of the entire canopy layer. It is determined by the quotient of the mean O_3 mixing ratio and the average temporal change $[d([O_3]^S(z_m))/dt]_{+/-}$ (average slope of ramp structures; see Rummel et al. (2005c)) obtained by the wavelet filtering scheme of high frequency O_3 time series at the measuring height z_m = 53 m:

$$\tau_b = -\frac{[O_3]}{\alpha\left[\frac{d}{dt}[O_3]^S\right]_{+/-}} \qquad (10)$$

According to the surface renewal theory (see Paw U et al. (1995)), the weighted temporal change $\alpha[d([O_3]^S(z_m))/dt]_{+/-}$ between consecutive large scale exchange events reflects the net effect of all source and sink processes in the air volume which is renewed by these events. Therefore the corresponding time scale τ_b for O_3 characterizes the bulk sink strength of the vegetation layer or which is equivalent, the O_3 flux. The similar magnitude of τ_b to the time scales of O_3 vegetation uptake τ_{u,i,O_3} points out the dominance of this canopy process as the main O_3 sink. This supports the findings for LBA-EUSTACH 1 campaign in Rummel et al. (2005a) and is in accordance with the wet season results of Fan et al. (1990) for the central Amazonian rain forest.

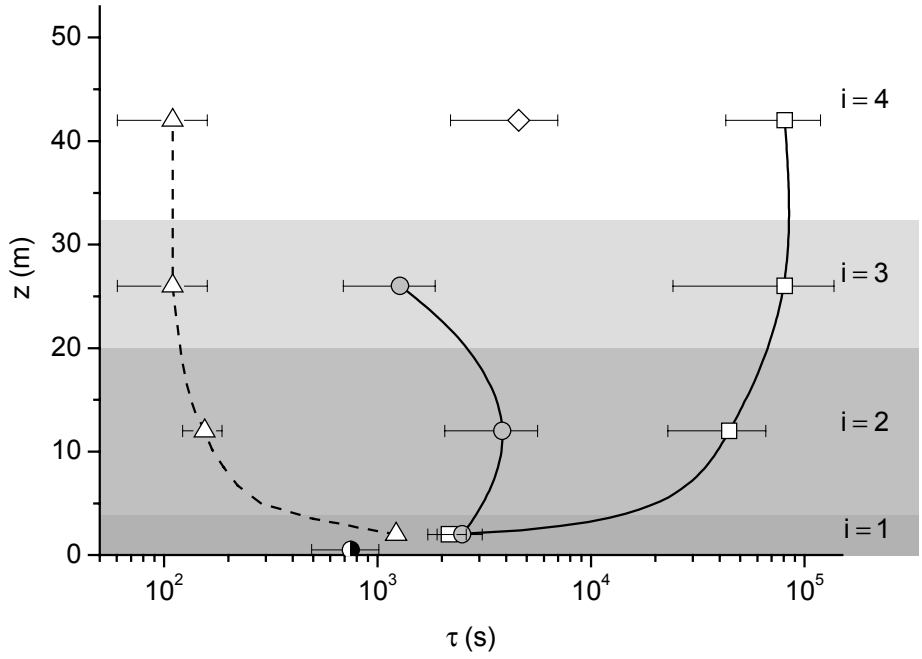

Fig. 3. Average vertical profiles (1000 LT-1400 LT) of O_3 exchange relevant time scales (chemical reaction with NO: open squares; turbulent transport: open triangles; vegetation uptake: gray circles; soil uptake: half open circle; ramp slope: open diamond). Error bars represent standard deviations from the ensemble average.

4.3 NO_x Exchange Relevant Time Scales (Daytime Situation)

Like in Fig. 3 of the previous Section, the time scales of processes which are relevant for the daytime forest-atmosphere exchange of NO_x are compared in Fig. 4. The chemical timescale of NO for the reaction with O_3 is closely connected to the time scale profile of turbulent transport. High O_3 mixing ratios above the canopy and effective downward transport of O_3 into the upper two canopy layers provides very short chemical timescales for NO there. These timescales are in the same order of magnitude than the transport timescales which means that, in contrast to O_3, chemical flux divergence has a considerable influence on NO fluxes measured above the forest canopy. The lowest canopy layer is also of special relevance for the canopy exchange of NO. Due to the damped turbulent transport in this layer the O_3 mixing ratio is also reduced. Despite that fact the chemical time scale of the $NO + O_3$ reaction is on average shorter by a factor of two, compared to the turbulent transport time scale. This agrees nicely with the findings of Rummel et al. (2002). Eddy covariance measurements of NO flux at 11 m height show no significant fluxes at daytime conditions during LBA-EUSTACH 2. Equivalent results were obtained for 20 and 21 May, the only two days these in-canopy NO flux measurements were carried out during LBA-EUSTACH 1 (results not shown). The effect of the chemical transformation of NO is also shown by the average daytime NO profiles in Fig. 6. Within the lowest 4 m almost all NO is oxidized by O_3 to NO_2. The contribution of NO oxidation via RO_2 and HO_2 radicals is assumed to be small in these lowest layer due to largely reduced photochemical production in the lowest part of the canopy. These radicals are also assumed to be deposited very fast to nearly all surfaces and therefore transport of high amounts down into the lowest layer might also be unlikely. Also due to the highly attenuated short wave radiation in the lowest layer a negligible amount of the produced NO_2 is transformed back by photolysis. The time scale of this reaction is more than one order of magnitude larger than the time scale for the oxidation of NO by O_3. The photolysis time scale decreases steadily with increasing height approaching a value comparable to the oxidation of NO by O_3 above the canopy.

In addition the time scales of vegetation and soil uptake of NO_2 are shown in Fig. 4. The displayed range of the vegetation uptake time scale results from considering or neglecting a mesophyll resistance (Section 3.2) according to Gut et al. (2002b). In the upper part of the canopy the vegetation uptake of NO_2 has the largest time scales of all processes which are compared in Fig. 4. Especially within the uppermost canopy layer ($i = 3$) the loss of NO_2 by photolysis is obviously substantially higher than the potential uptake capacity of the vegetation (although this layer has the highest LAI and the lowest stomatal resistances). In the middle vegetation layer ($i = 2$) both NO_2 loss terms show about the same order of

magnitude if a mesophyll contribution to the leaf resistance is negligible. In comparison to the turbulent transport the NO_2 vegetation uptake in the upper part of the canopy ($i = 1$ and 2) is rather slow.

In the lowest layer ($i = 1$) the time scale ratio between vegetation uptake and turbulent transport is considerably smaller than above. The characteristic time scale for soil surface uptake is about 2600 s (if the high aerodynamic resistance of the lowest meter above the forest floor is considered again (Gut et al., 2002b)), and therefore comparable to the vegetation uptake within that lowest layer. All this, together with the relative fast oxidation of soil emitted NO to NO_2 makes this lowest layer crucial for the net NO_x emission of the ecosystem during daytime.

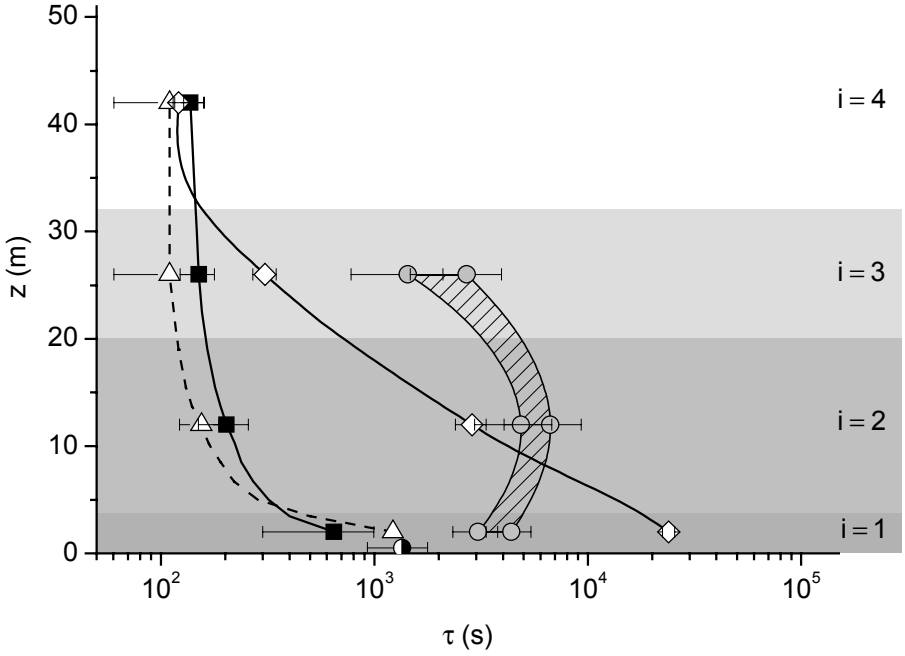

Fig. 4. Average vertical profiles (1000 LT-1400 LT) of NO_x exchange relevant time scales (chemical reaction with O_3: solid squares; photolysis: open diamonds; turbulent transport: open triangles; vegetation uptake: gray circles (the hatched area marks the range of NO_2 uptake time scales with and without mesophyll resistances, see text); soil uptake: half open circle). Error bars represent standard deviations from the ensemble average.

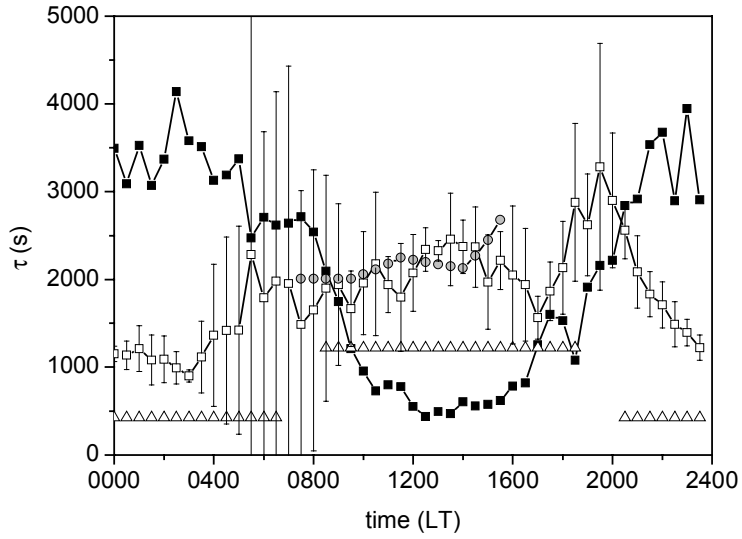

Fig. 5. Diel variation of mean characteristic time scales of the chemical reaction NO + O_3 (for O_3:open squares; for NO: full squares), vegetation uptake of O_3 (gray circles), and turbulent transport (open triangles) in the lowest canopy layer i = 1 (18 to 22 May). Error bars representing standard deviations from the ensemble are just shown for one curve in the interest of clarity.

4.4 Nocturnal Time Scales of the Lowest Canopy Layer

For the discussion of the nocturnal situation within the canopy, the diurnal course of time scales for the chemical reaction NO + O_3 and for turbulent transport in the lowest canopy layer are compared in Fig. 5. The night time conditions are substantially different from those found during day. In contrast to the upper canopy, where the turbulent transport is reduced during night, the nocturnal transport in the lowest part of the canopy is enhanced. Compared to daytime hours the corresponding time scale is considerably shorter during night. In addition the stable stratification in the upper crown layer (and above), suppresses effective incursion of O_3 from aloft. As a consequence the chemical timescale for NO in the lowest canopy layer is larger by a factor of 7 compared to daytime. This together with the shorter transport time scale enables relative constant NO mixing ratios of 1.5 - 2 ppb, to occur trough the main part of the nocturnal canopy (see Fig. 6).

The lack in a substantial chemical NO flux divergence in the lower canopy during night supports the relative good agreement found in Rummel et al. (2002) between soil NO emissions measured by dynamic chambers and the eddy covariance measurements of NO flux at 11 m height within the stem space. The relative large amount of NO which is mixed up to the crown layer during night, makes deep penetration of turbulent eddies not necessary to export considerable amounts of NO from the canopy.

4.5 *Impact of Uptake Processes on Biogenic NO_x*

The time scale of a single process is a measure to assess its relative weight compared to all parallel processes affecting a constituent simultaneously. For example, during daytime in the lowest canopy layer, the relative slow turbulent transport compared to (i) the oxidation of soil emitted NO to NO_2 and (ii) negligible photolysis of NO_2 ensures that almost no biogenic NO_x is able to leave the canopy as NO. On the other hand, for an absolute quantification of individual processes, e.g., chemical reactions, the corresponding mixing ratios are necessary.

Fig. 6 shows mean day and night time profiles of NO_x, NO, NO_2, and O_3 mixing ratios for the 4 day intensive investigation period at the end of LBA-EUSTACH 1. The daytime NO_2 profile (Fig. 6 (d)) is clearly divided into two parts, which can be at least qualitatively explained by the results of the preceding time scale analysis. Due to effective turbulent transport through the upper two third of the forest, only a weak NO_2 gradient is visible between 11 m and the roughness sub-layer above the vegetation. The mean daytime NO_2 mixing ratios above 11 m are below 0.1 ppb. The sub-canopy below 11 m shows higher average NO_2 mixing ratios up to 0.55 ppb due to (i) the longer residence time, (ii) missing photolysis of NO_2 (Fig. 6 (a)), and (iii) a high production rate by NO oxidation (see Fig. 4).

Comparing the obtained average mixing ratios with the compensation point range 0.53 - 1.6 ppb found by Sparks et al. (2001) suggests, that NO_2 uptake by vegetation seems to be most likely for the lowest canopy part. In the upper canopy layers the NO_2 mixing ratios are probably below corresponding compensation points. An indication for a positive correlation between compensation NO_2 mixing ratios and ultraviolet radiation for pine seeds was just found by Hari et al. (2003). An equivalent behavior of for tropical tree species would cause height dependent compensation points, increasing from the forest floor to the crown region due to increasing ultraviolet radiation levels. Consequently, an uptake of NO_2 within the upper layers of the canopy would therefore be even more unlikely (due to decreasing NO_2 mixing ratios).

However, because no leaf level measurements (cuvette) of NO_2 exchange were deduced during the LBA-EUSTACH field campaigns, there is no direct information available about possible compensation mixing ratios for the tree species at RBJ. The greenhouse fumigation experiments by Gut et al. (2002b) were carried out at NO_2 mixing ratios, which were 10 to 100 times higher than the NO_2 measured in the forest and provide therefore also no information on that concern. Owing to that, three possible scenarios were calculated (Fig. 7) to assess the spectrum of ecosystem effects on NO_x originating from biogenic soil emissions of NO during daytime. They base on a steady state budget estimation, including the NO_2 uptake by the three canopy layers (i = 1, 2, 3) and the soil surface (i = 0), which is closely oriented at the measured NO_2

mixing ratios. The budget for each layer is calculated with the mean NO_2 mixing ratio, the corresponding leaf resistance (Eq. (4) weighted by layer specific LAI), and the NO_2 soil deposition resistance (at RBJ) according to Gut et al. (2002b). The scenarios are characterized by different prescribed, vertically constant NO_2 leaf compensation points (mixing ratios), which are 1 ppb for scenario (a), 300 ppt for scenario (b), and scenario (c) without a compensation point. Hereby the NO_2 vegetation emission rates are assumed to correspond with the layer averaged emissions of the tropical forest investigated by Sparks et al. (2001). These single emission rates were normalized and weighted by the corresponding LAI fractions of the RBJ canopy layers.

In Fig. 7 possible influence of the single canopy layers and the soil surface on the net NO_x emission is shown in percent of the average NO soil emission during the investigation period here of about 4.1 ng N $m^{-2}s^{-1}$ (Gut et al., 2002a). In the following discussion all fluxes are quoted as percentage of this soil emission flux.

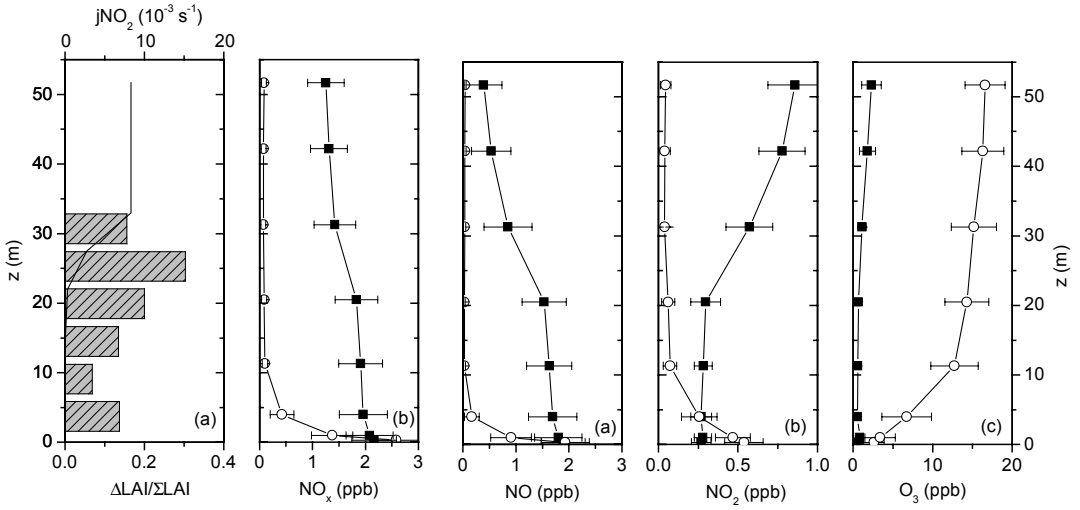

Fig. 6. Average vertical profiles of (b) NO_x, (c) NO, (d) NO_2, and (e) O_3 mixing ratios at daytime (1000 LT – 1400 LT; open circles) and night time (2200 LT – 0200 LT; full squares) for the investigation period 18 to 22 May. Error bars represent standard deviations from the ensemble average. Profiles of the relative LAI and j_{NO2} are shown in (a).

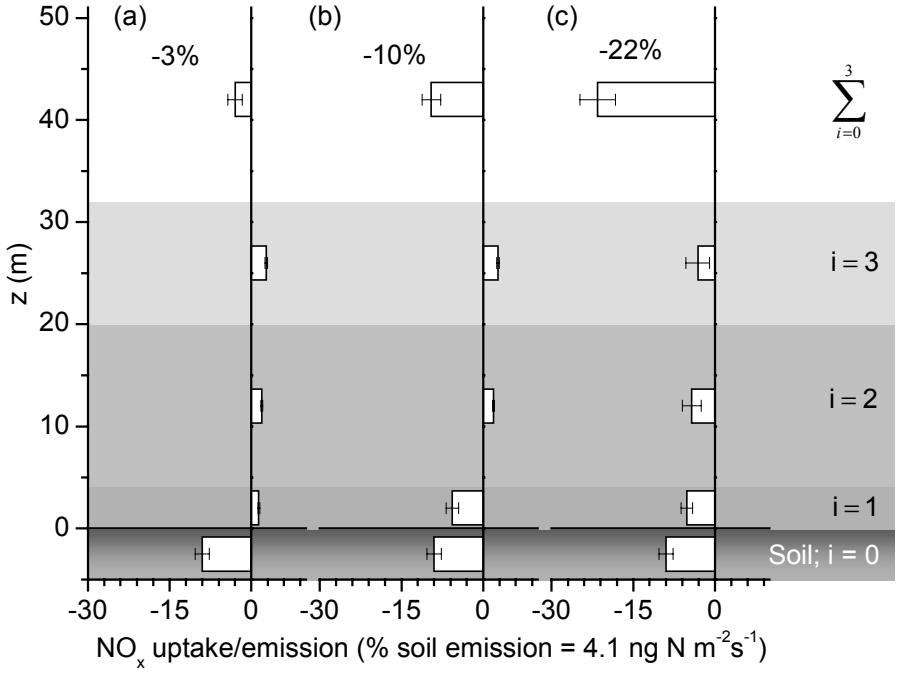

Fig. 7. Integral and layer wise mean modification of biogenic NO_x within the canopy volume during daytime (1000 LT – 1400 LT). Estimates have been performed for three scenarios of different compensation points:(a) 1 ppb, (b) 300 ppt, (c) no compensation point. Error bars represent standard deviations for the ensemble average.

The obtained NO_2 soil deposition flux here accounts for about -9% of the soil emission during day. This is significantly lower than the results of Gut et al. (2002b) and Jacob and Bakwin (1992). Gut et al. (2002b) got a mean daytime NO_2 deposition flux accounting for about -34% of the NO soil emission. Since their measurements were performed during the burning season (LBA-EUSTACH 2), they suspected a considerable part of the NO_2 deposited to the forest floor, to originate not from biogenic NO soil emissions, but from biomass burning (imported from above the canopy). The simulations of Jacob and Bakwin (1992) were performed for wet season conditions. During daytime, they got a relative NO_2 soil deposition of about -19% as a consequence of a lower soil resistance (compared to RBJ) and neglecting the aerodynamic resistance in the lowest part of the canopy. But, according to Gut et al. (2002b) this aerodynamic resistance is substantial (~700 s m^{-1} compared to mean a soil resistance of ~340 s m^{-1} for RBJ) and is the main limitation for NO_2 soil deposition during daytime. The fact, that it is included in the calculation for RBJ here, explains the differences in the relative NO_2 deposition rates to their results.

In scenarios (a) and (b) low NO_2 mixing ratios in the upper two canopy layers i = 2, 3, caused by effective turbulent transport, are below the assumed compensation points of

1 ppb and 300 ppt, respectively. The obtained emission rates are 1.9% and 2.7% for layer 2 and 3 respectively. The behavior of the lowest vegetation layer ($i = 1$) differs in both scenarios. Since the NO_2 mixing ratios in this layer have the highest probability to be above a potential compensation point, this case was considered in scenario (b) by the low compensation point of 300 ppt. Therefore, whereas in scenario (a) the NO_2 mixing ratio of layer ($i = 1$) is also below the assumed compensation point of 1 ppb, resulting in an additional emission rate of 1.4%, scenario (b) results in an uptake of -5.1% for this lowest vegetation layer. Setting the mesophyll resistance to zero, like in the calculations of Jacob and Bakwin (1992) would enhance this fraction to -7.4%, which is comparable to -6.7% they got for their lowest model layer. Their three times lower NO_2 mixing ratio in that layer was nearly compensated by a higher LAI fraction (compared to RBJ) and the low cuticula resistance they used for NO_2 equivalent to O_3 deposition (for a discussion on that issue, see below). Scenario (c) assumes no compensation point to exist, which results in a NO_2 uptake through the entire vegetation. The obtained NO_2 uptake rates of layers $i = 2$ and 3 are -4.3% and -3.2% respectively. Neglecting again the mesophyll resistance the uptake in these layers also increases to -5.9% ($i = 2$) and -6.3% ($i = 3$).

The integral effect of the ecosystem on NO_x originating from soil NO emissions, indicated by the uppermost bars in Fig. 7, shows a relatively wide range for the different scenarios. In scenario (a) the net effect is almost negligible with a reduction of only about -3 ± 1.3% (s.d). Here the soil deposition is nearly compensated by the bulk canopy emission. Additional NO_2 uptake in the lowest vegetation layer in scenario (b) reduces the soil emission by -10 ± 1.7%. NO_2 uptake by all three vegetation layers in scenario (c), which assumes no compensation points to exist, results in an integral reduction of about -22 ± 3.3%. The range of the resulting reduction effect caused by vegetation emphasizes the importance of a possibly existing compensation point (the conundrum raised by Lerdau et al. (2000)) for the chemical composition of the boundary layer, particularly during the wet season in remote areas of the tropics, where biogenic NO emission is a main source of atmospheric NO_x.

But the range of the possible vegetation effect is also largely dependent on the cuticula resistance. The results from the RBJ forest, show even for scenario (c) (with no NO_2 compensation point) much lower NO_x reduction compared to the results of Jacob and Bakwin (1992) and Jacob and Wofsy (1990) with an average reduction between -60% and -80% at noon time. A considerable cuticular NO_2 deposition was necessary in their model calculations. Otherwise the simulated nocturnal NO_x accumulation would have exceeded the NO_y mixing ratios Bakwin et al. (1990b) measured just above the canopy. The mean NO_y mixing ratio was quite constant during the course of the day and did not show a significant nocturnal increase.

In contrast to that, a pronounced nocturnal NO_x accumulation was registered for the experimental period here. As visible in the average night time profiles in Fig. 6, within the forest the main fraction of NO_x occurs as NO. Above the canopy the ratio changes towards NO_2, due to O_3 mixing ratios increasing with height. Fig. 8 shows the NO_x time series between dusk and midnight at three heights; within the stem space (11.3 m), at the top of the closed canopy (31.3 m), and at the uppermost measuring level (51.7 m) above the forest. Beside a slight reduction of the absolute NO_x mixing ratios from the stem space up to the top level, a fairly uniform and steady increase occurs at all heights. The average accumulation rate is about 0.22 ppb h^{-1}. The pronounced increase at the top level indicates, that despite the stable stratification within the crown layer and above, a considerable fraction of biogenic NO_x is able to leave the canopy during night.

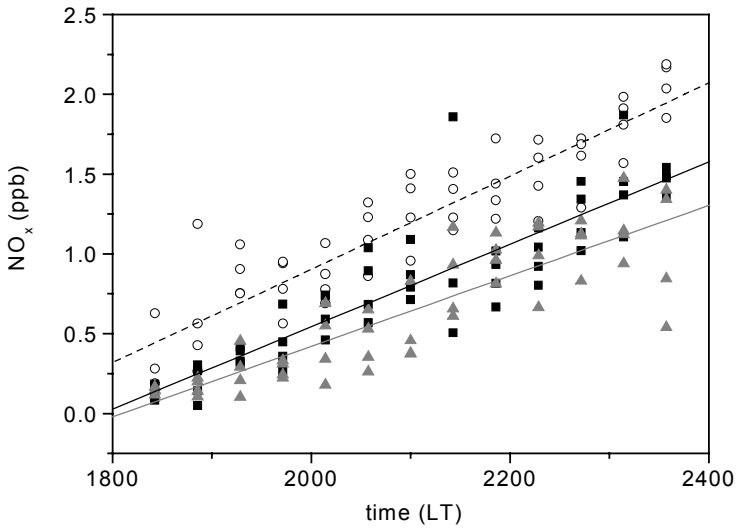

Fig. 8. NO_x time series between 1800 LT and 2400 LT for all 4 days of the investigation period 18 to 22 May, at 11.3 m (open circles), at 31.3 m (black squares), and at 51.7 m (gray triangles). The lines mark the correspondent trends obtained by linear regression analysis.

If the volume below the upper measuring level (51.7 m) is in idealized form assumed to be well mixed and exchange with layers above to be negligible (due to the vertically continuing stable stratification), a simple box budget estimate can be made for that volume. Considering integral (i = 1, 2, 3) plant surface NO_2 deposition (with the cuticula resistance of 20000 s m^{-1} used here), the average soil emission of NO, and the NO_2 ground deposition, results in NO_x accumulation rate of ~0.45 ppb h^{-1}. Despite the fact that all sink terms in the budget are based on the mean nighttime NO_2 mixing ratios (between 2200 LT and 0200 LT) which represent an upper limit for NO_2 values (and consequently also for the corresponding sink strength) in the time interval from 1800 LT to 2400 LT at each vegetation layer, the resulting NO_x accumulation is about a factor of 2 higher than the measured average accumulation. One possibility to reconcile this discrepancy is to assume, the cuticular deposition to be larger.

The sensitivity of the integral relative NO_x reduction (calculated by the steady state budget approach) on variation of the cuticula resistance for NO_2 is shown in Fig. 9 for day and night time conditions. Scenario (b) with a compensation point of 300 ppt and scenario (c) without a compensation mixing ratio are displayed for the daytime period. Especially in scenario (b) where net NO_2 uptake occurs just in the lowest vegetation layer, the NO_x reduction shows a only a weak dependence on the cuticula resistance. But also without any net plant emission of NO_2 (because of low mixing ratios; scenario (c)) a large effect on the relative NO_x reduction is just appearing for cuticula resistances below ~3000 s m^{-1}, due to the large stomatal uptake during daytime. Contrastingly, because of the largely reduced impact of stomatal uptake, the dependence of the relative NO_x reduction on the cuticula resistance is much stronger during night. The application of a cuticula resistance for NO_2 of 1000 s m^{-1} as used by Jacob and Wofsy (1990), results in an relative NO_x deposition of -61 ± 9.4% for night time conditions. This would reduce the calculated mean nocturnal NO_2 accumulation to ~0.20 ppb h^{-1} which agrees nicely the measured one (~0.22 ppb h^{-1}).

But such low cuticula resistances contradict the findings of leaf scale measurements at the IBAMA camp site (see Rummel et al. (2005a)) and the results of the greenhouse experiments by Gut et al. (2002b).

At the end of the LBA-EUSTACH 2 experiment branch cuvette measurements of O_3 exchange on the deciduous tree *Hymenaea courbaril* L. were performed at the IBAMA camp site. The results suggest a minimum cuticula resistance for O_3 of ~4000 s m^{-1}. Of course one has to bear in mind that these results are just obtained from one out of a large number of species of the tropical canopy.

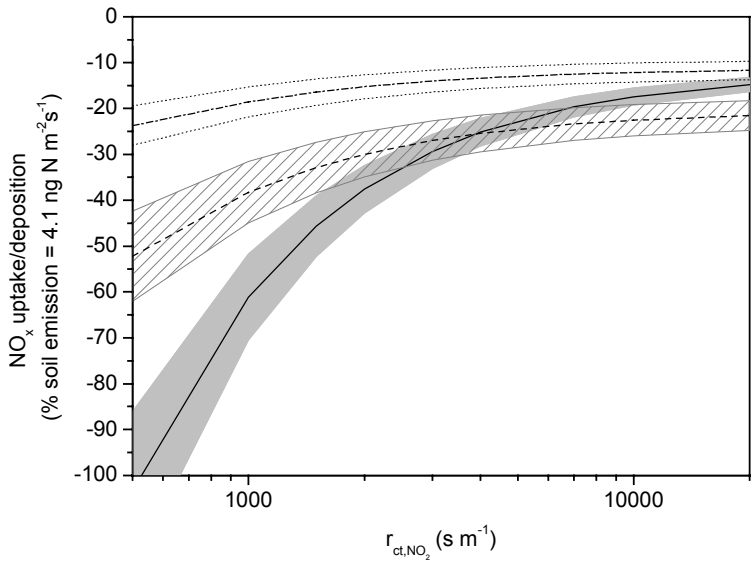

Fig. 9. Mean ecosystem NO_x uptake/deposition in % of the NO soil emission as function of the cuticula resistance for daytime hours (1000 LT - 1400 LT): scenario (b) (dashed dotted line); scenario (c) (dashed line) and during night time hours (2200 LT - 0200 LT) scenario (c) (solid line).The corresponding ranges represent standard deviations.

However, in addition the greenhouse cuvette measurements by Gut et al. (2002b) for another Amazonian tree species (*Pouteria glomerata*) were also indicating a considerable cuticula resistance for O_3 (with negligible mesophyll resistance). They obtained no significant O_3 deposition for night time and no statistically insignificant difference between leaf resistance and stomatal resistance for daytime hours. This supports the suspicion that the applied 4000 s m^{-1} is most likely a lower limit for r_{ct,O_3}. The cuticula resistance for NO_2 is usually assumed to be larger or at least not smaller than for O_3 (e.g. Wesely, 1989). Since Gut et al. (2002b) also determined stomatal and leaf resistances on two Amazonian tree species (*Laetia corymbulosa* and *Pouteria glomerata*) by fumigation experiments, cuticula resistances could be directly determined by the application of the leaf resistance model Eq. (4). Even for unrealistically high mesophyll resistances, minimum cuticula resistances of 5400 s m^{-1} and 9400 s m^{-1} are necessary for *Laetia corymbulosa* and *Pouteria glomerata*, respectively, to obtain their measured leaf resistances with the corresponding stomatal resistances.

At first glance, like the difference between leaf scale and canopy scale approaches concerning the existence of a NO_2 compensation point during daytime, raised by Lerdau et al. (2000), there is also a difference

between the cuticula resistances obtained from the leaf and canopy level measurements.

One thing has to be taken into account especially when nocturnal NO_2 surface uptake is discussed here in the tropics. The air is regularly saturated from 2200 LT until 0700 LT, which means a large fraction of the vegetation surfaces in the crown region is covered by dew during the main part of the night. This might be lightly different in the ventilated cuvette interior. Generally the NO_2 absorption into the aqueous phase should be rather small because of the relative poor solubility and low atmospheric mixing ratios (Schwartz and White, 1983). But NO_2 absorption depends also on the chemical composition of the liquid film. NO_2 uptake to aqueous solutions containing reducing constituents was found to be enhanced (for a review see also Schwartz and White, 1983). Is the solution alkaline, the uptake is additionally intensified. But the impact at the end of the wet season might be rather small. For the burning season, when much higher aerosol concentrations may lead to larger fractions of dissolved substances in the dew like found in rain water (Andreae et al., 1990) the effect could be larger. Its not very likely that dew water is alkaline, even if an enhanced input of ashes during the dry season would act in that direction.

Another NO_2 consuming process which occurs at wet surfaces is the heterogeneous hydrolysis forming HONO and HNO_3 :

$$2NO_2 + H_2O \xrightarrow{surface} HONO + HNO_3 \quad (11)$$

According to Kleffmann et al. (1998) the corresponding NO_2 removal rate shows a distinct proportionality to the surface area to volume ratio S/V and can be estimated by a relative simple parameterization:

$$\frac{dNO_2}{dt} = \frac{1}{4}\bar{\upsilon}_{NO_2}\gamma_{up}\frac{S_A}{V}NO_2 \quad (12)$$

Here $\bar{\upsilon}_{NO_2}$ is the average speed of NO_2 molecules and γ_{up} the accomodation coefficient found to be 10^{-6} for water. Applied to the vegetation and ground surface $S_A = LAI + A_{ground}$ within the air volume up to the top measuring height, an estimate for a potential reduction of NO_2 can be made. By using the highest average NO_2 mixing ratio (within the canopy) from the crown layer and the whole vegetation surface this estimate is rather an upper limit for the contribution of the process to the weakening of nocturnal NO_x accumulation in the volume. The obtained hourly NO_2 reduction rate of -0.02 ppb h^{-1} is about one order of magnitude to low to account for the discrepancy between the calculated and the measured nocturnal NO_x accumulation.

So far this discrepancy is based on the assumption, that at night time no vertical exchange of NO_x takes place with layers above the top measuring height. Under this assumption a cuticular NO_2 deposition as large as postulated by Jacob and Wofsy (1990) and Jacob and Bakwin (1992) is necessary. On the other hand, despite the stable stratification in the upper part of the crown layer and above, obviously a considerable fraction of NO_x is able to leave the canopy during night.

The temporal NO_x increase at the upper measuring level which is just slightly weaker than in the sub-canopy in the first half of the night (see Fig. 8), which is an indication that NO_x might even be transferred into heights above 51.7 m. A permanent growth of the nocturnal boundary layer during the course of the night from about 200 m (2000 LT) up to nearly 400 m (0500 LT) (reported by Nobre et al. (1996) for the Jaru forest site in July 1993) might provide a volume, which is large enough to hold the exported NO_x fraction and simultaneously prevent an effective downward transport of O_3 from the residuum layer above. With the assumed lower limit of the cuticula resistance of 4000 s m^{-1} (the value for O_3 determined by the branch cuvette measurements) the average integral reduction of NO_x is about -25 ± 3.0% at night (see Fig. 9) would require a volume height of ~90 m to result in the measured nocturnal NO_x accumulation. A 10 m higher volume would be necessary, when a cuticula resistance of 20000 s m^{-1} (Wesely, 1989) (which was used for the time scale estimates) is used, which leads to a nocturnal NO_x reduction of -14.8 ± 1.6%.

Even if a lot of potential feedbacks between different processes can not be estimated without a relatively complete vegetation and boundary layer model, the sum of experimental information gave some indication that the low cuticula resistances might not be absolutely necessary to explain the low night time accumulation of NO_x.

For daytime conditions the usage of r_{ct,NO_2} = 4000 s m^{-1} results also in an average integral NO_x reduction of -25 ± 4.0%. This higher daytime export of biogenic NO_x compared to the findings of Jacob and Bakwin (1992) mainly as a result of the effective transport mechanisms discussed in Rummel et al. (2005c) must have direct consequences on the photochemistry of the boundary layer. Taking into account the two times higher average soil emissions here (Gut et al., 2002a) compared to the ABLE 2B (wet season) experiment (Bakwin et al., 1990a) the absolute NO_x input to the tropical boundary layer in combination with relative high levels of biogenic VOCs (Kuhn et al., 2002a) might lead to higher photochemical production of O_3 in the lower boundary layer for all scenarios (a) to (c) during this experimental period at the end of the wet season. O_3 mixing ratios up to 20 ppb measured at the tower top, which is more than a factor 2 higher than the mixing ratios found during the ABLE 2B experiment by Fan et al. (1990), are an indication for that.

5 Summary and Conclusions

The comparison of time scales for different canopy processes provided information about their potential impact on O_3 and NO_x exchange between this Amazonian rainforest and the atmosphere.

1. It was found, that for daytime O_3 deposition the vegetation uptake within the uppermost canopy layer represents the main O_3 sink. On the

other hand, due to a highly efficient vertical turbulent transport, no significant chemical O_3 flux divergence occurs above the forest, which is a benefit for the applicability of flux measurement techniques.

2. For NO_x exchange, the lowest canopy layer turned out to play a crucial role. Here in the lowest part of the canopy the transport time scale gets considerably larger than the chemical time scale of NO oxidation by O_3 imported from aloft. This in concurrence with a negligible photolysis rate close to the ground ensures that nearly all soil emitted NO is transformed into NO_2 within the lowest 4 m of the canopy. Therefore during daytime the main fraction of biogenic NO_x is available as NO_2 for potential scavenging by vegetation over the whole depth of the canopy.

3. At night time a reversed ratio of transport and chemical ($NO + O_3$) time scales within the canopy enables NO to reach higher regions of the forest. Potential emission of NO_x as NO is therefore more likely during night.

The distinct turbulence partitioning of the canopy during daytime has an additional importance if the possibility of a bi-directional exchange between plant leaves and canopy air is considered. In the lowest layer of the canopy the probability is highest for NO_2 mixing ratios to be above a potential compensation point which controls the direction of the leaf-canopy air exchange.

Unfortunately the conundrum raised by Lerdau et al. (2000), about the existence of an NO_2 compensation mixing ratio can also not solved by the results obtained in this study. For this, beside canopy scale information, extensive leaf scale measurements of NO_2 exchange under environmental mixing ratio levels are necessary. Three scenarios characterized by different NO_2 compensation points were calculated instead on the basis of measured NO and NO_2 profiles. For daytime conditions, the resulting integral ecosystem NO_x reduction ranges from -3% (of average soil emission), in the case of NO_2 emitting vegetation, up to -25% for NO_x uptake by all vegetation layers. For night time condition the maximum NO_x reduction of also -25% was obtained for the vegetation-soil system. The considerably smaller vegetation reduction of NO_x compared to the prominent model estimations by Jacob et al. (1990) is mainly a consequence of a lower LAI and distinctively higher mesophyll and cuticula resistances used in the leaf model for RBJ forest. Although canopy scale measurements show some indication for NO_2 cuticula resistances as low as used by Jacob et al. (1990) (1000 s m^{-1}), there is experimental evidence by leaf level cuvette field and greenhouse measurements for a NO_2 minimum cuticula resistance of ~4000 s m^{-1}. Therefore, like the difference between leaf scale and canopy scale approaches concerning the existence of a NO_2 compensation point during daytime, raised by

Lerdau et al. (2000), the results from tropical tree species here suggest also a difference between the cuticula resistances obtained from leaf level (bottom-up) and canopy level (top-down) measurements.

Since more experimental effort is necessary to confirm or refute this additional night time "conundrum" on the cuticular NO_2 deposition, the application of sophisticated SVAT models on the basis of the LBA-EUSTACH dataset might be promising at that point. With a SVAT model the explicit influence of different parameters on the reduction capacity of the ecosystem can be investigated in more detail and under consideration of feedback mechanisms [*C. Ammann et al.,* manuscript in prep.].

However, the obtained higher input of biogenic NO_x from the forest ecosystem in Rondônia (higher NO soil emission in combination with a smaller NO_x reduction through the canopy) into the tropical boundary layer during LBA-EUSTACH 1 might cause enhanced photochemical production of O_3 in the lower boundary layer, compared to the ABLE2B (wet season) experiment. O_3 mixing ratios, measured above the forest, higher by more than a factor of 2 are a strong indication for that.

Acknowledgements

This research is supported by the "Environmental and Climate Programme" (Project LBA-EUSTACH, ENV4-CT97-0566) of the European Union, and by the Max Planck Society. We would like to thank the staff at INCRA (Instituto Nacional de Colonização e Reforma Agrária), especially Jaõ Luis Esteves, Eduardo Conceição, and Claudionor Rodrigues. Further, Carlos Brãndao and the staff of IBAMA (Instituto Brasileiro do Meio Ambiente e dos Recursos Naturais Renováveis) in Ji-Parana are gratefully acknowledged for their help in installing and maintaining the infrastructure at the forest. We are indebted to Beatriz E. Gomes (Universidade Federal de Rondonia, Ji Parana) for support concerning everything. We are also grateful to Monika Scheibe, Michael Welling, and Wesley Saores da Silva for assisting us in the field.

References

Andreae, M.O., Talbot, R.W., Berresheim, H., Beecher, K.M., 1990. Precipitation chemistry in central Amazonia. Journal of Geophysical Research, 95 (D10), 16987-16999.

Andreae, M.O., Artaxo, P., Brandao, C., Carswell, F.E., Ciccioli, P., da Costa, A.L., Culf, A., Esteves, J.L., Gash, J.H.C., Grace, J., Kabat, P., Lelieveld, J., Mahli, Y., Manzi, A.O., Meixner, F.X., Nobre, A.D., Nobre, C., Ruivo, M.d.L.P., Silva-Dias, M.A., P., S., Valentini, R., von Jouanne, J., Waterloo, M.J., 2002. Biogeochemical cycling of carbon, water, energy, trace gases, and aerosols in Amazonia. Journal of Geophysical Research, 107

(D20), 8066, doi: 10.1029/2001 JD000524.

Bakwin, P.S., Wofsy, S.C., Fan, S.-M., Keller, M., Trumbore, S., da Costa, J.M., 1990a. Emission of nitric oxide (NO) from tropical forest soils and exchange of NO between the forest canopy and atmospheric bounday layers. Journal of Geophysical Research, 95 (D10), 16'755-16'764.

Bakwin, P.S., Wofsy, S.C., Fan, S.M., 1990b. Measurements of Reactive Nitrogen-Oxides (NO_y) within and above a Tropical Forest Canopy in the Wet Season. Journal of Geophysical Research-Atmospheres, 95 (D10), 16765-16772.

Baldocchi, D., 1988. A multi-layer model for estimating sulfur dioxide deposition to a deciduous oak forest canopy. Atmospheric Environment, 22 (5), 869-884.

Beier, N., Schneewind, R., 1991. Chemical reactions of gases in tubes of probing systems and their influence on measured concentrations. Annales Geophysicae, 9, 703-707.

Chen, J.M., Ibbetson, A., Milford, J.R., 1988. Boundary-layer resistances of artificial leaves in turbulent air 2: leaves inclined to the mean flow. Boundary-Layer Meteorology, 45, 371-390.

Crutzen, P.J., 1979. The role of NO and NO_2 in the chemistry of the troposphere and the stratosphere. Annual Review of Earth and Planetary Sciences, 7, 443-472.

Crutzen, P.J. (Editor), 1986. The role of the tropics in atmospheric chemistry. The Geophysiology of Amazomia. John Wiley, New York, 107-130 pp.

Davidson, E.A., Kingerlee, W., 1997. A global inventory of nitric oxide emissions from soils. Nutrient Cycling in Agroeecosystems, 48, 37-50.

Fan, S.M., Wofsy, S.C., Bakwin, P.S., Jacob, D.J., Fitzjarrald, D.R., 1990. Atmosphere-biosphere exchange of CO_2 and O_3 in the central Amazon forest. Journal of Geophysical Research, 95 (D10), 16851-16864.

FAO, 2001. Global forest ressources assessment 2000, FAO Forestry Pap. No. 140, UN Food Agric. Org., Rome.

Finnigan, J., Raupach, M.R., 1987. Transfer processes in plant canopies in relation to stomatal characteristics. In: G. D. F. E. Zeiger, and I.R. Cowan (Editor), Stomatal Function. Stanford University Press, Stanford, California, pp. 385-427

Ganzeveld, L.N., Lilieveld, J., Dentener, F.J., Krol, M.C., Bouwman, A.J., Roelofs, G.-J., 2002. Global soil-biogenic NO_x emissions and the role of canopy processes. Journal of Geophysical Research, 107, 10.1029/2001JD001289.

Gash, J.H.C., Nobre, J.M., Roberts, J.M., Victoria, R.L., 1996. An overview of ABRACOS. In: J. H. C. Gash, J. M. Nobre, J. M. Roberts and R. L. Victoria (Editors), Amazonian Deforestation and Climate. John Wiley, New York

Grace, J., Wilson, J., 1976. The boundary layer over a Populus leave. J. exp. Bot., 27, 231-241.

Gut, A., van Dijk, S.M., Scheibe, M., Rummel, U., Welling, M., Ammann, C., Meixner, F.X., Andreae, M.O., Lehmann, B.E., 2002a. NO emission from an Amazonian rain forest soil: Continuous measurements of NO flux and soil compensation concentration. Journal of Geophysical Research, 107 (D20), 8057, doi: 10.1029/2001 JD000521.

Gut, A., Scheibe, M., Rottenberger, S., Rummel, U., Welling, M., Ammann, C., Kirkman, G.A., Kuhn, U., Meixner, F.X., Kesselmeier, J., Lehmann, B.E., Schmidt, J., Müller, E., Piedade, M.T.F., 2002b. Exchange fluxes of NO_2 and O_3 at soil and leaf surfaces in an Amazonian rain-forest. Journal of Geophysical Research, 107 (D20), 8060, doi:10.1029/2001JD000654.

Hari, P., Raivonen, M., Vesala, T., Munger, J.W., Pilegaard, K., M., K., 2003. Ultraviolet light and leaf emission of NO_x. Nature, 422, 134.

Harriss, R.C., Garstang, M., Wofsy, S.C., Beck, S.M., Bendura, R.J., Coelho, J.R.B., Drewry, J.W., Heoell Jr., J.M., Matson, P.A., McNeal, R.J., Molion, L.C.B., Navarro, J.W., Rabine, V., Snell, R.L., 1990. The Amazon boundary layer experiment: Wet season 1987. Journal of Geophysical Research, 95 (D10), 16721-16736.

Hicks, B.B., Baldocchi, D.D., Meyers, T.P., Hosker Jr., R.P., Matt, D.R., 1987. A preliminary multiple resistance routine for deriving dry deposition velocities from measured quantities. Water, Air and Soil Pollution, 36, 311-330.

Hosker, R.P., Lindberg, S.E., 1982. Review - Atmospheric deposition and plant assimilation of gases and particles. Atmospheric Environment, 16 (5), 889-910.

IPCC, 2001. Climate Change 2001: The Scientifc Basis - Contribution of Working Group I to the Third Assessment Report of the International Panel on Climate Change (IPCC). Cambridge University Press, Cambridge.

Jacob, D.J., Wofsy, S.C., 1990. Budgets of reactive nitrogen, hydrocarbons, and ozone over the Amazon-Forest during the wet season. Journal of Geophysical Research, 95 (D10), 16737-16754.

Jacob, D.J., Bakwin, P.S., 1992. Cycling of NO_x in tropical forest canopies. In: W.

B. Whitman (Editor), Microbial Production and Consumption of Greenhouse Gases. American Society of Microbiology, Washington, D.C., pp. 237-253

Johansson, C., 1987. Pine forest: A negligible sink for atmospheric NO_x in rural Sweden. Tellus (B), 39, 426-438.

Kaplan, W.A., Wofsy, S.C., Keller, M., da Costa, J.M., 1988. Emission of NO and deposition of O_3 in a tropical forest system. Journal of Geophysical Research, 93 (D2), 1389-1395.

Keller, M., Veldkamp, E., Weitz, A.M., Reiners, W.A., 1993. Effect of pasture age on soil trace-gas emissions from a deforested area of Costa Rica. Nature, 365, 244-246.

Kesselmeier, J., Kuhn, U., Rottenberger, S., Biesenthal, T., Wolf, A., Schebeske, G., Andreae, M.O., Ciccioli, P., Brancaleoni, E., Frattoni, M., Oliva, S.T., Botelho, M.L., Silva, C.M.A., Tavares, T.M., 2002. Concentrations and species composition of atmospheric volatile organic compounds (VOC) as observed during the wet and dry season in Rondonia (Amazonia). Journal of Geophysical Research, 107 (D20), 8053, doi: 10.1029/2000JD000267.

Kirkman, G.A., Gut, A., Ammann, C., Gatti, L.V., Cordova, A.M., Moura, M.A.L., Andreae, M.O., Meixner, F.X., 2002. Surface exchange of nitric oxide, nitrogen dioxide, and ozone at a pasture in Rondonia, Brazil. Journal of Geophysical Research, 107 (D20), 8083, doi: 10.1029/2001JD000523.

Kleffmann, J., Becker, H., Wiesen, P., 1998. Heterogeneous NO_2 conversion processes on acid surfaces: possible atmospheric implications. Atmospheric Environment, 32 (16), 2721-2729.

Kuhn, U., Rottenberger, S., Biesenthal, T., Wolf, A., Schebeske, G., Ciccioli, P., Brancaleoni, E., Frattoni, M., Tavares, T.M., Kesselmeier, J., 2002a. Isoprene and monoterpene emission of Amazonian tree species during the wet season: Direct and indirect investigations of controlling functions. Journal of Geophysical Research, 107 (D20), 8071, doi:10.1029/2001 JD000978.

Kuhn, U., Rottenberger, S., Biesenthal, T., Ammann, C., Wolf, A., Schebeske, G., Oliva, S.T., Tavares, T.M., Kesselmeier, J., 2002b. Exchange of short-chain monocarboxylic acids by vegetation at a remote tropical forest site in Amazonia. Journal of Geophysical Research, 107 (D20), 8069, doi:10.1029/2001JD000303.

Labrador, L.J., von Kuhlmann, R., Lawrence, M.G., 2004. Strong sensitivity of global mean OH concentration and the tropospheric oxidizing efficiency to source of NO_x from lightning.

Geophysical Research Letters, 31 (L06102), doi:10.1029/2003 GL019229.

Lee, D.S., Köhler, I., Grobler, E., Rohrer, F., Sausen, R., Gallardo-Klenner, L., Olivier, J.G.J., Dentener, F.J., Bouwman, A.F., 1997. Estimations of global NO_x emissions and their uncertainties. Atmospheric Environment, 31 (12), 1735-1749.

Lerdau, M., Munger, J.W., Jacob, D.J., 2000. The NO_2 flux conundrum. Science, 289, 2291-2293.

Levy, H., 1971. Normal atmosphere: Large radical and formaldehyde concentrations predicted. Science, 173, 141-143.

Ludwig, J., Weber, P., Meixner, F.X., Rennenberg, H. (Editors), 1992. Surface fluxes of NO and NO_2 by a dynamic chamber technique - Laboratory studies on wheat. Field measurtements and interpretation of species related to photooxidants and acid deposition, Air Pollution Research Report 39. Comission of the European Comunities, Directorate-Generale for Science, Brussels (B), 257-265 pp.

McKee, D.J. (Editor), 1993. Tropospheric ozone, human health and agricultural impacts, Lewis, Boca Raton, Fla.

McWilliam, A.-L.C., Cabral, O.M.R., Gomes, B.M., Esteves, J.L., Roberts, J.M., 1996. Forest and pasture leaf gas exchange in south-west Amazonia. In: J. H. C. Gash, C. A. Nobre, J. M. Roberts and R. L. Victoria (Editors), Amazonian deforestation and climate. John Wiley & Sons, Chichester, pp. 266-285

Meyers, T.P., 1987. The sensitivity of modeled SO_2 fluxes and profiles to stomatal and boundary layer resistances. Water Air and Soil Pollution, 35, 261-278.

Neff, J.C., Keller, M., Holland, E.A., Weitz, A.M., Veldkamp, E., 1995. Fluxes of nitric oxide from soils following the clearing and burning of secondary tropical rain forest. Journal of Geophysical Research, 100 (D12), 25913-25922.

Nobre, C.A., Fisch, G., da Rocha, H.R., Lyra, R.F.d.F., da Rocha, E.P., da Costa, A.C.L., Ubarana, V.N., 1996. Observations of the atmospheric boundary layer in Rondônia. In: J. H. C. Gash, C. A. Nobre, J. M. Roberts and R. L. Victoria (Editors), Amazonian deforestation and climate. John Wiley & Sons, Chichester, pp. 413-423

Paw U, K.T., Qiu, J., Su, H.B., Watnabe, T., Brunet, Y., 1995. Surface renewal analysis: a new method to obtain scalar fluxes. Agricultural and Forest Meteorology, 74, 119-137.

Portmann, R.W., Solomon, S., Fishman, J., Olson, J.R., Kiehl, J.T., Briegleb, B.,

1997. Reactive forcing of earth's climate due to tropical tropospheric ozone production. Journal of Geophysical Research, 102, 9409-9417.

Ribero, J.E.L.S., Berg, T.C., 1999. Guia de identificacao das plantas vasculares de uma floresta de terra-firme na Amazonia central. IMPA, Manaus, Brazil.

Roberts, J., Cabral, O.M.R., Deaguiar, L.F., 1990. Stomatal and Boundary-Layer Conductances in an Amazonian Terra-Firme Rain-Forest. Journal of Applied Ecology, 27 (1), 336-353.

Rondon, A., Johansson, C., Granat, L., 1993. dry deposition of nitrogen dioxide and ozone to coniferous forests. Journal of Geophysical Research, 98 (D3), 5159-5172.

Rondon, A., Granat, L., 1994. Studies on dry deposition of NO_2 to coniferous species at low NO_2 concentrations. Tellus, 46B, 339-352.

Rottenberger, S., Kuhn, U., Wolf, A., Schebeske, G., Oliva, S.T., Tavares, T.M., Kesselmeier, J., 2004. Exchange of short-chain aldehydes between Amazonian vegetation and the atmosphere. Ecological Applications, 14 (4), 247-262.

Rummel, U., Ammann, C., Gut, A., Meixner, F.X., andreae, M.O., 2002. Eddy covariance measurements of nitric oxide flux within an Amazonian rainforest. Journal of Geophysical Research, 107(D20), 8050, doi: 10.1029/ 2001 JD000520.

Rummel, U., Ammann, C., Kirkman, G.A., Moura, M.A.L., Rottenberger, S., Kuhn, U., Kesselmeier, J., Foken, T., Andreae, M.O., Meixner, F.X., 2005a. Seasonal variation of ozone deposition to a tropical rain forest in southwest Amazonia. Agricultural and Forest Meteorology, for submission.

Rummel, U., Ammann, C., Foken, T., Meixner, F.X., 2005b. Characterization of turbulent air motion within and above a tropical rain forest in Amazonia. Boundary-Layer Meteorology, for submission.

Rummel, U., Ammann, C., Foken, T., Andreae, M.O., Meixner, F.X., 2005c. Application of a surface renewal model for the determination of heat, carbon dioxide, and ozone fluxes from a tropical rain forest in Amazonia. Atmos. Chem. Phys., for submission.

Schuepp, P.H., 1971. Studies of forced-convection heat and mass transfer of fluttering realistic leaf models. Boundary-Layer Meteorology, 2, 263-274.

Schwartz, S.E., White, W.H. (Editors), 1983. Kinetics of reactive dissolution of nitrogen oxides into aqueous solution. Advances in Environmental Science

and Technology: Trace Atmospheric Constituents; Properties, Transformations, and Fates, 12. Jon Wiley and Sons, New York, 1-116 pp.

Shuttleworth, W.J., Gash, J.H.C., Lloyd, C.R., Moore, C.J., Roberts, J.M., Marques Filho, A.d.O., Fisch, G.F., Silva Filho, V.d.P., Ribero, J.E.L.S., Molion, L.C.B., Abreu Sa, L.D., Nobre, J.C.A., Cabral, O.M.R., Patel, S.R., de Moraes, J.C., 1984. Observation of radiation exchange above and below Amazonian Forest. Quarterly Journal of the Royal Meteorological Society, 110, 1163-1169.

Sparks, J.D., Monson, R.K., Sparks, K.L., Lerdau, M., 2001. Leaf uptake of nitrogen dioxide (NO_2) in a tropical wet forest: implications for tropospheric chemistry. Oecologia, 127, 214-221.

Stockwell, D.Z., Giannakopoulos, C., Plantevin, P.H., Carver, G.D., Chipperfield, M.P., Law, K.S., Pyle, J.A., Shallcross, D.E., Wang, K.-Y., 1999. Modelling NO_x from lightning and its impact on global chemical fields. Atmospheric Environment, 33, 4477-4493.

Thoene, B., Schröder, P., Papen, H., Egger, A., Rennenberg, H., 1991. Absorption of atmospheric NO_2 by spruce (Picea abies L. Karst.) trees. 1. NO_2 influxe and its correlation with nitrate reduction. New Phytol., 117, 575-585.

Thoene, B., Rennenberg, H., Weber, P., 1996. Absorption of atmospheric NO_2 by spruce (Picea abies) trees. 2. Parameterization of NO_2 fluxes by controlled dynamic chamber measurements. New Phytol., 134, 257-266.

Verchot, L.V., Davidson, E.A., Cattanio, J.H., Ackermann, I.L., Erickson, H.E., Keller, M., 1999. Land use change and biogechemical controls of nitrogen oxide emissions from soils in eastern Amazonia. Global Biogeochemical Cycles, 13, 31-46.

Weber, P., Rennenberg, H., 1996. Dependency of nitrogen dioxide (NO_2) fluxes to wheat(Triticum Aestivum L.) leaves from NO_2 concentration, light intensity, temperature and relative humidity determined from controlled dynamic chamber experiments. Atmospheric Environment, 30 (17), 3001-3009.

Wesely, M.L., 1989. Parameterization of surface resistances to gaseous dry deposition in regional-scale numerical models. Atmospheric Environment, 23 (6), 1293-1304.

Yienger, J., Levy, H., 1995. Empirical model of global soil-biogenic NO_x emission. Journal of Geophysical Research, 100 (D6), 11447-11464.

Erklärung

Hiermit erkläre ich, dass ich die vorliegende Arbeit selbstständig verfasst und keine anderen als die von mir angegebenen Quellen und Hilfsmittel benutzt habe.

Ferner erkläre ich, dass ich anderweitig mit oder ohne Erfolg nicht versucht habe, diese Dissertation einzureichen. Ich habe keine gleichartige Doktorprüfung an einer anderen Hochschule endgültig nicht bestanden.

Berlin, April 2005

Udo Rummel